STUDY OF ELASTODYNAMIC PROBLEMS IN MICROPOLAR THERMOELASTIC MEDIA

A Thesis Submitted for the Award of the Degree of

DOCTOR OF PHILOSOPHY

in

Mathematics

By

Arun Kochar

Registration Number: 41800354

Supervised By

Dr. Sachin Kaushal

Professor

Department of Mathematics,

School of Chemical Engineering and Physical Sciences

Lovely Professional University, Punjab

Co-Supervised by

Dr. Rajneesh Kumar

Professor

Department of Mathematics,

Kurukshetra University,

Kurukshetra-Haryana

LOVELY PROFESSIONAL UNIVERSITY
PHAGWARA-PUNJAB
2025

DECLARATION

I, hereby declared that the presented work in the thesis entitled "Study of Elastodynamic Problems in Micropolar Thermoelastic Media" in fulfilment of degree of **Doctor of Philosophy (Ph. D.)** is outcome of research work carried out by me under the supervision of Dr. Sachin Kaushal, working as Professor, in the Department of Mathematics, School of Chemical Engineering and Physical Sciences of Lovely Professional University, Punjab, India and co-supervision of Dr. Rajneesh Kumar, Professor, in the Department of Mathematics, Kurukshetra University, Kurukshetra-Haryana. In keeping with general practice of reporting scientific observations, due acknowledgements have been made whenever work described here has been based on findings of other investigator. This work has not been submitted in part or full to any other University or Institute for the award of any degree.

(Signature of Scholar)
ARUN KOCHAR
41800354
Department of Mathematics,
School of Chemical Engineering and Physical Sciences
Lovely Professional University, Punjab, India

CERTIFICATE

This is to certify that the work reported in the Ph. D. thesis entitled "Study of Elastodynamic Problems in Micropolar Thermoelastic Media" submitted in fulfillment of the requirement for the award of degree of **Doctor of Philosophy (Ph.D.)** in the Department of Mathematics, School of Chemical Engineering and Physical Sciences, is a research work carried out by Arun Kochar, 41800354, is bonafide record of his original work carried out under our supervision and that no part of thesis has been submitted for any other degree, diploma or equivalent course.

(Signature of Supervisor)

Dr. Sachin Kaushal
Professor,
Department of Mathematics,
School of Chemical Engineering and Physical Sciences
Lovely Professional University, Punjab

(Signature of Co-Supervisor)

Dr. Rajneesh Kumar
Professor,
Department of Mathematics,
Kurukshetra University,
Kurukshetra-Haryana

ABSTRACT

The thesis entitled "**Study of Elastodynamic Problems in Micropolar Thermoelastic Media**" is divided into six chapters and contribution of the chapters is as follows:

In the first chapter, an introduction is provided that includes a brief history to theories of micropolar elasticity, micropolar thermoelasticity, modified Green-Lindsay (MG-L) thermoelasticity, and Moore-Gibson-Thompson (MGT) thermoelasticity with hyperbolic two-temperature (HTT), two-temperature (TT), non-local (N-L), and voids. Additionally, a concise literature review of the relevant research in the area is presented.

Chapter 2 presents the reflection of plane waves in homogeneous, isotropic, micropolar thermoelastic (MT) half-space using the MG-L generalised thermoelasticity theory. The governing equations are rendered dimensionless for two-dimensional problem, and potential functions are employed to facilitate further simplification. When a plane wave (longitudinal displacement wave (LDW) or thermal wave (TW) or coupled transverse wave (CD-IW), or coupled microrotational wave (CD-IIW)) is incident on the surface $x_3 = 0$, four types of reflected waves are identified, namely LDW, TW, CD-IW, and CD-IIW. The impedance boundary restrictions are employed to calculate the amplitude ratios (AR) of these reflected waves. Graphs illustrate the impacts of impedance parameters on the AR of reflected waves for a variety of thermoelasticity theories. Some particular cases are also discussed.

A mathematical model of micropolar thermoelasticity is introduced in chapter 3, which is based on the MGT heat equation with N-L and HTT parameters. The governing equations are transformed into a two-dimensional problem, which is then simplified using potential functions and rendered dimensionless. Subsequently, a reflection-based methodology is implemented to solve the problem. Four types of reflected waves are identified when a plane wave (LDW or CD-IW) strikes the surface $x_3 = 0$, namely LDW, TW, CD-IW, and CD-IIW. The impedance boundary restrictions are employed to calculate the AR of these reflected waves. The graphic representation of numerical findings depicts the effects of N-L, HTT, TT, and impedance parameters on AR. Specific cases are also considered.

The reflection of plane waves in a micropolar elastic medium with voids at the non-free surface is the area of investigation in chapter 4. The governing equations are translated into a two-dimensional, dimensionless form for the model under consideration, and potential functions are employed to further simplify the formulation. Four types of reflected waves are identified when a plane wave (LDW or longitudinal void volume fraction wave (LVVFW) or CD-IW, or CD-IIW) is incident at the surface $x_3 = 0$, namely LDW, LVVFW, CD-IW, and CD-IIW. Using non-free boundary conditions, the AR of various reflected waves are

determined. The graphic representation of the AR with respect to the angle of incidence for both non-free and free surfaces is used to illustrate the effects of stiffnesses and voids. Specific cases are also deduced.

In chapter 5, the MGT heat equation is employed to solve a two-dimensional deformation problem in an isotropic, homogeneous MT half-space. The problem is solved under thermomechanical conditions, and N-L and HTT parameters are incorporated. Potential functions are employed to further simplify the governing equations, which are presented in dimensionless form. The problem is solved by employing the Laplace and Fourier transforms. The transformed domain is used to calculate physical quantities, such as components of displacement, force stresses, tangential couple stress, thermodynamic temperature, and conductive temperature, for a specific thermal source and normal force at the boundary surface. The quantities in the original domain are subsequently recovered using a numerical inversion technique. Graphs are used to demonstrate how the N-L, HTT, and TT parameters affect the resulting quantities. Certain cases are also deduced.

The primary objective of chapter 6 is to utilize the MGT heat equation to examine the axisymmetric deformity in homogeneous, isotropic, MT with N-L, and HTT parameters as a result of the distinct loads (ring load and disc load). The equations are reduced in two-dimensional form and then transformed by using dimensionless quantities and potential functions. The Laplace and Hankel transforms are employed to solve governing equations. The displacement components, force stresses, tangential couple stress, thermodynamic temperature, and conductive temperature are obtained in the transformed form. To recover physical quantities into the original domain, a numerical inversion technique is used. The graphic representation of numerical findings for force stress components, tangential couple stress and conductive temperature depicts the effects of N-L, HTT, and TT factors. Some cases of interest are also drawn.

Problems discussed in the thesis are published in the form of research papers in SCI and Scopus indexed journals with good impact factor.

ACKNOWLEDGEMENT

It is with great pleasure that I acknowledge the invaluable assistance I have received throughout the completion of my work. Foremost, I extend my heartfelt gratitude to my esteemed supervisor, **Dr. Sachin Kaushal**, Professor in the Department of Mathematics at Lovely Professional University, Phagwara, Punjab. His expert guidance, insightful suggestions, and unwavering encouragement have been instrumental in the progress of this thesis. His strong motivation and supportive attitude have consistently inspired me to work diligently. I am deeply indebted to him for his thorough review, analysis of the thesis structure, and valuable recommendations.

I would be remiss in my duties if I did not express my profound respect to **Dr. Rajneesh Kumar**, Professor in the Department of Mathematics at Kurukshetra University, Kurukshetra, for his stimulating guidance, continuous encouragement, and supervision throughout the course. His unwavering support and tireless guidance have been a constant source of inspiration for me. My gratitude to him extends far beyond this formal acknowledgment and cannot be fully expressed in words.

I sincerely pay tribute to my parents with deep reverence. Words cannot fully express their enduring love for me. I owe special thanks to my father, **Mr. Bal Krishan Kochar**, and my mother, **Mrs. Veena Rani**, for their unwavering support, love, and blessings, which have been a constant source of inspiration in bringing this thesis to fruition. I would like to express my deepest gratitude to my wife, **Mrs Nisha Kochar**, for her unwavering support and encouragement throughout the duration of my PhD. Her belief in me has been a constant source of motivation. I would like to thank my children, **Lavnya, Janvika and Shivaay**, for their love, patience, and understanding during this journey. I would also like to express my sincere thanks to **Mrs. Kumar** and **Mrs. Kaushal** for their kindness and blessings.

I express my deep sense of appreciation to my brother, **Mr. Pankaj Kochar**, and his wife, **Mrs. Neetu Kochar**, for their continuous support in the completion of this research work. I would also like to extend my sincere regards to **department of the Mathematics and Lovely Professional University** for their cooperation during this endeavour.

Ultimately, all my thanks are only a fraction of what is due to the Almighty for granting me the opportunity and divine grace to successfully accomplish this assignment.

Arun Kochar

CONTENTS

Chapter 1

Introduction

This chapter provides a brief introduction to the theories of micropolar elasticity, micropolar thermoelasticity, modified Green-Lindsay thermoelasticity, and Moore-Gibson-Thompson thermoelasticity with hyperbolic two-temperature, two-temperature, non-local, and voids. Various researchers' work on these aspects is briefly reviewed.

Chapter 1

1.1 Introduction

The classical theory of elasticity aligns well with experimental results for many structural materials under elastic conditions. However, it often falls short in scenarios where the material's microstructure plays a critical role. Notable discrepancies arise near stress concentrators such as holes, notches, and cracks in materials like steel, aluminum, and concrete. These inconsistencies become more pronounced in high-frequency phenomena, such as ultrasonic wave propagation, and in dynamic behaviors like vibrations of granular or multimolecular structures. Since most natural and engineered materials including metals, composites, soils, and concrete exhibit inherent microstructures, a more refined theory is needed to accurately capture their mechanical response.

Voigt (1887) [165] was the first to suggest that the interaction between two components in a material is described by both a force vector and a moment vector. This proposal addressed the shortcomings of classical elasticity and resulted in the development of couple stress theory. Cosserat and Cosserat (1909) [25] established an asymmetric elasticity theory for deformable bodies, taking into account a three-dimensional continuum in which material particles can move linearly and rotate during material deformation. As a result, a body's deformation is characterized by two vectors: displacement and independent rotation. Although the idea was innovative, the Cosserat brothers' work attracted little attention from researchers, and the theory remained largely overlooked during their lifetime, possibly due to its non-linear nature. After several years of Cosserat's work, some researchers Gunthier (1958) [55], Grioli (1960) [54], Truesdell and Toupin (1960) [164], and Mindlin and Tiersten (1962) [107] extended Cosserat continuum theory as Cosserat Pseudocontinuum.

Eringen (1964) [34] developed the theory of simple microfluids, incorporating the concept of microinertia conservation. Later, Eringen and Suhubi (1964) [45], along with Suhubi and Eringen (1964) [158], formulated a general theory for nonlinear microelastic solids. This theory considers the internal motions of microelements within the macrovolume and introduces new balance laws for continuum mechanics.

Green and Rivlin (1964) [53] and Green (1965) [48] devised a multipolar continuum theory that appears to be a specific instance of Eringen and Suhubi (1964) [45] theory. A micromorphic continuum is composed of materials that exhibit both classical motion and

deformation, with the assumption that the deformation is affine. Consequently, the material point in the micromorphic medium possesses twelve degrees of freedom, with three of these degrees being dedicated to macro motion and nine to micro motion. Eringen (1966) [35] renamed the theory of micromorphic continuum that Eringen and Suhubi devised in 1964. Micromorphic continuum theory, which encompasses both Cosserat continuum theory and indeterminate couple stress theory, presents challenges in its application due to its complexity.

Eringen (1966 [36], 1966 [37]) later simplified the theory of the micromorphic continuum and introduced the term "micropolar elasticity" in his papers. In micropolar elasticity, the body is considered to be composed of interconnected material particles, resembling small rigid bodies that can move both rotationally and translationally. The motion of these particles is characterized by both deformation and microrotation, resulting in six degrees of freedom. They are free to rotate independently. Consequently, the interaction between two regions of a material's constituents is transmitted through both force and torque, resulting in asymmetric force and couple stresses within the material. Examples of materials in this category include solid propellant granules, polymeric compounds and fiberglass.

Nowacki (1968) [109] and Eringen (1970) [39] introduced thermal effects into the theory of micropolar materials, leading to the development of micropolar coupled thermoelasticity theory. This theory is based on the conduction equation and stress-strain relation, both of which are influenced by thermal processes or heat. Tauchert et al. (1968) [159] formulated the fundamental equations for the linear theory of micropolar thermoelasticity, encompassing the constitutive equations, displacement components, microrotation, and coupling stresses. Nowacki (1970) [110] established the "second" plane problem in micropolar elastic solid.

Iesan (1971) [57] also developed the existence theorems using the fundamental three-dimensional boundary value problems in micropolar elastic solids. Nowacki (1971 [111], 1972 [112]) studied axisymmetric problems in micropolar elasticity. Boschi and Iesan (1973) [20] used Green and Lindsay's (G-L) (1972) [49] entropy production inequality to investigate the linear theory of generalised thermoelasticity for a homogeneous micropolar continuum. Rao and Rao (1983) [125] investigated longitudinal wave propagation in a long, circular cylinder of linear micropolar elastic material. The theory of micropolar thermoelasticity, which has heat flux as one of its constitutive variables, was devised by Chandrasekharaiah (1986) [21].

Eringen (1999) [43] presented the connections between several microcontinuity theories. Kumar and Deswal (2000) [73] studied the steady-state response of a micropolar generalized thermoelastic solid under the influence of a moving force applied normal to the boundary, accounting for the effects of microrotation. Kumar et al. (2007) [90] employed the eigenvalue method to examine thermal and mechanical disturbances in a micropolar thermoelastic (MT) medium.

In the context of the Green and Naghdi III (GN-III) (1992) [51] theory of thermoelasticity, Partap and Kumar (2010) [116] employed the separation of variables technique to solve the resultant equation that governs an isotropic, homogeneous MT cylindrical curved plate in a circumferential direction. The axisymmetric problem of micropolar porous thermoelastic materials under thermal source and normal force was investigated by Kumar and Gupta (2010) [75] using the potential function.

Shaw and Mukhopadhyay (2011) [148] used Lord-Shulman's (L-S) (1967) [98] generalised theory of thermoelasticity to explore the properties of waves in various modes on an isotropic MT plate. Zhang et al. (2015) [171] calculated the energy flux ratios of reflected waves at the non-free surface in a micropolar elastic semi-solid. Abouelregal and Zenkour (2017) [4] calculated thermodynamic and conductive temperatures, micro-rotation, and stresses when surface waves propagate in MT media. Singh et al. (2019) [151] derived the reflection coefficients and energy ratios for various reflected waves in a generalized MT medium.

Khan and Tanveer (2022) [69] studied the refraction and reflection of waves at the interface between micropolar solid and liquid layers. Kumar and Partap (2022) [91] used normal mode (NM) analysis technique to derive wave dispersion relation in a MT plate with memory dependent derivatives. Othman and Abbas (2023) [114] developed the phase lag theory to investigate the impact of rotation for the two-dimensional MT medium by employing the eigenvalue approach.

Somaiah and Kumar (2023) [155] formulated secular equations to analyze Rayleigh wave propagation in a homogeneous, isotropic micropolar elastic solid coupled with a viscous liquid, and studied the nature of different Rayleigh waves. Sahu et al. (2023) [128] studied propagation of Rayleigh wave in a micropolar semi-space and explored the impacts of material density and micropolarity on phase velocity.

By combining a linear TT theory with a higher-order derivative in a micropolar thermoelasticity semi-solid, Abouelregal and Rashid (2024) [3] employed a NM analysis approach to demonstrate the effects of initial stress and magnetic Hall current on wave fields and media characteristics. Bhat et al. (2024) [18] studied the behaviour of Rayleigh waves caused by seismic surface pulses in both an isotropic micropolar elastic semi-space and multilayered micropolar media.

The non-locality postulates, when viewed through the lens of functional basic relations, reveal a study of every particle's behaviour within a physical material. According to the non-local (N-L) theory of elasticity, the condition of each place inside the substance influences a specific property of a particle. This property differentiates N-L theory of elasticity from classical theory of elasticity. N-L atomic interactions have a significant impact on material characteristics in solid-state physics. This theory focuses on an internal characteristic length parameter crucial for accurately describing the physical behaviour of materials at the nanoscale.

With the help of universal balance laws along with thermodynamic second law, Eringen and Edelen (1972) [44] established the N-L theory of thermoelastic solids. Eringen (1972) [40] evolved a N-L theory of polar elastic continua. In this theory, he formulated the constitutive equations by using N-L thermodynamics and invariance under rigid motions of N-L micromorphic elastic solid. N-L theory of elasticity evaluates strain at every point in the medium, as compared to classical theory of elasticity, which only considers strain at a single point. N-L thermoelasticity theory serves as a bridge between the classical continuum limit and the atomic lattice theory. It incorporates surface, thermal and elastic effects, providing a framework to analyze solids with finite boundaries. This approach enables a more comprehensive treatment of material behavior, particularly at scales where classical theories may not adequately describe phenomena due to their inherent assumptions about locality and boundary conditions.

Eringen (1974) [41] formulated the foundational equations of N-L theory of thermoelasticity, establishing a framework that considers the N-L effects in thermal and elastic behavior of materials. Eringen (1984) [42] developed the dispersion relation for transverse plane waves in N-L micropolar elastic materials. Yu et al. (2016) [169] introduced a N-L thermoelasticity theory to investigate the effects of elastic deformation and heat conduction in nanoscale structures.

Kalkal et al. (2020) [63] studied the effects of N-L, rotational, and micropolar parameters on the energy ratios and reflection coefficients of different reflected waves in a rotating MT medium. Sahrawat et al. (2023) [127] studied the reflection and refraction phenomena of waves at an interface in a N-L MT media. They also computed the reflection and refraction coefficients of various waves concerning their angle of incidence and angular frequency. Poonam et al. (2024) [117] investigated the basic solution in an isotropic N-L MT materials with voids. They also explored how N-L and void parameters affected the attenuation coefficients and phase velocity of distinct waves. With the NM analysis approach, Dhankhar et al. (2024) [31] investigated thermo-mechanical interactions in functionally graded MT half-space with N-L impact due to inclined load.

A linear elastic material with voids consists of microscopic pores. In classical elasticity theory, the volume of these pores is typically ignored. However, the volume of these pores is crucial and must be considered as an independent kinematic variable. Voids are common in the composite manufacturing process and have the potential to change stiffness, strength, and fracture characteristics. Incorporating voids into micropolar media enriches the model by introducing additional physical phenomena such as porosity-induced wave modes and coupling effects. This extended model is vital for simulating and analysing real-world materials where porosity and microstructure significantly influence mechanical behaviour. The study of wave propagation in such media supports advanced material design, geophysical exploration etc. As a result, many researchers have worked on void-containing materials in various fields of study and applications.

Nunziato and Cowin (1979) [113] developed a hypothesis that was predicated on the existence of apertures in non-linear elastic materials. Cowin and Nunziato (1983) [26] expanded this concept to include linear elastic materials with apertures. Iesan (1985) [58] investigated shock wave propagation in micropolar elastic materials containing voids. Iesan (1986) [59] built on Cowin and Nunziato's (1983) linear theory of thermoelastic solids with voids by incorporating thermal effects. Marin (1996) [100] employed elliptic equation theory to establish the existence and uniqueness of solutions for boundary value problems in micropolar elastic materials with apertures.

The dynamic problem of isotropic, homogeneous semi-space that contain voids under a normal point source was investigated by Kumar and Choudhary (2003) [72]. Miglani and

Kaushal (2011) [105] studied a two-dimensional problem involving micropolar elastic solids with voids in an inviscid fluid. Othman and Atwa (2012) [115] used the Green and Naghdi type I (GN-I) (1991) [50] and type II (GN-II) (1993) [52] thermoelasticity theories to explore the deformation of MT solids with cavities under the effect of various sources at the boundary. Singh and Singh (2013) [153] used the eigenvalue method to solve the field equations for an axisymmetric problem in a micropolar elastic medium with apertures.

Marin (2016) [101] proposed a heat-flux theory for micropolar porous media that incorporates both the heat-flux vector and its accompanying evolution equation. Lianngenga, & Singh and Lianngenga (2017 [96], 2017 [154]) examined various wave analysis problems in micropolar elastic and MT material containing cavities. Marin et al. (2019) [102] used advanced mathematical techniques to generalize Dafermos's results to prove the existence and uniqueness of finite energy solutions in thermoelasticity for micropolar materials with pores. With the help of NM analysis approach, Alharbi et al. (2020) [15] obtained expressions of temperature, volume fraction fields, displacement components, microrotation and stresses in the micropolar medium with voids using the three-phase-lag model of thermoelasticity and studied the impacts of heat source, temperature dependence and void parameters on resulting quantities.

In order to investigate thermomechanical interactions in a N-L MT semi-space that was initially stressed and contained pores, Kundu et al. (2023) [94] implemented a NM analysis approach under a moving thermal load. Jangra et al. (2024) [62] applied NM analysis approach to derive expression of stresses, temperature, and pore pressure and studied the impacts of time, velocity of the load, micropolarity and void parameters on these quantities in MT saturated porous medium, under the framework of G-L theory of thermoelasticity.

Chen and Gurtin (1968) [22] and Chen et al. (1969) [23] presented the thermoelasticity hypothesis of the two temperatures (TT). This hypothesis is based on two temperatures: thermodynamic temperature and conductive temperature. The thermodynamic temperature was caused by mechanical interactions between particles, but the conductive temperature was caused by thermal interactions. Quintanilla (2003) [119] obtained TT theory of thermoelasticity and characterized its properties, including structural stability, convergence, and spatial behaviour.

Youssef (2006) [167] proposed a model of heat conduction that considers two types of temperatures: dynamic and conductive. The difference in temperatures is related to the amount of heat given. In this model, thermal wave propagates at infinite speed. The TT model was

updated to the hyperbolic two-temperature (HTT) model by Youssef and El-Bary (2018) [168]. In this model the difference between the second derivatives of dynamical temperature and conductive temperature is proportional to heat supply over time and it creates a thermal wave with limited speed.

Kumar and Abbas (2013) [71] studied the substantial impacts of TT on displacement, stresses, microrotation, temperature field, and conductive temperature after incorporating a thermal source at the boundary in MT materials with TT under L-S theory. Sharma et al. (2013) [140] established the equations for leaky and non-leaky Lamb waves in MT materials with TT. Kumar et al. (2014) [78] explored wave propagation in an MT plate with TT, using secular equations under stress-free, insulated, and isothermal scenarios.

Kumar and Kaur (2015) [76] used the GN-III theory of thermoelasticity to investigate wave propagation at the interface of two MT mediums and studied the impacts of TT and stiffness on the amplitude ratios (AR) of various reflected and transmitted waves. Kumar et al. (2017) [82] explored the impacts of thermodynamic and conductive temperatures on the transmission and reflection coefficients at the interface of two separate micropolar visco-thermoelastic solid semi-spaces using the G-L theory of thermoelasticity.

Kumar et al. (2018) [84] studied the deformation of a micropolar porous circular plate using a three-phase lag model in conjunction with the TT theory of thermoelasticity. Bayones et al. (2022) [16] used NM analysis technique to explore the impacts of the Thomson and TT parameters on physical quantities in MT materials with voids. El-Sapa et al. (2023) [33] examined the impacts of rotation and viscosity on generalized micropolar thermoelasticity with TT, considering various thermoelasticity theories such as L-S, G-L, GN-II, and GN-III.

To account for microscopic characteristics in materials, Abouelregal et al. (2023) [6] investigated the propagation of planar waves in rotating MT media using the TT thermoelastic model with higher-order time derivatives and dual-phase latency. With help of NM analysis approach, Abouelregal et al. (2024) [11] computed theoretical and graphical results, showing significant effects of higher-order phase delays and TT facts on deformations in MT model under Hall current. Rani et al. (2025) [124] employed the normal mode analysis technique to investigate wave behavior and thermomechanical deformation in a porous thermoelastic medium with microtemperature, considering non-local effects and dual phase lag theory. They evaluated various wave characteristics and deformation parameters which offer valuable insights for

applications in material engineering, geophysical studies, and related scientific areas. Abouelregal et al. (2025) [8] presented a novel dual-phase-lag (DPL) thermoelastic theory by incorporating non-local elasticity and micropolar effects to analyzes temperature, displacement, and stress responses under laser pulse heating at the boundary which effectively offering valuable insights for nanoscale applications such as laser heating, nanomaterials, and MEMS.

Green and Lindsay (G-L) (1972) [49] developed a thermoelasticity theory with two relaxation times by including the rate of temperature change among the constitutive variables, all while adhering to Fourier's law of heat conduction. Yu et al. (2018) [170] introduced a new model, the modified Green-Lindsay (MG-L) model, by integrating the strain rate term into the G-L thermoelastic model using principles from extended thermodynamics. This model further refines this framework by incorporating additional physical effects such as non-locality and temperature-dependent material properties. This enhancement allows for a more accurate representation of complex thermoelastic behaviours in advanced materials, such as micropolar materials, where classical assumptions may fall short. Consequently, the MG-L theory offers a more comprehensive tool for analysing and predicting the behaviour of materials under thermal and mechanical loads, accommodating a broader range of real-world applications.

Within the framework of the MG-L model, Quintanilla (2018) [120] demonstrated the exponential decay of solutions and analysed their spatial behaviour. Sarkar et al. (2020) [131] used the MG-L model with TT effects to study the reflection of magneto-thermoelastic plane waves from stress-free and thermally insulated barriers. Sarkar and Mondal (2020) [130] utilized the MG-L model with TT effects to examine the reflection of thermoelastic plane waves from thermally insulated and stress-free boundary. They also compared the reflection coefficients for L-S and G-L models.

Shakeriaski et al. (2021) [133] created a non-linear numerical technique for solving the governing equations in a highly deformed elastic medium under thermal shock using the MG-L model. Kumar et al. (2022) [79] studied the impacts of heat source and thermomechanical loading on stresses, components of displacement, thermodynamic and conductive temperatures using the MG-L model with N-L and TT parameters.

Kaushal et al. (2023) [67] studied the effects of HTT and N-L factors, as well as various thermoelasticity theories, on the temperature distribution, conductive temperature, and stresses under the application of a ramp-type thermal source and normal force at the boundary using the

MG-L thermoelasticity theory. Kaushal et al. (2024) [68] examined the effects of N-L and TT parameters on displacement components, stresses, and temperature fields in generalized thermoelastic medium under the MG-L theory of thermoelasticity. Ailawalia and Priyanka (2024) [13] investigated the impact of thermal conductivity on photothermal interaction in a semiconducting medium under the MG-L theory of thermoelasticity.

The Moore-Gibson-Thompson (MGT) heat equation has attracted considerable attention in recent years due to its wide range of applications in industrial and medical fields. Consequently, it is not surprising that many studies have focused on the use of high-intensity ultrasound. The MGT thermoelasticity theory was formulated to characterize high-amplitude sound vibrations, which have various potential applications in medicine and industry, including lithotripsy, heat therapy, and ultrasound cleaning.

Thompson (1972) [161] established this theory based on a third-order differential equation that highlighted the significance of specific fluid dynamics concepts. Quintanilla (2019) [121] later developed an innovative MGT thermoelasticity theory that gained serious attention from researchers, which is a combination (or generalization) of the Lord-Shulman and Green-Naghdi thermoelasticity theory of type III. L-S and GN-III models can be recovered when we omit the dependence with respect to suitable variables in this model. The MGT equation for thermal conductivity was presented by Quintanilla (2020) [122] with TT effects. The solutions are well-presented and decrease substantially when the constitutive parameters are set correctly.

Jangid and Mukhopadhyay (2021) [61] formulated several theorems to tackle heat flux and natural stress problems within the MGT theory of thermoelasticity. Meanwhile, Fernandez and Quintanilla (2021) [46] examined linear thermoelastic deformations in dielectrics using the MGT theory of thermoelasticity. In context of MGT thermoelastic theory, Bazarra et al. (2021) [17] analysed radially symmetric solutions and establish their exponential decay with respect to (w.r.t) time using energy arguments.

Abouelregal et al. (2022) [9] studied thermal and mechanical wave characteristics in a thermoviscoelastic orthotropic cylinder using a Kelvin-Voigt viscoelastic model under MGT theory of thermoelasticity. Tiwari et al. (2022) [163] studied thermoelastic vibrations of a clamped nano-beam under a variable axial load using Euler–Bernoulli beam theory and the Moore–Gibson generalized thermoelastic (MGTE) model. They employed Laplace transform

technique for analytical solutions, and analyzed significant effects of thermoelastic models, axial load, and ramping time on nano-beam responses.

Within the framework of the MGT theory of thermoelasticity, Megahid et al. (2023) [104] utilized the NM analysis approach to explore the relationship between the modulus of modified Ohm's law and rotation across various physical parameters. Kumar et al. (2024) [81] examined a two-dimensional axisymmetric thermoelastic problem incorporating fractional order derivatives and analysed the effects of HTT and N-L parameters on temperature distribution, conductive temperature, stress components, and displacement in the context of the MGT heat equation under mechanical loading.

1.2 Research Gap

Over the past decade, significant progress has been made in the field of generalized thermoelasticity, particularly in developing various models that incorporate thermal relaxation and non-classical heat conduction effects. These advancements are largely driven by the need to understand the thermoelastic responses of structures such as railways, bridges, and aerospace components under dynamic loading conditions. Despite this progress, a comprehensive mathematical treatment of micropolar thermoelastic media that integrates non-local effects, energy dissipation, and hyperbolic two temperature remains limited. In particular, the application of modified Green–Lindsay (MG-L) theory, coupled with nonlocal parameters, fractional calculus, and Moore-Gibson-Thompson (MGT) heat conduction, has not been adequately addressed in existing literature. Furthermore, the role of additional physical phenomena such as viscosity, porosity, and mass diffusion within the framework of two-temperature and hyperbolic two-temperature theories has not been thoroughly explored. This highlights a critical need for interdisciplinary approaches that bridge theoretical modeling with practical engineering applications.

The current study aims to fill this gap by developing and analyzing new mathematical models in micropolar thermoelasticity that incorporate these advanced features. These models will be investigated under various boundary conditions relevant to the physical context and evaluated through numerical simulations. Comparative analyses with existing models will be conducted to assess improvements in predictive capability, and parametric studies will be used to illustrate the influence of key factors such as relaxation times, diffusion coefficients, non-local parameters, and void effects on the thermoelastic response.

1.3 Foundation of Waves

For the wave equation $\frac{\partial^2 y}{\partial x^2} = \frac{1}{c^2}\frac{\partial^2 y}{\partial t^2}$, a plane wave travelling with speed c in the positive x-direction is represented by $y(x,t) = Ae^{i(kx-\omega t)}$, where A is the amplitude of wave, k is the number, $\omega = ck$ is the angular frequency.

In the framework of micropolar thermoelasticity, a wave is a disturbance that transmits energy through a medium by inducing both translational and micro-rotational motion of material particles, without causing permanent deformation. Seismic waves are generated by natural events like earthquakes or artificial explosions are studied extensively using seismometers, which record wave amplitudes and help in the exploration of subsurface features such as oil and mineral deposits. These waves are broadly categorized into body waves and surface waves. Body waves traverse the interior of the earth, bending due to spatial variation in modulus, density, and thermal properties caused by changes in temperature and material composition. Primary waves (P-waves), also referred to as longitudinal, compressional, or irrotational waves, are the fastest and first to appear on a seismogram. In micropolar thermoelastic media, they involve not only compressional motion but also couple with thermal fields and micro-rotational effects. The particles oscillate in the direction of wave propagation, and the velocity of these waves is $\sqrt{\frac{\lambda+2\mu+K}{\rho}}$, where λ and μ are Lamé constants, ρ is the mass density and K is micropolar constant. Secondary waves (S-waves) arrive after P-waves and are known as transverse, shear, or rotational waves. In the micropolar context, these waves gain added complexity, as the particle motion perpendicular to the wave vector now includes micro-rotation and couple stress effects. Their speed is approximately $\sqrt{\frac{\mu+K}{\rho}}$. Surface waves, which propagate along the earth's surface, travel slower than body waves but are often more destructive due to their larger amplitudes and longer durations. Their amplitude decays exponentially with depth, and their sensitivity to surface defects makes them useful in non-destructive testing. Thus, the inclusion of micropolar and thermoelastic effects provides a more complete understanding of wave behavior, especially in materials with internal structure or subjected to thermal gradients.

The reflection of waves at material interfaces is a classical problem in continuum mechanics and mathematical physics. It arises in numerous fields including elasticity, acoustics, thermoelasticity and micropolar thermoelasticity. The study of wave propagation with their

reflection in micropolar thermoelastic medium at boundary surfaces or interfaces, has long been a subject of considerable interest. Numerous researchers have investigated these phenomena using various theoretical models, resulting in a substantial body of work available in the scientific literature.

1.4 Constitutive Relations and Basic Equations for Different Mathematical Models

The classical theory of elasticity is a foundational branch of continuum mechanics, focusing on the stress and deformation responses of elastic materials under the influence of external forces or thermal variations. The derivation of constitutive relations and basic equations used in this study are as follows:

1.4.1 Classical Elasticity

Strain-displacement relations

$$e_{ij} = \frac{1}{2}\left(u_{i,j} + u_{j,i}\right), \quad (i,j = 1,2,3) \tag{1.1}$$

where e_{ij} is the strain tensor and u_i is the displacement component.

Strain compatibility equations

$$e_{ij,kl} + e_{kl,ij} - e_{ik,jl} - e_{jl,ik} = 0, \quad (i,j,k,l = 1,2,3) \tag{1.2}$$

Stress- strain relations

For homogeneous isotropic material, Hooke's law becomes

$$t_{ij} = \lambda u_{k,k}\delta_{ij} + 2\mu e_{ij} \tag{1.3}$$

where λ, μ are Lame's constants, δ_{ij} is Kronecker's delta, t_{ij} represents stress tensor and $u_{k,k}$ is the dilatation.

Equations of motion

For homogeneous isotropic medium

$$t_{ij,j} + \rho F_i = \rho \ddot{u}_i \tag{1.4}$$

where $t_{ij,j}$ represents divergence of stress tensor t_{ij}, F_i is the component of external body force per unit mass, $\ddot{u}_i$ is second time derivative of displacement component u_i and ρ is the mass density.

1.4.2 Classical Thermoelasticity

The classical theory of thermoelasticity (CTE) originated with the work of Duhamel (1837) [32] who formulated equations to describe how strain distributes within an elastic medium subjected

to temperature gradients. Building on this foundation, Neumann (1885) [108] introduced the Duhamel–Neumann stress, strain and temperature relation, which remains a cornerstone of CTE.

Stress-strain-temperature relations

$$t_{ij} = 2\mu e_{ij} + (\lambda u_{k,k} - \beta T)\delta_{ij} \quad (i, j, k = 1,2,3) \tag{1.5}$$

where $\beta = (3\lambda + 2\mu)\alpha_t$, α_t - coefficient for linear thermal expansion of the material, T is the increase in temperature above the reference temperature T_0 such that $\left|\frac{T}{T_0}\right| << 1$.

Fourier's law of heat conduction

$$q_i = -K^* T_{,i} \tag{1.6}$$

where q_i indicate the component of the heat flux vector $\mathbf{q}$ and K^* is the thermal conductivity.

Energy equation

$$-q_{i,i} + \rho Q = \rho C_e \dot{T} \tag{1.7}$$

where C_e is the specific heat at constant strain, Q is the heat source and t is the time.

Heat equation

The equations (1.6) and (1.7) together yield the parabolic heat transport equation as

$$K^* T_{,ii} + \rho Q = \rho C_e \dot{T} \tag{1.8}$$

This theory predicts two events that contradict physical observations. First, there are no elastic factors in this theory's heat conduction equation. Second, the heat equation is of the parabolic type, predicting infinite speeds of propagation for heat waves.

Equations (1.4), (1.5) and (1.8) constitute the complete mathematical model of the classical thermoelasticity.

1.4.3 Classical Coupled Thermoelasticity

Biot (1956) [19] proposed the theory of classical coupled thermoelasticity. The governing equations of this theory are coupled, which eliminates the first paradox of the classical theory of thermoelasticity.

Energy equation

$$-q_{i,i} + \rho Q = \rho C_e \dot{T} + \beta T_0 \dot{u}_{k,k} \tag{1.9}$$

where the term $\beta T_0 \dot{u}_{k,k}$ introduces a thermo-mechanical coupling between the temperature field and the mechanical deformation.

Heat Equation

By eliminating q_i between equations (1.6) and (1.9), we get parabolic type heat transport equation

$$K^* T_{,ii} + \rho Q = \rho C_e \dot{T} + \beta T_0 \dot{u}_{k,k} \quad (1.10)$$

Equation (1.10), describes the coupling between the thermal and elastic fields. This suggests that thermal signals propagate at infinite speed, a conclusion that is physically unrealistic.

Equations (1.4), (1.5) and (1.10) together constitute the complete mathematical model of the classical coupled thermoelasticity.

1.4.4 Lord-Shulman Model [L-S Model]

To address the paradox inherent in classical coupled thermoelasticity, Lord and Shulman (1967) [98] proposed a generalized theory of thermoelasticity by introducing a modification to the classical Fourier heat conduction law as

Modified Fourier law of heat conduction

$$\left(1 + \tau_0 \frac{\partial}{\partial t}\right) q_i = -K^* T_{,i} \quad (1.11)$$

Heat equation

Eliminating q_i from equations (1.9) and (1.11), one gets the following generalization of the heat conduction equation

$$K^* T_{,ii} = \left(1 + \tau_0 \frac{\partial}{\partial t}\right) [\, \rho C_e \dot{T} + \beta T_0 \dot{u}_{k,k} - \rho Q] \quad (1.12)$$

where τ_0 is called relaxation time. This model yields hyperbolic type heat transport equation with finite speed of thermal wave.

Equation (1.12) together with equations (1.4), (1.5) constitute the field equations of L-S model.

1.4.5 Green-Lindsay Model [G-L Model]

Green and Lindsay (G-L) (1972) [49] proposed a generalized thermoelasticity theory that introduces notable distinctions from the L-S model, which employs a single relaxation time parameter. Unlike the L-S theory, the G-L model retains the classical Fourier law of heat conduction but modifies both the energy equation and the constitutive relations between stress, strain, and temperature.

Stress-strain-temperature relations

$$t_{ij} = 2\mu e_{ij} + \lambda u_{k,k} \delta_{ij} - \beta(T + \tau_1 \dot{T}) \delta_{ij} \quad (1.13)$$

Fourier law of heat conduction

$$q_i = -K^* T_{,i} \quad (1.14)$$

Energy Equation

$$-q_{i,i} + \rho Q = \rho C_e \left(\dot{T} + \tau_0 \ddot{T}\right) + \beta T_0 \dot{u}_{k,k} \quad (1.15)$$

Heat equation

Elimination of q_i from equations (1.14) and (1.15), give the following heat conduction equation

$$K^* T_{,ii} + \rho Q = \rho C_e \left(\dot{T} + \tau_0 \ddot{T}\right) + \beta T_0 \dot{u}_{k,k} \quad (1.16)$$

where τ_1 is relaxation time. τ_1 and τ_0 satisfy $\tau_1 \geq \tau_0 > 0$ for G-L model only. However, it has been proved by Strunin (2001) [157] that the inequalities $\tau_1 \geq \tau_0 > 0$ are not mandatory for τ_0 and τ_1 to follow. This theory gives hyperbolic type heat transport equation with finite speed of thermal wave.

The system of equations (1.4), (1.13) and (1.16) constitute the complete mathematical model for G-L model.

1.4.6 Modified Green-Lindsay Model [MG-L Model]

Yu et al. (2018) [170] proposed the MG-L model by incorporating the strain rate term into the G-L thermoelastic framework. This enhancement was achieved based on the principles of extended thermodynamics, aiming to capture more realistic thermo-mechanical coupling effects, especially in materials with microstructural interactions or under high-frequency excitations.

Stress-strain-temperature relations

$$t_{ij} = \left(1 + \eta_1 \tau_1 \frac{\partial}{\partial t}\right)\left(2\mu e_{ij} + \lambda u_{k,k}\delta_{ij}\right) - \beta(T + \eta_2 \tau_1 \dot{T})\delta_{ij} \quad (1.17)$$

Energy Equation

$$-q_{i,i} + \rho Q = \rho C_e \left(\dot{T} + \eta_3 \tau_0 \ddot{T}\right) + \beta T_0 \left(1 + \eta_4 \tau_0 \frac{\partial}{\partial t}\right) \dot{u}_{k,k} \quad (1.18)$$

Heat equation

Elimination of q_i from equations (1.14) and (1.18), give the following heat conduction equation

$$K^* T_{,ii} + \rho Q = \rho C_e \left(\dot{T} + \eta_3 \tau_0 \ddot{T}\right) + \beta T_0 \left(1 + \eta_4 \tau_0 \frac{\partial}{\partial t}\right) \dot{u}_{k,k} \quad (1.19)$$

where η_1, η_2, η_3 and η_4 are constants and by replacing $\eta_1 = \eta_4 = 0,\ \eta_2 = \eta_3 = 1$, this model reduces to G-L model.

The system of equations (1.4), (1.17) and (1.19) constitute the complete mathematical model for MG-L model.

1.4.7 Green-Naghdi Model II (GN II (1993))

The governing equations of the generalized thermoelasticity proposed by Green and Naghdi [52] are

Law of heat conduction

$$q_i = -K_1^* \vartheta_{,i} \quad (1.20)$$

where ϑ is the thermal displacement such that $\dot{\vartheta} = T$ and K_1^* is thermal conductivity rate.

Heat equation

Eliminating q_i from the equations (1.20) and (1.9), we get

$$K_1^* T_{,ii} + \rho\dot{Q} = \rho C_e \ddot{T} + \beta T_0 \dot{u}_{k,k} \tag{1.21}$$

Equations (1.4), (1.5) and (1.21) constitute the complete mathematical model of GN II model.

A re-examination of equations (1.5) and (1.21) within the framework of the GN II model indicates the absence of any damping term in the governing equations. As a result, the GN II model is commonly referred to as thermoelasticity without energy dissipation.

1.4.8 Green-Naghdi model III (GN III (1992))

The modified heat conduction law proposed by Green and Naghdi [51] are

Law of heat conduction

$$q_i = -(K^* T_{,i} + K_1^* \vartheta_{,i}) \tag{1.22}$$

Heat equation

Equations (1.9) and (1.22) together give the generalized heat transport equation

$$K^* \dot{T}_{,ii} + K_1^* T_{,ii} + \rho\dot{Q} = \rho C_e \ddot{T} + \beta T_0 \ddot{u}_{k,k} \tag{1.23}$$

Equations (1.4), (1.5) and (1.23) constitute the complete mathematical model of GN III model. This theory is also known as thermoelasticity with energy dissipation.

By putting $K^* = 0$ in the equations of GN III model, we obtain the GN II model. When $K_1^* = 0$, the equations of GN III model reduce to GN I model, which is identical with the classical theory of thermoelasticity.

1.4.9 Moore Gibson Thompson (MGT) Model

Quintanilla (2019) [121] proposed a modified heat conduction law by incorporating the relaxation parameter τ_0 into the GN-III theory of thermoelasticity as

Modified Law of heat conduction

$$\left(1 + \tau_0 \frac{\partial}{\partial t}\right) q_i = -(K^* T_{,i} + K_1^* \vartheta_{,i}) \tag{1.24}$$

Heat equation

Eliminating q_i from (1.24) and (1.9), one can get heat conduction equation (in absence of heat source) as

$$\left(1 + \tau_0 \frac{\partial}{\partial t}\right)\left[\rho C_e \ddot{T} + \beta T_0 \ddot{u}_{k,k}\right] = \left(K^* \frac{\partial}{\partial t} + K_1^*\right) T_{,ii}. \tag{1.25}$$

This theory is useful for studying wave propagation and thermomechanical problems particularly under conditions involving rapid thermal or mechanical disturbances.

1.4.10 Micropolar Thermoelasticity

The constitutive equations of linear micropolar thermoelasticity for homogenous isotropic medium given by Tauchert et al. (1968) [159] are

$$t_{ij} = \lambda u_{k,k}\delta_{ij} + \mu(u_{i,j} + u_{j,i}) + K(u_{j,i} - \varepsilon_{ijk}\phi_k) - \gamma_1 T\delta_{ij} \quad (1.26)$$

$$m_{ij} = \alpha\phi_{k,k}\delta_{ij} + \eta\phi_{i,j} + \zeta\phi_{j,i} \quad (1.27)$$

$$-q_{i,i} + \rho Q = \rho C_e \dot{T} + \gamma_1 T_0 \dot{u}_{k,k} \quad (1.28)$$

where $\gamma_1 = (3\lambda + 2\mu + K)\alpha_t$, α_t - coefficient for linear thermal expansion of the material, m_{ij} denote couple stress tensor, ϕ_k represents component of microrotation vector, ε_{ijk} represents alternating tensor and K, η, α, ζ are micropolar constants. Index after comma denotes the partial derivative.

As per the Eringen's (1966) [36]

Equation of motion:

$$t_{ij,j} + \rho(F_i - \ddot{u}_i) = 0 \quad (1.29)$$

$$m_{ij,j} + \epsilon_{ijk}t_{jk} + \rho\left(l_i - J\ddot{\phi}_i\right) = 0 \quad (1.30)$$

where l_i is body couple per unit mass, J is microrotation inertia.

Using constitutive equations (1.26) -(1.27) into field equations (1.29) -(1.30), we get

$$(\lambda + \mu)u_{i,ji} + (\mu + K)u_{j,ij} + K\epsilon_{ijk}\phi_{k,j} - \gamma_1 T_{,i} + \rho(F_i - \ddot{u}_i) = 0, \quad (1.31)$$

$$(\alpha + \eta)\phi_{i,jj} + \zeta\phi_{j,ij} + K\epsilon_{ijk}u_{k,j} - 2K\phi_i + \rho\left(l_i - J\ddot{\phi}_i\right) = 0. \quad (1.32)$$

Eliminating q_i from equations (1.28) and (1.11), we get

$$K^* T_{,ii} = \left(1 + \tau_0 \frac{\partial}{\partial t}\right)[\rho C_e \dot{T} + \gamma_1 T_0 \dot{u}_{k,k} - \rho Q] \quad (1.33)$$

1.5 Thesis Layout

This section briefly explains the problems mentioned in chapter 1 to chapter 6 of the thesis. In chapter 1, an introduction is provided that contains a brief history and basic concepts of the problem under consideration. In addition, a brief literature review in the field under consideration is provided.

The MG-L generalised thermoelasticity theory is used in Chapter 2 to study the reflection of plane waves in homogeneous, isotropic MT half-space. The governing equations are rendered

dimensionless for two-dimensional problem, and potential functions are employed to facilitate further simplification. When a plane wave (longitudinal displacement wave (LDW) or thermal wave (TW) or coupled transverse wave (CD-IW), or coupled microrotational wave (CD-IIW)) is incident at the surface $x_3 = 0$, four types of reflected waves are identified as LDW, TW, CD-IW, and CD-IIW. The impedance boundary restrictions are employed to calculate the AR of these reflected waves numerically. The graphs depict the effects of impedance parameters on the AR of reflected waves across different theories of thermoelasticity. Several specific cases are also analysed.

Chapter 3 introduces a mathematical model of micropolar thermoelasticity based on the MGT heat equation and the N-L and HTT parameters. The governing equations are transformed into a two-dimensional problem, which is then simplified using potential functions and rendered dimensionless. Subsequently, a reflection-based methodology is implemented to solve the problem. Four types of reflected waves are identified when a plane wave (LDW or CD-IW) is incident at the surface $x_3 = 0$, namely LDW, TW, CD-IW, and CD-IIW. The impedance boundary restrictions are employed to calculate the AR of these reflected waves. The graphic representation of numerical findings depicts the effects of N-L, HTT, TT, and impedance parameters on AR. Specific cases are also considered.

The reflection of plane waves in a micropolar elastic medium with voids at the non-free surface is presented in Chapter 4. The governing equations are translated into a two-dimensional, dimensionless form for the model under consideration, and potential functions are employed to further simplify the formulation. Four types of reflected waves are identified when a plane wave (LDW or longitudinal void volume fraction wave (LVVFW) or CD-IW, or CD-IIW) is incident at the surface $x_3 = 0$, namely LDW, LVVFW, CD-IW, and CD-IIW. Using non-free boundary conditions, the AR of various reflected waves are determined. The graphic representation of the AR with respect to the angle of incidence for both non-free and free surfaces is used to illustrate the effects of stiffnesses and voids. Specific cases are also deduced.

In Chapter 5, the MGT heat equation is used to solve a two-dimensional deformation problem in an isotropic and homogeneous MT half-space. The problem is solved under thermomechanical conditions, and N-L and HTT parameters are incorporated. Potential functions are employed to further simplify the governing equations, which are presented in dimensionless form. The problem is addressed using the Laplace and Fourier transforms. In the

transformed domain, physical quantities such as displacement components, force stresses, thermodynamic temperature, and conductive temperature are calculated for a specific thermal source and normal force applied at the boundary surface. The quantities in the original domain are subsequently recovered using a numerical inversion technique. Graphs are used to demonstrate how the N-L, HTT, and TT parameters affect the resulting quantities. Certain cases are also deduced.

The primary objective of chapter 6 is to utilize the MGT heat equation to examine the axisymmetric deformity in homogeneous, isotropic MT with N-L, and HTT parameters as a result of the distinct loads (ring load and disc load). The equations are reduced in two-dimensional form and then transformed by using dimensionless quantities and potential functions. The governing equations are solved using the Laplace and Hankel transforms. In the transformed domain, the displacement components, force stresses, tangential couple stress, thermodynamic temperature, and conductive temperature are obtained. A numerical inversion technique is then applied to recover the physical quantities in the original domain. The graphic representation of numerical findings for stress components, conductive temperature and tangential couple stress depicts the effects of N-L, HTT, and TT factors. Some cases of interest are also drawn.

Chapter 2

Wave propagation in a micropolar thermoelastic media under impedance boundary in the framework of modified Green-Lindsay theory of thermoelasticity

The work from this chapter has been published in the form of research paper entitled "Response of impedance parameters on waves in the micropolar thermoelastic medium under modified Green-Lindsay theory", ZAMM-Journal of Applied Mathematics and Mechanics, 102(9), 2022, https://doi.org/10.1002/zamm.202200109.

Indexing: SCI, Scopus, Impact Factor:2.3

Chapter 2

Wave propagation in a micropolar thermoelastic media under impedance boundary in the framework of modified Green-Lindsay theory of thermoelasticity

2.1 Introduction

Sharma and Marin (2013) [139] studied the impact of two temperature (TT) parameter on plane wave propagation in a micropolar thermoelastic (MT) medium. Kumar et al. (2018) [89] derived a secular equation for Rayleigh wave propagation in a MT half-space incorporating impedance parameters. In context of modified Green-Lindsay (MG-L) theory of generalized thermoelasticity, Sarkar et al. (2020) [132] calculated the amplitude ratios (AR) of reflected waves at boundaries that are both stress-free and isothermal.

In order to examine the influence of laser radiation in a two-dimensional thermoelastic half-space, Tayel et al. (2021) [160] implemented the MG-L model. Singh and Kaur (2022) [150] examined the variation in the speed of Rayleigh waves due to impedance boundary in micropolar elastic media. In order to investigate the propagation of plane waves in MT media with TT, Abouelregal et al. (2022) [5] implemented the normal mode analysis technique. Energy ratios and reflection coefficients for reflected waves in a rotating micropolar double porous thermoelastic medium were determined by Sheoran et al. (2024) [149]. They also examined the impact of angular velocity, micropolarity, and double porosity on these energy ratios.

Kaushal et al. (2024) [66] examined the reflection of plane waves using the MG-L theory of thermoelasticity and analyzed how TT, non-local (N-L) parameters, and different thermoelasticity theories affect the AR of the reflected waves. Kumar et al. (2024) [92] explored wave propagation in MT plates by incorporating memory-dependent derivatives and employing the normal mode analysis technique.

This chapter presents the reflection of plane waves in an isotropic, homogeneous MT half-space within the framework of the MG-L theory of generalized thermoelasticity. For the two-dimensional problem, governing equations are rendered dimensionless and potential functions are employed to facilitate further simplification. When a plane wave (longitudinal displacement wave (LDW) or thermal wave (TW) or coupled transverse wave (CD-IW) or coupled microrotational wave (CD-IIW)) is incident on the surface $x_3 = 0$, four types of reflected waves are identified as LDW, TW, CD-IW, and CD-IIW. An impedance boundary is used to determine the AR of these reflected waves. The wave characteristics and material

properties of the medium influence the AR, which depend upon the angle of incidence, frequency, and impedance parameters. Graphs are used to demonstrate the effects of impedance on the AR of various reflected waves in relation to different thermoelasticity theories. Several special cases are also included for comparison.

This study is motivated by the limitations of classical wave reflection theories, which fail to capture the complex interactions arising from microstructural effects, thermal relaxation, and impedance related phenomena in advanced materials. To address these shortcomings, a refined and unified framework is developed for analyzing wave propagation in micropolar thermoelastic media. Based on the MG-L theory of thermoelasticity, the proposed model integrates micro-rotational behavior, thermal relaxations, and impedance interactions into a single formulation. This novel approach not only improves the accuracy of wave reflection analysis but also deepens the theoretical understanding of wave behavior in microstructured environments.

2.2 Governing Equations

The following are the field equations and constitutive relations for micropolar thermoelasticity under the MG-L model after removing body couples, body forces, and heat sources (as described by Eringen (1966) [36] and Yu et al. (2018) [170]):

$$\left(1+\eta_1\tau_1\frac{\partial}{\partial t}\right)[(\lambda+\mu)\nabla(\nabla.\mathbf{u})+(\mu+K)\Delta\mathbf{u}+K(\nabla\times\boldsymbol{\phi})] - \left(1+\eta_2\tau_1\frac{\partial}{\partial t}\right)\gamma_1\nabla T=\rho\frac{\partial^2\mathbf{u}}{\partial t^2}, \tag{2.1}$$

$$\gamma\Delta\boldsymbol{\phi}+(\alpha+\beta)\nabla(\nabla.\boldsymbol{\phi})+K[(\nabla\times\mathbf{u})-2\boldsymbol{\phi}]=\rho\hat{j}\frac{\partial^2\boldsymbol{\phi}}{\partial t^2}, \tag{2.2}$$

$$K^*\Delta T=\rho C_e\left(1+\eta_3\tau_0\frac{\partial}{\partial t}\right)\frac{\partial T}{\partial t}+\left(1+\eta_4\tau_0\frac{\partial}{\partial t}\right)\gamma_1 T_0\frac{\partial}{\partial t}(u_{h,h}), \tag{2.3}$$

$$t_{pq}=\left(1+\eta_1\tau_1\frac{\partial}{\partial t}\right)\left[\lambda u_{h,h}\delta_{pq}+\mu\left(u_{p,q}+u_{q,p}\right)+K\left(u_{q,p}-\varepsilon_{pqh}\phi_h\right)\right] - \gamma_1\left(1+\eta_2\tau_1\frac{\partial}{\partial t}\right)T\delta_{pq}, \tag{2.4}$$

$$m_{pq}=\alpha\phi_{h,h}\delta_{pq}+\beta\phi_{p,q}+\gamma\phi_{q,p}, \qquad (p,q,h=1-3), \tag{2.5}$$

In above, microrotation vector - $\boldsymbol{\phi}$, displacement vector – $\mathbf{u}$, thermodynamic temperature - T, micropolar constants - K, β, α, γ, density - ρ, microrotation inertia - $\hat{j}$, Lame's constants - λ, μ , thermal conductivity - K^*, components of force stress tensor - t_{pq}, time - t, relaxation times - τ_0 and τ_1, $\gamma_1=(3\lambda+2\mu+K)\alpha_t$, α_t - coefficient for linear thermal expansion, components of couple stress tensor - m_{pq}, specific heat - C_e, η_1, η_2, η_3 and η_4 - constants, reference temperature - T_0, Kronecker's delta - δ_{pq}, alternating tensor - ε_{pqh} , Laplacian operator - Δ, nabla (gradient) operator - ∇.

Following cases arises:

(i) $\eta_1 = \eta_2 = 0,\ \eta_3 = \eta_4 = 1$: Lord-Shulman (L-S) theory (1967) [98],

(ii) $\eta_1 = \eta_4 = 0,\ \eta_2 = \eta_3 = 1$: Green-Lindsay (G-L) theory (1972) [49],

(iii) $\eta_1 = \eta_2 = \eta_3 = \eta_4 = 0$: Coupled thermoelasticity (C-T) theory (1980) [30],

(iv) $\eta_1 = \eta_2 = \eta_3 = \eta_4 = 1$: MG-L theory (2018) [170].

Equations (2.1) -(2.5), in components form for Cartesian coordinates (x_1, x_2, x_3) are written as

$$\left(1+\eta_1\tau_1\frac{\partial}{\partial t}\right)\left[(\lambda+\mu)\frac{\partial}{\partial x_1}\left(\frac{\partial u_1}{\partial x_1}+\frac{\partial u_2}{\partial x_2}+\frac{\partial u_3}{\partial x_3}\right)+(\mu+K)\Delta u_1+K\left(\frac{\partial \phi_3}{\partial x_2}-\frac{\partial \phi_2}{\partial x_3}\right)\right] - \left(1+\eta_2\tau_1\frac{\partial}{\partial t}\right)\gamma_1\frac{\partial T}{\partial x_1}=\rho\frac{\partial^2 u_1}{\partial t^2}, \tag{2.6}$$

$$\left(1+\eta_1\tau_1\frac{\partial}{\partial t}\right)\left[(\lambda+\mu)\frac{\partial}{\partial x_2}\left(\frac{\partial u_1}{\partial x_1}+\frac{\partial u_2}{\partial x_2}+\frac{\partial u_3}{\partial x_3}\right)+(\mu+K)\Delta u_2+K\left(\frac{\partial \phi_1}{\partial x_3}-\frac{\partial \phi_3}{\partial x_1}\right)\right] - \left(1+\eta_2\tau_1\frac{\partial}{\partial t}\right)\gamma_1\frac{\partial T}{\partial x_2}=\rho\frac{\partial^2 u_2}{\partial t^2}, \tag{2.7}$$

$$\left(1+\eta_1\tau_1\frac{\partial}{\partial t}\right)\left[(\lambda+\mu)\frac{\partial}{\partial x_3}\left(\frac{\partial u_1}{\partial x_1}+\frac{\partial u_2}{\partial x_2}+\frac{\partial u_3}{\partial x_3}\right)+(\mu+K)\Delta u_3+K\left(\frac{\partial \phi_2}{\partial x_1}-\frac{\partial \phi_1}{\partial x_2}\right)\right] - \left(1+\eta_2\tau_1\frac{\partial}{\partial t}\right)\gamma_1\frac{\partial T}{\partial x_3}=\rho\frac{\partial^2 u_3}{\partial t^2}, \tag{2.8}$$

$$\gamma\Delta\phi_1+(\alpha+\beta)\frac{\partial}{\partial x_1}\left(\frac{\partial \phi_1}{\partial x_1}+\frac{\partial \phi_2}{\partial x_2}+\frac{\partial \phi_3}{\partial x_3}\right)+K\left(\left(\frac{\partial u_3}{\partial x_2}-\frac{\partial u_2}{\partial x_3}\right)-2\phi_1\right)=\rho\hat{j}\frac{\partial^2 \phi_1}{\partial t^2}, \tag{2.9}$$

$$\gamma\Delta\phi_2+(\alpha+\beta)\frac{\partial}{\partial x_2}\left(\frac{\partial \phi_1}{\partial x_1}+\frac{\partial \phi_2}{\partial x_2}+\frac{\partial \phi_3}{\partial x_3}\right)+K\left(\left(\frac{\partial u_1}{\partial x_3}-\frac{\partial u_3}{\partial x_1}\right)-2\phi_2\right)=\rho\hat{j}\frac{\partial^2 \phi_2}{\partial t^2}, \tag{2.10}$$

$$\gamma\Delta\phi_3+(\alpha+\beta)\frac{\partial}{\partial x_3}\left(\frac{\partial \phi_1}{\partial x_1}+\frac{\partial \phi_2}{\partial x_2}+\frac{\partial \phi_3}{\partial x_3}\right)+K\left(\left(\frac{\partial u_2}{\partial x_1}-\frac{\partial u_1}{\partial x_2}\right)-2\phi_3\right)=\rho\hat{j}\frac{\partial^2 \phi_3}{\partial t^2}, \tag{2.11}$$

$$K^*\Delta T=\rho C_e\left(1+\eta_3\tau_0\frac{\partial}{\partial t}\right)\frac{\partial T}{\partial t}+\left(1+\eta_4\tau_0\frac{\partial}{\partial t}\right)\gamma_1 T_0\frac{\partial}{\partial t}\left(\frac{\partial u_1}{\partial x_1}+\frac{\partial u_2}{\partial x_2}+\frac{\partial u_3}{\partial x_3}\right), \tag{2.12}$$

$$t_{11}=\left(1+\eta_1\tau_1\frac{\partial}{\partial t}\right)\left[\lambda\left(\frac{\partial u_1}{\partial x_1}+\frac{\partial u_2}{\partial x_2}+\frac{\partial u_3}{\partial x_3}\right)+(2\mu+K)\frac{\partial u_1}{\partial x_1}\right]-\gamma_1\left(1+\eta_2\tau_1\frac{\partial}{\partial t}\right)T, \tag{2.13}$$

$$t_{22}=\left(1+\eta_1\tau_1\frac{\partial}{\partial t}\right)\left[\lambda\left(\frac{\partial u_1}{\partial x_1}+\frac{\partial u_2}{\partial x_2}+\frac{\partial u_3}{\partial x_3}\right)+(2\mu+K)\frac{\partial u_2}{\partial x_2}\right]-\gamma_1\left(1+\eta_2\tau_1\frac{\partial}{\partial t}\right)T, \tag{2.14}$$

$$t_{33}=\left(1+\eta_1\tau_1\frac{\partial}{\partial t}\right)\left[\lambda\left(\frac{\partial u_1}{\partial x_1}+\frac{\partial u_2}{\partial x_2}+\frac{\partial u_3}{\partial x_3}\right)+(2\mu+K)\frac{\partial u_3}{\partial x_3}\right]-\gamma_1\left(1+\eta_2\tau_1\frac{\partial}{\partial t}\right)T, \tag{2.15}$$

$$t_{31}=\left(1+\eta_1\tau_1\frac{\partial}{\partial t}\right)\left[\mu\left(\frac{\partial u_3}{\partial x_1}+\frac{\partial u_1}{\partial x_3}\right)+K\left(\frac{\partial u_1}{\partial x_3}-\phi_2\right)\right], \tag{2.16}$$

$$t_{32}=\left(1+\eta_1\tau_1\frac{\partial}{\partial t}\right)\left[\mu\left(\frac{\partial u_3}{\partial x_2}+\frac{\partial u_2}{\partial x_3}\right)+K\left(\frac{\partial u_2}{\partial x_3}+\phi_1\right)\right], \tag{2.17}$$

$$t_{21}=\left(1+\eta_1\tau_1\frac{\partial}{\partial t}\right)\left[\mu\left(\frac{\partial u_2}{\partial x_1}+\frac{\partial u_1}{\partial x_2}\right)+K\left(\frac{\partial u_1}{\partial x_2}+\phi_3\right)\right], \tag{2.18}$$

$$m_{11}=\alpha\left(\frac{\partial \phi_1}{\partial x_1}+\frac{\partial \phi_2}{\partial x_2}+\frac{\partial \phi_3}{\partial x_3}\right)+(\beta+\gamma)\frac{\partial \phi_1}{\partial x_1}, \tag{2.19}$$

$$m_{22} = \alpha\left(\frac{\partial \phi_1}{\partial x_1} + \frac{\partial \phi_2}{\partial x_2} + \frac{\partial \phi_3}{\partial x_3}\right) + (\beta + \gamma)\frac{\partial \phi_2}{\partial x_2}, \tag{2.20}$$

$$m_{33} = \alpha\left(\frac{\partial \phi_1}{\partial x_1} + \frac{\partial \phi_2}{\partial x_2} + \frac{\partial \phi_3}{\partial x_3}\right) + (\beta + \gamma)\frac{\partial \phi_3}{\partial x_3}, \tag{2.21}$$

$$m_{31} = \beta\frac{\partial \phi_3}{\partial x_1} + \gamma\frac{\partial \phi_1}{\partial x_3}, \tag{2.22}$$

$$m_{32} = \beta\frac{\partial \phi_3}{\partial x_2} + \gamma\frac{\partial \phi_2}{\partial x_3}, \tag{2.23}$$

$$m_{12} = \beta\frac{\partial \phi_1}{\partial x_2} + \gamma\frac{\partial \phi_2}{\partial x_1}, \tag{2.24}$$

where

$\Delta = \frac{\partial^2}{\partial x_1^2} + \frac{\partial^2}{\partial x_2^2} + \frac{\partial^2}{\partial x_3^2}$.

2.3 Problem Statement

A micropolar MG-L half-space that is homogeneous and isotropic, and has an impedance boundary, is examined. We employ a rectangular Cartesian coordinate system (x_1, x_2, x_3), with the origin positioned at the plane boundary at $x_3 = 0$. The x_3-axis extends vertically downward into the medium, while the x_1-axis is oriented horizontally, as illustrated in figure 2.1. The x_2-axis is aligned along the direction where the plane wave front intersects the plane surface. The field variables are contingent upon x_1, x_3 and t, if we restrict our analysis to the $x_1 - x_3$ plane, we assume that

$$\mathbf{u} = (u_1(x_1, x_3, t), 0, u_3(x_1, x_3, t)), \quad \boldsymbol{\phi} = (0, \phi_2(x_1, x_3, t), 0), \quad T = T(x_1, x_3, t). \tag{2.25}$$

Using equation (2.25) in (2.6) - (2.12), (2.15), (2.16) and (2.23), recast as

$$\left(1 + \eta_1\tau_1\frac{\partial}{\partial t}\right)\left[(\lambda + \mu)\frac{\partial}{\partial x_1}\left(\frac{\partial u_1}{\partial x_1} + \frac{\partial u_3}{\partial x_3}\right) + (\mu + K)\Delta u_1 - K\frac{\partial \phi_2}{\partial x_3}\right] - \left(1 + \eta_2\tau_1\frac{\partial}{\partial t}\right)\gamma_1\frac{\partial T}{\partial x_1} = \rho\frac{\partial^2 u_1}{\partial t^2}, \tag{2.26}$$

$$\left(1 + \eta_1\tau_1\frac{\partial}{\partial t}\right)\left[(\lambda + \mu)\frac{\partial}{\partial x_3}\left(\frac{\partial u_1}{\partial x_1} + \frac{\partial u_3}{\partial x_3}\right) + (\mu + K)\Delta u_3 + K\frac{\partial \phi_2}{\partial x_1}\right] - \left(1 + \eta_2\tau_1\frac{\partial}{\partial t}\right)\gamma_1\frac{\partial T}{\partial x_3} = \rho\frac{\partial^2 u_3}{\partial t^2}, \tag{2.27}$$

$$\gamma\Delta\phi_2 + K\left[\left(\frac{\partial u_1}{\partial x_3} - \frac{\partial u_3}{\partial x_1}\right) - 2\phi_2\right] = \rho\hat{j}\frac{\partial^2 \phi_2}{\partial t^2}, \tag{2.28}$$

$$K^*\Delta T = \rho C_e\left(1 + \eta_3\tau_0\frac{\partial}{\partial t}\right)\frac{\partial T}{\partial t} + \left(1 + \eta_4\tau_0\frac{\partial}{\partial t}\right)\gamma_1 T_0\frac{\partial}{\partial t}\left(\frac{\partial u_1}{\partial x_1} + \frac{\partial u_3}{\partial x_3}\right), \tag{2.29}$$

$$t_{33} = \left(1 + \eta_1\tau_1\frac{\partial}{\partial t}\right)\left[\lambda\left(\frac{\partial u_1}{\partial x_1} + \frac{\partial u_3}{\partial x_3}\right) + (2\mu + K)\frac{\partial u_3}{\partial x_3}\right] - \gamma_1\left(1 + \eta_2\tau_1\frac{\partial}{\partial t}\right)T, \tag{2.30}$$

$$t_{31} = \left(1 + \eta_1\tau_1\frac{\partial}{\partial t}\right)\left[\mu\left(\frac{\partial u_3}{\partial x_1} + \frac{\partial u_1}{\partial x_3}\right) + K\left(\frac{\partial u_1}{\partial x_3} - \phi_2\right)\right], \tag{2.31}$$

$$m_{32} = \gamma\frac{\partial \phi_2}{\partial x_3}, \tag{2.32}$$

where

$\Delta = \frac{\partial^2}{\partial x_1^2} + \frac{\partial^2}{\partial x_3^2}$.

To simplify further, we consider the dimensionless quantities as follows:

$(x_i', u_i') = \frac{\omega_1}{c_1}(x_i, u_i)$, $t_{3i}' = \frac{1}{\gamma_1 T_0} t_{3i}$, $m_{32}' = \frac{\omega_1}{\gamma_1 c_1 T_0} m_{32}$, $\phi_2' = \frac{\rho c_1^2}{\gamma_1 T_0}\phi_2$,

$(t', \tau_0', \tau_1') = \omega_1(t, \tau_0, \tau_1)$, $T' = \frac{T}{T_0}$, $(z_1', z_2') = \frac{c_1}{\gamma_1 T_0}(z_1, z_2)$, $z_3' = \frac{{\omega_1}^2}{\rho {c_1}^3} z_3$,

$z_4' = \frac{c_1}{K^*} z_4$, $\omega' = \frac{\omega}{\omega_1}$, $(i = 1,3)$, (2.33)

where

$c_1^2 = \frac{\lambda + 2\mu + K}{\rho}$ and $\omega_1 = \frac{\rho C_e c_1^2}{K^*}$. (2.34)

Using (2.33) in (2.26) -(2.32) after suppressing the primes, yield

$$\left(1 + \eta_1\tau_1 \frac{\partial}{\partial t}\right)\left[a_1 \frac{\partial}{\partial x_1}\left(\frac{\partial u_1}{\partial x_1} + \frac{\partial u_3}{\partial x_3}\right) + a_2 \Delta u_1 - a_3 \frac{\partial \phi_2}{\partial x_3}\right] - a_4 \left(1 + \eta_2\tau_1 \frac{\partial}{\partial t}\right)\frac{\partial T}{\partial x_1} = \frac{\partial^2 u_1}{\partial t^2}, \quad (2.35)$$

$$\left(1 + \eta_1\tau_1 \frac{\partial}{\partial t}\right)\left[a_1 \frac{\partial}{\partial x_3}\left(\frac{\partial u_1}{\partial x_1} + \frac{\partial u_3}{\partial x_3}\right) + a_2 \Delta u_3 + a_3 \frac{\partial \phi_2}{\partial x_1}\right] - a_4 \left(1 + \eta_2\tau_1 \frac{\partial}{\partial t}\right)\frac{\partial T}{\partial x_3} = \frac{\partial^2 u_3}{\partial t^2}, \quad (2.36)$$

$$a_5 \Delta\phi_2 + a_6\left(\frac{\partial u_1}{\partial x_3} - \frac{\partial u_3}{\partial x_1}\right) - a_7\phi_2 = \frac{\partial^2 \phi_2}{\partial t^2}, \quad (2.37)$$

$$\Delta T = \left(1 + \eta_3\tau_0 \frac{\partial}{\partial t}\right)\frac{\partial T}{\partial t} + a_8\left(1 + \eta_4\tau_0 \frac{\partial}{\partial t}\right)\frac{\partial}{\partial t}\left(\frac{\partial u_1}{\partial x_1} + \frac{\partial u_3}{\partial x_3}\right), \quad (2.38)$$

$$t_{33} = \left(1 + \eta_1\tau_1 \frac{\partial}{\partial t}\right)\left(a_{12}\frac{\partial u_3}{\partial x_3} + a_{13}\frac{\partial u_1}{\partial x_1}\right) - \left(1 + \eta_2\tau_1 \frac{\partial}{\partial t}\right)T, \quad (2.39)$$

$$t_{31} = \left(1 + \eta_1\tau_1 \frac{\partial}{\partial t}\right)\left(a_9\frac{\partial u_1}{\partial x_3} + a_{10}\frac{\partial u_3}{\partial x_1} - a_{11}\phi_2\right), \quad (2.40)$$

$$m_{32} = a_{14}\frac{\partial \phi_2}{\partial x_3}, \quad (2.41)$$

where

$a_1 = \frac{\lambda + \mu}{\rho c_1^2}$, $a_2 = \frac{\mu + K}{\rho c_1^2}$, $a_3 = \frac{K\gamma_1 T_0}{\rho^2 c_1^4}$, $a_4 = \frac{\gamma_1 T_0}{\rho c_1^2}$, $a_5 = \frac{\gamma}{\rho c_1^2 j}$, $a_6 = \frac{K c_1^2}{j\gamma_1 \omega_1^2 T_0}$,

$a_7 = \frac{2K}{j\rho\omega_1^2}$, $a_8 = \frac{\gamma_1 c_1^2}{K^*\omega_1}$, $a_9 = \frac{\mu + K}{\gamma_1 T_0}$, $a_{10} = \frac{\mu}{\gamma_1 T_0}$, $a_{11} = \frac{K}{\rho c_1^2}$, $a_{12} = \frac{\rho c_1^2}{\gamma_1 T_0}$,

$a_{13} = \frac{\lambda}{\gamma_1 T_0}$, $a_{14} = \frac{\gamma\omega_1^2}{\rho c_1^4}$. (2.42)

2.4 Solution Procedure

With the help of Helmholtz decomposition, u_1 and u_3 can be expressed as

$u_1 = \frac{\partial q}{\partial x_1} - \frac{\partial \psi}{\partial x_3}$, $u_3 = \frac{\partial q}{\partial x_3} + \frac{\partial \psi}{\partial x_1}$. (2.43)

After using (2.43), equations (2.35) -(2.38) reduce to the following equations:

$$\left(1 + \eta_1\tau_1 \frac{\partial}{\partial t}\right)\Delta q - a_4\left(1 + \eta_2\tau_1 \frac{\partial}{\partial t}\right)T = \frac{\partial^2 q}{\partial t^2}, \quad (2.44)$$

$$\left(1 + \eta_1\tau_1 \frac{\partial}{\partial t}\right)(a_2\Delta\psi + a_3\phi_2) = \frac{\partial^2 \psi}{\partial t^2}, \quad (2.45)$$

$$a_5\Delta\phi_2 - a_6\Delta\psi - a_7\phi_2 = \frac{\partial^2\phi_2}{\partial t^2}, \tag{2.46}$$

$$\left(1 + \eta_3\tau_0\frac{\partial}{\partial t}\right)\frac{\partial T}{\partial t} + a_8\left(1 + \eta_4\tau_0\frac{\partial}{\partial t}\right)\frac{\partial}{\partial t}\Delta q = \Delta T. \tag{2.47}$$

Assuming harmonic motion and aiming to solve equations, (2.44) -(2.47), we adopt the solutions in the form:

$$(q, T, \psi, \phi_2) = (q^o, T^o, \psi^o, \phi_2^o)e^{\iota\kappa(x_1\sin\theta_0 - x_3\cos\theta_0 + vt)}, \tag{2.48}$$

where $q^o, T^o, \psi^o, \phi_2^o$ represent the wave amplitudes, ν denotes phase speed, ι is known as iota, κ is indicated wave number, θ_0 is angle of inclination, and ω is angular frequency having the relation $\omega = \kappa v$.

Simplifying equations (2.44) - (2.47) by inserting the values of q, T, ψ, ϕ_2 from (2.48), yield the following equations

$$(\upsilon^4 + C_{01}\upsilon^2 + C_{02})(q^o, T^o) = 0, \tag{2.49}$$

$$(\upsilon^4 + C_{03}\upsilon^2 + C_{04})(\psi^o, \phi_2^o) = 0, \tag{2.50}$$

where

$$C_{01} = \frac{\omega(\tau_e\tau_\theta + a_4a_8\tau_f\tau_g) - \iota}{\iota\tau_e}, \qquad C_{02} = \frac{-\omega\tau_\theta}{\iota\tau_e}, \qquad C_{03} = \frac{\iota\omega\tau_\theta(a_2a_7 - a_3a_6 - a_2\omega^2) - a_5\omega^2}{\omega^2 - a_7},$$

$$C_{04} = \frac{a_2a_5\iota\omega^3\tau_\theta}{\omega^2 - a_7},$$

and

$$\tau_\theta = \left(\tau_1\eta_1 - \frac{\iota}{\omega}\right), \qquad \tau_e = \left(\tau_0\eta_3 - \frac{\iota}{\omega}\right), \quad \tau_f = \left(\tau_1\eta_2 - \frac{\iota}{\omega}\right), \qquad \tau_g = \left(\tau_0\eta_4 - \frac{\iota}{\omega}\right).$$

Let υ_i(i = 1,2) denote the roots of the characteristic equation $(\upsilon^4 + C_{01}\upsilon^2 + C_{02}) = 0$, which correspond to the velocities of the LDW and TW in decreasing order. In the same way, the roots of the characteristic equation $(\upsilon^4 + C_{03}\upsilon^2 + C_{04}) = 0$, are represented by υ_j (j = 3, 4) and correspond to velocities of CD-IW and CD-IIW in decreasing order.

2.5 Reflection Phenomenon of Waves

Consider a plane harmonic wave (LDW or TW or CD-IW or CD-IIW) that form an angle θ_0 with the normal to the surface at $x_3 = 0$. When any incident wave (LDW or TW or CD-IW or CD-IIW) strikes the boundary, it generates four reflected waves (LDW, TW, CD-IW and CD-IIW). These reflected waves make angles $\theta_1, \theta_2, \theta_3$, and θ_4 with the positive x_3- axis, as illustrated in figure 2.1. The complete wave field structure in the half-space, incorporating both incident and reflected waves, can be expressed as follows:

$$q = \sum_{i=1}^{2}\left[A_{0i}e^{\iota\kappa_0(x_1\sin\theta_0 - x_3\cos\theta_0) + \iota\omega t} + A_ie^{\iota\kappa_i(x_3\cos\theta_i + x_1\sin\theta_i) + \iota\omega t}\right], \tag{2.51}$$

$$T = \sum_{i=1}^{2}\left[d_i\left(A_{0i}e^{\iota\kappa_0(x_1\sin\theta_0 - x_3\cos\theta_0) + \iota\omega t} + A_ie^{\iota\kappa_i(x_3\cos\theta_i + x_1\sin\theta_i) + \iota\omega t}\right)\right], \tag{2.52}$$

$$\psi = \sum_{i=1}^{2}\left[B_{0i}e^{\iota\kappa_0(x_1\sin\theta_0 - x_3\cos\theta_0) + \iota\omega t} + B_ie^{\iota\kappa_j(x_3\cos\theta_j + x_1\sin\theta_j) + \iota\omega t}\right], \tag{2.53}$$

$$\phi_2 = \sum_{i=1}^{2}\left[f_i\left(B_{0i}e^{\iota\kappa_0(x_1\sin\theta_0 - x_3\cos\theta_0)+\iota\omega t} + B_i e^{\iota\kappa_j(x_3\cos\theta_j + x_1\sin\theta_j)+\iota\omega t}\right)\right], \quad (2.54)$$

where

$$d_i = \frac{\omega - \kappa_i{}^2\iota\tau_\theta}{a_4\iota\tau_f}, \quad f_i = \frac{a_6\kappa_j^2}{a_5\kappa_j^2 + a_7 - \omega^2}, (i = 1,2), (j = 3,4),$$

and, the amplitudes of the incident LDW, TW, CD-IW and CD-IIW are designated as A_{01}, A_{02}, B_{01} and B_{02}, respectively. A_1, A_2, B_1 and B_2 represent the amplitudes of the reflected LDW, TW, CD-IW and CD-IIW respectively.

2.6 Boundary Conditions

Generally, when seismic waves interact with discontinuities, an ideally welded contact surface is often assumed, ensuring continuity of displacement and stress components. Impedance boundary conditions typically involve a linear combination of the unknown functions and their derivatives, defined at the boundary. Therefore, following the formulations by Tiersten (1969) [162] and Malischewsky (1987) [99], the impedance boundary conditions at $x_3 = 0$ are as follows:

$$\text{(i) } t_{33} + \omega z_1 u_3 = 0, \qquad \text{(ii) } t_{31} + \omega z_2 u_1 = 0,$$

$$\text{(iii) } m_{32} + \omega z_3 \phi_2 = 0, \qquad \text{(iv) } K^* \frac{\partial T}{\partial x_3} + \omega z_4 T = 0, \quad (2.55)$$

where z_1, z_2 represent impedance parameters with dimensions of N sec m^{-3}, while z_3 and z_4 denote impedance parameters with dimensions of N sec m^{-1} and N $m^{-1}K^{-1}$ respectively.

Equation (2.55) reduces as following after using equation (2.33)

$$\text{(i) } t_{33} + \omega z_1 u_3 = 0, \qquad \text{(ii) } t_{31} + \omega z_2 u_1 = 0,$$

$$\text{(iii) } m_{32} + \omega z_3 \phi_2 = 0, \qquad \text{(iv) } \frac{\partial T}{\partial x_3} + \omega z_4 T = 0. \quad (2.56)$$

Using equation (2.43) into the equations (2.39) and (2.40), yield

$$t_{33} = \left(1 + \eta_1\tau_1\frac{\partial}{\partial t}\right)\left[(a_{12} - a_{13})\frac{\partial^2\psi}{\partial x_1\,\partial x_3} + a_{12}\frac{\partial^2 q}{\partial x_3^2} + a_{13}\frac{\partial^2 q}{\partial x_1^2}\right] - \left(1 + \eta_2\tau_1\frac{\partial}{\partial t}\right)T, \quad (2.57)$$

$$t_{31} = \left(1 + \eta_1\tau_1\frac{\partial}{\partial t}\right)\left[(a_9 + a_{10})\frac{\partial^2 q}{\partial x_1\,\partial x_3} - a_9\frac{\partial^2\psi}{\partial x_3^2} + a_{10}\frac{\partial^2\psi}{\partial x_1^2} - a_{11}\phi_2\right]. \quad (2.58)$$

The angles of the reflected waves must satisfy a specific relationship with the angle of the incident wave in order to meet the boundary condition (2.56) at $x_3 = 0$ as follows:

$$\kappa_0 \sin\theta_0 = \kappa_i \sin\theta_i, \quad (i = 1 \cdots 4) \quad (2.59)$$

Relation (2.59) can be written as

$$\frac{\sin\theta_0}{v_0} = \frac{\sin\theta_i}{v_i}, \qquad (i = 1 \cdots 4) \quad (2.60)$$

where

$$\upsilon_0 = \begin{cases} \upsilon_1, & \text{incident LDW}, \\ \upsilon_2, & \text{incident TW}, \\ \upsilon_3, & \text{incident CD} - \text{IW}, \\ \upsilon_4, & \text{incident CD} - \text{IIW}. \end{cases}$$

Replacing the values of q, T, ψ, ϕ_2 from (2.51) -(2.54) into the equation (2.56), along with equations (2.41), (2.43) and (2.57) -(2.60), determine following system of equations as:

$$\sum_{i=1}^{4} b_{ij} R_j = Y_{i,} \qquad (j = 1 \cdots 4), \tag{2.61}$$

where

$$b_{1p} = \iota\tau_\theta\omega\left[a_{13}\sin^2\theta_p + a_{12}\cos^2\theta_p\right]\kappa_p^2 + \iota\omega\left[\tau_f d_p - \kappa_p z_1 \cos\theta_p\right],$$

$$b_{1q} = -\iota\omega\kappa_q\left[\kappa_q(a_{13} - a_{12})\tau_\theta \sin\theta_q \cos\theta_q + z_1 \sin\theta_q\right],$$

$$b_{2p} = \iota\omega\kappa_p\left[\kappa_p(a_9 + a_{10})\tau_\theta \sin\theta_p \cos\theta_p - z_2 \sin\theta_p\right],$$

$$b_{2q} = \kappa_q^2\iota\tau_\theta\omega\left[-a_9\cos^2\theta_q + a_{10}\sin^2\theta_q\right] + \iota\omega\left[a_{11} f_p \tau_\theta + \kappa_q z_2 \cos\theta_q\right],$$

$$b_{3p} = 0, \qquad b_{3q} = -f_p(a_{14}\iota\kappa_q \cos\theta_q + \omega z_3), \qquad b_{4p} = -d_p\left[\iota\kappa_p \cos\theta_p + \omega z_4\right],$$

$$b_{4q} = 0, \qquad (p = 1,2), (q = 3,4), \tag{2.62}$$

and R_1, R_2, R_3 and R_4 denote the AR of reflected LDW, TW, CD-IW and CD-IIW, each making an angle $\theta_1, \theta_2, \theta_3$, and θ_4 respectively, as depicted in figure 2.1 and these are given as

$$R_1 = \frac{A_1}{B^*}, \qquad R_2 = \frac{A_2}{B^*}, \qquad R_3 = \frac{B_1}{B^*}, \qquad R_4 = \frac{B_2}{B^*}. \tag{2.63}$$

For incident LDW:

$$B^* = A_{01} \text{ and } A_{02} = B_{01} = B_{02} = 0,$$

$$Y_1 = -\iota\omega\tau_\theta[a_{13}\sin^2\theta_0 + a_{12}\cos^2\theta_0]\kappa_0^2 - \iota\omega[\tau_f d_1 + \kappa_0 z_1 \cos\theta_0],$$

$$Y_2 = \iota\omega\kappa_0[\kappa_0(a_9 + a_{10})\tau_\theta \sin\theta_0 \cos\theta_0 + z_2 \sin\theta_0],$$

$$Y_3 = 0,$$

$$Y_4 = -d_1[\iota\kappa_0 \cos\theta_0 - \omega z_4]. \tag{2.64}$$

For incident TW:

$$B^* = A_{02} \text{ and } A_{01} = B_{01} = B_{02} = 0,$$

$$Y_1 = -\iota\omega\tau_\theta[a_{13}\sin^2\theta_0 + a_{12}\cos^2\theta_0]\kappa_0^2 - \iota\omega[\tau_f d_2 + \kappa_0 z_1 \cos\theta_0],$$

$$Y_2 = \iota\omega\kappa_0[\kappa_0(a_9 + a_{10})\tau_\theta \sin\theta_0 \cos\theta_0 + z_2 \sin\theta_0],$$

$$Y_3 = 0,$$

$$Y_4 = -d_2[\iota\kappa_0 \cos\theta_0 - \omega z_4]. \tag{2.65}$$

For incident CD-IW:

$$B^* = B_{01} \text{ and } A_{01} = A_{02} = B_{02} = 0,$$

$$Y_1 = -\iota\omega\kappa_0[\kappa_0(a_{13} - a_{12})\tau_\theta \sin\theta_0 \cos\theta_0 - z_1 \sin\theta_0],$$

$$Y_2 = -\kappa_0^2 \iota\omega\tau_\theta[-a_9\cos^2\theta_0 + a_{10}\sin^2\theta_0] - \iota\omega[a_{11}f_1\tau_\theta - \kappa_0 z_2\cos\theta_0],$$

$$Y_3 = -(a_{14}\iota\kappa_0\cos\theta_0 - \omega z_3)f_1,$$

$$Y_4 = 0. \qquad (2.66)$$

For incident CD-IIW:

$$B^* = B_{02} \text{ and } A_{01} = A_{02} = B_{01} = 0,$$

$$Y_1 = -\iota\omega\kappa_0[\kappa_0(a_{13} - a_{12})\tau_\theta \sin\theta_0 \cos\theta_0 - z_1 \sin\theta_0],$$

$$Y_2 = -\kappa_0^2 \iota\omega\tau_\theta[-a_9\cos^2\theta_0 + a_{10}\sin^2\theta_0] - \iota\omega[a_{11}f_2\tau_\theta - \kappa_0 z_2\cos\theta_0],$$

$$Y_3 = -(a_{14}\iota\kappa_0\cos\theta_0 - \omega z_3)f_2,$$

$$Y_4 = 0. \qquad (2.67)$$

It is noted that the AR, $R_i (i = 1 \cdots 4)$ are influenced by the angle of incidence θ_0 and the material parameters of the MT medium under MG-L theory of thermoelasticity.

2.7 Validations

i) By establishing $\alpha = \beta = \gamma = K = 0$ and $\eta_1 = \eta_2 = \eta_3 = \eta_4 = 1$, the equations (2.49) and (2.50) reduces as

$$(\upsilon^4 + C_1\upsilon^2 + C_2)(q^o, T^o) = 0, \qquad (2.68)$$

$$(\upsilon^2 - C_3)\psi^o = 0, \qquad (2.69)$$

with changed values of

$$C_1 = \frac{\omega^2 - \iota\omega R_1 R_2(1+a_3 a_4)}{\iota\omega R_2}, \qquad C_2 = \frac{-\omega R_1}{\iota R_2}, \qquad C_3 = (1 + \tau_1\iota\omega)a_2,\ S_1 = (1 + \tau_1\iota\omega),$$

$$S_2 = (1 + \tau_0\iota\omega), \quad a_2 = \frac{\mu}{\rho c_1^2}, \quad a_3 = \frac{\gamma_1 T_0}{\rho c_1^2}, \quad a_4 = \frac{\gamma_1 c_1^2}{K^*\omega_1}, \quad a_5 = \frac{\lambda+2\mu}{\gamma_1 T_0}, \quad a_6 = \frac{\lambda}{\gamma_1 T_0}$$

$$a_7 = \frac{\mu}{\gamma_1 T_0}, \qquad \gamma_1 = (3\lambda + 2\mu)\alpha_t, \quad c_1^2 = \frac{\lambda+2\mu}{\rho}.$$

Also, the system of equations (2.61) reduces to

$$\sum_{i=1}^{3} a_{ij}Z_j = Y_{i,} \qquad (j = 1 \cdots 3), \qquad (2.70)$$

where

$$a_{1p} = -S_1\left[a_5\cos^2\theta_p + a_6\sin^2\theta_p\right]\kappa_p^2 + S_1 d_p - \iota\kappa_p\omega z_1\cos\theta_p,$$

$$a_{13} = \kappa_3^2(a_6 - a_5)S_1 \sin\theta_3 \cos\theta_3 + \iota\kappa_3\omega z_1 \sin\theta_3,$$

$$a_{2p} = -2S_1 a_7\kappa_p^2 \sin\theta_p \cos\theta_p + \iota\kappa_p\omega z_2 \sin\theta_p,$$

$$a_{23} = S_1 a_7\kappa_3^2(\cos^2\theta_3 - \sin^2\theta_3) - \iota\kappa_3\omega z_2\cos\theta_3,$$

$$a_{3p} = d_p\left[\iota\kappa_p\cos\theta_p + \omega z_3\right],\ d_p = \frac{\iota\omega a_4 S_2{\kappa_3}^2}{{\kappa_3}^2 + \iota\omega S_2}, \qquad (p = 1,2). \qquad (2.71)$$

The above equations are obtained for MG-L model with impedance boundary and these are consistent with those obtained by Kaushal et al. (2024) [65] (In absence of N-L and TT effects).

ii) In absence of impedance parameters along with the conditions $\eta_1 = \eta_2 = 0,\ \eta_3 = \eta_4 = 1$, the equations (2.49) and (2.50) reduces

$$(\upsilon^4 + W_{01}\upsilon^2 + W_{02})(q^o, T^o) = 0, \tag{2.72}$$

$$(\upsilon^4 + W_{03}\upsilon^2 + W_{04})(\psi^o, \phi_2^o) = 0, \tag{2.73}$$

with changed values of

$$W_{01} = \frac{-(1+\tau_e+a_4a_8\tau_e)}{\tau_e}, \quad W_{02} = \frac{1}{\tau_e}, \quad W_{03} = \frac{a_2a_7-a_3a_6-\omega^2(a_2+a_5)}{\omega^2-a_7}, \quad W_{04} = \frac{a_2a_5\omega^2}{\omega^2-a_7},$$

$$\tau_e = \left(\tau_0 - \frac{\iota}{\omega}\right).$$

Also, the system of equations (2.61) reduces to

$$\sum_{i=1}^{4} b_{ij}R_j = Y_{i,} \qquad (j = 1 \cdots 4), \tag{2.74}$$

where

$$b_{1p} = \left[a_{13}\sin^2\theta_p + a_{12}\cos^2\theta_p\right]\kappa_p^2 + d_p,$$

$$b_{1q} = -\kappa_q^2\left[(a_{13} - a_{12})\sin\theta_q\cos\theta_q\right],$$

$$b_{2p} = \kappa_p^2\left[(a_9 + a_{10})\sin\theta_p\cos\theta_p\right],$$

$$b_{2q} = \kappa_q^2\left[-a_9\cos^2\theta_q + a_{10}\sin^2\theta_q\right] + a_{11}f_p,$$

$$b_{3p} = 0, \quad b_{3q} = -f_pa_{14}\iota\kappa_q\cos\theta_q, \quad b_{4p} = -d_p\iota\kappa_p\cos\theta_p, \quad b_{4q} = 0,$$

$$d_p = \frac{\omega^2-{\kappa_p}^2}{a_4}, \quad f_p = \frac{a_6\kappa_q^2}{a_5\kappa_q^2+a_7-\omega^2}\,(p = 1,2), (q = 3,4). \tag{2.75}$$

The equation (2.75) is obtained for the micropolar generalized thermoelasticity (L-S model) without impedance boundary and these are identical as obtained by Sharma and Marin (2013) [139] (In absence of TT parameter).

iii) By taking $\eta_1 = \eta_4 = 0,\ \eta_2 = \eta_3 = 1$ along with $z_1 = z_2 = z_3 = z_4 = 0$, the equations (2.49) and (2.50) reduces as

$$(\upsilon^4 + L_{01}\upsilon^2 + L_{02})(q^o, T^o) = 0, \tag{2.76}$$

$$(\upsilon^4 + L_{03}\upsilon^2 + L_{04})(\psi^o, \phi_2^o) = 0, \tag{2.77}$$

With changed values of

$$L_{01} = \frac{-(1+\tau_e+a_4a_8\tau_f)}{\tau_e}, \quad L_{02} = \frac{1}{\tau_e}, \quad L_{03} = \frac{a_2a_7-a_3a_6-\omega^2(a_2+a_5)}{\omega^2-a_7}, \quad L_{04} = \frac{a_2a_5\omega^2}{\omega^2-a_7},$$

$$\tau_e = \left(\tau_0 - \frac{\iota}{\omega}\right), \qquad \tau_f = \left(\tau_1 - \frac{\iota}{\omega}\right).$$

Also, the system of equations (2.61) reduces to

$$\sum_{i=1}^{4} b_{ij}R_j = Y_{i,} \qquad (j = 1 \cdots 4), \tag{2.78}$$

where

$$b_{1p} = \left[a_{13}\sin^2\theta_p + a_{12}\cos^2\theta_p\right]\kappa_p^2 + \iota\omega\tau_f d_p,$$

$$b_{1q} = -\kappa_q^2\left[(a_{13} - a_{12})\sin\theta_q \cos\theta_q\right],$$

$$b_{2p} = \kappa_p^2\left[(a_9 + a_{10})\sin\theta_p \cos\theta_p\right],$$

$$b_{2q} = \kappa_q^2\left[-a_9\cos^2\theta_q + a_{10}\sin^2\theta_q\right] + a_{11}f_p,$$

$$b_{3p} = 0, \qquad b_{3q} = -f_p a_{14}\iota\kappa_q \cos\theta_q, \qquad b_{4p} = -d_p\iota\kappa_p \cos\theta_p, \qquad b_{4q} = 0,$$

$$d_p = \frac{\omega^2 - {\kappa_p}^2}{a_4\iota\omega\tau_f}, \quad f_p = \frac{a_6\kappa_q^2}{a_5\kappa_q^2 + a_7 - \omega^2}. \qquad (p = 1,2), (q = 3,4). \qquad (2.79)$$

The results obtained in equation (2.79) are for micropolar generalized thermoelasticity (G-L model) and these results tally with those obtained by Sharma (2013) [136] in a particular case when TT parameter is absent.

2.7.1 Unique Cases

(i) To obtain the corresponding expressions for AR in micropolar MG-L generalized thermoelastic half-space with normal impedance parameter, substitute $z_2 = z_3 = z_4 = 0$ in (2.61).

(ii) The results are inferred for micropolar MG-L generalized thermoelastic half-space with tangential impedance parameter by adopting $z_1 = z_3 = z_4 = 0$ in (2.61).

(iii) By substituting $z_1 = z_2 = z_4 = 0$ in (2.61), the resulting expressions are determined for micropolar MG-L generalized thermoelastic half-space with tangential coupled stress impedance parameter.

(iv) By setting $z_1 = z_2 = z_3 = 0$ in (2.61), the resulting expressions are obtained for micropolar MG-L generalized thermoelastic half- space with thermal conducted impedance parameter.

2.8 Discussion and Numerical Results

To proceed with numerical results and discussions for the micropolar MG-L generalized thermoelastic half-space with impedance parameter, we utilized aluminum-epoxy material with the physical constants given by Gauthier (1982) [47],

$\mu = 1.89 \times 10^{10}\text{Nm}^{-2}$, $\quad K = 0.0149 \times 10^{10}\text{Nm}^{-2}$, $\quad \gamma = 0.268 \times 10^{6}\text{N}$,

$C_e = 2.361 \times 10^{10}\text{m}^2\text{sec}^{-2}\text{K}^{-1}$, $\quad \rho = 2.7 \times 10^{3}\ \text{Kgm}^{-3}$, $\quad T_0 = 298\ \text{K}$,

$\alpha_t = 2.36 \times 10^{-6}\text{K}^{-1}$, $\quad \tau_0 = 0.2\text{sec}$, $\quad \tau_1 = 0.4\text{sec}$, $\quad \lambda = 7.59 \times 10^{10}\text{Nm}^{-2}$,

$\hat{\jmath} = 0.196 \times 10^{4}\text{m}^2$, $\quad K^* = 0.492 \times 10^{2}\text{Nsec}^{-1}\text{K}^{-1}$.

Graphical representations illustrate the AR of reflected waves versus the angle of incidence θ_0 for MT MG-L model, G-L model, and L-S model. This includes scenarios with impedance parameters ($z_1 = 1,\ z_2 = 5,\ z_3 = 2,\ z_4 = 3$) and without impedance parameters ($z_1 =$

$z_2 = z_3 = z_4 = 0$).

The computation for following cases is considered as:

- The micropolar MG-L model with impedance parameters (IMGL) is represented by the solid line (—)
- The micropolar MG-L model without impedance parameters (NIMGL) is represented by the solid line with the center symbol diamond (—◇—).
- The micropolar G-L model with impedance parameters (IGL) is denoted by the large dashed line (− − −).
- The micropolar G-L model without impedance parameters (NIGL) is represented by the large dashed line with a central symbol circle (−o −).
- The micropolar L-S model with impedance parameters (ILS) is denoted by the small dashed line (---).
- The micropolar L-S model without impedance parameters (NILS) is represented by the small dashed line with a triangle symbol at the center (--Δ--).

Figures 2.2-2.5 are for LDW, figures 2.6-2.9 are for TW, figures 2.10-2.13 are for CD-IW and figures 2.14-2.17 are for CD-IIW.

2.8.1 LD-Wave

The variations of $|R_1|$ vs. θ_0 are displayed in figure 2.2. It is evident that the values of $|R_1|$ for L-S and G-L models (with and without impedance) show ascending trend whereas in case of MG-L model opposite behaviour is noticed for $|R_1|$ in presence and absence of impedance parameters.

The variations of $|R_2|$ vs. θ_0 are illustrated in figure 2.3. The magnitude of $|R_2|$ show a declining trend for all the examined cases, however the magnitude of $|R_2|$ for IMGL remain high for entire range except some values of θ_0.

Figure 2.4 depicts the variations of $|R_3|$ vs. θ_0. It is evident that due to impedance parameters the magnitude of $|R_3|$ is higher for all the considered models i.e. for ILS, IGL and IMGL when compared with NILS, NIGL and NIMGL respectively.

Figure 2.5 shows the variations of $|R_4|$ vs. θ_0. The magnitude of $|R_4|$ follow similar trend for all studied cases, however the magnitude of $|R_4|$ for IMGL, IGL and ILS is higher than NIMGL, NIGL and NILS, respectively.

2.8.2 T-Wave

The figure 2.6 demonstrates the variations of $|R_1|$ vs. θ_0. $|R_1|$ follows monotonic ascending trend for NILS and NIGL, whereas steady state behavior is noticed for NIMGL. It is also

noted that in presence of impedance i.e. ILS, IGL and IMGL, $|R_1|$ shows steady state variation with distinct magnitude.

Figure 2.7 depicts the variations of $|R_2|$ vs. θ_0. It is seen that the magnitude of $|R_2|$ exhibits steady state behavior due to presence of impedance parameters, whereas descending trend is noticed in absence of impedance parameters for all considered models, magnitude of $|R_2|$ remain high for MG-L model as compared to other models.

Figure 2.8 depicts the variations of $|R_3|$ vs. θ_0. The magnitude of $|R_3|$ depicts ascending behaviour for NIGL and NILS, attaining maximum value at $\theta_0 = 54^o$ before decreasing in the rest of interval, whereas $|R_3|$ shows increasing trend throughout the interval for all the remaining cases, magnitude $|R_3|$ remains high for G-L model compared to L-S model.

Figure 2.9 displays the variations of $|R_4|$ vs. θ_0. It is seen that the magnitude of $|R_4|$ shows an upward trend for all cases that are being considered, with a significant difference in their magnitude.

2.8.3 CD-I-Wave

Figure 2.10 demonstrates the variations of $|R_1|$ vs. θ_0. The values of $|R_1|$ follow a similar trend for all studied cases however, the magnitude of $|R_1|$ for MG-L model (with and without impedance) remains high when compared to other models, except some values of θ_0.

Figure 2.11 depicts the variations of $|R_2|$ vs. θ_0. In absence of impedance parameters, the magnitude of $|R_2|$ reveals oscillatory behaviour whereas due to impedance boundary, the values of $|R_2|$ exhibit a downward trend for entire range except some values of θ_0.

Figure 2.12 demonstrates the variations of $|R_3|$ vs. θ_0. The magnitude of $|R_3|$ exhibits a decreasing trend for NIMGL, NIGL, NILS, IGL and ILS in the interval $0^o \leq \theta_0 \leq 83^o$ and increases in left over the interval. However, the values of $|R_3|$ for IMGL exhibit an oscillatory trend, indicating the effects of impedance parameters.

Figure 2.13 depicts the variations of $|R_4|$ vs. θ_0. It is evident that $|R_4|$ decreases monotonically and reaches a minimum value at $\theta_0 = 74^o$. When $\theta_0 > 74^o$, $|R_4|$ exhibits ascending behaviour for all studied models in absence of impedance parameters and oscillating trend is noticed in presence of impedance parameters.

2.8.4 CD-II-Wave

Figure 2.14 is plot of $|R_1|$ vs. θ_0. It is seen that the magnitude of $|R_1|$ follows oscillatory trend for all the examined cases but magnitude of $|R_1|$ remain high for IMGL.

Figure 2.15 reveals the variations of $|R_2|$ vs. θ_0. Impedance parameters increase the magnitude of $|R_2|$ near and far away from boundary, except for some values of θ_0 whereas

in absence of impedance, $|R_2|$ follow oscillatory behavior for all the studied models but magnitude of $|R_2|$ remain higher for G-L model.

Figure 2.16 displays the variations of $|R_3|$ vs. θ_0. It is noticed that the magnitude of $|R_3|$ decrease abruptly for IGL, ILS, NIGL and NILS whereas $|R_3|$ shows oscillating behavior with decreasing magnitude for IMGL in entire range. It is also noted that the values of $|R_3|$ increase monotonically in the range $0^o \leq \theta_0 \leq 45^o$ and decrease in the remaining interval in the case of NIMGL.

The variations of $|R_4|$ vs. θ_0 are illustrated in figure 2.17. It is seen that the values of $|R_4|$ for IMGL and NIMGL (in the interval $0^o \leq \theta_0 \leq 18^o$), IGL and NIGL, ILS and NILS respectively (in the interval $0^o \leq \theta_0 \leq 24^o$), show opposite trend whereas similar behavior is noticed in the rest of the interval.

2.9 Conclusion

This chapter presents a formulation for a MT medium using the MG-L theory of generalised thermoelasticity. In order to simplify two-dimensional problem, potential functions and dimensionless quantities are implemented. The impedance boundary restrictions are employed to investigate the reflection of plane waves in an assumed model. In the model under consideration, the plane wave (LDW or TW or CD-IW or CD-IIW) is incident, resulting in four reflected waves (LDW, TW, CD-IW, and CD-IIW). The AR of these reflected waves are determined in accordance with the impedance boundary restrictions. The AR of various reflected waves are numerically calculated and graphically presented for generalized thermoelasticity theories, including MG-L, G-L, and L-S. The influence of impedance characteristics is examined, and the following conclusions are derived from the numerical results:

i. The AR of reflected LDW, CD-IW and CD-IIW across the MG-L, L-S and G-L theories of thermoelasticity are intensified by impedance parameters when LDW is incident. At the same time, the AR of the reflected TW for NILS and NIGL are higher than those observed for ILS and IGL, respectively.
ii. It has been observed that the magnitude of AR for all reflected waves is increased due to the presence of impedance parameters in the MG-L theory of thermoelasticity when a TW is incident. Conversely, the L-S and G-L theories of thermoelasticity exhibit a comparable pattern, albeit with significant variations in the magnitude of AR.
iii. The AR exhibit consistent behavior across the L-S and G-L theories of thermoelasticity when a CD-IW or CD-IIW is incident, with significant differences in their magnitudes under both the cases (with and without impedance parameters).

However, the MG-L theory of thermoelasticity exhibits oscillatory behavior. Thus, the study provides critical insights into the impact of impedance parameters on the AR during wave propagation and underscores the significance of impedance and thermal relaxation effects in the design of materials for aerospace, defense and engineering applications. By employing dimensionless analysis, potential functions and harmonic solutions, the structure facilitates analytical tractability while preserving physical realism. The developed model not only generalizes existing theories but also establishes a robust foundation for future research involving N-L effects, anisotropic media and layered structure.

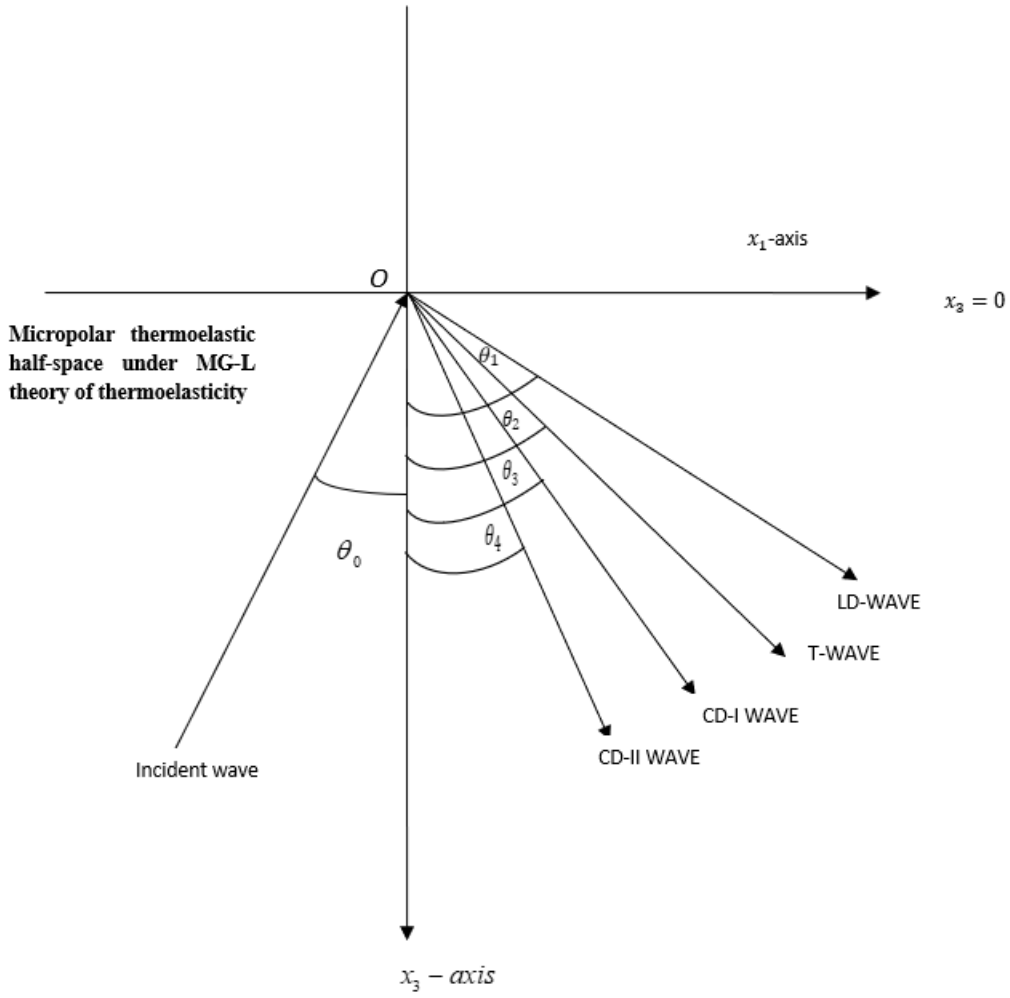

Fig. 2.1: Geometry of the problem

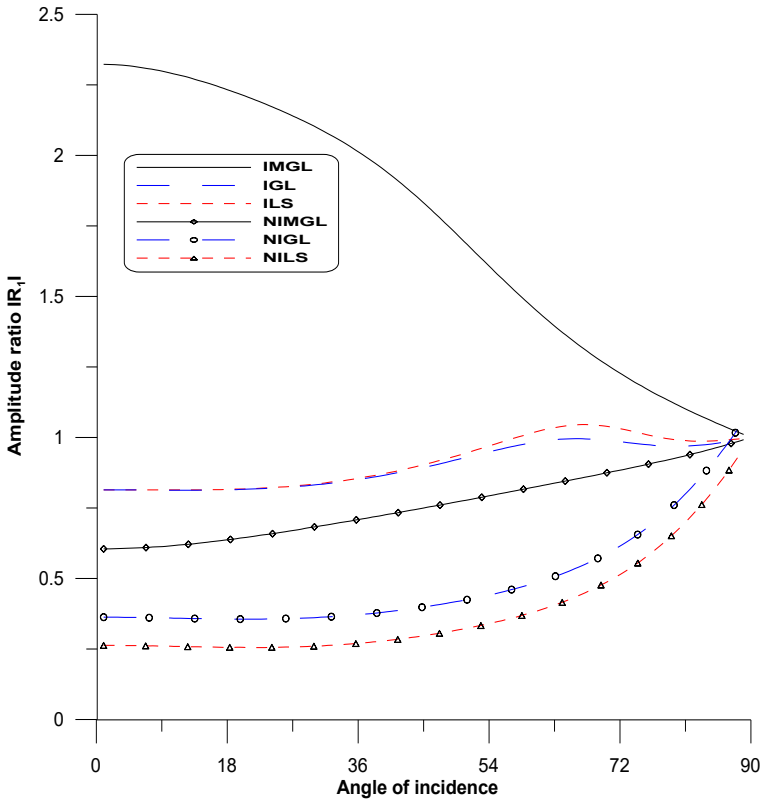

Fig. 2.2: $|R_1|$ vs. θ_0 (LD-wave)

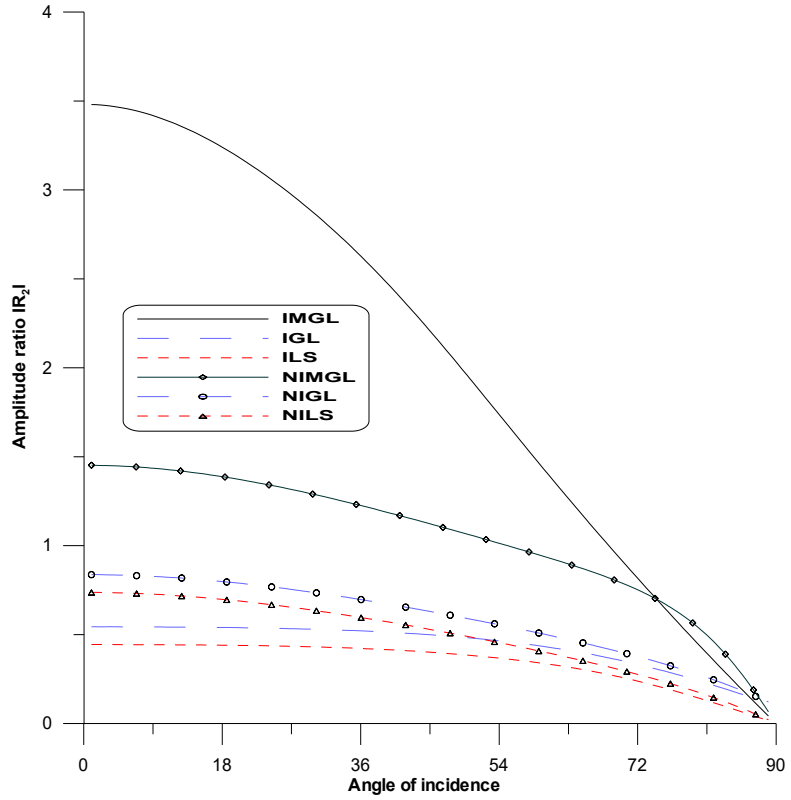

Fig. 2.3: $|R_2|$ vs. θ_0 (LD-wave)

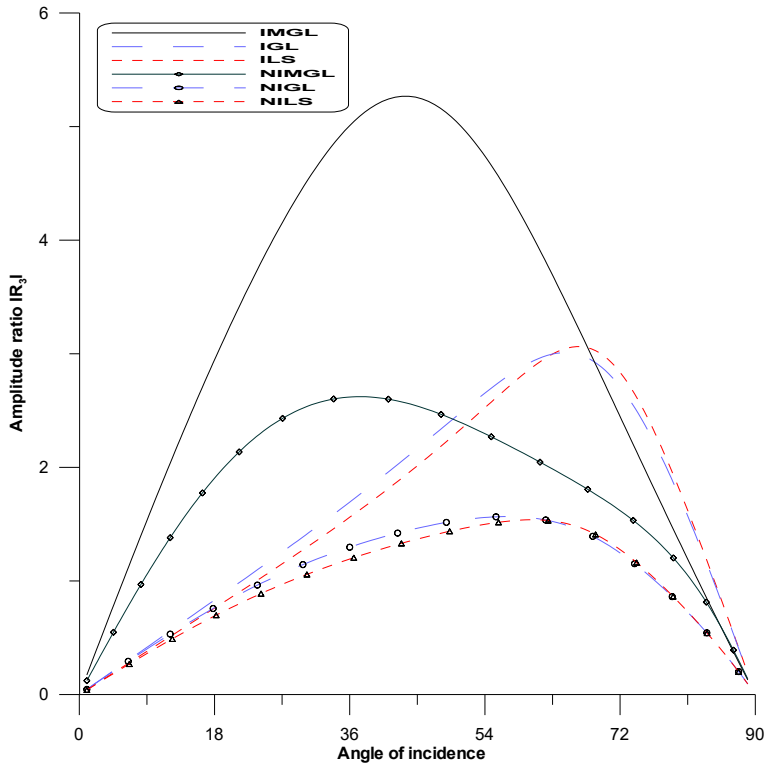

Fig. 2.4: $|R_3|$ vs. θ_0 (LD-wave)

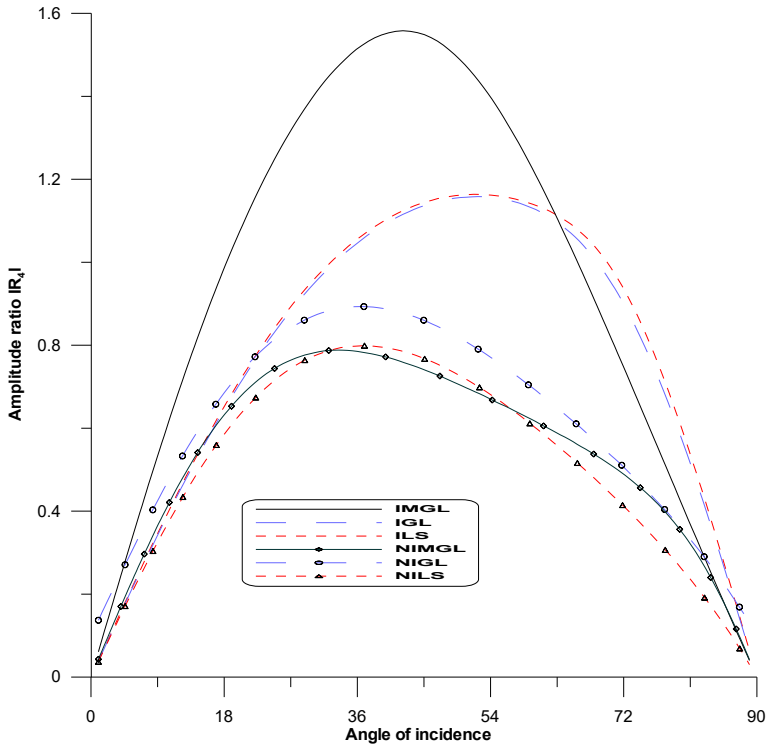

Fig. 2.5: $|R_4|$ vs. θ_0 (LD-wave)

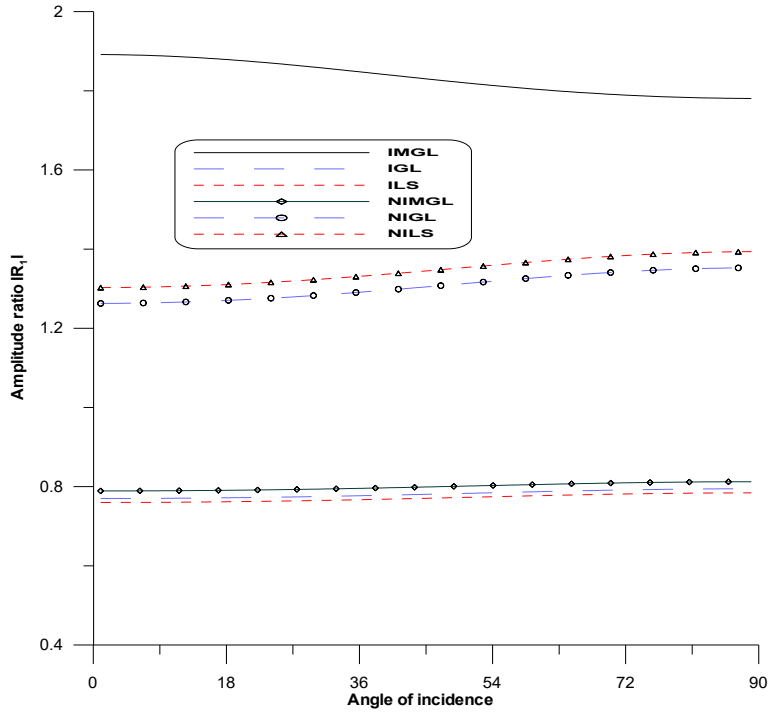

Fig. 2.6: $|R_1|$ vs. θ_0
(T-wave)

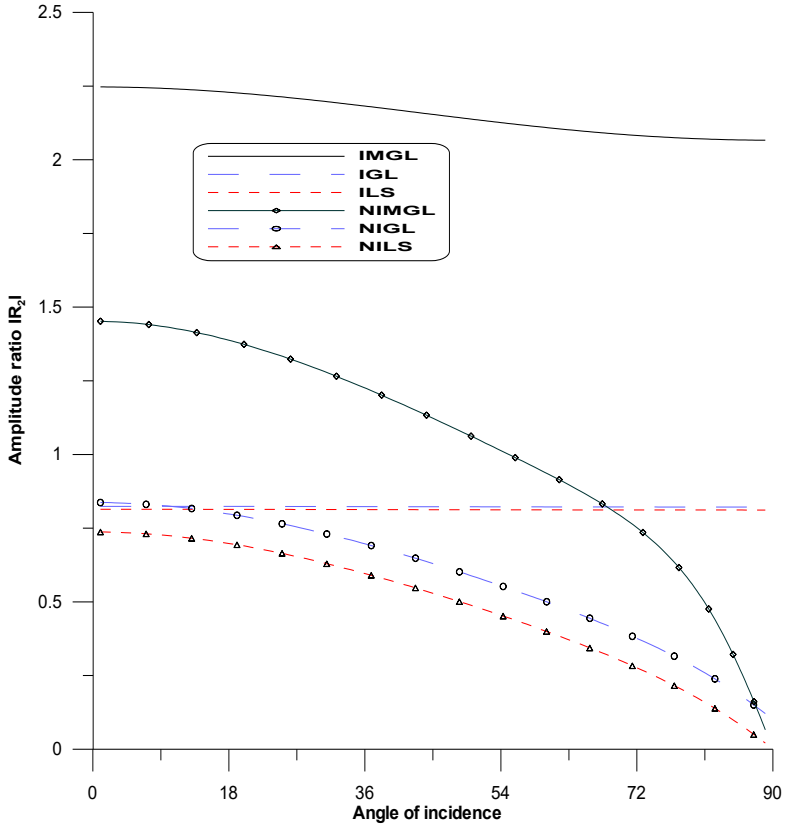

Fig. 2.7: $|R_2|$ vs. θ_0
(T-wave)

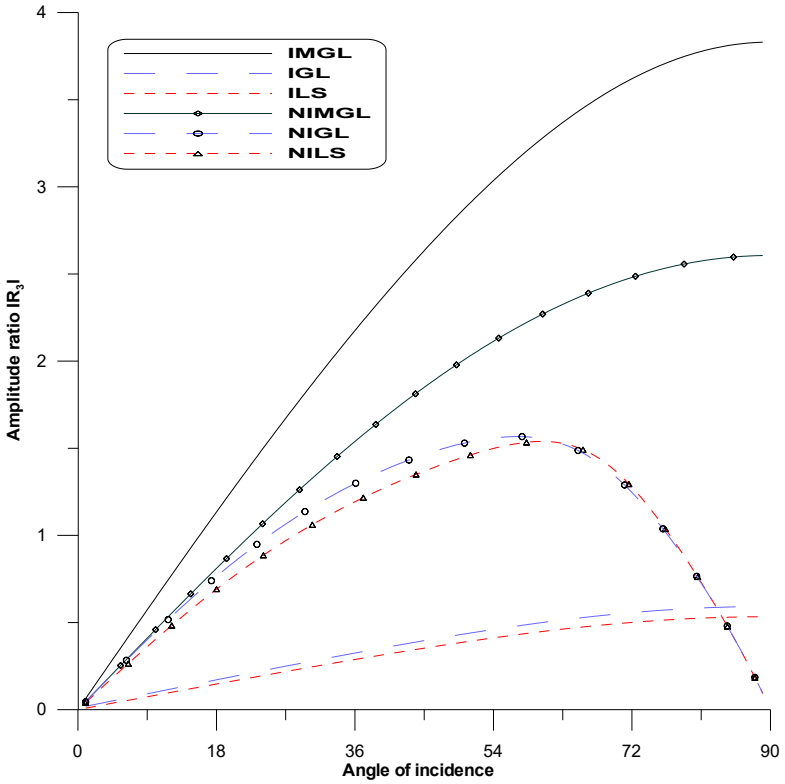

Fig. 2.8: $|R_3|$ vs. θ_0
(T-wave)

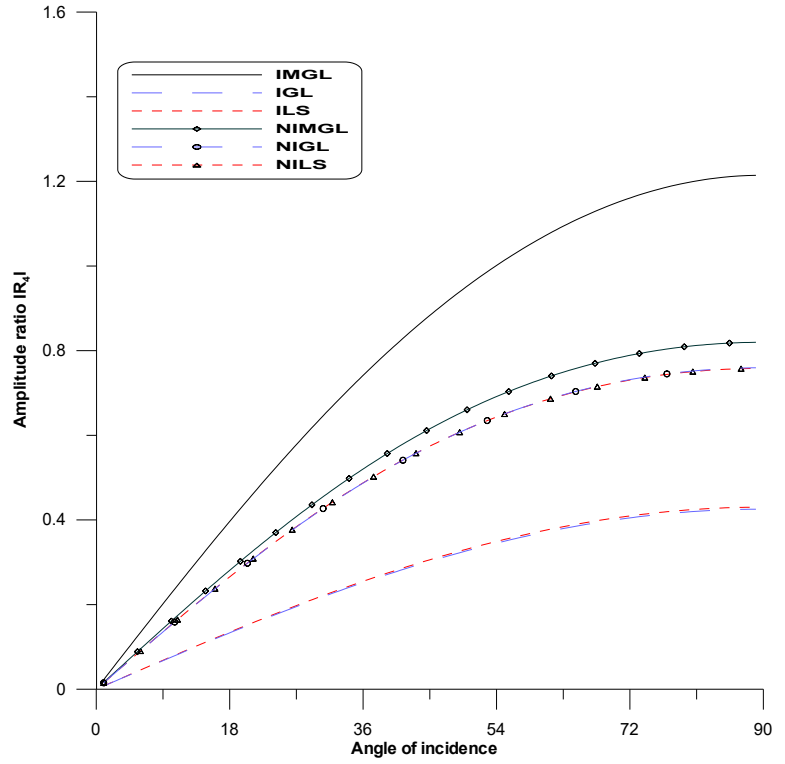

Fig. 2.9: $|R_4|$ vs. θ_0
(T-wave)

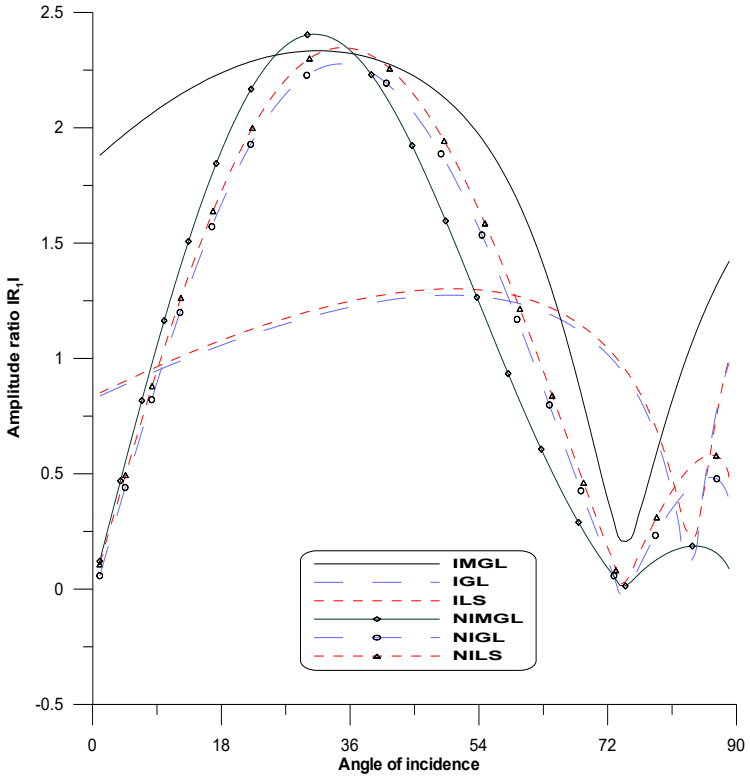

Fig. 2.10: $|R_1|$ vs. θ_0
(CD-I wave)

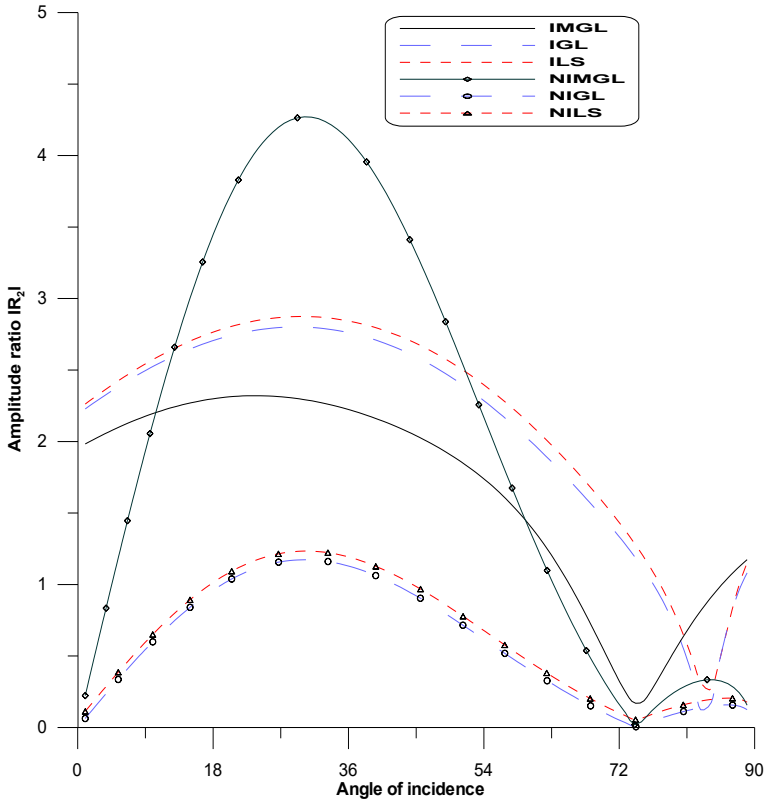

Fig. 2.11: $|R_2|$ vs. θ_0
(CD-I wave)

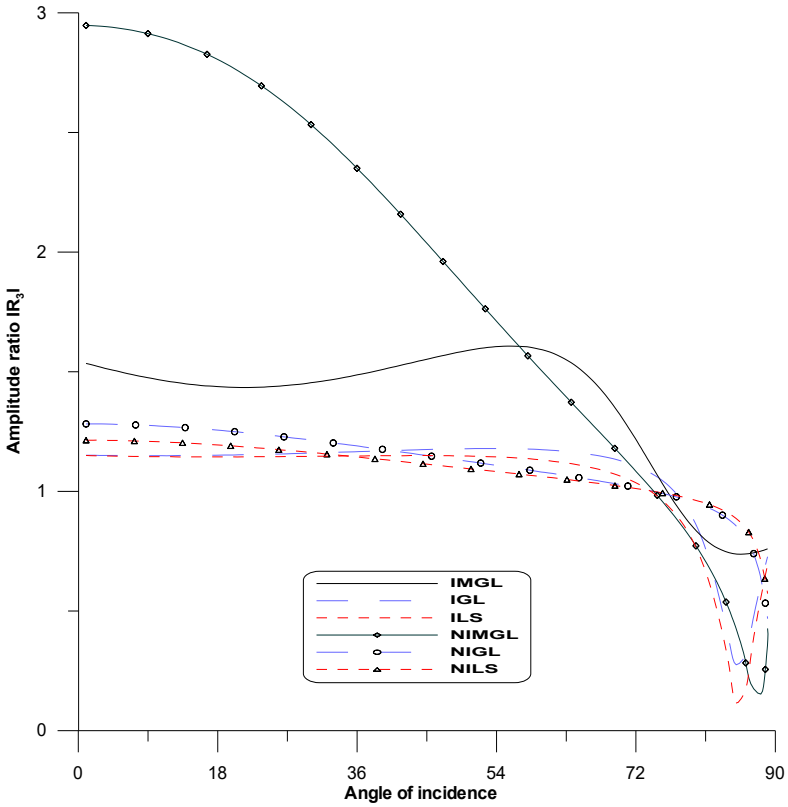

Fig. 2.12: $|R_3|$ vs. θ_0
(CD-I wave)

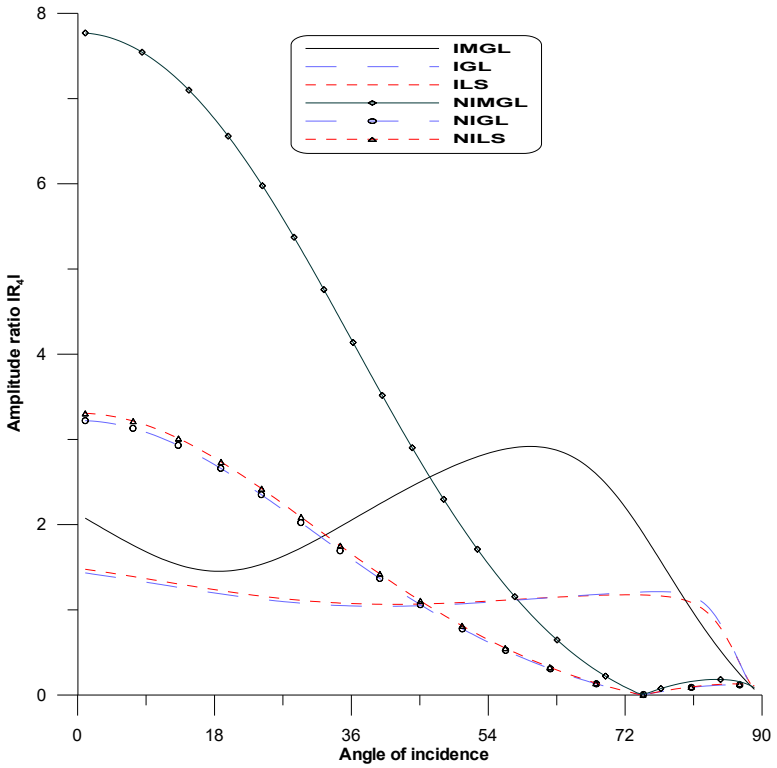

Fig. 2.13: $|R_4|$ vs. θ_0
(CD-I wave)

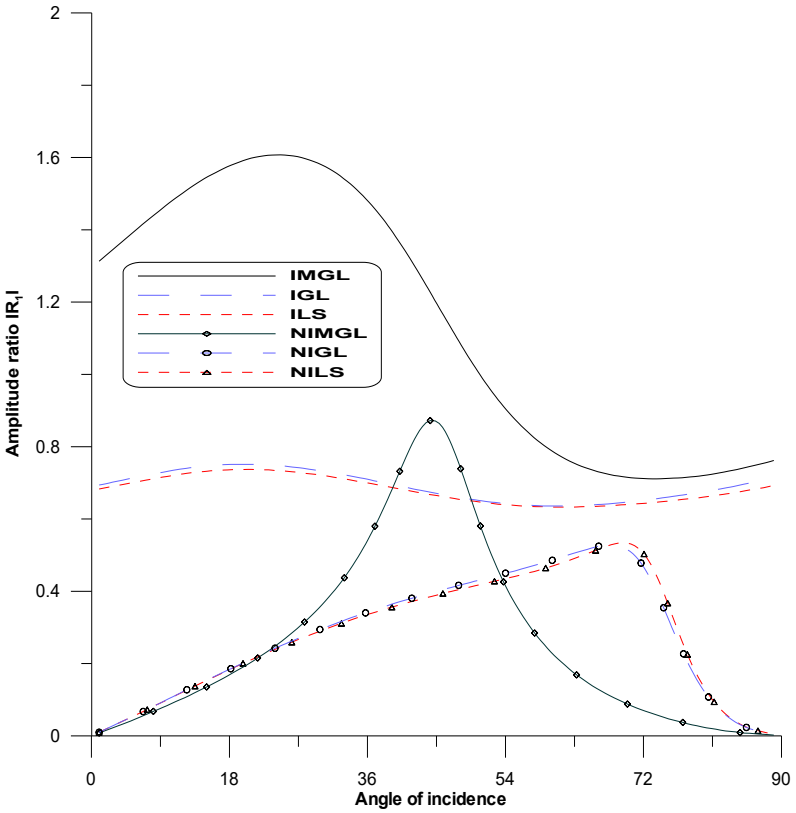

Fig. 2.14: $|R_1|$ vs. θ_0
(CD-II wave)

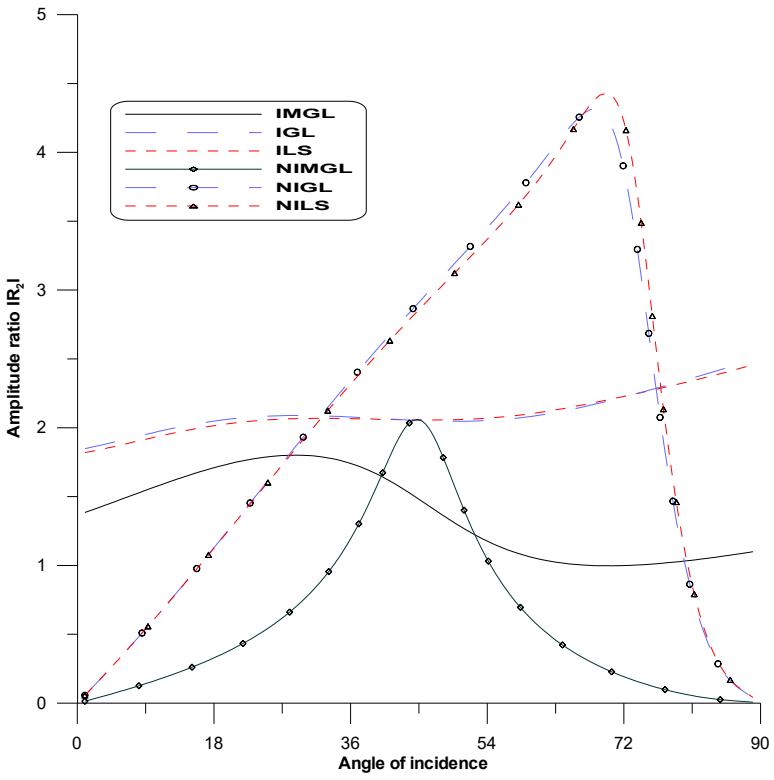

Fig. 2.15: $|R_2|$ vs. θ_0
(CD-II wave)

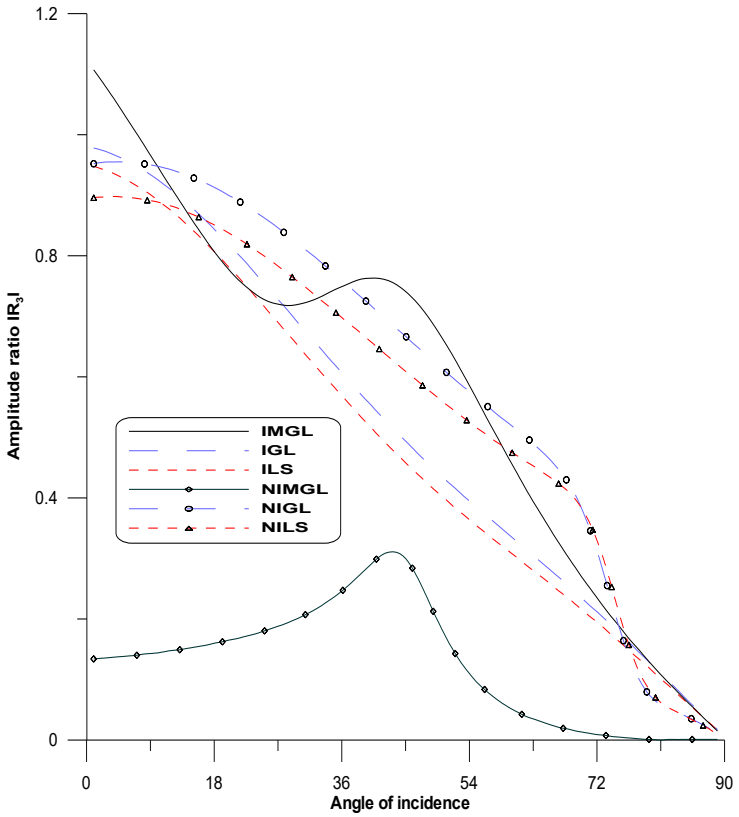

Fig. 2.16: $|R_3|$ vs. θ_0
(CD-II wave)

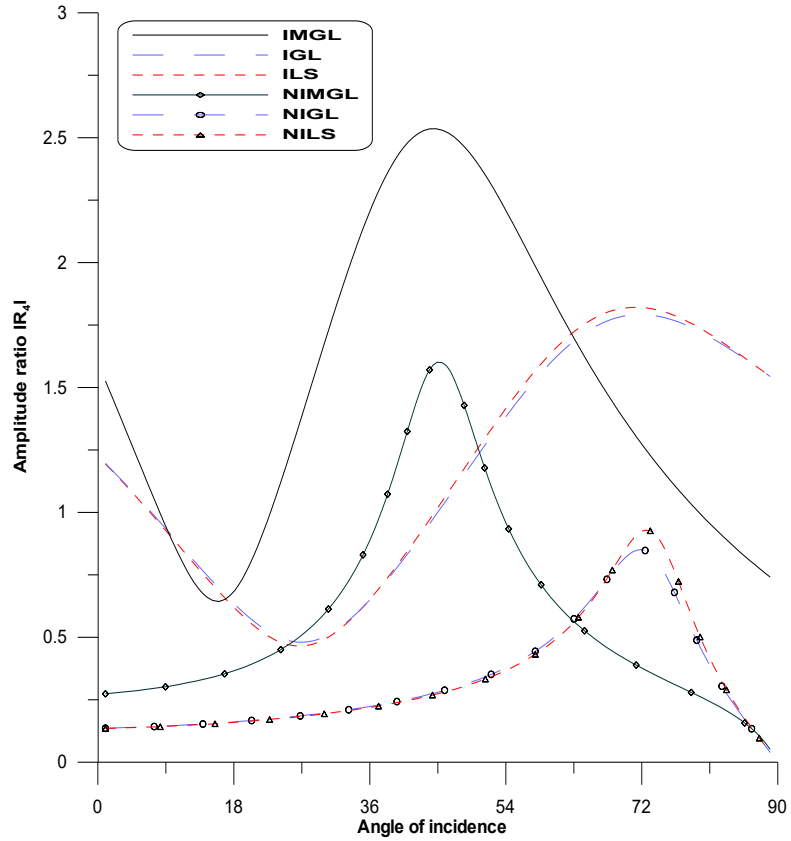

Fig. 2.17: $|R_4|$ vs. θ_0
(CD-II wave)

Chapter 3

Propagation of plane waves in a micropolar thermoelastic medium based on the Moore-Gibson-Thompson heat equation, including non-local effects and hyperbolic two-temperature effects

The work from this chapter has been published in the form of research paper entitled "Analysis of Wave Motion in Micropolar Thermoelastic Medium Based on Moore–Gibson–Thompson Heat Equation Under Non-local and Hyperbolic Two-Temperature", International Journal of Applied and Computational Mathematics, 10(50), 2024, https://doi.org/10.1007/s40819-023-01667-4.

Indexing: Scopus, SJR:0.377

Chapter 3

Propagation of plane waves in a micropolar thermoelastic medium based on the Moore-Gibson-Thompson heat equation, including non-local effects and hyperbolic two-temperature effects

3.1 Introduction

Sharma (2013) [136] studied how two temperature (TT) parameter effects the reflection coefficients of various reflected waves in a micropolar thermoelastic (MT) semi-space. Sharma et al. (2014) [147] investigated the propagation of waves in an electro-microstretch elastic solid. Kaushal et al. (2021) [64] explored the influence of impedance parameters, diffusion and relaxation time on the amplitude ratios (AR) of reflected waves in a thermoelastic medium.

Das et al. (2023) [27] studied the reflection problem at an insulated, isothermal and stress-free plane boundary and explored the influence of non-local (N-L) parameters on reflection coefficients and energy ratios of various reflected waves within the framework of the Moore-Gibson-Thompson (MGT) theory of thermoelasticity. Kumar et al. (2023) [88] investigated the fundamental solution and plane wave propagation in photothermoelastic under the MGT heat equation. They also calculated attenuation coefficient and phase velocity of plane waves using various thermoelastic theories.

Deswal et al. (2024) [29] investigated how micropolarity, N-L parameters, and temperature affected the energy ratios and AR of reflected plane waves. Kumar et al. (2024) [70] calculated the phase speed, energy ratios, and reflection/transmission coefficients of various reflected and transmitted waves at the interface of two distinct N-L triclinic MT semi-spaces to study the effects of N-L and micropolar parameters on the resulting quantities. Said (2024) [129] studied the effect of viscosity and gravitational field on different reflected waves in a MT media.

This chapter presents a novel mathematical formulation for analyzing wave propagation in micropolar thermoelastic media by incorporating the MGT heat conduction equation together with hyperbolic two-temperature (HTT) and N-L effects. After being converted to a two-dimensional case, the governing equations are rendered dimensionless, and potential functions are implemented to facilitate additional simplification. In order to solve the problem, a reflection technique is implemented. Four types of reflected waves are identified when a plane wave (longitudinal displacement wave (LDW) or coupled transverse wave (CD-IW)) is incident on the surface $x_3 = 0$, namely LDW, thermal wave (TW), CD-IW, and

coupled microrotational wave (CD-IIW). The impedance boundary restrictions are employed to calculate the AR of these reflected waves. The effects of N-L, HTT, TT, and impedance factors on these AR are graphically represented. Some special cases are also covered.

This study is motivated by the increasing need to better understand how waves propagate through complex materials with microstructures, where traditional theories cannot fully explain micro-rotational effects. It is especially important for modern technologies like microscale thermal sensors, where having accurate models is essential for improving design and performance. The novelty of this work is embodied in its integration of the MGT thermoelasticity theory with N-L and HTT parameters within a micropolar continuum framework. This unified model enables a rigorous evaluation of how N-L effects, HTT behavior, and impedance boundary conditions influence AR of various reflected waves. By bridging microstructural mechanics and advanced thermal modeling, the study offers a more comprehensive and realistic approach to wave analysis in next-generation engineered materials.

3.2 Fundamental Equations

Eringen (1966) [36], Youssef and El-Bary (2018) [168], and Quintanilla (2019) [121] provide the field equations and constitutive relations for MT medium under the MGT heat equation, encompassing N-L effects and HTT, after eliminating body couples, heat sources, and body forces as

$$(\lambda+\mu)\nabla(\nabla.\mathbf{u})+(\mu+K)\Delta\mathbf{u}+K(\nabla\times\boldsymbol{\phi})-\gamma_1\nabla T=\rho\left(1-{\xi_1}^2\Delta\right)\frac{\partial^2\mathbf{u}}{\partial t^2}, \tag{3.1}$$

$$(\alpha+\beta)\nabla(\nabla.\boldsymbol{\phi})+\gamma\Delta\boldsymbol{\phi}+K(\nabla\times\mathbf{u})-2K\boldsymbol{\phi}=\rho\hat{\jmath}\left(1-{\xi_2}^2\Delta\right)\frac{\partial^2\boldsymbol{\phi}}{\partial t^2}, \tag{3.2}$$

$$\left(1+\tau_0\frac{\partial}{\partial t}\right)\left[\rho C_e\frac{\partial^2 T}{\partial t^2}+\gamma_1 T_0\frac{\partial^2}{\partial t^2}(\nabla.\mathbf{u})\right]=K^*\frac{\partial}{\partial t}\Delta\varphi+K_1^*\Delta\varphi, \tag{3.3}$$

$$t_{pq}=\lambda u_{h,h}\delta_{pq}+\mu\left(u_{p,q}+u_{q,p}\right)+K\left(u_{q,p}-\varepsilon_{pqh}\phi_h\right)-\gamma_1 T\delta_{pq}, \tag{3.4}$$

$$m_{pq}=\alpha\phi_{h,h}\delta_{pq}+\beta\phi_{p,q}+\gamma\phi_{q,p}, \tag{3.5}$$

$$\ddot{T}=\ddot{\varphi}-\beta^*\Delta\varphi, \qquad (p,q,h=1-3), \tag{3.6}$$

where φ - conductive temperature, β^* - HTT parameter, $K_1^*=\frac{(\lambda+2\mu)C_e}{4}$ - rate of the thermal conductivity, ξ_1 and ξ_2 -non-local parameters and other symbols $\mathbf{u}, \boldsymbol{\phi}, T, \lambda, \mu, K, \hat{\jmath}, K^*, \beta, C_e$, $\gamma_1, t, t_{pq}, m_{pq}, \tau_0, \alpha, \gamma, T_0, \delta_{pq}, \rho, \varepsilon_{pqh}, \Delta, \nabla$ are as defined in section 2.2 [Chapter 2].

Following cases arises:

(i) For Lord-Shulman (L-S) theory (1967) [98]: $K_1^*=0$,

(ii) For Coupled theory of thermoelasticity (1980) [30]: $K_1^*=\tau_0=0$,

(iii) For Green-Naghdi–II (GN-II) theory (1993) [52]: $K^*=\tau_0=0$,

(iv) For Green-Naghdi–III (GN-III) theory (1992) [51]: $\tau_0 = 0$.

Equations (3.1) -(3.6) in components form for Cartesian coordinates (x_1, x_2, x_3) are written as

$$(\lambda+\mu)\frac{\partial}{\partial x_1}\left(\frac{\partial u_1}{\partial x_1}+\frac{\partial u_2}{\partial x_2}+\frac{\partial u_3}{\partial x_3}\right)+(\mu+K)\Delta u_1+K\left(\frac{\partial \phi_3}{\partial x_2}-\frac{\partial \phi_2}{\partial x_3}\right)-\gamma_1\frac{\partial T}{\partial x_1} = \rho\left(1-{\xi_1}^2\Delta\right)\frac{\partial^2 u_1}{\partial t^2}, \tag{3.7}$$

$$(\lambda+\mu)\frac{\partial}{\partial x_2}\left(\frac{\partial u_1}{\partial x_1}+\frac{\partial u_2}{\partial x_2}+\frac{\partial u_3}{\partial x_3}\right)+(\mu+K)\Delta u_2+K\left(\frac{\partial \phi_1}{\partial x_3}-\frac{\partial \phi_3}{\partial x_1}\right)-\gamma_1\frac{\partial T}{\partial x_2} = \rho\left(1-{\xi_1}^2\Delta\right)\frac{\partial^2 u_2}{\partial t^2}, \tag{3.8}$$

$$(\lambda+\mu)\frac{\partial}{\partial x_3}\left(\frac{\partial u_1}{\partial x_1}+\frac{\partial u_2}{\partial x_2}+\frac{\partial u_3}{\partial x_3}\right)+(\mu+K)\Delta u_3+K\left(\frac{\partial \phi_2}{\partial x_1}-\frac{\partial \phi_1}{\partial x_2}\right)-\gamma_1\frac{\partial T}{\partial x_3} = \rho\left(1-{\xi_1}^2\Delta\right)\frac{\partial^2 u_3}{\partial t^2}, \tag{3.9}$$

$$(\alpha+\beta)\frac{\partial}{\partial x_1}\left(\frac{\partial \phi_1}{\partial x_1}+\frac{\partial \phi_2}{\partial x_2}+\frac{\partial \phi_3}{\partial x_3}\right)+\gamma\Delta\phi_1+K\left(\left(\frac{\partial u_3}{\partial x_2}-\frac{\partial u_2}{\partial x_3}\right)-2\phi_1\right) = \rho\hat{j}\left(1-{\xi_2}^2\Delta\right)\frac{\partial^2 \phi_1}{\partial t^2}, \tag{3.10}$$

$$(\alpha+\beta)\frac{\partial}{\partial x_2}\left(\frac{\partial \phi_1}{\partial x_1}+\frac{\partial \phi_2}{\partial x_2}+\frac{\partial \phi_3}{\partial x_3}\right)+\gamma\Delta\phi_2+K\left(\left(\frac{\partial u_1}{\partial x_3}-\frac{\partial u_3}{\partial x_1}\right)-2\phi_2\right) = \rho\hat{j}\left(1-{\xi_2}^2\Delta\right)\frac{\partial^2 \phi_2}{\partial t^2}, \tag{3.11}$$

$$(\alpha+\beta)\frac{\partial}{\partial x_3}\left(\frac{\partial \phi_1}{\partial x_1}+\frac{\partial \phi_2}{\partial x_2}+\frac{\partial \phi_3}{\partial x_3}\right)+\gamma\Delta\phi_3+K\left(\left(\frac{\partial u_2}{\partial x_1}-\frac{\partial u_1}{\partial x_2}\right)-2\phi_3\right) = \rho\hat{j}\left(1-{\xi_2}^2\Delta\right)\frac{\partial^2 \phi_3}{\partial t^2}, \tag{3.12}$$

$$\left(1+\tau_0\frac{\partial}{\partial t}\right)\left[\rho C_e\frac{\partial^2 T}{\partial t^2}+\gamma_1 T_0\frac{\partial^2}{\partial t^2}\left(\frac{\partial u_1}{\partial x_1}+\frac{\partial u_2}{\partial x_2}+\frac{\partial u_3}{\partial x_3}\right)\right] = K^*\frac{\partial}{\partial t}\Delta\varphi+K_1^*\Delta\varphi, \tag{3.13}$$

$$t_{11} = \lambda\left(\frac{\partial u_1}{\partial x_1}+\frac{\partial u_2}{\partial x_2}+\frac{\partial u_3}{\partial x_3}\right)+(2\mu+K)\frac{\partial u_1}{\partial x_1}-\gamma_1 T, \tag{3.14}$$

$$t_{22} = \lambda\left(\frac{\partial u_1}{\partial x_1}+\frac{\partial u_2}{\partial x_2}+\frac{\partial u_3}{\partial x_3}\right)+(2\mu+K)\frac{\partial u_2}{\partial x_2}-\gamma_1 T, \tag{3.15}$$

$$t_{33} = \lambda\left(\frac{\partial u_1}{\partial x_1}+\frac{\partial u_2}{\partial x_2}+\frac{\partial u_3}{\partial x_3}\right)+(2\mu+K)\frac{\partial u_3}{\partial x_3}-\gamma_1 T, \tag{3.16}$$

$$t_{31} = \mu\left(\frac{\partial u_3}{\partial x_1}+\frac{\partial u_1}{\partial x_3}\right)+K\left(\frac{\partial u_1}{\partial x_3}-\phi_2\right), \tag{3.17}$$

$$t_{32} = \mu\left(\frac{\partial u_3}{\partial x_2}+\frac{\partial u_2}{\partial x_3}\right)+K\left(\frac{\partial u_2}{\partial x_3}+\phi_1\right), \tag{3.18}$$

$$t_{21} = \mu\left(\frac{\partial u_2}{\partial x_1}+\frac{\partial u_1}{\partial x_2}\right)+K\left(\frac{\partial u_1}{\partial x_2}+\phi_3\right), \tag{3.19}$$

$$\ddot{T} = \ddot{\varphi}-\beta^*\Delta\varphi, \tag{3.20}$$

and the values of m_{11}, m_{22}, m_{33} m_{31}, m_{32} and m_{12} are as given by equations (2.19) -(2.24) in section 2.2 [Chapter 2]. Additionally, the value of Δ is as described in section 2.2 [Chapter 2].

3.3 Problem Formulation

We are examining a MT half-space that is homogeneous and isotropic, governed by the MGT heat equation, and subjected to impedance boundary conditions. This half-space also includes N-L and HTT effects. We consider a rectangular Cartesian coordinate system (x_1, x_2, x_3), with the origin positioned at the plane boundary $x_3 = 0$. The x_3 -axis extends vertically downward into the medium, while the x_1 – axis runs horizontally. The x_2-axis is aligned with the direction of the line where the plane wave front intersects the plane surface. The field variables are contingent upon x_1, x_3, and t, if we confine our analysis to a plane strain problem in $x_1 - x_3$ plane.

In the case of a two-dimensional problem, we consider the following:

$$\mathbf{u} = (u_1(x_1, x_3, t), 0, u_3(x_1, x_3, t)), \qquad \boldsymbol{\phi} = (0, \phi_2(x_1, x_3, t), 0), \qquad T = T(x_1, x_3, t),$$
$$\varphi = \varphi(x_1, x_3, t), \tag{3.21}$$

Using equation (3.21) in (3.7) -(3.13), (3.16), (3.17), (2.23) and (3.20), yield

$$(\lambda + \mu)\frac{\partial}{\partial x_1}\left(\frac{\partial u_1}{\partial x_1} + \frac{\partial u_3}{\partial x_3}\right) + (\mu + K)\Delta u_1 - K\frac{\partial \phi_2}{\partial x_3} - \gamma_1 \frac{\partial T}{\partial x_1} = \rho\left(1 - {\xi_1}^2 \Delta\right)\frac{\partial^2 u_1}{\partial t^2}, \tag{3.22}$$

$$(\lambda + \mu)\frac{\partial}{\partial x_3}\left(\frac{\partial u_1}{\partial x_1} + \frac{\partial u_3}{\partial x_3}\right) + (\mu + K)\Delta u_3 + K\frac{\partial \phi_2}{\partial x_1} - \gamma_1 \frac{\partial T}{\partial x_3} = \rho\left(1 - {\xi_1}^2 \Delta\right)\frac{\partial^2 u_3}{\partial t^2}, \tag{3.23}$$

$$\gamma\Delta\phi_2 + K\left(\left(\frac{\partial u_1}{\partial x_3} - \frac{\partial u_3}{\partial x_1}\right) + 2\phi_2\right) = \rho\hat{j}\left(1 - {\xi_2}^2 \Delta\right)\frac{\partial^2 \phi_2}{\partial t^2}, \tag{3.24}$$

$$\left(1 + \tau_0 \frac{\partial}{\partial t}\right)\left[\rho C_e \frac{\partial^2 T}{\partial t^2} + \gamma_1 T_0 \frac{\partial^2}{\partial t^2}\left(\frac{\partial u_1}{\partial x_1} + \frac{\partial u_3}{\partial x_3}\right)\right] = K^* \frac{\partial}{\partial t}\Delta\varphi + K_1^* \Delta\varphi, \tag{3.25}$$

$$t_{33} = \lambda\left(\frac{\partial u_1}{\partial x_1} + \frac{\partial u_3}{\partial x_3}\right) + (2\mu + K)\frac{\partial u_3}{\partial x_3} - \gamma_1 T, \tag{3.26}$$

$$t_{31} = \mu\left(\frac{\partial u_3}{\partial x_1} + \frac{\partial u_1}{\partial x_3}\right) + K\frac{\partial u_1}{\partial x_3} - K\phi_2, \tag{3.27}$$

$$m_{32} = \gamma\frac{\partial \phi_2}{\partial x_3}, \tag{3.28}$$

$$\ddot{T} = \ddot{\varphi} - \beta^*\Delta\varphi, \tag{3.29}$$

where the value of Δ is as defined in section 2.3 [Chapter 2].

To simplify further, we consider the dimensionless quantities as follows:

$$(x_i', u_i') = \frac{\omega_1}{c_1}(x_i, u_i), \quad t_{3i}' = \frac{1}{\gamma_1 T_0} t_{3i}, \qquad (T', \varphi') = \frac{1}{T_0}(T, \varphi), \quad \phi_2' = \frac{\rho c_1^2}{\gamma_1 T_0}\phi_2,$$

$$m_{32}' = \frac{\omega_1}{\gamma_1 c_1 T_0} m_{32}, \qquad (t', \tau_0') = \omega_1(t, \tau_0), \qquad (z_1', z_2') = \frac{c_1}{\gamma_1 T_0}(z_1, z_2), \qquad z_3' = \frac{{\omega_1}^2}{\rho {c_1}^3} z_3,$$

$$z_4' = \frac{c_1}{K^*} z_4, \ (\xi_1', \xi_2') = \frac{\omega_1}{c_1}(\xi_1, \xi_2), \quad \beta^{*\prime} = \frac{1}{c_1^2}\beta^*, \qquad \omega' = \frac{\omega}{\omega_1}, \quad (i = 1,3), \tag{3.30}$$

where

$$c_1^2 = \frac{\lambda+2\mu+K}{\rho} \text{ and } \omega_1 = \frac{\rho C_e c_1^2}{K^*}. \tag{3.31}$$

Using (3.30) in (3.22) -(3.29) after suppressing the primes, yield

$$a_1 \frac{\partial}{\partial x_1}\left(\frac{\partial u_1}{\partial x_1} + \frac{\partial u_3}{\partial x_3}\right) + a_2 \Delta u_1 - a_3 \frac{\partial \phi_2}{\partial x_3} - a_4 \frac{\partial T}{\partial x_1} = \left(1 - {\xi_1}^2 \Delta\right) \frac{\partial^2 u_1}{\partial t^2}, \tag{3.32}$$

$$a_1 \frac{\partial}{\partial x_3}\left(\frac{\partial u_1}{\partial x_1} + \frac{\partial u_3}{\partial x_3}\right) + a_2 \Delta u_3 + a_3 \frac{\partial \phi_2}{\partial x_1} - a_4 \frac{\partial T}{\partial x_3} = \left(1 - {\xi_1}^2 \Delta\right) \frac{\partial^2 u_3}{\partial t^2}, \tag{3.33}$$

$$a_5 \Delta \phi_2 + a_6 \left(\frac{\partial u_1}{\partial x_3} - \frac{\partial u_3}{\partial x_1}\right) - a_7 \phi_2 = \left(1 - {\xi_2}^2 \Delta\right) \frac{\partial^2 \phi_2}{\partial t^2}, \tag{3.34}$$

$$\frac{\partial}{\partial t} \Delta \varphi + a_8 \Delta \varphi = \left(1 + \tau_0 \frac{\partial}{\partial t}\right) \left[\frac{\partial^2 T}{\partial t^2} + a_9 \frac{\partial^2}{\partial t^2}\left(\frac{\partial u_1}{\partial x_1} + \frac{\partial u_3}{\partial x_3}\right)\right], \tag{3.35}$$

$$t_{33} = a_{13} \frac{\partial u_1}{\partial x_1} + a_{14} \frac{\partial u_3}{\partial x_3} - T, \tag{3.36}$$

$$t_{31} = a_{10} \left(\frac{\partial u_3}{\partial x_1} + \frac{\partial u_1}{\partial x_3}\right) + a_{11} \frac{\partial u_1}{\partial x_3} - a_{12} \phi_2, \tag{3.37}$$

$$m_{32} = a_{15} \frac{\partial \phi_2}{\partial x_3}, \tag{3.38}$$

$$\ddot{T} = \ddot{\varphi} - \beta^* \Delta \varphi, \tag{3.39}$$

where a_i $(i = 1 \cdots 7)$ are as given by equation (2.42) [Chapter 2] and

$$a_8 = \frac{K_1^*}{\omega_1 K^*}, \quad a_9 = \frac{\gamma_1 c_1^2}{\omega_1 K^*}, \quad a_{10} = \frac{\mu}{\gamma_1 T_0}, \quad a_{11} = \frac{\mu+K}{\gamma_1 T_0}, \quad a_{12} = \frac{K}{\rho c_1^2},$$

$$a_{13} = \frac{\lambda}{\gamma_1 T_0}, \quad a_{14} = \frac{(\lambda+2\mu+K)}{\gamma_1 T_0}, \quad a_{15} = \frac{\gamma \omega_1^2}{\rho c_1^4}. \tag{3.40}$$

3.4 Solution Procedure

Relation between displacement components and scalar potentials is as given by equation (2.43) [Chapter 2].

Using equation (2.43) in equations (3.32) -(3.35), yield

$$\Delta q - a_4 T = \left(1 - {\xi_1}^2 \Delta\right) \frac{\partial^2 q}{\partial t^2}, \tag{3.41}$$

$$a_2 \Delta \psi + a_3 \phi_2 = \left(1 - {\xi_1}^2 \Delta\right) \frac{\partial^2 \psi}{\partial t^2}, \tag{3.42}$$

$$a_5 \Delta \phi_2 - a_6 \Delta \psi - a_7 \phi_2 = \left(1 - {\xi_2}^2 \Delta\right) \frac{\partial^2 \phi_2}{\partial t^2}, \tag{3.43}$$

$$\frac{\partial}{\partial t} \Delta \varphi + a_8 \Delta \varphi = \left(1 + \tau_0 \frac{\partial}{\partial t}\right) \left(\frac{\partial^2 T}{\partial t^2} + a_9 \frac{\partial^2}{\partial t^2} \Delta q\right). \tag{3.44}$$

To solve the system of equations (3.41) - (3.44), we approach the solution as follows:

$$(q, T, \varphi, \psi, \phi_2) = (\bar{q}, \bar{T}, \bar{\varphi}, \bar{\psi}, \bar{\phi}_2) e^{\iota\kappa(x_1 \sin\theta_0 - x_3 \cos\theta_0 + \nu t)}, \tag{3.45}$$

where ω, ι, θ_0, ν, and κ are as defined in section 2.4 [Chapter 2] and quantities such as $\bar{q}, \bar{T}, \bar{\varphi}, \bar{\psi}$ and $\bar{\phi}_2$ are constants representing the wave amplitudes.

Substituting the value of T from equation (3.45) in (3.39), (after removing the bars) yields

$$T = \varphi + \varsigma\Delta\varphi, \tag{3.46}$$

where

$$\varsigma = \begin{cases} \frac{\beta^*}{\omega^2}, \text{for (HTT)} \\ a, \text{for (TT)} \\ 0, \text{for one temperature (1T).} \end{cases}$$

Using the equation (3.46) in equations (3.41) and (3.44), yield

$$\Delta q - a_4(1 + \varsigma\Delta)\varphi = \left(1 - {\xi_1}^2\Delta\right)\frac{\partial^2 q}{\partial t^2}, \tag{3.47}$$

$$\frac{\partial}{\partial t}\Delta\varphi + a_8\Delta\varphi = \left(1 + \tau_0\frac{\partial}{\partial t}\right)\left[\frac{\partial^2}{\partial t^2}(1 + \varsigma\Delta)\varphi + a_9\frac{\partial^2}{\partial t^2}\Delta q\right], \tag{3.48}$$

The following equations are obtained by simplifying and inserting the values of q, φ, ψ and ϕ_2 from the equation (3.45) into equations (3.47), (3.48), (3.42), and (3.43)

$$(\upsilon^4 + G_{01}\upsilon^2 + G_{02})(\bar{q}, \bar{\varphi}) = 0, \tag{3.49}$$

$$(\upsilon^4 + G_{03}\upsilon^2 + G_{04})(\bar{\psi}, \bar{\phi}_2) = 0, \tag{3.50}$$

where

$$G_{01} = \frac{-\left((\iota\omega + a_8) + \iota\omega\tau_e\left(1 - {\xi_1}^2\omega^2 + a_4a_9 + \omega^2\varsigma\right)\right)}{\iota\omega\tau_e}, \qquad G_{02} = \frac{(\iota\omega + a_8)(1 - {\xi_1}^2\omega^2) + \iota\tau_e\omega^3\varsigma\left(1 - {\xi_1}^2\omega^2 + a_4a_9\right)}{\iota\omega\tau_e},$$

$$G_{03} = \frac{\omega^2\left(a_2 + a_5 + a_7{\xi_1}^2 - \omega^2\left({\xi_1}^2 + {\xi_2}^2\right)\right) - a_2a_7 + a_3a_6}{a_7 - \omega^2}, \quad G_{04} = \frac{\omega^4\left(a_5{\xi_1}^2 - \omega^2{\xi_1}^2{\xi_2}^2 + a_2{\xi_2}^2\right) - \omega^2(a_2a_5)}{a_7 - \omega^2},$$

$$\tau_e = \left(\tau_0 - \frac{\iota}{\omega}\right).$$

Let $\upsilon_i (i = 1,2)$ designate the roots of the characteristic equation $(\upsilon^4 + G_{01}\upsilon^2 + G_{02}) = 0$, which correspond to the velocities of the LDW and TW in decreasing order. In the same way, the roots of the characteristic equation $(\upsilon^4 + G_{03}\upsilon^2 + G_{04}) = 0$ are represented by υ_j (j = 3, 4) and correspond to velocities of CD-IW and CD-IIW in decreasing order.

3.5 Wave Reflection Phenomenon

Consider a plane harmonic wave (LDW or CD-IW) that forms an angle θ_0 with normal to the surface at $x_3 = 0$, as illustrated in figure 3.1. When any incident wave (LDW or CD-IW) hits at the boundary $x_3 = 0$, four types of reflected waves are generated in the medium namely LDW, TW, CD-IW, and CD-IIW. These reflected waves make angles $\theta_1, \theta_2, \theta_3$, and θ_4 with the positive x_3-axis. The wave field for the half-space, encompassing both incident and reflected waves, can be expressed as:

$$q = \sum_{i=1}^{2}\left[E_{0i}e^{\iota\kappa_0(x_1\sin\theta_0 - x_3\cos\theta_0) + \iota\omega t} + E_ie^{\iota\kappa_i(x_3\cos\theta_i + x_1\sin\theta_i) + \iota\omega t}\right], \tag{3.51}$$

$$\varphi = \sum_{i=1}^{2}\left[r_i\left(E_{0i}e^{\iota\kappa_0(x_1\sin\theta_0 - x_3\cos\theta_0) + \iota\omega t} + E_ie^{\iota\kappa_i(x_3\cos\theta_i + x_1\sin\theta_i) + \iota\omega t}\right)\right], \tag{3.52}$$

$$\psi = \sum_{i=1}^{2}\left[F_{0i}e^{\iota\kappa_0(x_1\sin\theta_0 - x_3\cos\theta_0) + \iota\omega t} + F_ie^{\iota\kappa_j(x_3\cos\theta_j + x_1\sin\theta_j) + \iota\omega t}\right], \tag{3.53}$$

$$\phi_2 = \sum_{i=1}^{2}\left[s_i\left(F_{0i}e^{\iota\kappa_0(x_1\sin\theta_0 - x_3\cos\theta_0)+\iota\omega t} + F_i e^{\iota\kappa_j(x_3\cos\theta_j + x_1\sin\theta_j)+\iota\omega t}\right)\right], \qquad (3.54)$$

where r_i and s_i are coupling constants, defined as

$$r_i = \frac{\left[\omega^2\left(1+{\xi_1}^2{\kappa_i}^2\right)-{\kappa_i}^2\right]}{a_4\left(1-\varsigma{\kappa_i}^2\right)}, \quad s_i = \frac{a_2\kappa_j^2-\omega^2\left(1+{\xi_1}^2{\kappa_j}^2\right)}{a_3}, (i = 1,2), (j = 3,4),$$

and $E_{0i}(i = 1,2)$ denote the amplitudes of incident LDW and TW, respectively. $F_{0i}(i = 1,2)$ represent the amplitudes of incident CD-IW and CD-IIW. $E_i(i = 1,2)$ denote the amplitudes of the reflected LDW and TW whereas $F_i(i = 1,2)$ corresponds to the amplitudes of the reflected CD-IW and CD-IIW respectively.

3.6 Boundary Conditions

Following Tiersten (1969) [162] and Malischewsky (1987) [99], the appropriate impedance boundary restrictions at $x_3 = 0$ are

$$\text{(i) } t_{33} + \omega z_1 u_3 = 0, \qquad \text{(ii) } t_{31} + \omega z_2 u_1 = 0,$$

$$\text{(iii) } m_{32} + \omega z_3 \phi_2 = 0, \qquad \text{(iv) } K^* \frac{\partial\varphi}{\partial x_3} + \omega z_4 \varphi = 0, \qquad (3.55)$$

where z_1, z_2 are impedance parameters with dimension N sec m^{-3}. z_3 and z_4 are impedance parameters have dimensions N sec m^{-1} and N $m^{-1}K^{-1}$ respectively. Taking $z_1 = z_2 = z_3 = z_4 = 0$ yields stress free boundary conditions.

Using non-dimensional quantities given by (3.30) on equation (3.55), yield

$$\text{(i) } t_{33} + \omega z_1 u_3 = 0, \qquad \text{(ii) } t_{31} + \omega z_2 u_1 = 0,$$

$$\text{(iii) } m_{32} + \omega z_3 \phi_2 = 0, \qquad \text{(iv) } \frac{\partial\varphi}{\partial x_3} + \omega z_4 \varphi = 0, \qquad (3.56)$$

Using equation (2.43) in equations (3.36), (3.37) and with the aid of equation (3.46), yield

$$t_{33} = a_{13}\left[\frac{\partial^2 q}{\partial x_1^2} - \frac{\partial^2\psi}{\partial x_1\,\partial x_3}\right] + a_{14}\left[\frac{\partial^2\psi}{\partial x_1\,\partial x_3} + \frac{\partial^2 q}{\partial x_3^2}\right] - (1+\varsigma\Delta)\varphi, \qquad (3.57)$$

$$t_{31} = (2a_{10}+a_{11})\left(\frac{\partial^2 q}{\partial x_1\,\partial x_3}\right) - (a_{10}+a_{11})\frac{\partial^2\psi}{\partial x_3^2} + a_{10}\frac{\partial^2\psi}{\partial x_1^2} - a_{12}\phi_2. \qquad (3.58)$$

To meet the boundary condition (3.56) at $x_3 = 0$, the angles of the reflected waves must follow a precise connection with the angle of the incident wave as

$$\kappa_0 \sin\theta_0 = \kappa_1 \sin\theta_i, \qquad (i = 1\cdots 4) \qquad (3.59)$$

Relation (3.59) can be written as

$$\frac{\sin\theta_0}{\upsilon_0} = \frac{\sin\theta_i}{\upsilon_i}, \qquad (i = 1\cdots 4) \qquad (3.60)$$

where

$$\upsilon_0 = \begin{cases} \upsilon_1, & \text{incident LDW} \\ \upsilon_2, & \text{incident TW} \\ \upsilon_3, & \text{incident CD}-\text{IW} \\ \upsilon_4, & \text{incident CD}-\text{IIW}. \end{cases}$$

By inserting the values of q, φ, ψ, ϕ_2 from equations (3.51) -(3.54) into the boundary condition (3.56) with the assistance of equations (2.43), (3.38) and (3.57) -(3.60), we derive the following system of equations:

$$\sum_{i=1}^{4} c_{ij} R_j = X_{i,} \qquad (j = 1 \cdots 4), \tag{3.61}$$

where

$$\begin{aligned}
&c_{1p} = \left[a_{13}\sin^2\theta_p + a_{14}\cos^2\theta_p\right]\kappa_p^2 + \left(1 - \varsigma\kappa_p^2\right)r_p - \kappa_p z_1 \iota\omega\cos\theta_p,\\
&c_{1q} = \left[\kappa_q^2(a_{14} - a_{13})\cos\theta_q - \kappa_q z_1 \iota\omega\right]\sin\theta_q,\\
&c_{2p} = \kappa_p^2 \sin\theta_p \cos\theta_p (2a_{10} + a_{11}) - \kappa_p z_2 \iota\omega \sin\theta_p,\\
&c_{2q} = -\kappa_q^2\left[(a_{10} + a_{11})\cos^2\theta_q - a_{10}\sin^2\theta_q\right] + a_{12}s_p + \kappa_q z_2 \iota\omega\cos\theta_q,\\
&c_{3p} = 0, \quad c_{3q} = -(a_{15}\iota\kappa_q \cos\theta_p + \omega z_3)s_p,\\
&c_{4p} = -r_p\left[\iota\kappa_p \cos\theta_p + \omega z_4\right],\\
&c_{4q} = 0, \qquad (p = 1,2), (q = 3,4),
\end{aligned} \tag{3.62}$$

and, the AR of reflected waves, denoted as $R_j (j = 1 \cdots 4)$ are given by:

$$R_1 = \frac{E_1}{A^*}, \quad R_2 = \frac{E_2}{A^*}, \quad R_3 = \frac{F_1}{A^*}, \quad R_4 = \frac{F_2}{A^*}. \tag{3.63}$$

For incident LDW, $A^* = E_{01}$ and $E_{02} = F_{01} = F_{02} = 0$,

$$\begin{aligned}
&X_1 = -[a_{13}\sin^2\theta_0 + a_{14}\cos^2\theta_0]\kappa_0^2 - (1 - \varsigma\kappa_0^2)r_1 - \kappa_0 z_1 \iota\omega\cos\theta_0,\\
&X_2 = \kappa_0^2 \sin\theta_0 \cos\theta_0 (2a_{10} + a_{11}) + \kappa_0 z_2 \iota\omega \sin\theta_0,\\
&X_3 = 0,\\
&X_4 = -r_1[\iota\kappa_0 \cos\theta_0 - \omega z_4].
\end{aligned} \tag{3.64}$$

For incident CD-IW, $A^* = F_{01}$ and $E_{01} = E_{02} = F_{02} = 0$,

$$\begin{aligned}
&X_1 = [\kappa_0^2(a_{14} - a_{13})\cos\theta_0 + \kappa_0 z_1 \iota\omega]\sin\theta_0,\\
&X_2 = \kappa_0^2[(a_{10} + a_{11})\cos^2\theta_0 - a_{10}\sin^2\theta_0] - a_{12}s_1 + \kappa_0 z_2 \iota\omega\cos\theta_0,\\
&X_3 = -(a_{15}\iota\kappa_0 \cos\theta_0 - \omega z_3)s_1,\\
&X_4 = 0.
\end{aligned} \tag{3.65}$$

3.7 Validations

i) By considering $\xi_1 = 0, \xi_2 = 0, \tau_0 = 0$ and $\varsigma = 0$ along with $z_1 = z_2 = z_3 = z_4 = 0$, equations (3.49) and (3.50) reduces as

$$(\upsilon^4 + G_{01}\upsilon^2 + G_{02})(\bar{q}, \bar{T}) = 0, \tag{3.66}$$

$$(\upsilon^4 + G_{03}\upsilon^2 + G_{04})(\bar{\psi}, \bar{\phi}_2) = 0, \tag{3.67}$$

with changed values of

$$G_{01} = -(\iota\omega + a_8 + 1 + a_4 a_9) \qquad G_{02} = (\iota\omega + a_8), \qquad G_{03} = \frac{a_2 a_7 - a_3 a_6 - \omega^2(a_2 + a_5)}{\omega^2 - a_7},$$

$$G_{04} = \frac{\omega^2(a_2 a_5)}{\omega^2 - a_7}.$$

Also, equation (3.61) reduces as

$$\sum_{i=1}^{4} c_{ij}R_j = X_{i,} \qquad (j = 1 \cdots 4), \tag{3.68}$$

where

$$c_{1p} = \left[a_{13}\sin^2\theta_p + a_{14}\cos^2\theta_p\right]\kappa_p^2 + r_p,$$
$$c_{1q} = \kappa_q^2(a_{14} - a_{13})\cos\theta_q \sin\theta_q,$$
$$c_{2p} = \kappa_p^2 \sin\theta_p \cos\theta_p (2a_{10} + a_{11}),$$
$$c_{2q} = -\kappa_q^2\left[(a_{10} + a_{11})\cos^2\theta_q - a_{10}\sin^2\theta_q\right] + a_{12}s_p,$$
$$c_{3p} = 0, \quad c_{3q} = -\iota\kappa_q\, a_{15}\cos\theta_p s_p$$
$$c_{4p} = -\iota\kappa_p r_p \cos\theta_p, \quad c_{4q} = 0,$$
$$r_p = \frac{(\omega^2 - \kappa_p{}^2)}{a_4}, \quad s_p = \frac{a_2\kappa_q^2 - \omega^2}{a_3}, (p = 1,2), (q = 3,4). \tag{3.69}$$

In equation (3.69), we obtained resulting expressions for MT with energy dissipation (GN-III model) and these are consistent with those obtained by Kumar et al. (2014) [85] for the particular case.

ii) By taking $K_1^* = 0$ along with absence of N-L, HTT and impedance parameters, the equations (3.49) and (3.50) reduces as

$$(\upsilon^4 + G_{01}\upsilon^2 + G_{02})(\bar{q}, \bar{T}) = 0, \tag{3.70}$$

$$(\upsilon^4 + G_{03}\upsilon^2 + G_{04})(\bar{\psi}, \bar{\phi}_2) = 0, \tag{3.71}$$

with changed values of

$$G_{01} = -\frac{(1+\tau_e(1+a_4a_8))}{\tau_e} \qquad G_{02} = \frac{1}{\tau_e}, \qquad G_{03} = \frac{\omega^2(a_2+a_5) - a_2a_7 + a_3a_6}{a_7 - \omega^2},$$

$$G_{04} = \frac{-\omega^2 a_2 a_5}{a_7 - \omega^2}, \quad \tau_e = \left(\tau_0 - \frac{\iota}{\omega}\right), \quad a_8 = \frac{\gamma_1 c_1^2}{\omega_1 K^*}, \qquad a_9 = \frac{\mu}{\gamma_1 T_0}, \qquad a_{10} = \frac{\mu+K}{\gamma_1 T_0},$$

$$a_{11} = \frac{K}{\rho c_1^2}, \qquad a_{12} = \frac{\lambda}{\gamma_1 T_0}, \qquad a_{13} = \frac{(\lambda+2\mu+K)}{\gamma_1 T_0}, \qquad a_{14} = \frac{\gamma\omega_1^2}{\rho c_1^4}.$$

Also, equation (3.61) reduces as

$$\sum_{i=1}^{4} c_{ij}R_j = X_{i,} \qquad (j = 1 \cdots 4), \tag{3.72}$$

where

$$c_{1p} = \left[a_{12}\sin^2\theta_p + a_{13}\cos^2\theta_p\right]\kappa_p^2 + r_p,$$
$$c_{1q} = \kappa_q^2(a_{13} - a_{12})\cos\theta_q \sin\theta_q,$$
$$c_{2p} = \kappa_p^2 \sin\theta_p \cos\theta_p (2a_9 + a_{10}),$$
$$c_{2q} = -\kappa_q^2\left[(a_9 + a_{10})\cos^2\theta_q - a_9\sin^2\theta_q\right] + a_{11}s_p,$$
$$c_{3p} = 0, \quad c_{3q} = -\iota\kappa_q\, a_{14}\cos\theta_p s_p$$
$$c_{4p} = -\iota\kappa_p r_p \cos\theta_p, \quad c_{4q} = 0,$$
$$r_p = \frac{[\omega^2 - \kappa_p{}^2]}{a_4}, \quad s_p = \frac{a_2\kappa_q^2 - \omega^2}{a_3}, (p = 1,2), (q = 3,4). \tag{3.73}$$

In equation (3.73), we obtained resulting expressions for micropolar generalized thermoelasticity (L-S model) and these results tally with those obtained by Yadav (2024) [166] (In absence of diffusion and void parameters).

iii) In absence of N-L and impedance parameters along with $K_1^* = \tau_0 = 0, \varsigma = a$

the equations (3.49) and (3.50) reduces as

$$(\upsilon^4 + G_{01}\upsilon^2 + G_{02})(\bar{q}, \bar{T}) = 0, \tag{3.74}$$

$$(\upsilon^4 + G_{03}\upsilon^2 + G_{04})(\bar{\psi}, \bar{\phi}_2) = 0, \tag{3.75}$$

with changed values of

$$G_{01} = -(\iota\omega + 1 + \omega^2 a + a_4 a_8) \qquad G_{02} = (\iota\omega + \omega^2 a(1 + a_4 a_8)),$$

$$G_{03} = \frac{\omega^2(a_2+a_5)-a_2 a_7+a_3 a_6}{a_7-\omega^2}, \quad G_{04} = \frac{-\omega^2 a_2 a_5}{a_7-\omega^2}, \quad a_8 = \frac{\gamma_1 c_1^2}{\omega_1 K^*}, \; a_9 = \frac{\mu}{\gamma_1 T_0}, \; a_{10} = \frac{\mu+K}{\gamma_1 T_0},$$

$$a_{11} = \frac{K}{\rho c_1^2}, \; a_{12} = \frac{\lambda}{\gamma_1 T_0}, \qquad a_{13} = \frac{(\lambda+2\mu+K)}{\gamma_1 T_0}, \; a_{14} = \frac{\gamma\omega_1^2}{\rho c_1^4}.$$

Also, equation (3.61) reduces as

$$\sum_{i=1}^{4} c_{ij} R_j = X_{i,} \qquad (j = 1 \cdots 4), \tag{3.76}$$

where

$$\begin{aligned}
c_{1p} &= \left[a_{12}\sin^2\theta_p + a_{13}\cos^2\theta_p\right]\kappa_p^2 + (1 - a\kappa_p^2) r_p, \\
c_{1q} &= \kappa_q^2(a_{13} - a_{12})\cos\theta_q \sin\theta_q, \\
c_{2p} &= \kappa_p^2 \sin\theta_p \cos\theta_p (2a_9 + a_{10}), \\
c_{2q} &= -\kappa_q^2\left[(a_9 + a_{10})\cos^2\theta_q - a_9\sin^2\theta_q\right] + a_{11} s_p, \\
c_{3p} &= 0, \quad c_{3q} = -\iota\kappa_q\, a_{14}\cos\theta_p s_p \\
c_{4p} &= -\iota\kappa_p r_p \cos\theta_p, \quad c_{4q} = 0, \\
r_p &= \frac{(\omega^2 - {\kappa_p}^2)}{(1-a\kappa_p^2)a_4}, \quad s_p = \frac{a_2\kappa_q^2 - \omega^2}{a_3}, (p = 1,2), (q = 3,4).
\end{aligned} \tag{3.77}$$

In equation (3.77), we obtained resulting expressions for micropolar thermoelasticity with TT and these results tally with those obtained by Kumar et al. (2014) [85] in the particular case.

3.7.1 Particular Cases

(i) Substituting $\alpha = \beta = \gamma = K = 0$ into equation (3.61), reduce the results for MGT thermoelastic half-space with N-L, HTT parameters with impedance boundary.

(ii) Taking $K_1^* = 0$ and $\tau_0 = 0$ into equation (3.61), reduce the results for micropolar thermoelasticity with N-L and HTT effects under impedance boundary.

3.8 Discussion and Numerical Results

Numerical calculations are implemented for different cases in order to examine the impact of numerous parameters: (i) N-L parameters ξ_1 and ξ_2 (ii) impedance parameters, HTT and TT parameters for the AR in the MT medium under the MGT theory of thermoelasticity.

Using a material like Magnesium crystal for numerical results and discussions, the values of the micropolar constants are as follows (Eringen (1984) [42]):

$\mu = 4 \times 10^{10}\ \mathrm{Nm^{-2}}$, $\rho = 1.74 \times 10^{3}\ \mathrm{Kgm^{-3}}$, $\gamma = 0.779 \times 10^{-9}\mathrm{N}$,

$\lambda = 9.4 \times 10^{10}\ \mathrm{Nm^{-2}}$, $K = 1.0 \times 10^{10}\mathrm{Nm^{-2}}$, $\hat{\jmath} = 0.2 \times 10^{-19}\mathrm{m^2}$,

Thermal parameters according to Dhaliwal and Singh (1980) [30]:

$K^* = 1.7 \times 10^{2}\ \mathrm{Nsec^{-1}K^{-1}}$, $\tau_0 = 0.2\mathrm{sec}$, $\alpha_t = 2.36 \times 10^{-6}\mathrm{K^{-1}}$,

$T_0 = 298\ \mathrm{K}$, $C_e = 1.04 \times 10^{10}\mathrm{m^2 sec^{-2}K^{-1}}$.

3.8.1 Non-Local Effect

We consider HTT parameter and impedance parameters ($z_1 = 1,\ z_2 = 5, z_3 = 2$ and $z_4 = 3$) for the range $0^o \le \theta_0 \le 90^o$.

The computations of graphs are as following:

- In absence of N-L parameters ($\xi_1 = 0$ and $\xi_2 = 0$), the curve is presented by solid line (——).
- In presence of ξ_1 only i.e., ($\xi_1 = 0.25$ and $\xi_2 = 0.0$), the curve is presented by big dashed line (− − −).
- The curve is presented by solid line with centered symbol triangle (-△-) in presence of ξ_2 only i.e., ($\xi_1 = 0.0$ and $\xi_2 = 0.5$).
- In presence of both N-L parameters ($\xi_1 = 0.35$ and $\xi_2 = 0.75$), the curve is presented by big dashed line with centered symbol diamond (−◇−).

3.8.1.1 LD-Wave

Figure 3.2 demonstrate the variations of $|R_1|$ vs. θ_0. The magnitude of $|R_1|$ follow ascending trend for the interval $0^o \le \theta_0 \le 64^o$ for ($\xi_1 = 0.0$ and $\xi_2 = 0.0$), ($\xi_1 = 0.25$ and $\xi_2 = 0.0$) and ($\xi_1 = 0.0$ and $\xi_2 = 0.5$) respectively and attain maximum value at $\theta_0 = 64^o$ then depicts descending trend for the rest of the interval whereas in case of presence of both N-L parameters, $|R_1|$ follow increasing trend in entire range.

Figure 3.3 depicts variations of $|R_2|$ vs. θ_0. It is seen that the values of $|R_2|$ exhibit a descending trend across the entire range but magnitude of $|R_2|$ is smallest when both N-L parameters are absent.

The plot of $|R_3|$ vs. θ_0 is depicted in figure 3.4. The values of $|R_3|$ exhibit an increasing trend for the range $0^o \le \theta_0 \le 45^o$ and a decreasing trend for the rest of the interval across all considered cases. Furthermore, the magnitude of $|R_3|$ is noted to be greater in the presence of both N-L parameters in all other scenarios.

The plot of $|R_4|$ vs. θ_0 is illustrated in figure 3.5. It is noted that values of $|R_4|$ exhibit a similar pattern across all considered cases but magnitude of $|R_4|$ is lowest in absence of both N-L parameters as compared to other cases.

3.8.1.2 CD-I-Wave

Figure 3.6 depicts the variations of $|R_1|$ vs. θ_0. The magnitude of $|R_1|$ exhibits an increasing trend near the boundary then descending trend in the rest of interval across all the considered cases however, the magnitude of $|R_1|$ is higher for $(\xi_1 = 0.25 \text{ and } \xi_2 = 0.0)$ compared to other cases, highlighting the impact N-L parameter ξ_1.

Figure 3.7 depicts variations of $|R_2|$ vs. θ_0. It is noticed that the values of $|R_2|$ show an oscillatory trend across all the considered cases, with a substantial difference in their magnitudes.

The variations of $|R_3|$ vs. θ_0 are illustrated in figure 3.8. The values of $|R_3|$ exhibit a descending trend for the range $0^o \leq \theta_0 \leq 54^o$ across all cases, except $(\xi_1 = 0.25 \text{ and } \xi_2 = 0.0)$, whereas an opposite trend is noticed for $(\xi_1 = 0.0 \text{ and } \xi_2 = 0.50)$ in the remaining interval. Additionally, it is noticed that the magnitude of $|R_3|$ depicts almost static behavior for $(\xi_1 = 0.25 \text{ and } \xi_2 = 0)$ in the range $0^o \leq \theta_0 \leq 81^o$ and decreasing in remaining range.

Figure 3.9 exhibits the variations of $|R_4|$ vs. θ_0. The magnitude of $|R_4|$ shows opposite trend in the range $0^o \leq \theta_0 \leq 63^o$ when both N-L parameters are present, compared to other cases i.e. $(\xi_1 = 0.0 \text{ and } \xi_2 = 0.0)$ and $(\xi_1 = 0.0 \text{ and } \xi_2 = 0.5)$. Beyond this range, similar behavior is noticed, though with significant differences in magnitude. Additionally, for $(\xi_1 = 0.25 \text{ and } \xi_2 = 0.0)$, $|R_4|$ exhibits small variations in the interval $0^o \leq \theta_0 \leq 70^o$ before showing a descending trend in remaining interval.

3.8.2 The effects of HTT and TT with Impedance

For the range $0^o \leq \theta_0 \leq 90^o$, we consider N-L parameters $(\xi_1 = 0.35 \text{ and } \xi_2 = 0.75)$ and impedance parameters $(z_1 = 1,\ z_2 = 5, z_3 = 2 \text{ and } z_4 = 3)$.

Graphs are computed as follows:

- The curves with HTT $(\varsigma = 0.75)$ and impedance parameters are depicted by solid line (——) **(IHT)**.
- The curves without HTT $(\varsigma = 0)$ and with impedance parameters are depicted by small dashed line (---) **(IWHT)**.
- The curves with TT $(a = 0.104)$ and impedance parameters are depicted by big dashed line $(- - -)$ **(ITT)**.
- The curves with HTT $(\varsigma = 0.75)$ and without impedance are depicted as solid line with central symbol triangle (—△—) **(NIHT)**.
- The curves without HTT $(\varsigma = 0)$ and impedance parameters are shown by small dashed line with the central symbol diamond (--◇--) **(NIWHT)**.

- The curves with TT ($a = 0.0104$) and without impedance parameters are indicated by big dashed line with center symbol circle ($-o-$) **(NITT)**.

3.8.2.1 LD-Wave

Figure 3.10 demonstrates the variations of $|R_1|$ vs. θ_0. The values of $|R_1|$, for IHT show opposite behavior when compared with IWHT and ITT. It is also noticed that, $|R_1|$ shows similar trend for NIHT, NIWHT and NITT with a substantial difference in their magnitudes. The variations of $|R_2|$ vs. θ_0 are illustrated in figure 3.11. It is evident that the values of $|R_2|$ exhibit a downward trend in the presence of impedance parameters, while $|R_2|$ has an oscillating behavior with a decreasing magnitude for NIHT, NITT, and NIWHT.

Figure 3.12 depicts the variations of $|R_3|$ vs. θ_0. The magnitude of $|R_3|$ depicts ascending behaviour for IHT and NIHT in the range $0^o \leq \theta_0 \leq 48^o$ and as θ_0 increases it start decreasing for the rest of interval whereas $|R_3|$ shows oscillating trend for IWHT, ITT NIWHT and NITT in the entire interval.

Figure 3.13 depicts the variations of $|R_4|$ vs. θ_0. $|R_4|$ is significantly affected by the HTT parameter, as the magnitude of $|R_4|$ for NIHT is greater than that of NIWHT and NITT and this trend is reversed in the presence of impedance parameters.

3.8.2.2 CD-I-Wave

The trends of $|R_1|$ vs. θ_0 are illustrated in figure 3.14. It is evident that $|R_1|$ follow similar trend across all considered cases. However, its magnitude is higher for IHT, IWHT and ITT compared to NIHT, NIWHT, and NITT, respectively.

Figure 3.15 reveals the variations of $|R_2|$ vs. θ_0. The magnitude of $|R_2|$ exhibits an increasing trend for IHT, IWHT and ITT in the interval $0^o \leq \theta_0 \leq 54^o$ and for NIHT, NIWHT and NITT in the interval $0^o \leq \theta_0 \leq 60^o$. For all cases that are taken into account, the value of $|R_2|$ decreases beyond these intervals.

The variations of $|R_3|$ vs. θ_0 are illustrated in figure 3.16. The magnitude of $|R_3|$ exhibits steady behaviour for NIHT, NIWHT and NITT in the interval $0^o \leq \theta_0 \leq 65^o$, followed by an abrupt decrease in the remaining interval. In contrast, for impedance boundary conditions, $|R_3|$ shows a decreasing trend across the entire range θ_0, highlighting the significant impact of impedance parameters on AR.

Figure 3.17 exhibits the trend of $|R_4|$ vs. θ_0. Initially, the magnitude of $|R_4|$ follows a reverse trend for NIHT, NIWHT and NITT compared to IHT, IWHT and ITT, respectively, in the range $0^o \leq \theta_0 \leq 54^o$. A similar trend is observed for all the cases that are considered beyond

this range. Additionally, it is noted that due to TT parameter, the magnitude of $|R_4|$ is higher for ITT compared to IHT.

3.9 Conclusion

This chapter presents the reflection of plane waves in an isotropic, homogeneous, MT half-space within framework of the MGT heat equation, considering both N-L and HTT effects. The problem is converted into two-dimensional and simplified by using dimensionless quantities and potential functions. Four types of reflected waves are identified when a plane wave (LDW or CD-IW) is incident at the surface $x_3 = 0$, namely LDW, TW, CD-IW, and CD-IIW. Under impedance boundary conditions, the AR of these reflected waves are determined. The AR of various reflected waves have been analyzed and presented graphically to depict the impact of N-L, HTT, TT, and impedance parameters on these AR. The numerical results yielded the following critical observations:

i) The magnitude of AR exhibits a similar trend in the absence of N-L parameters and in the presence of the N-L parameter ξ_2 alone when LDW is incident. However, the values of these AR are consistently higher due to presence of N-L parameter (ξ_2) for all reflected waves.

ii) In the presence of both N-L parameters, the magnitude of AR corresponding to reflected TW, CD-IW, and CD-IIW is higher than in other cases when LDW is incident. Conversely, a reverse trend is observed for the AR of the reflected LDW.

iii) The magnitude of AR associated with reflected CD-IW and CD-IIW demonstrates oscillatory behavior as a result of the HTT parameter. Conversely, the magnitude of AR for the reflected LDW exhibits an opposite trend compared to the reflected TW throughout the entire range, with the exception of certain values of θ_0, when LDW is incident.

iv) The HTT parameter increases the magnitude of AR associated with reflected LDW and CD-IIW when a CD-IW is incident. Conversely, the magnitude of AR for reflected TW and CD-IW exhibits a decreasing trend in the presence of impedance parameters.

v) When CD-IW is incident, N-L parameter (ξ_1) enhances the magnitude of AR for all reflected waves.

vi) It is observed that the impedance parameters amplify the magnitude of AR of all reflected waves across the entire range for the incident LDW, with the exception of certain values of θ_0 in the case of ITT and IWHT.

vii) The magnitudes of AR corresponding to reflected LDW, TW, and CD-IIW exhibit oscillatory behavior throughout the entire range when CD-IW is incident. Conversely,

the AR of the reflected CD-IW exhibit a decreasing trend as a result of the impedance parameters.

The presented results offer an analytical and numerical framework for investigating wave reflection phenomena in N-L micropolar thermoelastic media incorporating HTT effects. This study provides valuable insights into the complex interplay between physical parameters namely nonlocality, HTT, and impedance highlight their significant influence on AR of reflected waves. The theoretical findings have broad applicability in engineering, geophysics, and materials science, particularly in domains where high-frequency wave propagation, microstructural interactions, and thermal effects are of paramount importance. Furthermore, the characterization and control of multiple reflected waves enhance our understanding of wave material interactions at the microscale with direct implications for the design of advanced materials.

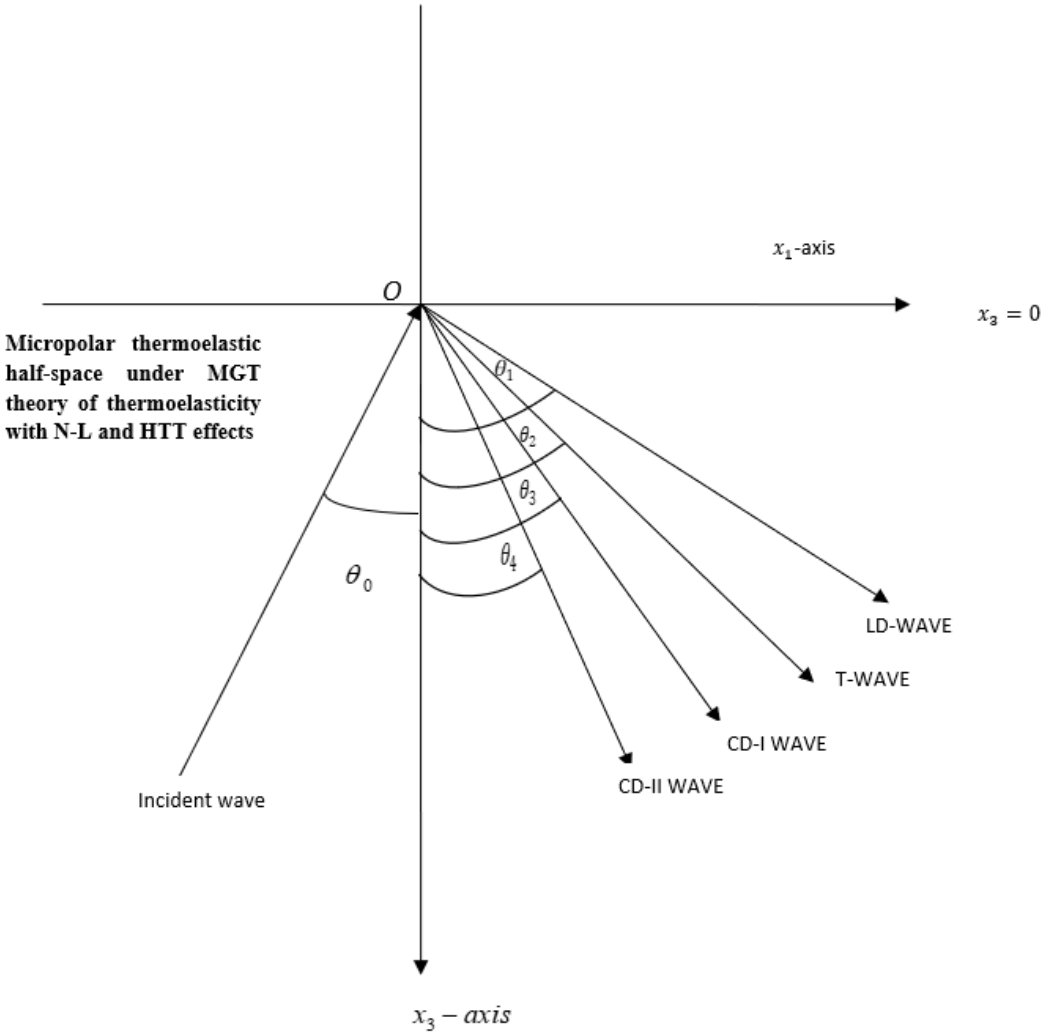

Figure 3.1 Geometry of the problem

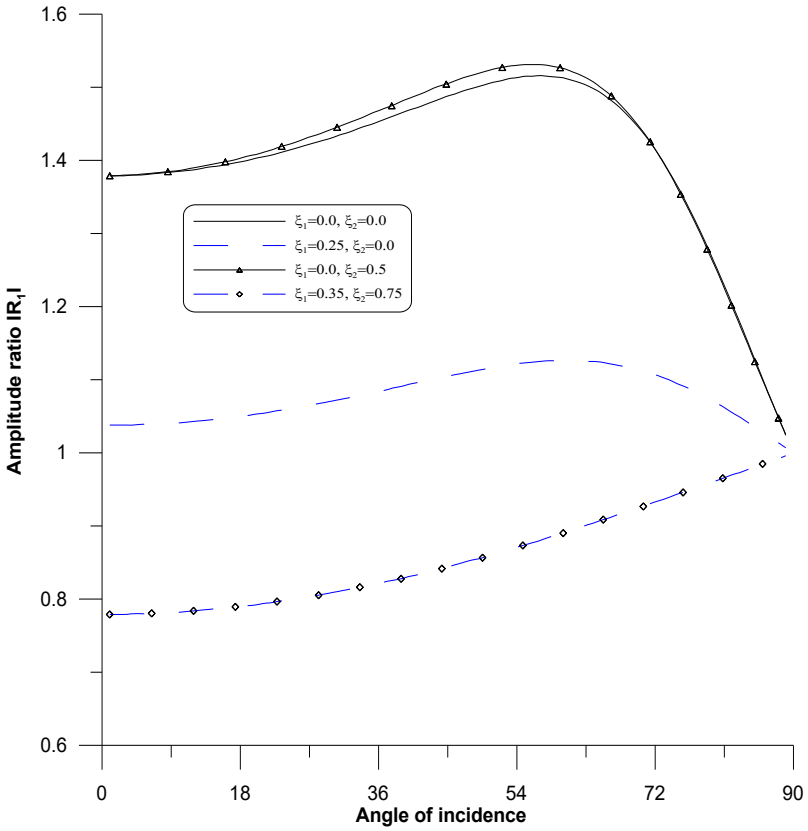

Fig. 3.2 $|R_1|$ w.r.t θ_0 for LD-wave

(Impact of N-L parameters)

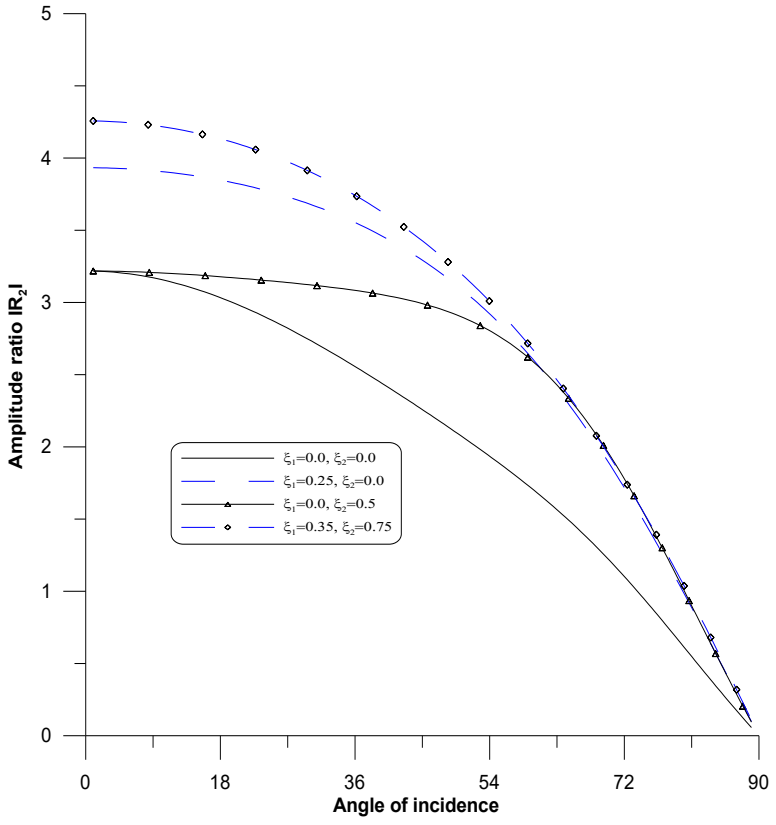

Fig. 3.3 $|R_2|$ w.r.t θ_0 for LD-wave

(Impact of N-L parameters)

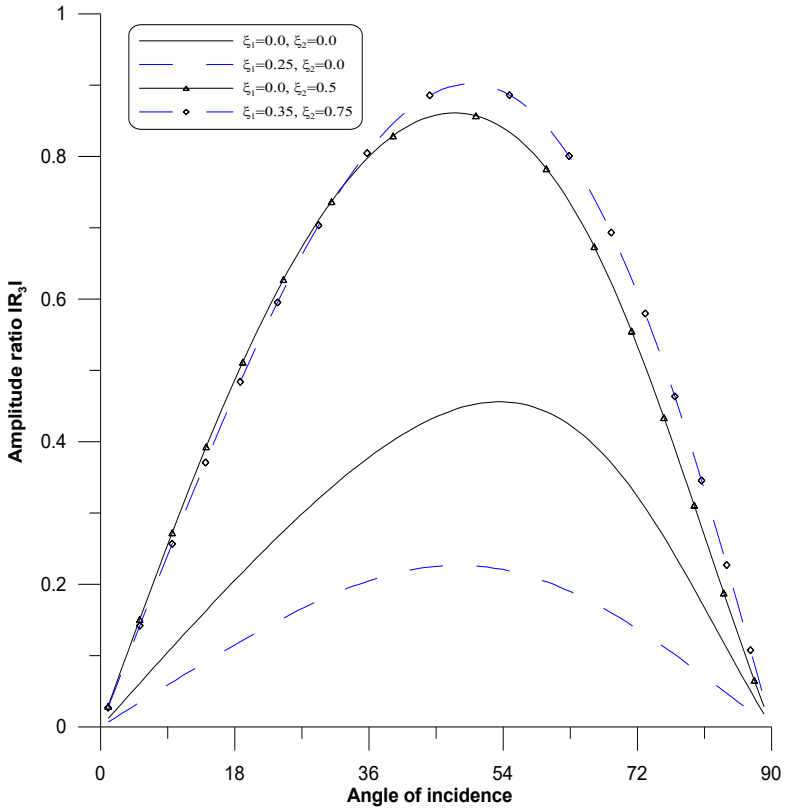

Fig. 3.4 $|R_3|$ w.r.t θ_0 for LD-wave

(Impact of N-L parameters)

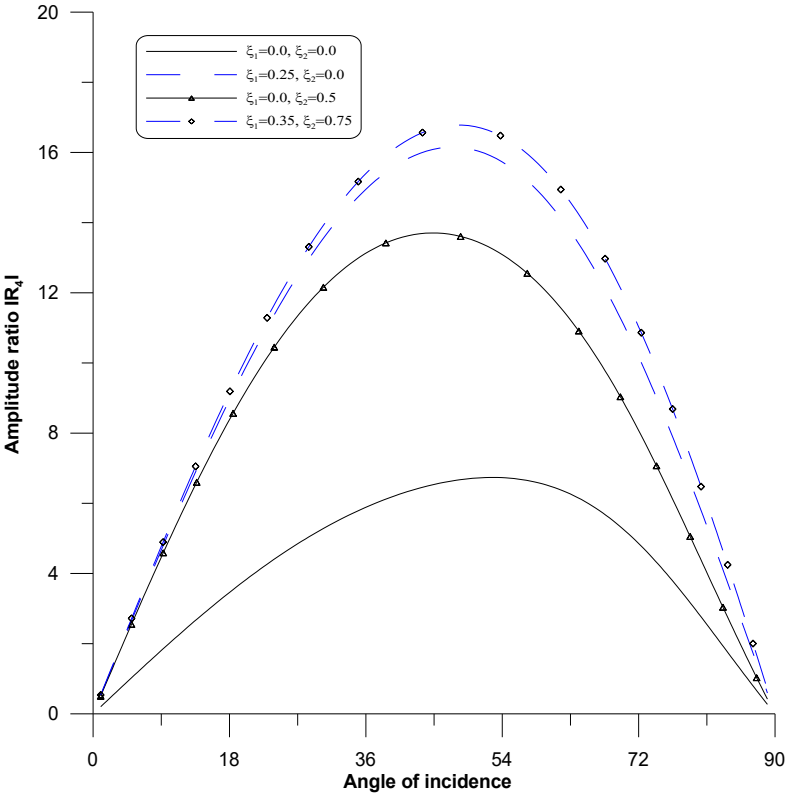

Fig. 3.5 $|R_4|$ w.r.t θ_0 for LD-wave

(Impact of N-L parameters)

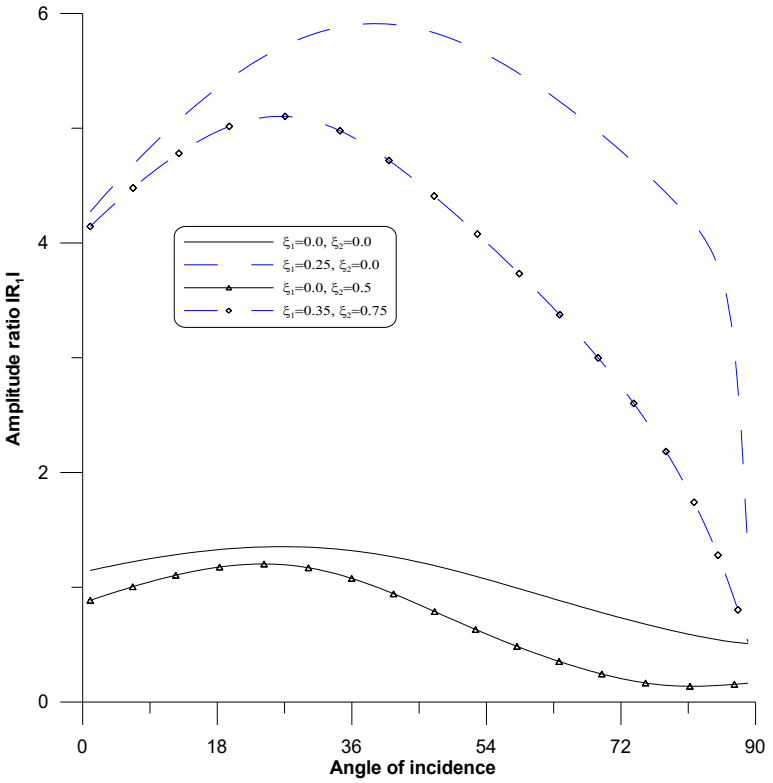

Fig. 3.6 $|R_1|$ w.r.t θ_0 for CD-I wave

(Impact of N-L parameters)

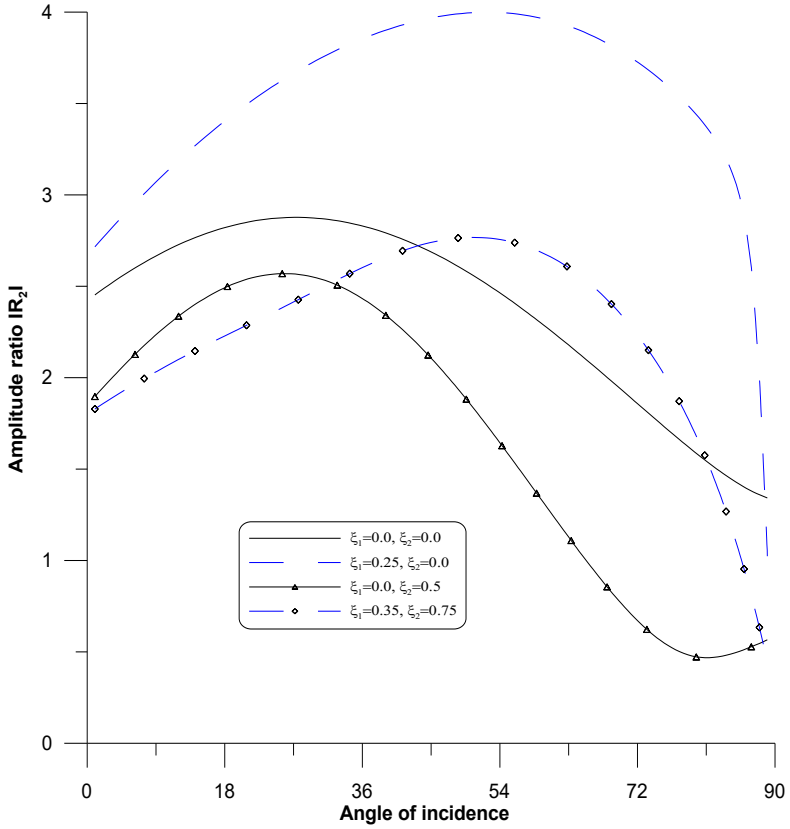

Fig.3.7 $|R_2|$ w.r.t θ_0 for CD-I wave

(Impact of N-L parameters)

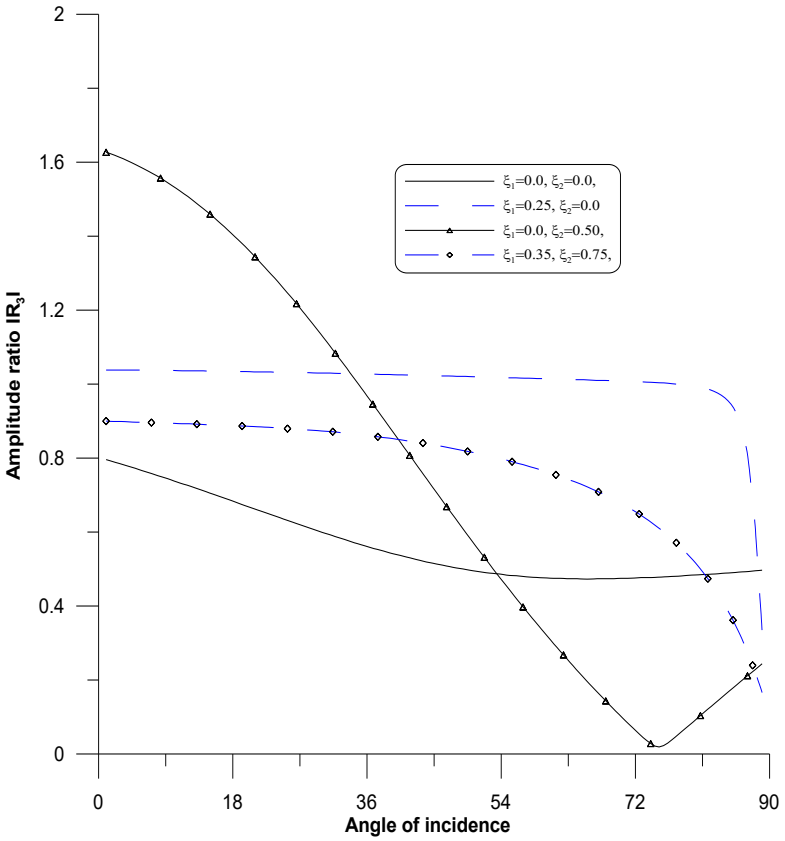

Fig. 3.8 $|R_3|$ w.r.t θ_0 for CD-I wave

(Impact of N-L parameters)

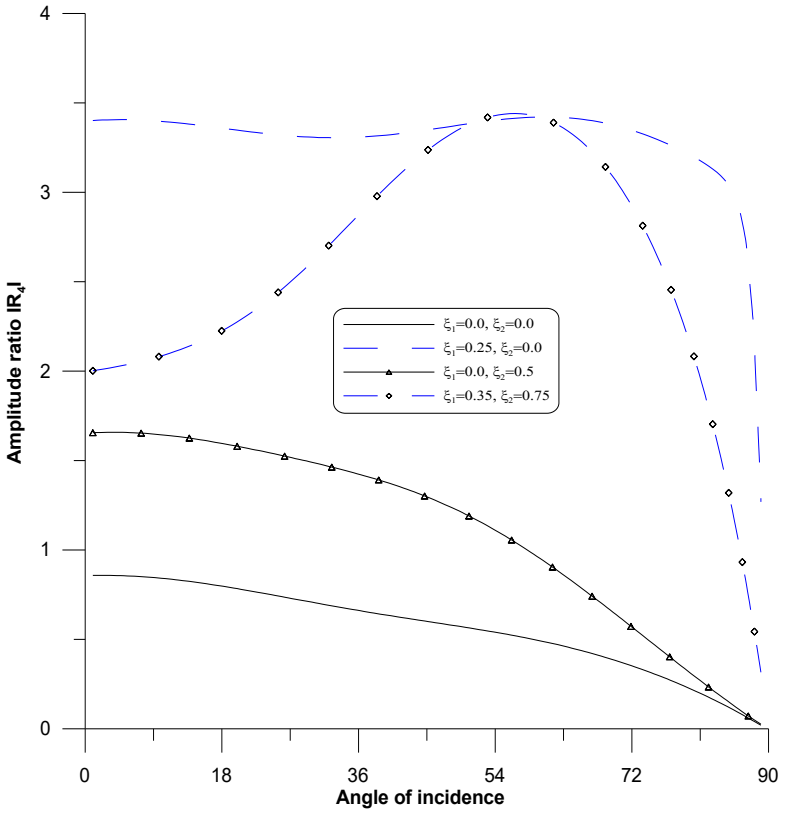

Fig.3.9 $|R_4|$ w.r.t θ_0 for CD-I wave

(Impact of N-L parameters)

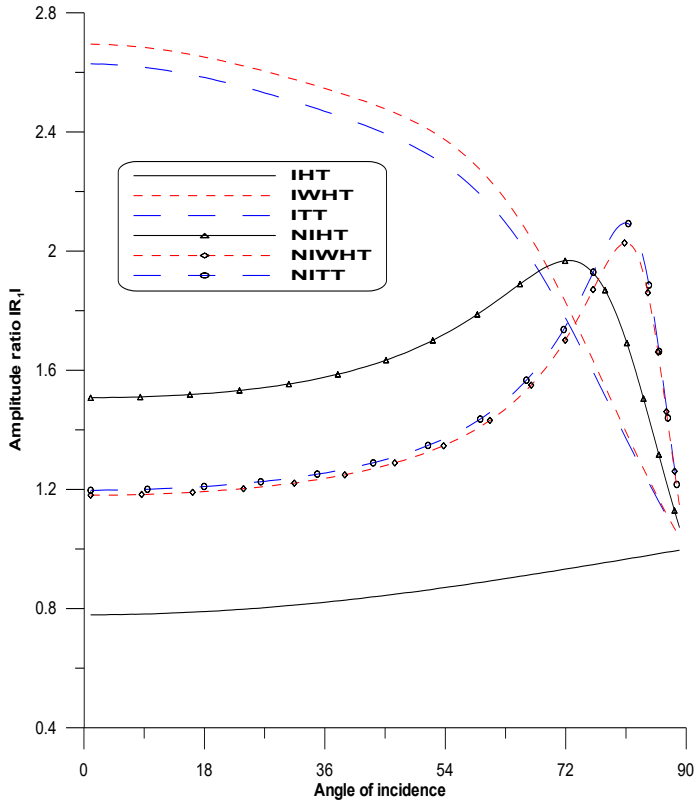

Fig. 3.10 $|R_1|$ w.r.t θ_0 for LD-wave

(Impact of impedance parameters with HTT and TT)

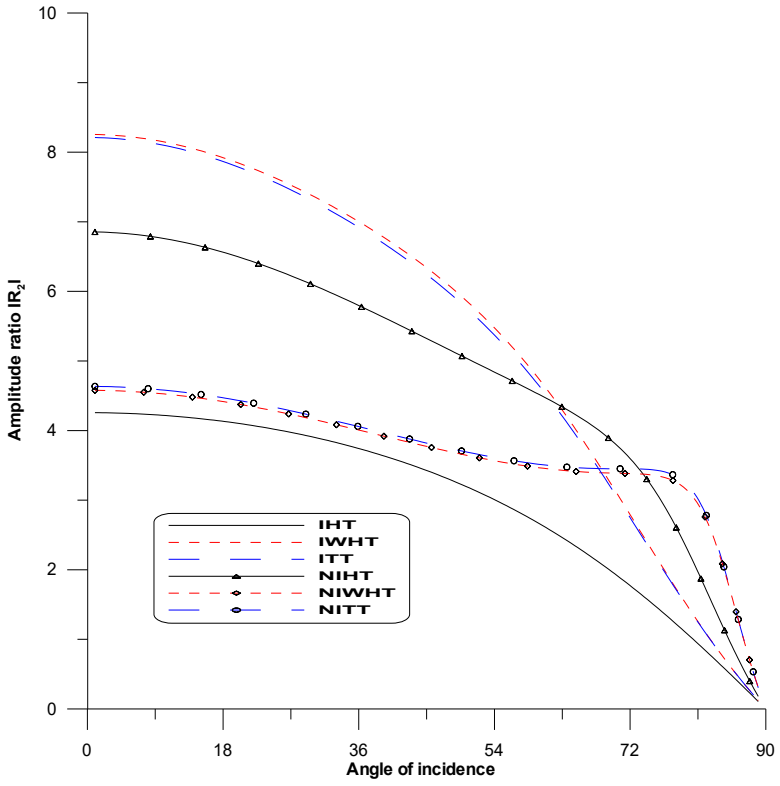

Fig. 3.11 $|R_2|$ w.r.t θ_0 for LD-wave

(Impact of impedance parameters with HTT and TT)

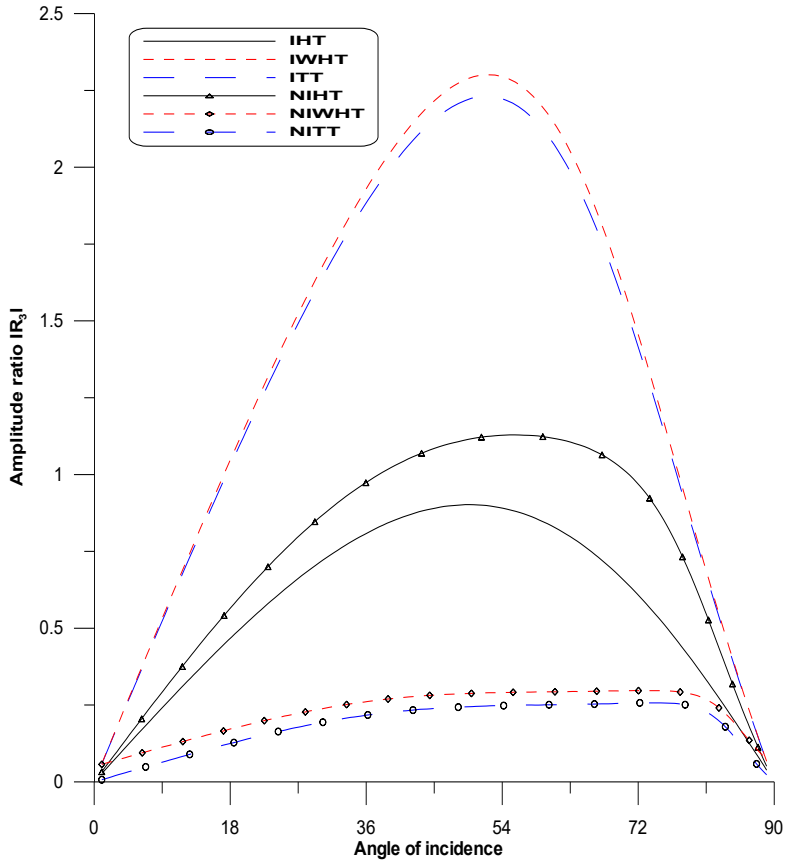

Fig. 3.12 $|R_3|$ w.r.t θ_0 for LD-wave

(Impact of impedance parameters with HTT and TT)

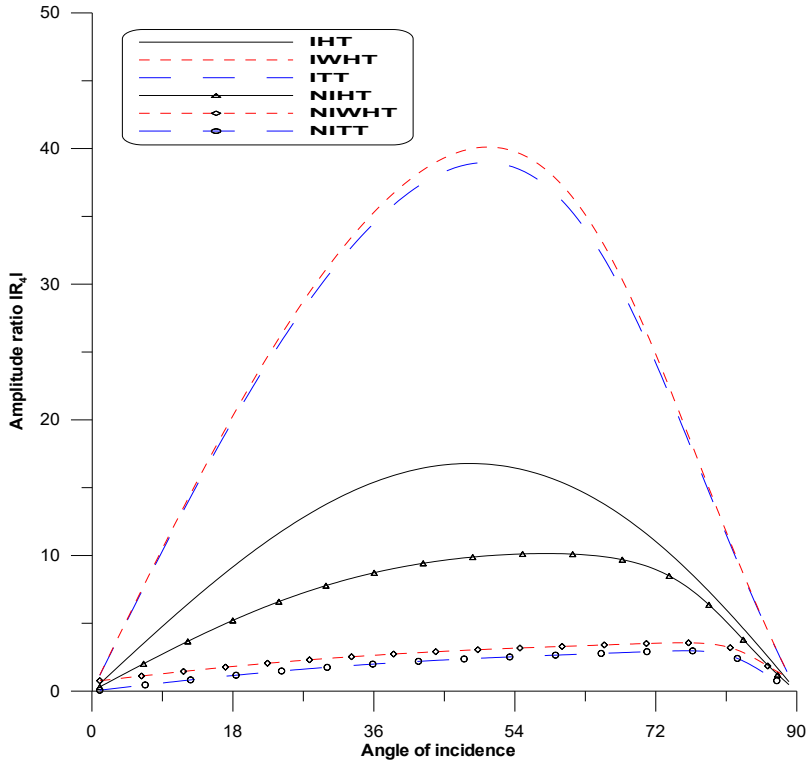

Fig. 3.13 $|R_4|$ w.r.t θ_0 for LD-wave

(Impact of impedance parameters with HTT and TT)

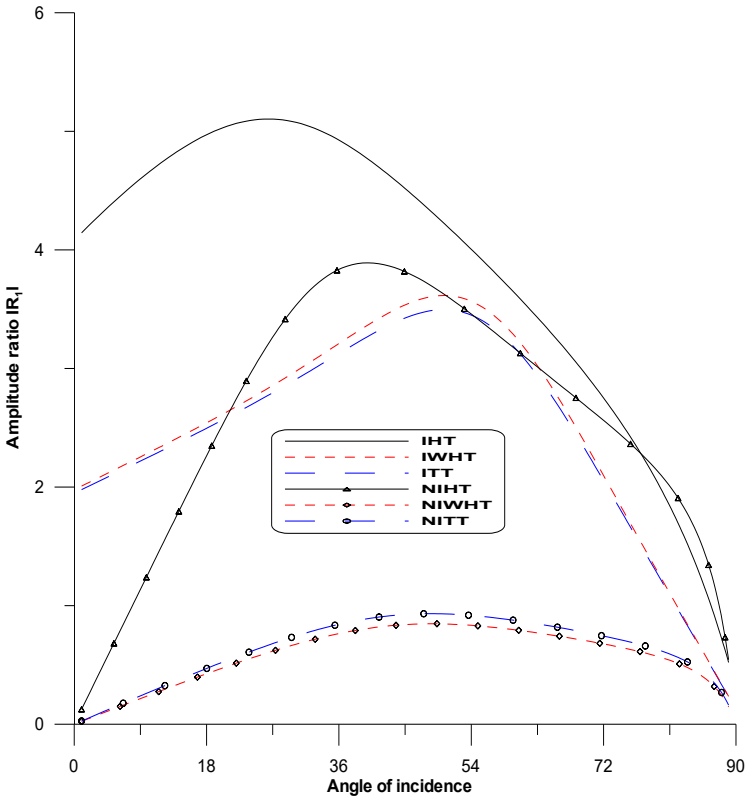

Fig. 3.14 $|R_1|$ w.r.t θ_0 for CD-I wave

(Impact of impedance parameters with HTT and TT)

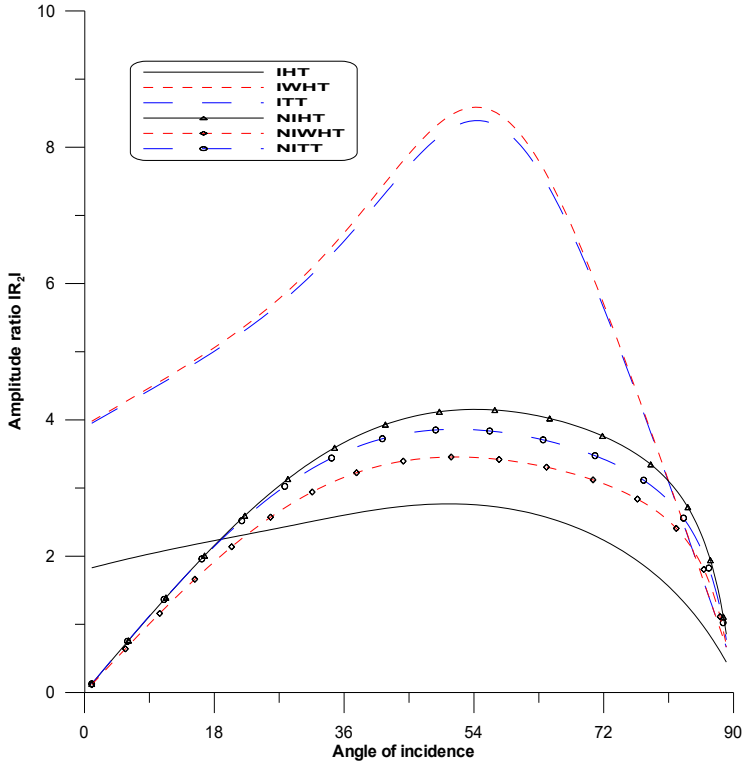

Fig. 3.15 $|R_2|$ w.r.t θ_0 for CD-I wave

(Impact of impedance parameters with HTT and TT)

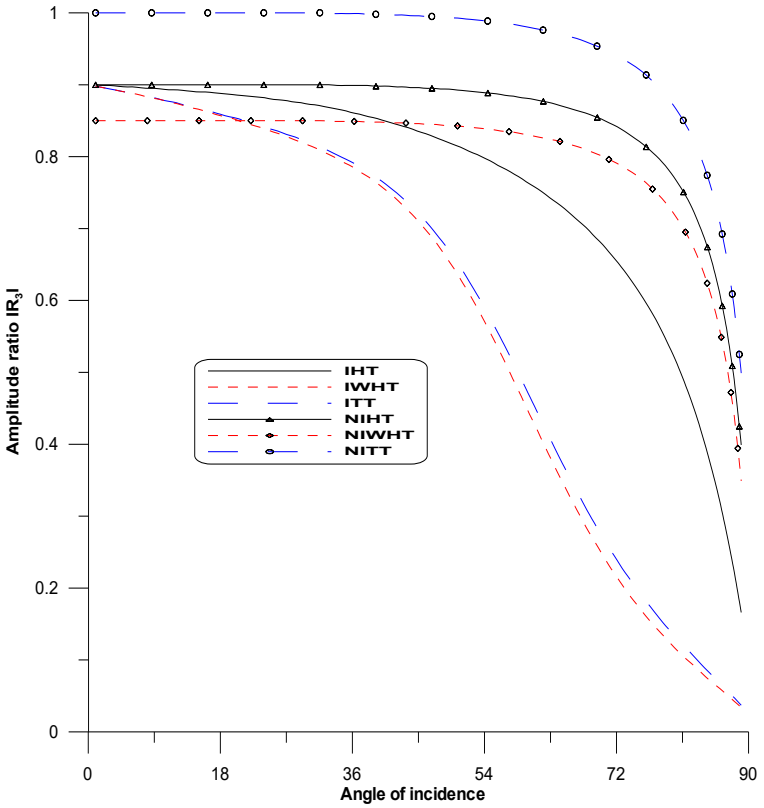

Fig. 3.16 $|R_3|$ w.r.t θ_0 for CD-I wave

(Impact of impedance parameters with TT and HTT)

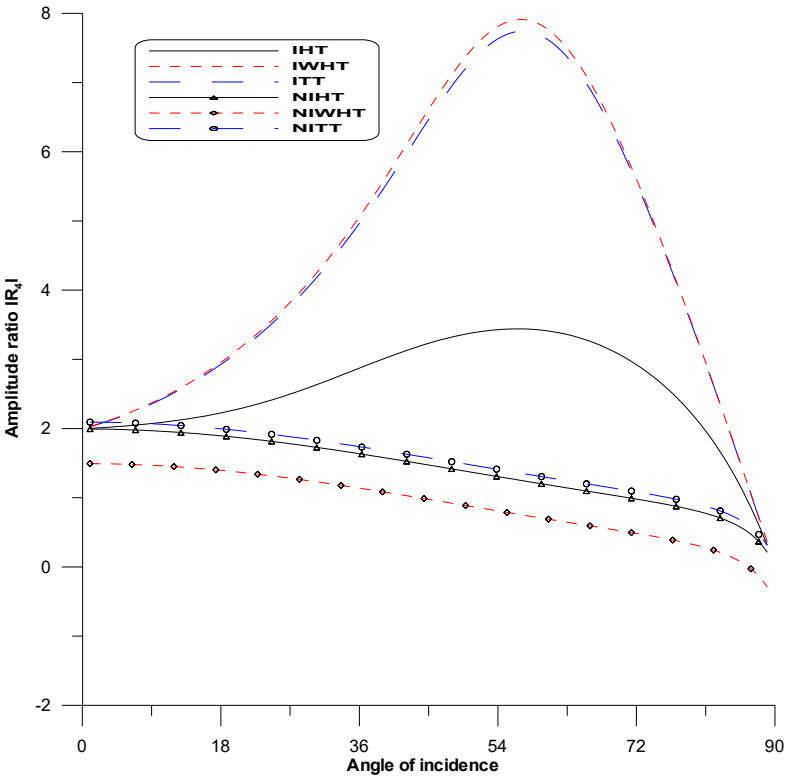

Fig. 3.17 $|R_4|$ w.r.t θ_0 for CD-I wave

(Impact of impedance parameters with TT and HTT)

Chapter 4

Propagation of plane waves in a micropolar elastic medium affected by voids and non-free surfaces

The work from this chapter has been published in the form of research paper entitled “Wave propagation under the influence of voids and non-free surfaces in a micropolar elastic medium”, Materials Physics & Mechanics, 50(2), 2022, DOI:10.18149/MPM.5022022_4.

Indexing: RSCI, Scopus, Impact Factor: 0.285

Chapter 4

Propagation of plane waves in a micropolar elastic medium affected by voids and non-free surfaces

4.1 Introduction

Sharma (2012) [135] investigated the reflection of plane waves in a thermodiffusive elastic half-space that included voids. Sharma and Kumar (2013) [138] explored how plane waves propagated through a thermoviscoelastic material with voids. Sharma and Bhargava (2014) [137] calculated the amplitude ratios (AR) of different transmitted and reflected waves at imperfect barriers and investigated the impacts of material stiffness and thermal parameters on these ratios. Kumari and Kaliraman (2018) [93] determined the AR of various reflected and refracted waves against the angle of incidence in a micropolar elastic material that contained voids.

Lianngenga (2022) [97] examined the impact of impedance parameters on the reflection coefficients of different reflected waves in a porous micropolar thermoelastic material. Jahangir et al. (2023) [60] calculated velocity, attenuation coefficient, and specific heat loss for various reflected waves in viscoelastic solids using the non-local (N-L) elasticity theory and the revised heat conduction model. Rajkumar et al. (2024) [123] investigated the impact of impedance parameters and micropolarity on propagation of elastic wave along a cylindrical rod with impedance boundary conditions.

This chapter presents the reflection of plane waves in micropolar elastic media with voids at non-free surface. The model-specific governing equations are formulated. These equations are then converted into two dimensions, transformed into dimensionless form, and potential functions are employed for further simplification. Four types of reflected waves are identified when a plane wave (longitudinal displacement wave (LDW) or longitudinal void volume fraction wave (LVVFW) or coupled transverse wave (CD-IW) or coupled microrotational wave (CD-IIW)) is incident at the surface $x_3 = 0$, namely LDW, LVVFW, CD-IW, and CD-IIW. Using non-free boundary conditions, the AR of various reflected waves are determined. The variations of these AR with angle of incidence are also shown graphically for both the non-free surface and the free surfaces, highlighting the influences of stiffnesses and voids. Certain cases are also deduced.

The reason for this study stems from the inadequacy of classical elastic models in capturing the complex wave behavior in materials with microstructures, voids, and non-free boundary conditions. Accurate modeling of such phenomena is essential for understanding

the dynamic response of materials like geological formations, porous foams, and composites, which exhibit significant microscale interactions. The motivation is driven by the need to enhance the predictive capability of wave propagation models for use in structural diagnostics, performance evaluation and advanced engineering applications. The novelty of this work lies in its incorporation of voids and non-free surface boundaries within a micropolar elastic framework, offering a more realistic and physically representative model. Unlike conventional theories that assume idealized free surfaces, this study accounts for non-free boundary constraints, thereby improving the fidelity of wave structure interaction analysis and contributing to the design of more robust and accurate material systems.

4.2 Governing equations

The field equations and constitutive relations for a micropolar elastic semi-space with voids, excluding body couples, body forces, and heat sources (as described by Eringen (1968) [38] and Iesan (1985) [58]), are as follows:

$$(\lambda+\mu)\nabla(\nabla.\mathbf{u})+(\mu+K)\Delta\mathbf{u}+K(\nabla\times\boldsymbol{\phi})+\beta_1^*\nabla q^*=\rho\frac{\partial^2\mathbf{u}}{\partial t^2}, \tag{4.1}$$

$$(\alpha+\beta)\nabla(\nabla.\boldsymbol{\phi})+\gamma\Delta\boldsymbol{\phi}+K[(\nabla\times\mathbf{u})-2\boldsymbol{\phi}]=\rho\hat{j}\frac{\partial^2\boldsymbol{\phi}}{\partial t^2}, \tag{4.2}$$

$$\alpha^*\Delta q^*-\omega^*\dot{q}^*-\xi^*q^*-\beta_1^*(\nabla.\mathbf{u})=\rho\kappa^*\frac{\partial^2 q^*}{\partial t^2}, \tag{4.3}$$

$$t_{pq}=\lambda u_{h,h}\delta_{pq}+\mu\left(u_{p,q}+u_{q,p}\right)+K\left(u_{q,p}-\varepsilon_{pqh}\phi_h\right)+\beta_1^*q^*\delta_{pq}, \tag{4.4}$$

$$m_{pq}=\alpha\phi_{h,h}\delta_{pq}+\beta\phi_{p,q}+\gamma\phi_{q,p}, \qquad (p,q,h=1-3), \tag{4.5}$$

where

$\omega^*,\beta_1^*,\alpha^*,\xi^*,\kappa^*$- void parameters, q^*- void fraction field and other symbols $\mathbf{u},\boldsymbol{\phi}$, $\mu,\lambda,\gamma,K,\rho,\hat{j},t,t_{pq},m_{pq},\beta,\alpha,\delta_{pq},\varepsilon_{pqh},\Delta,\nabla$ are as described in section 2.2 [Chapter 2].

Equations (4.1) -(4.5) in components form for Cartesian coordinates (x_1,x_2,x_3) are expressed as

$$(\lambda+\mu)\frac{\partial}{\partial x_1}\left(\frac{\partial u_1}{\partial x_1}+\frac{\partial u_2}{\partial x_2}+\frac{\partial u_3}{\partial x_3}\right)+(\mu+K)\Delta u_1+K\left(\frac{\partial\phi_3}{\partial x_2}-\frac{\partial\phi_2}{\partial x_3}\right)+\beta_1^*\frac{\partial q^*}{\partial x_1}=\rho\frac{\partial^2 u_1}{\partial t^2}, \tag{4.6}$$

$$(\lambda+\mu)\frac{\partial}{\partial x_2}\left(\frac{\partial u_1}{\partial x_1}+\frac{\partial u_2}{\partial x_2}+\frac{\partial u_3}{\partial x_3}\right)+(\mu+K)\Delta u_2+K\left(\frac{\partial\phi_1}{\partial x_3}-\frac{\partial\phi_3}{\partial x_1}\right)+\beta_1^*\frac{\partial q^*}{\partial x_2}=\rho\frac{\partial^2 u_2}{\partial t^2}, \tag{4.7}$$

$$(\lambda+\mu)\frac{\partial}{\partial x_3}\left(\frac{\partial u_1}{\partial x_1}+\frac{\partial u_2}{\partial x_2}+\frac{\partial u_3}{\partial x_3}\right)+(\mu+K)\Delta u_3+K\left(\frac{\partial\phi_2}{\partial x_1}-\frac{\partial\phi_1}{\partial x_2}\right)+\beta_1^*\frac{\partial q^*}{\partial x_3}=\rho\frac{\partial^2 u_3}{\partial t^2}, \tag{4.8}$$

$$(\alpha+\beta)\frac{\partial}{\partial x_1}\left(\frac{\partial\phi_1}{\partial x_1}+\frac{\partial\phi_2}{\partial x_2}+\frac{\partial\phi_3}{\partial x_3}\right)+\gamma\Delta\phi_1+K\left(\left(\frac{\partial u_3}{\partial x_2}-\frac{\partial u_2}{\partial x_3}\right)-2\phi_1\right)=\rho\hat{j}\frac{\partial^2\phi_1}{\partial t^2}, \tag{4.9}$$

$$(\alpha+\beta)\frac{\partial}{\partial x_2}\left(\frac{\partial\phi_1}{\partial x_1}+\frac{\partial\phi_2}{\partial x_2}+\frac{\partial\phi_3}{\partial x_3}\right)+\gamma\Delta\phi_2+K\left(\left(\frac{\partial u_1}{\partial x_3}-\frac{\partial u_3}{\partial x_1}\right)-2\phi_2\right)=\rho\hat{j}\frac{\partial^2\phi_2}{\partial t^2}, \tag{4.10}$$

$$(\alpha+\beta)\frac{\partial}{\partial x_3}\left(\frac{\partial \phi_1}{\partial x_1}+\frac{\partial \phi_2}{\partial x_2}+\frac{\partial \phi_3}{\partial x_3}\right)+\gamma\Delta\phi_3+K\left(\left(\frac{\partial u_2}{\partial x_1}-\frac{\partial u_1}{\partial x_2}\right)-2\phi_3\right)=\rho\hat{j}\frac{\partial^2\phi_3}{\partial t^2}, \quad (4.11)$$

$$\alpha^*\Delta q^*-\omega^*\dot{q}^*-\xi^* q^*-\beta_1^*\left(\frac{\partial u_1}{\partial x_1}+\frac{\partial u_2}{\partial x_2}+\frac{\partial u_3}{\partial x_3}\right)=\rho\kappa^*\frac{\partial^2 q^*}{\partial t^2}, \quad (4.12)$$

$$t_{11}=\left[\lambda\left(\frac{\partial u_1}{\partial x_1}+\frac{\partial u_2}{\partial x_2}+\frac{\partial u_3}{\partial x_3}\right)+(2\mu+K)\frac{\partial u_1}{\partial x_1}\right]+\beta_1^* q^*, \quad (4.13)$$

$$t_{22}=\left[\lambda\left(\frac{\partial u_1}{\partial x_1}+\frac{\partial u_2}{\partial x_2}+\frac{\partial u_3}{\partial x_3}\right)+(2\mu+K)\frac{\partial u_2}{\partial x_2}\right]+\beta_1^* q^*, \quad (4.14)$$

$$t_{33}=\left[\lambda\left(\frac{\partial u_1}{\partial x_1}+\frac{\partial u_2}{\partial x_2}+\frac{\partial u_3}{\partial x_3}\right)+(2\mu+K)\frac{\partial u_3}{\partial x_3}\right]+\beta_1^* q^*, \quad (4.15)$$

$$t_{31}=\left[\mu\left(\frac{\partial u_3}{\partial x_1}+\frac{\partial u_1}{\partial x_3}\right)+K\left(\frac{\partial u_1}{\partial x_3}-\phi_2\right)\right], \quad (4.16)$$

$$t_{32}=\left[\mu\left(\frac{\partial u_3}{\partial x_2}+\frac{\partial u_2}{\partial x_3}\right)+K\left(\frac{\partial u_2}{\partial x_3}+\phi_1\right)\right], \quad (4.17)$$

$$t_{21}=\left[\mu\left(\frac{\partial u_2}{\partial x_1}+\frac{\partial u_1}{\partial x_2}\right)+K\left(\frac{\partial u_1}{\partial x_2}+\phi_3\right)\right], \quad (4.18)$$

and the values of m_{11}, m_{22}, m_{33}, m_{31}, m_{32} and m_{12} are as given by equations (2.19) -(2.24) [Chapter 2]. Additionally, the value of Δ is as provided in section 2.2 [Chapter 2].

4.3 Problem Statement

We consider an isotropic, homogeneous micropolar elastic semi-space that includes voids. A rectangular Cartesian coordinate system (x_1, x_2, x_3) is employed, with the origin positioned at the plane boundary $x_3 = 0$. The x_3 - axis extends vertically downward into the medium, while the x_1 – axis runs horizontally. The x_2-axis is aligned with the direction of the line where the plane wave front intersects the plane surface. The field variables are contingent upon x_1, x_3, and t, if we confine our analysis to the $x_1 - x_3$ plane.

Consider the following two-dimensional problem: $\mathbf{u} = \left(u_1(x_1, x_3, t), 0, u_3(x_1, x_3, t)\right)$,

$$\boldsymbol{\phi} = (0, \phi_2(x_1, x_3, t), 0), \qquad q^* = q^*(x_1, x_3, t). \quad (4.19)$$

Employing equation (4.19) in equations (4.6) -(4.12), (4.15), (4.16) and (2.23), yield

$$(\lambda+\mu)\frac{\partial}{\partial x_1}\left(\frac{\partial u_1}{\partial x_1}+\frac{\partial u_3}{\partial x_3}\right)+(\mu+K)\Delta u_1-K\frac{\partial \phi_2}{\partial x_3}+\beta_1^*\frac{\partial q^*}{\partial x_1}=\rho\frac{\partial^2 u_1}{\partial t^2}, \quad (4.20)$$

$$(\lambda+\mu)\frac{\partial}{\partial x_3}\left(\frac{\partial u_1}{\partial x_1}+\frac{\partial u_3}{\partial x_3}\right)+(\mu+K)\Delta u_3+K\frac{\partial \phi_2}{\partial x_1}+\beta_1^*\frac{\partial q^*}{\partial x_3}=\rho\frac{\partial^2 u_3}{\partial t^2}, \quad (4.21)$$

$$\gamma\Delta\phi_2+K\left[\left(\frac{\partial u_1}{\partial x_3}-\frac{\partial u_3}{\partial x_1}\right)+2\phi_2\right]=\rho\hat{j}\frac{\partial^2\phi_2}{\partial t^2}, \quad (4.22)$$

$$\alpha^*\Delta q^*-\omega^*\dot{q}^*-\xi^* q^*-\beta_1^*\left(\frac{\partial u_1}{\partial x_1}+\frac{\partial u_3}{\partial x_3}\right)=\rho\kappa^*\frac{\partial^2 q^*}{\partial t^2}, \quad (4.23)$$

$$t_{33}=\left[\lambda\left(\frac{\partial u_1}{\partial x_1}+\frac{\partial u_3}{\partial x_3}\right)+(2\mu+K)\frac{\partial u_3}{\partial x_3}\right]+\beta_1^* q^*, \quad (4.24)$$

$$t_{31}=\left[\mu\left(\frac{\partial u_3}{\partial x_1}+\frac{\partial u_1}{\partial x_3}\right)+K\left(\frac{\partial u_1}{\partial x_3}-\phi_2\right)\right], \quad (4.25)$$

$$m_{32} = \gamma \frac{\partial \phi_2}{\partial x_3}, \tag{4.26}$$

where Δ is as defined in section 2.3 [Chapter 2].

For further simplification, following dimensionless quantities are taken as

$$(x_i', u_i') = \frac{\omega_1}{c_1}(x_i, u_i), \qquad t_{3i}' = \frac{1}{\mu} t_{3i}, \qquad q^{*\prime} = \frac{\kappa^* {\omega_1}^2}{c_1^2} q^*, \qquad \phi_2' = \frac{\hat{\jmath} {\omega_1}^2}{c_1^2} \phi_2,$$

$$t' = \omega_1 t, \qquad m_{32}' = \frac{\hat{\jmath}\omega_1}{\gamma c_1} m_{32}, \qquad (S_1', S_2') = \frac{c_1}{\mu \omega_1}(S_1, S_2), \qquad S_3' = \frac{c_1}{\gamma \omega_1} S_3, (i = 1,3), \tag{4.27}$$

where

$$c_1^2 = \frac{\lambda + 2\mu + K}{\rho} \quad \text{and} \quad \omega_1^2 = \frac{K}{\rho \hat{\jmath}}. \tag{4.28}$$

Using (4.27) in equations (4.20) -(4.26) after suppressing the primes, yield

$$b_1^0 \frac{\partial}{\partial x_1}\left(\frac{\partial u_1}{\partial x_1} + \frac{\partial u_3}{\partial x_3}\right) + b_2^0 \Delta u_1 - b_3^0 \frac{\partial \phi_2}{\partial x_3} + b_4^0 \frac{\partial q^*}{\partial x_1} = \frac{\partial^2 u_1}{\partial t^2}, \tag{4.29}$$

$$b_1^0 \frac{\partial}{\partial x_3}\left(\frac{\partial u_1}{\partial x_1} + \frac{\partial u_3}{\partial x_3}\right) + b_2^0 \Delta u_3 + b_3^0 \frac{\partial \phi_2}{\partial x_1} + b_4^0 \frac{\partial q^*}{\partial x_3} = \frac{\partial^2 u_3}{\partial t^2}, \tag{4.30}$$

$$b_5^0 \Delta \phi_2 + b_6^0 \left(\frac{\partial u_1}{\partial x_3} - \frac{\partial u_3}{\partial x_1}\right) - b_7^0 \phi_2 = \frac{\partial^2 \phi_2}{\partial t^2}, \tag{4.31}$$

$$b_8^0 \Delta q^* - b_9^0 q^* - b_{10}^0 \frac{\partial q^*}{\partial t} - b_{11}^0 \left(\frac{\partial u_1}{\partial x_1} + \frac{\partial u_3}{\partial x_3}\right) = \frac{\partial^2 q^*}{\partial t^2}, \tag{4.32}$$

$$t_{33} = b_{14}^0 \frac{\partial u_1}{\partial x_1} + b_{15}^0 \frac{\partial u_3}{\partial x_3} + b_{16}^0 q^*, \tag{4.33}$$

$$t_{31} = b_{12}^0 \frac{\partial u_1}{\partial x_3} + \frac{\partial u_3}{\partial x_1} - b_{13}^0 \phi_2, \tag{4.34}$$

$$m_{32} = \frac{\partial \phi_2}{\partial x_3}, \tag{4.35}$$

where

$$b_1^0 = \frac{\lambda + \mu}{\rho c_1^2}, \quad b_2^0 = \frac{\mu + K}{\rho c_1^2}, \quad b_3^0 = \frac{K}{\hat{\jmath}\rho\omega_1^2}, \quad b_4^0 = \frac{\beta_1^*}{\kappa^* \omega_1^2 \rho}, \quad b_5^0 = \frac{\gamma}{\rho c_1^2 \hat{\jmath}}, \quad b_6^0 = \frac{K}{\rho c_1^2},$$

$$b_7^0 = \frac{2K}{\hat{\jmath}\rho\omega_1^2}, \quad b_8^0 = \frac{\alpha^*}{\kappa^* \rho c_1^2}, \quad b_9^0 = \frac{\xi^*}{\kappa^* \rho \omega_1^2}, \quad b_{10}^0 = \frac{\omega^*}{\kappa^* \rho \omega_1}, \quad b_{11}^0 = \frac{\beta_1^*}{\rho c_1^2}, \quad b_{12}^0 = \frac{\mu + K}{\mu},$$

$$b_{13}^0 = \frac{K c_1^2}{\mu \hat{\jmath} \omega_1^2}, \quad b_{14}^0 = \frac{\lambda}{\mu}, \quad b_{15}^0 = \frac{\lambda + 2\mu + K}{\mu}, \quad b_{16}^0 = \frac{\beta_1^* c_1^2}{\kappa^* \omega_1^2}.$$

4.4 Solution Procedure

Relation between displacement components and scalar potentials is as given by equation (2.43) [Chapter 2].

Using (2.43) in equations (4.29) -(4.32), we get

$$\left(\Delta - \frac{\partial^2}{\partial t^2}\right) q + b_4^0 q^* = 0, \tag{4.36}$$

$$\left(b_2^0 \Delta - \frac{\partial^2}{\partial t^2}\right) \psi + b_3^0 \phi_2 = 0, \tag{4.37}$$

$$\left(b_5^0\Delta - \frac{\partial^2}{\partial t^2} - b_7^0\right)\phi_2 - b_6^0\Delta\psi = 0, \tag{4.38}$$

$$\left(b_8^0\Delta - \frac{\partial^2}{\partial t^2} - b_9^0 - b_{10}^0\frac{\partial}{\partial t}\right)q^* - b_{11}^0\Delta q = 0. \tag{4.39}$$

For solving equations (4.36) -(4.39), we assume the solution as

$$(q, q^*, \psi, \phi_2) = (\bar{q}, \overline{q^*}, \bar{\psi}, \bar{\phi}_2)e^{\iota\kappa(x_1\sin\theta_0 - x_3\cos\theta_0 + vt)}, \tag{4.40}$$

where ι, v, ω, κ and θ_0 are as defined in [Chapter 2]. Quantities like $\bar{q}$, $\overline{q^*}$, $\bar{\psi}$ and $\bar{\phi}_2$ are described the wave amplitudes.

The following equations are obtained by simplifying and inserting the values of q, q^*, ψ and ϕ_2 from equation (4.40) into equations (4.36) -(4.39):

$$(v^4 + D_{01}v^2 + D_{02})(\overline{q^*}, \bar{q}) = 0, \tag{4.41}$$

$$(v^4 + D_{03}v^2 + D_{04})(\bar{\psi}, \bar{\phi}_2) = 0, \tag{4.42}$$

where

$$D_{01} = \frac{-(b_4^0 b_{11}^0 - b_9^0 + (b_8^0+1)\omega^2 - \iota\omega b_{10}^0)}{\omega^2 - b_9^0 - \iota\omega b_{10}^0}, \qquad D_{02} = \frac{b_8^0\omega^2}{\omega^2 - b_9^0 - \iota\omega b_{10}^0},$$

$$D_{03} = \frac{b_2^0 b_7^0 - b_3^0 b_6^0 - (b_5^0 + b_2^0)\omega^2}{\omega^2 - b_7^0}, \qquad D_{04} = \frac{b_2^0 b_5^0 \omega^2}{\omega^2 - b_7^0}.$$

Let v_i (i = 1,2) be roots of characteristic equation $(v^4 + D_{01}v^2 + D_{02}) = 0$, which correspond to velocities of LDW and LVVFW, respectively in decreasing order. Similarly, v_j (j = 3, 4) designate the roots of the characteristic equation $(v^4 + D_{03}v^2 + D_{04}) = 0$, which correspond to the velocities of CD-IW and CD-IIW, respectively in decreasing order.

4.5. Reflection at boundary surface

Let a plane harmonic wave (LDW or LVVFW or CD-IW or CD-IIW) form an angle θ_0 with the normal to the surface at $x_3 = 0$. When any incident wave (LDW or LVVFW or CD-IW or CD-IIW) strikes the boundary, it generates four reflected waves (LDW, LVVFW, CD-IW and CD-IIW). These reflected waves make angles $\theta_1, \theta_2, \theta_3$, and θ_4 with the positive x_3-axis, as illustrated in figure 4.1. The complete wave field structure in the half-space, consisting of both incident and reflected waves, can be expressed as:

$$q = \sum_{i=1}^{2}\left[\widetilde{A}_{0i}e^{\iota\kappa_0(x_1\sin\theta_0 - x_3\cos\theta_0)+\iota\omega t} + \widetilde{A}_i e^{\iota\kappa_i(x_3\cos\theta_i + x_1\sin\theta_i)+\iota\omega t}\right], \tag{4.43}$$

$$q^* = \sum_{i=1}^{2}\left[\tilde{d}_i\left(\widetilde{A}_{0i}e^{\iota\kappa_0(x_1\sin\theta_0 - x_3\cos\theta_0)+\iota\omega t} + \widetilde{A}_i e^{\iota\kappa_i(x_3\cos\theta_i + x_1\sin\theta_i)+\iota\omega t}\right)\right], \tag{4.44}$$

$$\psi = \sum_{i=1}^{2}\left[\widetilde{B}_{0i}e^{\iota\kappa_0(x_1\sin\theta_0 - x_3\cos\theta_0)+\iota\omega t} + \widetilde{B}_i e^{\iota\kappa_j(x_3\cos\theta_j + x_1\sin\theta_j)+\iota\omega t}\right], \tag{4.45}$$

$$\phi_2 = \sum_{i=1}^{2}\left[\tilde{f}_i\left(\widetilde{B}_{0i}e^{\iota\kappa_0(x_1\sin\theta_0 - x_3\cos\theta_0)+\iota\omega t} + \widetilde{B}_i e^{\iota\kappa_j(x_3\cos\theta_j + x_1\sin\theta_j)+\iota\omega t}\right)\right], \tag{4.46}$$

where

$$\tilde{d}_i = \frac{\kappa_i{}^2 - \omega^2}{b_4^0}, \qquad \tilde{f}_i = \frac{b_6^0\kappa_j^2}{b_5^0\kappa_j^2 + b_7^0 - \omega^2}, \quad (i = 1,2), (j = 3,4),$$

also, $\widetilde{A}_{0i}$ and $\widetilde{B}_{0i}(i = 1,2)$ indicate the amplitudes of incident LDW, LVVFW, CD-IW and CD-IIW, respectively. Similarly, $\widetilde{A}_i$ and $\widetilde{B}_i(i = 1,2)$ describe the amplitudes of the reflected LDW, LVVFW, CD-IW, and CD-IIW, respectively.

4.6 Restrictions on Boundary

The stress components (force stress and couple stress) are zero on the free surface. However, at the non-free surface, these stress components can have finite values proportional to both displacement and rotational components, namely

$$\begin{bmatrix} t_{33} \\ t_{31} \\ m_{32} \end{bmatrix} = -\iota \begin{bmatrix} S_1 & 0 & 0 \\ 0 & S_2 & 0 \\ 0 & 0 & S_3 \end{bmatrix} \begin{bmatrix} u_3 \\ u_1 \\ \phi_2 \end{bmatrix}, \tag{4.47}$$

where S_1, S_2 and S_3 are proportional coefficients representing the stiffness of the normal, tangential, and rotational elastic supports, respectively. The free surface condition is restored when $S_1, S_2, S_3 \to 0$, whereas the fixed surface condition is achieved when $S_1, S_2, S_3 \to \infty$.

A negative imaginary number $-\iota$ is multiplied on right hand side of equation (4.47) to remove the phase shift between stress (force stress and couple stress) field, displacement field and microrotation field. We also require the gradient of the volume fraction field to vanish at the surface $x_3 = 0$.

Thus, the suitable boundary conditions at $x_3 = 0$ are:

$$\text{(i) } t_{33} = -\iota S_1 u_3, \qquad \text{(ii)} t_{31} = -\iota S_2 u_1,$$

$$\text{(iii)} m_{32} = -\iota S_3 \phi_2, \qquad \text{(iv)} \frac{\partial q^*}{\partial x_3} = 0. \tag{4.48}$$

Using equation (2.43) into equations (4.33) and (4.34), yield

$$t_{33} = (b_{15}^0 - b_{14}^0)\frac{\partial^2 \psi}{\partial x_1 \partial x_3} + b_{14}^0 \frac{\partial^2 q}{\partial x_1^2} + b_{15}^0 \frac{\partial^2 q}{\partial x_3^2} + b_{16}^0 q^*, \tag{4.49}$$

$$t_{31} = (b_{12}^0 + 1)\frac{\partial^2 q}{\partial x_1 \partial x_3} - b_{12}^0 \frac{\partial^2 \psi}{\partial x_3^2} + \frac{\partial^2 \psi}{\partial x_1^2} - b_{13}^0 \phi_2. \tag{4.50}$$

To meet the boundary condition (4.48) at $x_3 = 0$, the angle of incident wave must be connected to the angles of reflected waves using the following relation:

$$\kappa_0 \sin\theta_0 = \kappa_i \sin\theta_i, \qquad (i = 1 \cdots 4) \tag{4.51}$$

Relation (4.51) can be written as

$$\frac{\sin\theta_0}{\upsilon_0} = \frac{\sin\theta_i}{\upsilon_i}, \qquad (i = 1 \cdots 4) \tag{4.52}$$

where

$$\upsilon_0 = \begin{cases} \upsilon_1, & \text{incident LDW} \\ \upsilon_2, & \text{incident LVVFW} \\ \upsilon_3, & \text{incident CD} - \text{IW} \\ \upsilon_4, & \text{incident CD} - \text{IIW} \end{cases}.$$

Substituting the values of $q, q^*, \psi, \text{and } \phi_2$ from (4.43) - (4.46) in (4.48) with the aid of equations (2.43), (4.35), (4.49)- (4.52), yield the following system of equations as

$$\sum_{i=1}^{4} g_{ij} R_j = X_{i,} \qquad (j = 1 \cdots 4), \tag{4.53}$$

where

$$g_{1p} = \left[b_{14}^0 \sin^2\theta_p + b_{15}^0 \cos^2\theta_p\right]\kappa_p^2 - b_{16}^0 \tilde{d}_p + S_1 \kappa_p \cos\theta_p,$$

$$g_{1q} = -\kappa_q\left[\kappa_q (b_{14}^0 - b_{15}^0)\sin\theta_q \cos\theta_q - S_1 \sin\theta_q\right],$$

$$g_{2p} = \kappa_p\left[\kappa_p (b_{12}^0 + 1)\sin\theta_p \cos\theta_p + S_2 \sin\theta_p\right],$$

$$g_{2q} = -\kappa_q^2\left[b_{12}^0 \cos^2\theta_q - \sin^2\theta_q\right] + b_{13}^0 \tilde{f}_p - \kappa_q S_2 \cos\theta_q,$$

$$g_{3p} = 0, \qquad g_{3q} = -\iota(\cos\theta_q \kappa_q + S_3)\tilde{f}_p,$$

$$g_{4p} = -\iota\kappa_p \tilde{d}_p \cos\theta_p, \qquad g_{4q} = 0, \qquad (p = 1,2), (q = 3,4), \tag{4.54}$$

and the AR of reflected waves, denoted as $R_j (j = 1 \cdots 4)$ are given by:

$$R_1 = \frac{\widetilde{A}_1}{A^*}, \quad R_2 = \frac{\widetilde{A}_2}{A^*}, \quad R_3 = \frac{\widetilde{B}_1}{A^*}, \quad R_4 = \frac{\widetilde{B}_2}{A^*}.$$

For incident LDW:

$$A^* = \widetilde{A}_{01} \text{ and } \widetilde{A}_{02} = \widetilde{B}_{01} = \widetilde{B}_{02} = 0,$$

$$X_1 = -[b_{14}^0 \sin^2\theta_0 + b_{15}^0 \cos^2\theta_0]\kappa_0^2 + b_{16}^0 \tilde{d}_1 + S_1 \kappa_0 \cos\theta_0,$$

$$X_2 = \kappa_0[\kappa_0 (b_{12}^0 + 1)\sin\theta_0 \cos\theta_0 - S_2 \sin\theta_0],$$

$$X_3 = 0,$$

$$X_4 = -\iota\kappa_0 \tilde{d}_1 \cos\theta_0. \tag{4.55}$$

For incident LVVFW:

$$A^* = \widetilde{A}_{02} \text{ and } \widetilde{A}_{01} = \widetilde{B}_{01} = \widetilde{B}_{02} = 0,$$

$$X_1 = -[b_{14}^0 \sin^2\theta_0 + b_{15}^0 \cos^2\theta_0]\kappa_0^2 + b_{16}^0 \tilde{d}_2 + S_1 \kappa_0 \cos\theta_0,$$

$$X_2 = \kappa_0[\kappa_0 (b_{12}^0 + 1)\sin\theta_0 \cos\theta_0 - S_2 \sin\theta_0],$$

$$X_3 = 0,$$

$$X_4 = -\iota\kappa_0 \tilde{d}_2 \cos\theta_0. \tag{4.56}$$

For incident CD-IW:

$$A^* = \widetilde{B}_{01} \text{ and } \widetilde{A}_{01} = \widetilde{A}_{02} = \widetilde{B}_{02} = 0,$$

$$X_1 = -[b_{14}^0 - b_{15}^0]\kappa_0^2 \sin\theta_0 \cos\theta_0 - S_1 \kappa_0 \cos\theta_0,$$

$$X_2 = \kappa_0^2[b_{12}^0 \cos^2\theta_0 - \sin^2\theta_0] - b_{13}^0 \tilde{f}_1 - \kappa_0 S_2 \cos\theta_0,$$

$$X_3 = -\iota(\cos\theta_0 \kappa_0 - S_3)\tilde{f}_1,$$

$$X_4 = 0. \tag{4.57}$$

For incident CD-IIW:

$A^* = \widetilde{B}_{02}$ and $\widetilde{A}_{01} = \widetilde{A}_{02} = \widetilde{B}_{01} = 0,$

$X_1 = -[b_{14}^0 - b_{15}^0]\kappa_0^2 \sin\theta_0 \cos\theta_0 - S_1\kappa_0 \cos\theta_0,$

$X_2 = \kappa_0^2[b_{12}^0 \cos^2\theta_0 - \sin^2\theta_0] - b_{13}^0 \tilde{f}_2 - \kappa_0 S_2 \cos\theta_0,$

$X_3 = -\iota(\cos\theta_0 \kappa_0 - S_3)\tilde{f}_2,$

$X_4 = 0.$ (4.58)

4.7 Specific Cases

4.7.1 Micropolar Elastic media

Taking $\alpha^* = \beta^* = \xi^* = \omega^* = \kappa^* = 0$ in equations (4.41) and (4.42) reduce to following form as

$(\nu^2 - 1)\bar{q} = 0,$

$(\nu^4 + D_{03}\nu^2 + D_{04})(\bar{\psi}, \bar{\phi}_2) = 0,$

where

$D_{03} = \frac{b_2^0 b_7^0 - b_3^0 b_6^0 - (b_5^0 + b_2^0)\omega^2}{\omega^2 - b_7^0}, \quad D_{04} = \frac{b_2^0 b_5^0 \omega^2}{\omega^2 - b_7^0},$

also, the system of equations (4.53) reduces to

$\sum_{i=1}^{3} g_{ij}^0 R_j^0 = X_{i,}^0 \qquad (j = 1 \cdots 3),$ (4.59)

where

$g_{1p}^0 = \left[b_{14}^0 \sin^2\theta_p + b_{15}^0 \cos^2\theta_p\right]\kappa_p^2 + S_1\kappa_p \cos\theta_p,$

$g_{1q}^0 = -\kappa_q\left[\kappa_q(b_{14}^0 - b_{15}^0)\sin\theta_q \cos\theta_q - S_1 \sin\theta_q\right],$

$g_{2p}^0 = \kappa_p\left[\kappa_p(b_{12}^0 + 1)\sin\theta_p \cos\theta_p + S_2 \sin\theta_p\right],$

$g_{2q}^0 = -\kappa_q^2\left[b_{12}^0 \cos^2\theta_q - \sin^2\theta_q\right] + b_{13}^0 \tilde{f}_p - \kappa_q S_2 \cos\theta_q,$

$g_{3p}^0 = 0, \qquad g_{3q}^0 = -\iota(\cos\theta_q \kappa_q + S_3)\tilde{f}_p, \qquad (p = 1), (q = 2,3),$ (4.60)

and the AR of reflected LDW, CD-IW and CD-IIW, denoted as $R_j^0 (j = 1 \cdots 3)$ are given by

$R_1^0 = \frac{\widetilde{A}_1}{A^*}, \qquad R_2^0 = \frac{\widetilde{B}_1}{A^*}, \qquad R_3^0 = \frac{\widetilde{B}_2}{A^*}.$

For incident LDW:

$A^* = \widetilde{A}_{01}$ and $\widetilde{B}_{01} = \widetilde{B}_{02} = 0,$

$X_1^0 = -[b_{14}^0 \sin^2\theta_0 + b_{15}^0 \cos^2\theta_0]\kappa_0^2 + S_1\kappa_0 \cos\theta_0,$

$X_2^0 = \kappa_0[\kappa_0(b_{12}^0 + 1)\sin\theta_0 \cos\theta_0 - S_2 \sin\theta_0],$

$X_3^0 = 0.$ (4.61)

For incident CD-IW:

$A^* = \widetilde{B}_{01}$ and $\widetilde{A}_{01} = \widetilde{B}_{02} = 0,$

$X_1^0 = -[b_{14}^0 - b_{15}^0]\kappa_0^2 \sin\theta_0 \cos\theta_0 - S_1\kappa_0 \cos\theta_0,$

$$X_2^0 = \kappa_0^2[b_{12}^0\cos^2\theta_0 - \sin^2\theta_0] - b_{13}^0\tilde{f}_1 - \kappa_0 S_2\cos\theta_0,$$

$$X_3^0 = -\iota(\cos\theta_0\kappa_0 - S_3)\tilde{f}_1. \quad (4.62)$$

For incident CD-IIW:

$$A^* = \widetilde{B}_{02} \text{ and } \widetilde{A}_{01} = \widetilde{A}_{02} = \widetilde{B}_{01} = 0,$$

$$X_1^0 = -[b_{14}^0 - b_{15}^0]\kappa_0^2 \sin\theta_0\cos\theta_0 - S_1\kappa_0\cos\theta_0,$$

$$X_2^0 = \kappa_0^2[b_{12}^0\cos^2\theta_0 - \sin^2\theta_0] - b_{13}^0\tilde{f}_2 - \kappa_0 S_2\cos\theta_0,$$

$$X_3^0 = -\iota(\cos\theta_0\kappa_0 - S_3)\tilde{f}_2. \quad (4.63)$$

and these results consistent with those reported by Zhang et al. (2015) [171].

4.7.2 Elastic Medium with Void

Taking $\alpha = \beta = \gamma = K = 0$ in equations (4.41) and (4.42) reduce to following form as
$(\nu^4 + D_{01}\nu^2 + D_{02})(\overline{q^*}, \bar{q}) = 0,$

$(\nu^2 - b_2^0)\,\bar{\psi} = 0,$

where

$$D_{01} = \frac{-(b_4^0 b_{11}^0 - b_9^0 + (b_8^0+1)\omega^2 - \iota\omega b_{10}^0)}{\omega^2 - b_9^0 - \iota\omega b_{10}^0}, \quad D_{02} = \frac{b_8^0\omega^2}{\omega^2 - b_9^0 - \iota\omega b_{10}^0}, \; b_2^0 = \frac{\mu}{\rho c_1^2}, \qquad b_{15}^0 = \frac{\lambda+2\mu}{\mu},$$

also, the system of equations (4.53) reduces to

$$\sum_{i=1}^{3} g_{ij}^* R_j^* = X_i^*, \qquad (j = 1\cdots 3), \quad (4.64)$$

where

$$g_{1p}^* = \left[b_{14}^0\sin^2\theta_p + b_{15}^0\cos^2\theta_p\right]\kappa_p^2 - b_{16}^0\tilde{d}_p + S_1\kappa_p\cos\theta_p,$$

$$g_{1q}^* = -\kappa_q\left[\kappa_q(b_{14}^0 - b_{15}^0)\sin\theta_q\cos\theta_q - S_1\sin\theta_q\right],$$

$$g_{2p}^* = \kappa_p\left[\kappa_p(b_{12}^0 + 1)\sin\theta_p\cos\theta_p + S_2\sin\theta_p\right],$$

$$g_{2q}^* = -\kappa_q^2\left[b_{12}^0\cos^2\theta_q - \sin^2\theta_q\right] - \kappa_q S_2\cos\theta_q,$$

$$g_{3p}^* = -\iota\kappa_p\tilde{d}_p\cos\theta_p, \qquad g_{3q}^* = 0, \qquad (p = 1,2), (q = 3), \quad (4.65)$$

and the AR of reflected LDW, LVVFW and CD-IIW, denoted as $R_j^*(j = 1\cdots 3)$ are given by

$$R_1^* = \frac{\widetilde{A}_1}{A^*}, \; R_2^* = \frac{\widetilde{A}_2}{A^*}, \; R_3^* = \frac{\widetilde{B}_1}{A^*}.$$

For incident LDW:

$$A^* = \widetilde{A}_{01} \text{ and } \widetilde{A}_{02} = \widetilde{B}_{01} = 0,$$

$$X_1^* = -[b_{14}^0\sin^2\theta_0 + b_{15}^0\cos^2\theta_0]\kappa_0^2 + b_{16}^0\tilde{d}_1 + S_1\kappa_0\cos\theta_0,$$

$$X_2^* = \kappa_0[\kappa_0(b_{12}^0 + 1)\sin\theta_0\cos\theta_0 - S_2\sin\theta_0],$$

$$X_3^* = -\iota\kappa_0\tilde{d}_1\cos\theta_0. \quad (4.66)$$

For incident LVVFW:

$$A^* = \widetilde{A}_{02} \text{ and } \widetilde{A}_{01} = \widetilde{B}_{01} = 0,$$

$$X_1^* = -[b_{14}^0\sin^2\theta_0 + b_{15}^0\cos^2\theta_0]\kappa_0^2 + b_{16}^0\tilde{d}_2 + S_1\kappa_0\cos\theta_0,$$

$X_2^* = \kappa_0[\kappa_0(b_{12}^0 + 1)\sin\theta_0\cos\theta_0 - S_2\sin\theta_0]$,

$X_3^* = -\iota\kappa_0\tilde{d}_2\cos\theta_0$. (4.67)

For incident CD-IW:

$A^* = \widetilde{B}_{01}$ and $\widetilde{A}_{01} = \widetilde{A}_{02} = 0$,

$X_1^* = -[b_{14}^0 - b_{15}^0]\kappa_0^2\sin\theta_0\cos\theta_0 - S_1\kappa_0\cos\theta_0$,

$X_2^* = \kappa_0^2[b_{12}^0\cos^2\theta_0 - \sin^2\theta_0] - \kappa_0 S_2\cos\theta_0$,

$X_3^* = 0$. (4.68)

and these results are consistent with those reported by Singh et al. (2017) [152] (In absence of N-L parameter).

4.7.3 For Free-Surface

In absence of S_1, S_2 and S_3, the results given by equation (4.53) are reduced for micropolar elastic media with void for free surface and these results align with those obtained by Kumar and Deswal (2006) [74].

4.8 Discussion and Numerical Results

According to numerical calculations and conversations, the material under consideration is similar to Magnesium crystal. The numerical values for micropolar constants following Eringen (1984) [42] are as given in section 3.8 [Chapter 3], and the values of the void parameters following Iesan (1985) [58] are taken as

$\beta_1^* = 1.1384 \times 10^{10}\ \mathrm{Nm^{-2}}$, $\xi^* = 1.147 \times 10^{10}\ \mathrm{Nm^{-2}}$, $\kappa^* = 1.175 \times 10^{-19}\mathrm{m^2}$,

$\alpha^* = 3.688 \times 10^{-9}$ N, $\omega^* = 0.0787 \times 10^{-1}$ N sec $\mathrm{m^{-2}}$.

A comparison of values of the AR of different reflected waves against the angle of incidence θ_0 are represented graphically for micropolar non-free surface i.e. $S_1 = 2,\ S_2 = 1,\ S_3 = 3$ (with the void and without void) and for free surface i.e. $S_1 = S_2 = S_3 = 0$ (with the void and without void).

The graphs are computed as follow:

- For micropolar free surface without voids (MFS) is denoted by the solid line (—).
- For micropolar non-free surface without voids (MNFS) is represented by the small dashed line (---).
- For micropolar free surface with voids (MVFS) is denoted by the solid line with central symbols diamond (-◇-).
- For micropolar non-free surface with voids (MVNFS) is represented by the small dashed line with central symbols circle (--o--).

4.8.1 LD-Wave

Figure 4.2 depicts the variations of $|R_1|$ vs. θ_0. It is evident that the magnitude of $|R_1|$ exhibits an opposite trend for MNFS compared to MVFS and MVNFS, respectively, whereas a steady state behavior of $|R_1|$ is noted for MFS.

The variations of $|R_2|$ vs. θ_0 are illustrated in figure 4.3. The magnitude of $|R_2|$ follow descending trend in the entire interval for MVFS and MVNFS but due to stiffness impact the magnitude of $|R_2|$ is higher for MVNFS.

Figure 4.4 displays the plot of $|R_3|$ vs. θ_0. The behavior of $|R_3|$ is similar across all the cases considered, although notable differences in magnitude. However, the magnitude of $|R_3|$ for MFS is higher compared to remaining cases.

Figure 4.5 clearly shows that the magnitude of $|R_4|$ for MVFS and MFS increase in the first half of the interval and then decrease later. The magnitude of $|R_4|$ remains high for MFS and MNFS compared to MVFS and MVNFS, respectively.

4.8.2 LVVF–Wave

The variations of $|R_1|$ vs. θ_0 are illustrated in figure 4.6. The magnitude of $|R_1|$ decreases for MVNFS and MVFS as θ_0 increases. Additionally, it is noted that magnitude of $|R_1|$ is higher for MVNFS compared to those observed for MVFS.

Figure 4.7 exhibits the variations of $|R_2|$ vs. θ_0. It is seen that the magnitude of $|R_2|$ for MVFS decreases for small values of θ_0 and as θ_0 increases, $|R_2|$ shows an ascending trend for both MVFS & MVNFS. The magnitude of $|R_2|$ for MVNFS is higher compared to MVFS, due to presence of stiffness.

Figure 4.8 shows how $|R_3|$ varies with respect to θ_0. The magnitude of $|R_3|$ exhibits a similar trend for MVFS and MVNFS, initially increasing and reaching its maximum value at $\theta_0 = 45^0$ for MVFS and at $\theta_0 = 15^0$ for MVNFS, respectively, and then decreasing as θ_0 increases.

Figure 4.9 depicts the variations of $|R_4|$ vs. θ_0. It is seen that the values of $|R_4|$ follow the same trend as noted for $|R_3|$, with significant difference in their magnitudes.

4.8.3 CD-I–Wave

Figure 4.10 displays the variations of $|R_1|$ vs. θ_0. The values of $|R_1|$ show an ascending trend for MNFS and MVFS in the first half of interval, and a decreasing trend in latter half. However, due to presence of stiffness, $|R_1|$ for MVNFS shows an increasing trend for the range $0^o \leq \theta_0 \leq 9^o$ and a descending behavior for the rest of the interval. Additionally, $|R_1|$ exhibits an oscillatory behaviour for MFS.

From figure 4.11, it is seen that the values of $|R_2|$ for MVNFS and MVFS follow oscillatory trend in entire interval. However, magnitude of $|R_2|$ is higher MVFS.

Figure 4.12 depicts variations of $|R_3|$ vs. θ_0. The values of $|R_3|$ for MFS and MVNFS exhibit ascending behavior near and far away from boundary and a descending trend in the rest of the interval. However, due to stiffness, reverse trend is noticed for MNFS. It is also seen that, due to void parameter, $|R_3|$ follows an oscillatory behaviour for MVFS.

Figure 4.13 demonstrates that the values of $|R_4|$ follow same trend as noticed for $|R_3|$ but have a significant difference in magnitude.

4.8.4 CD-II-Wave

Figure 4.14 depicts the variations of $|R_1|$ vs. θ_0. It is seen that the magnitude of $|R_1|$ exhibits an increasing trend for MFS and MNFS, whereas an oscillatory behaviour is noticed for MVFS and MVNFS.

Figure 4.15 demonstrates that the magnitude of $|R_2|$ for MVNFS increases near the boundary and reaches the maximum at $\theta_0 = 18^o$, then decreases in the remaining interval. However, an oscillatory trend is noted for MVFS.

Figure 4.16 exhibits the variations of $|R_3|$ vs. θ_0. It is evident that $|R_3|$ follows steady state behaviour for MNFS whereas small variations are noticed for MFS. It is also noticed that the magnitudes of $|R_3|$ follow oscillatory behaviour for MVNFS and MVFS.

Figure 4.17 indicates that the magnitude of $|R_4|$, depicts mirror image throughout the whole range for MFS and MVFS. Additionally, it is noted that magnitude of $|R_4|$ follows a similar trend for MNFS and MVNFS near the boundary and exhibits a reverse trend for rest of the interval.

4.9 Conclusion

In this chapter, we study the reflection of plane waves from a non-free surface in a micropolar elastic material that includes voids. The governing equations are transformed into two-dimensional forms, then dimensionless quantities and potential functions are utilized for further simplifications. The plane wave (LDW or LVVFW or CD-IW or CD-IIW) is incident in the assumed model, resulting in four reflected waves namely LDW, LVVFW, CD-IW, and CD-IIW. The AR of these reflected waves are calculated for both free and non-free surfaces. The impacts of stiffness and void parameters on the AR of various reflected waves are calculated numerically and displayed graphically.

The numerically generated findings yielded the following observations:

(i) The results indicate that due to presence of stiffness, the magnitude of AR corresponding to reflected LDW, CD-IW and CD-IIW are smaller across the entire

range compared to those obtained for free surface, except at certain values of θ_0 when LDW is incident. In contrast, the magnitude of AR of reflected LVVFW exhibits the opposite trend.

(ii) When an LVVFW is incident, it is noted that the AR of the reflected LDW and LVVFW show opposite trends. Furthermore, the AR of the reflected CD-IW and CD-IIW display oscillatory behavior with distinct magnitudes.

(iii) The AR of reflected LDW and LVVFW demonstrate oscillatory behavior, while a opposite trend is observed for the reflected CD-IW and CD-IIW in the cases of MNFS and MVNFS across all angles of incidence. This highlights the influence of void parameters on the AR when CD-IW is incident.

(iv) It has been demonstrated that when CD-IIW is incident, the magnitude of AR for all reflected waves exhibits oscillatory behavior in the cases of MVFS and MVNFS, each with distinct magnitudes.

The above analysis provides a comprehensive understanding of wave boundary interactions in microstructured media, illustrating how variations in boundary constraints (free vs. non-free surfaces) and internal material characteristics such as voids and microrotation significantly influence AR of reflected waves. These insights are crucial for the tailored design of advanced materials and engineered structures in applications where precise control over wave propagation is vital, such as in geophysical exploration and acoustic metamaterials.

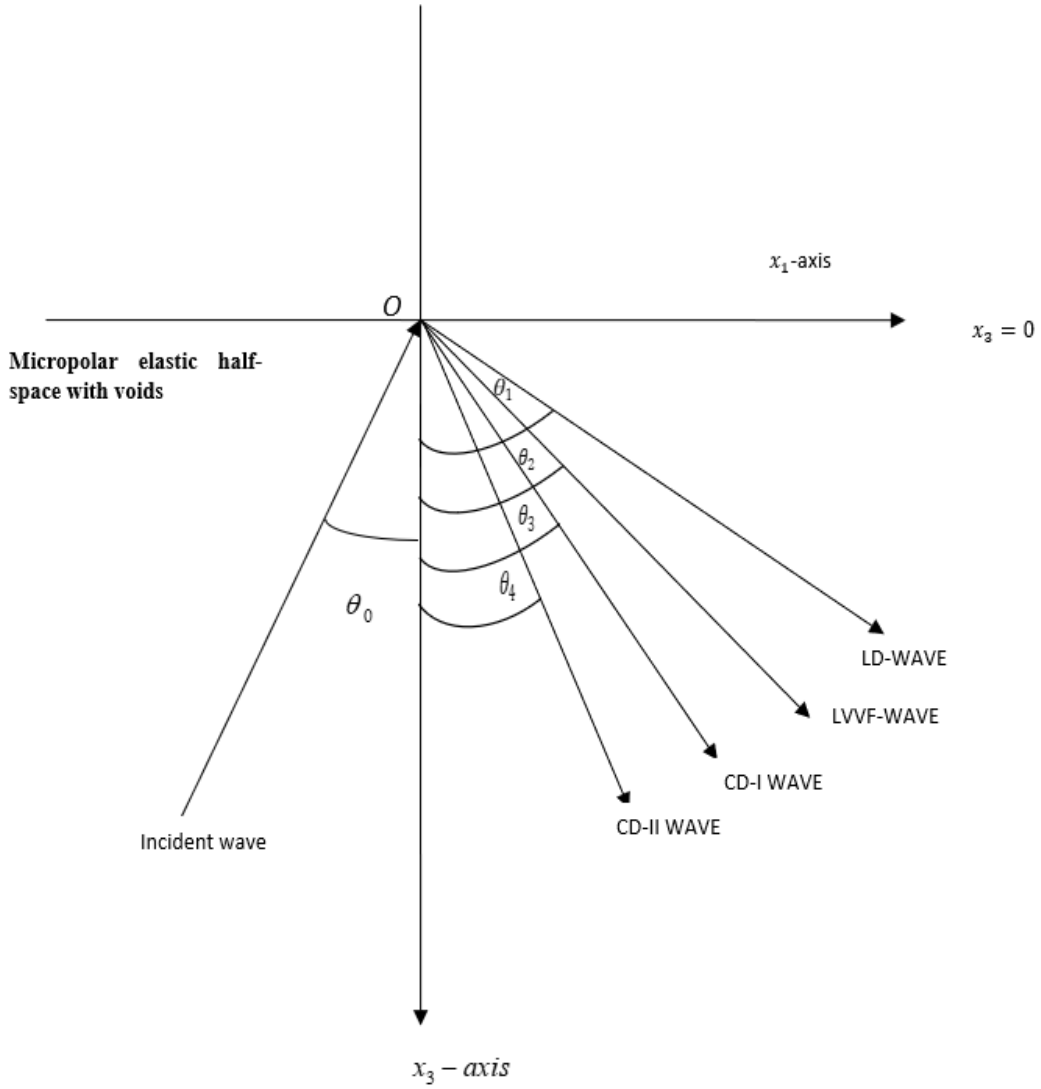

Figure 4.1 Geometry of the problem

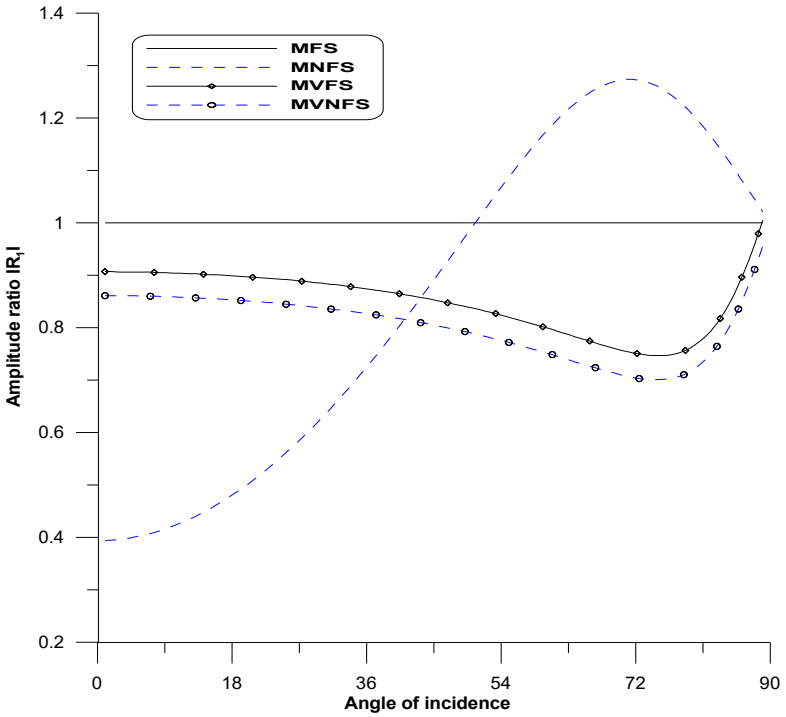

Fig. 4.2: $|R_1|$ vs. θ_0 (LD-wave)

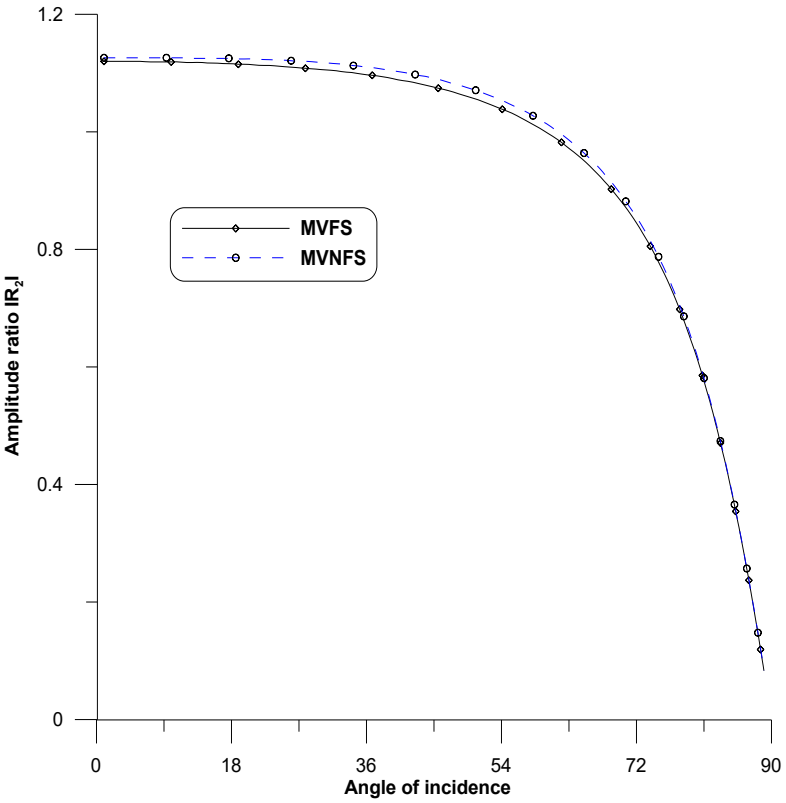

Fig. 4.3: $|R_2|$ vs. θ_0 (LD-wave)

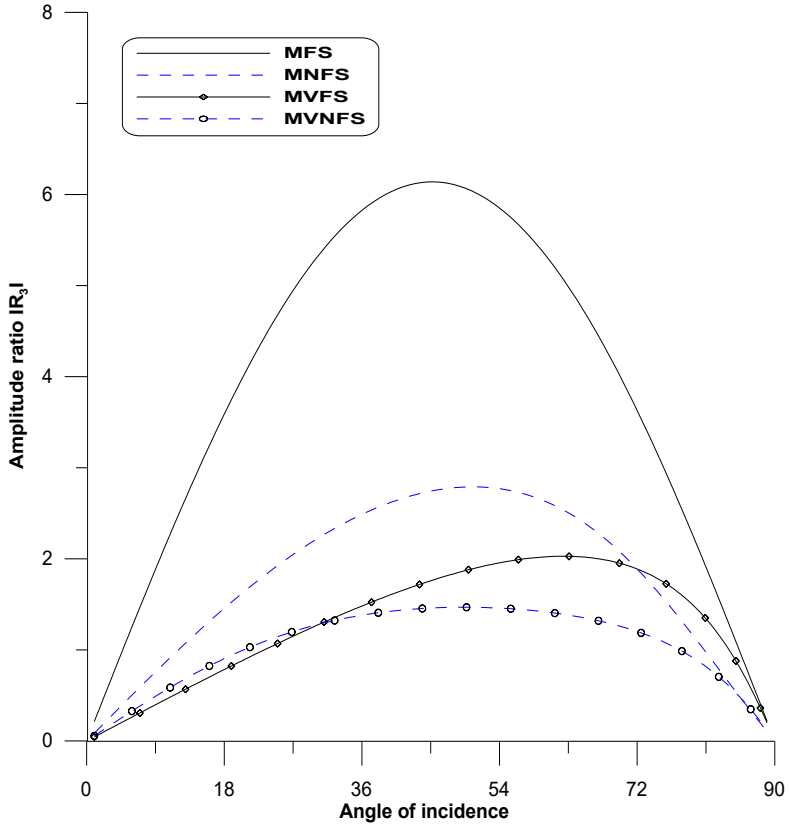

Fig. 4.4: $|R_3|$ vs. θ_0 (LD-wave)

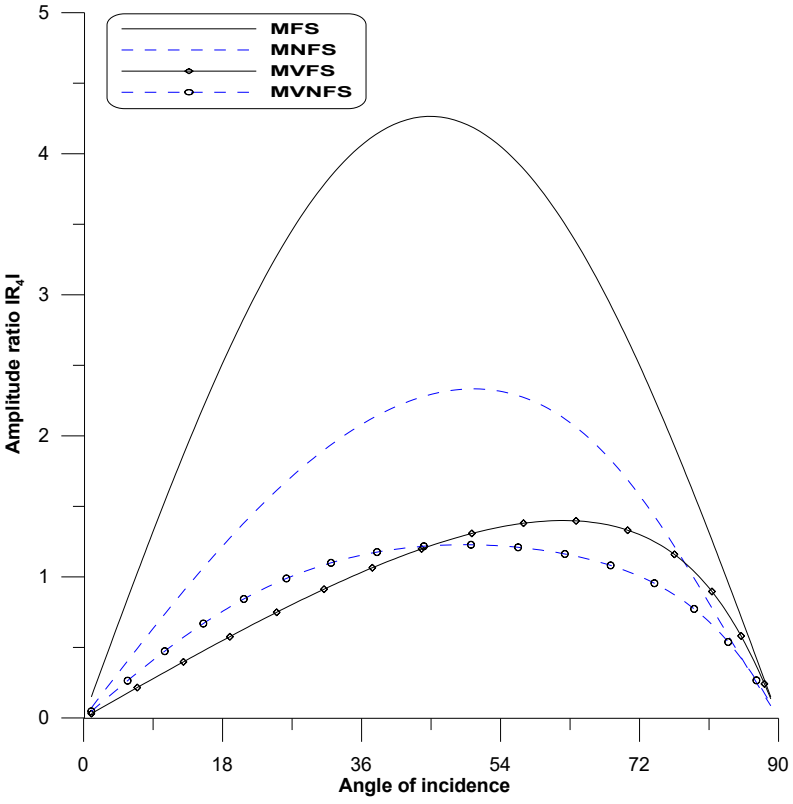

Fig. 4.5: $|R_4|$ vs. θ_0 (LD-wave)

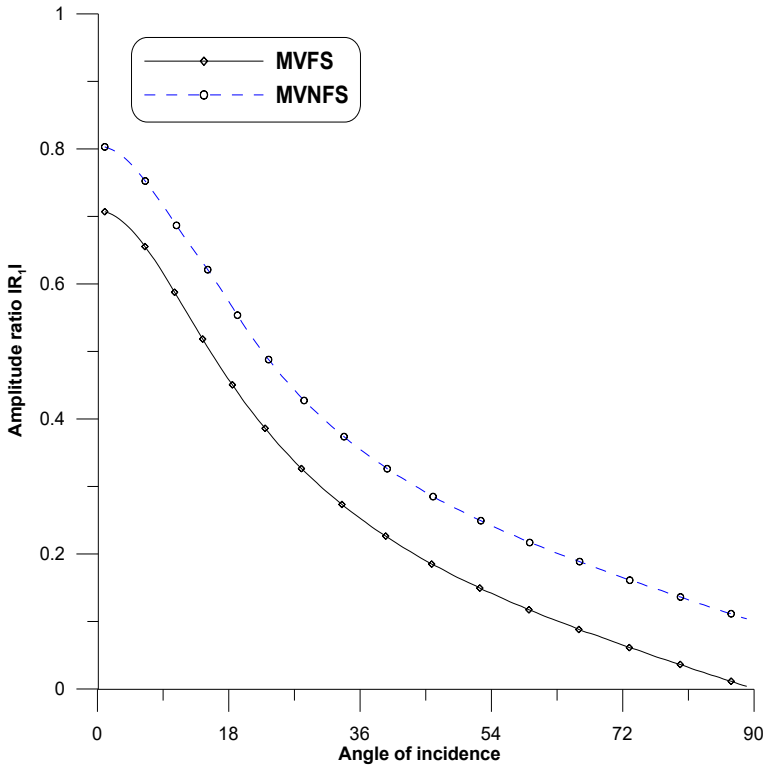

Fig. 4.6: $|R_1|$ vs. θ_0 (LVVF-wave)

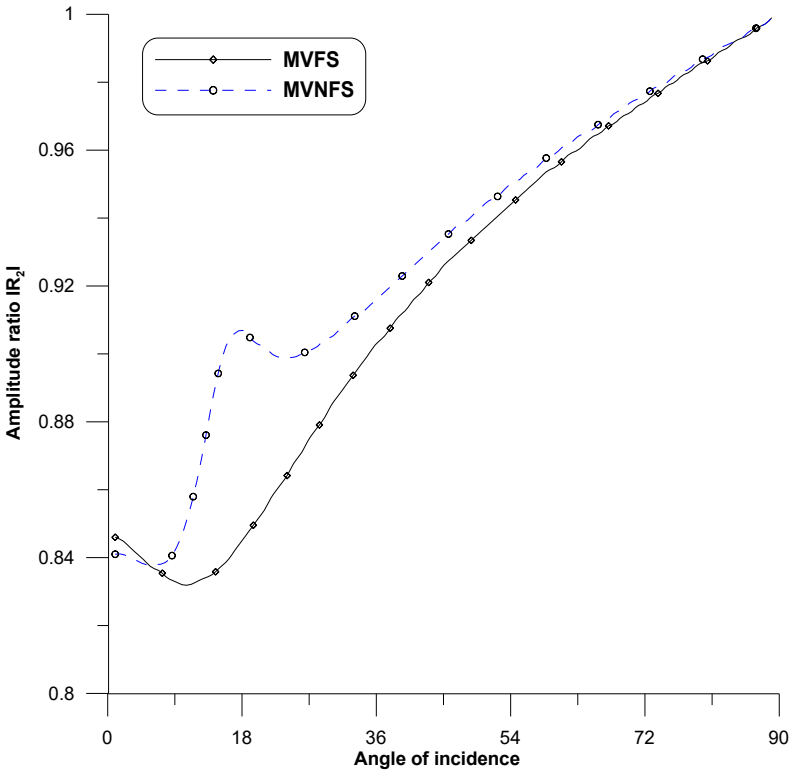

Fig. 4.7: $|R_2|$ vs. θ_0 (LVVF-wave)

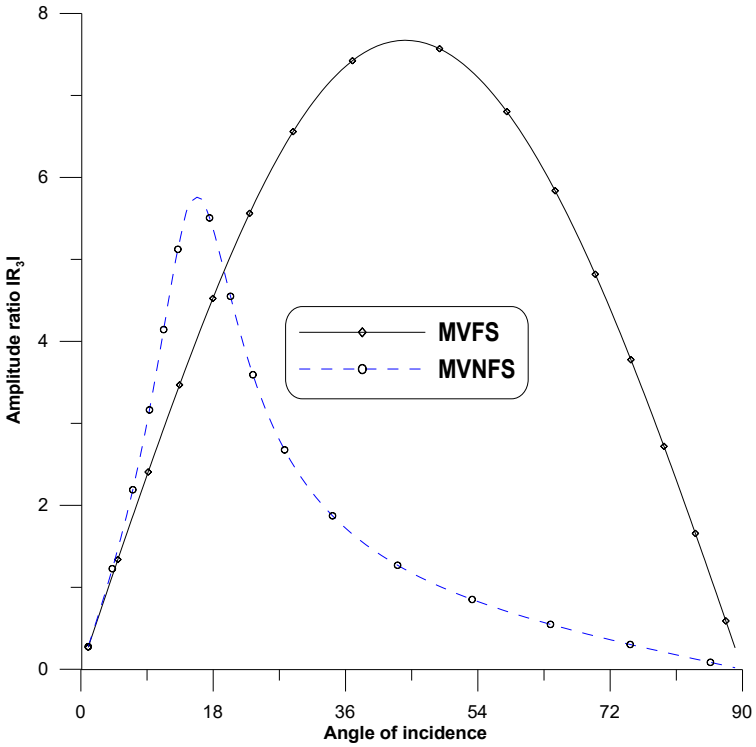

Fig. 4.8: $|R_3|$ vs. θ_0 (LVVF-wave)

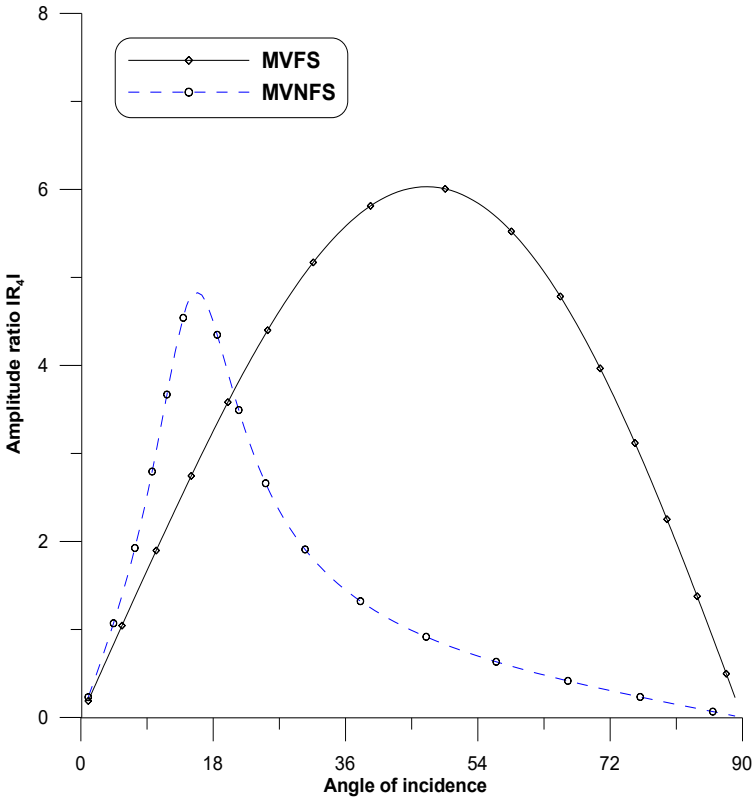

Fig. 4.9: $|R_4|$ vs. θ_0 (LVVF-wave)

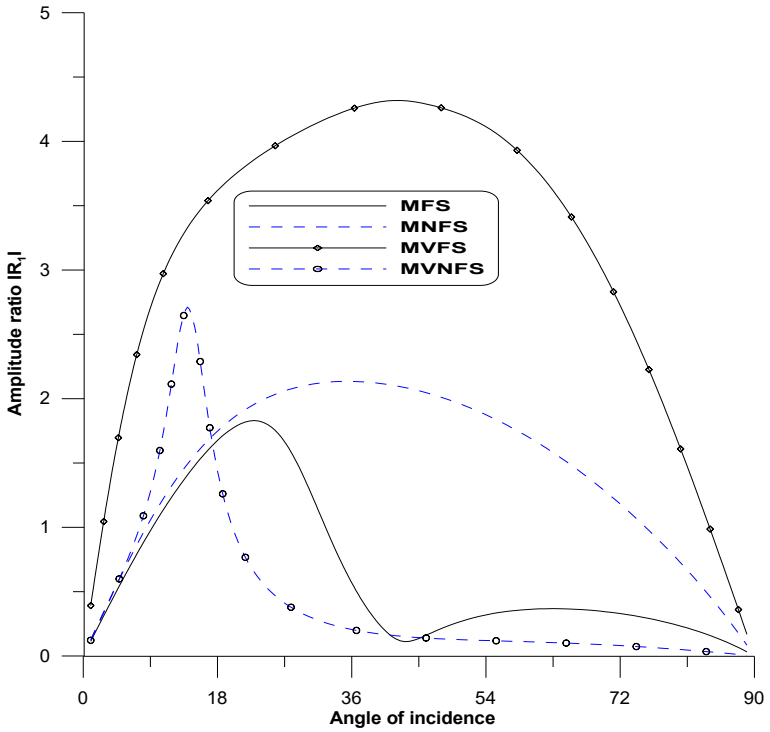

Fig. 4.10:$|R_1|$ vs. θ_0
(CD-I wave)

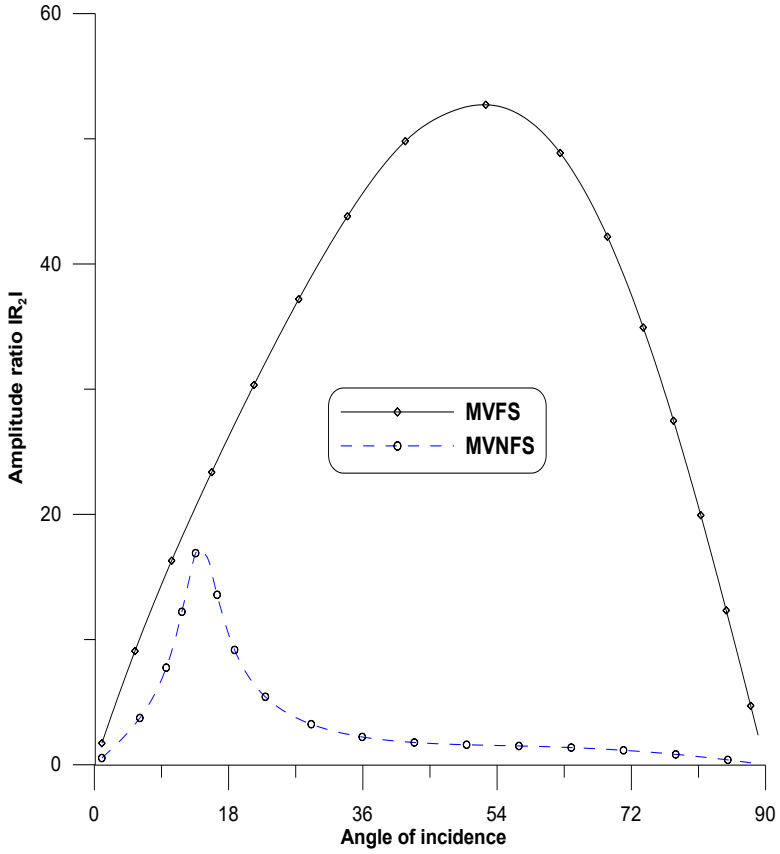

Fig. 4.11:$|R_2|$ vs. θ_0
(CD-I wave)

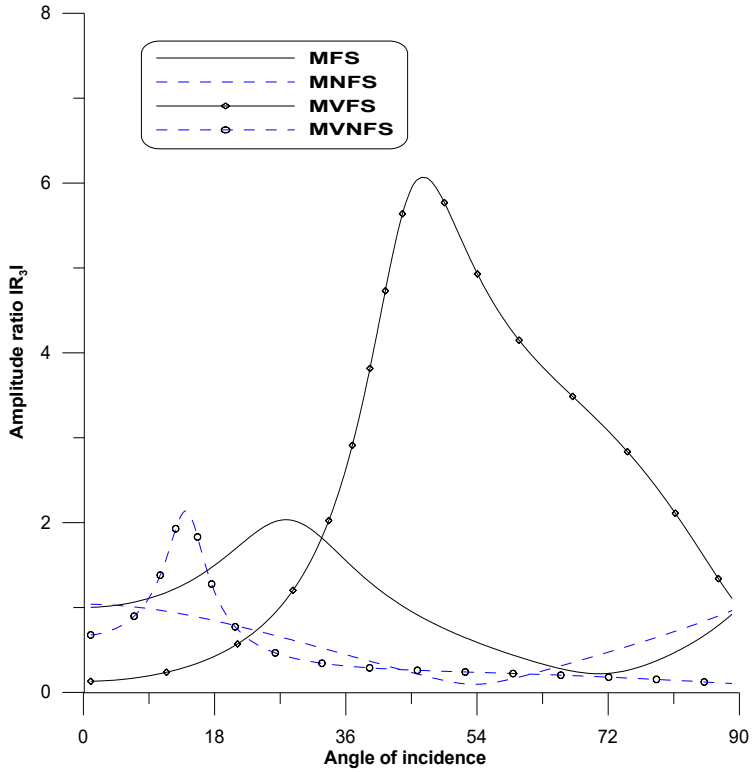

Fig. 4.12:$|R_3|$ vs. θ_0
(CD-I wave)

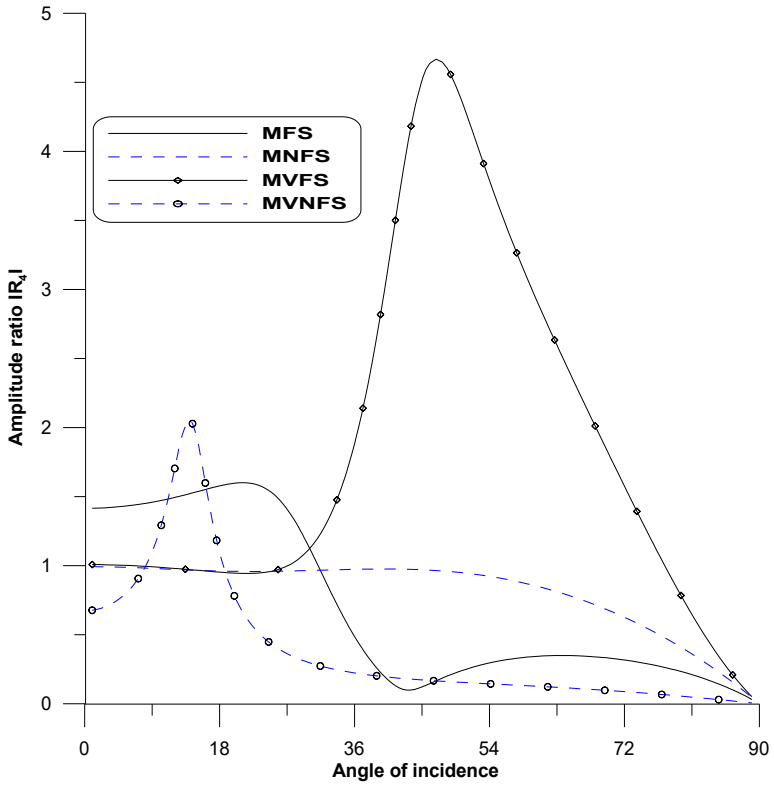

Fig. 4.13: $|R_4|$ vs. θ_0
(CD-I wave)

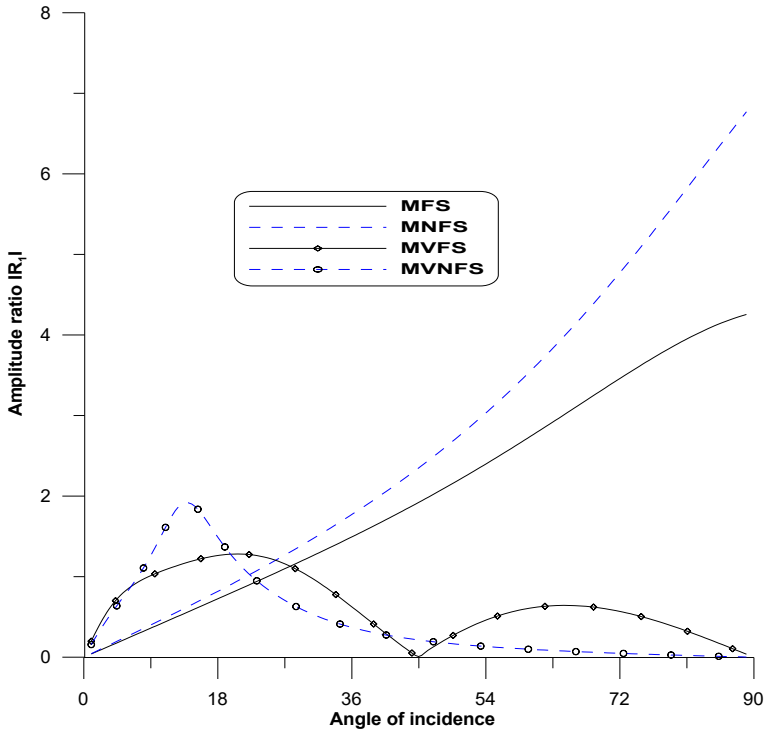

Fig. 4.14: $|R_1|$ vs. θ_0
(CD-II wave)

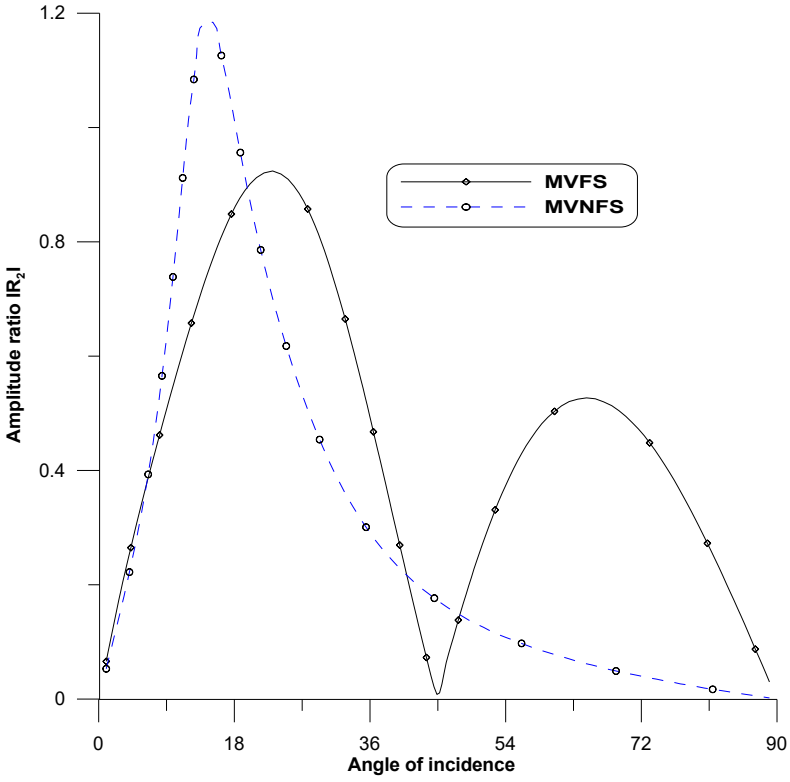

Fig. 4.15: $|R_2|$ vs. θ_0
(CD-II wave)

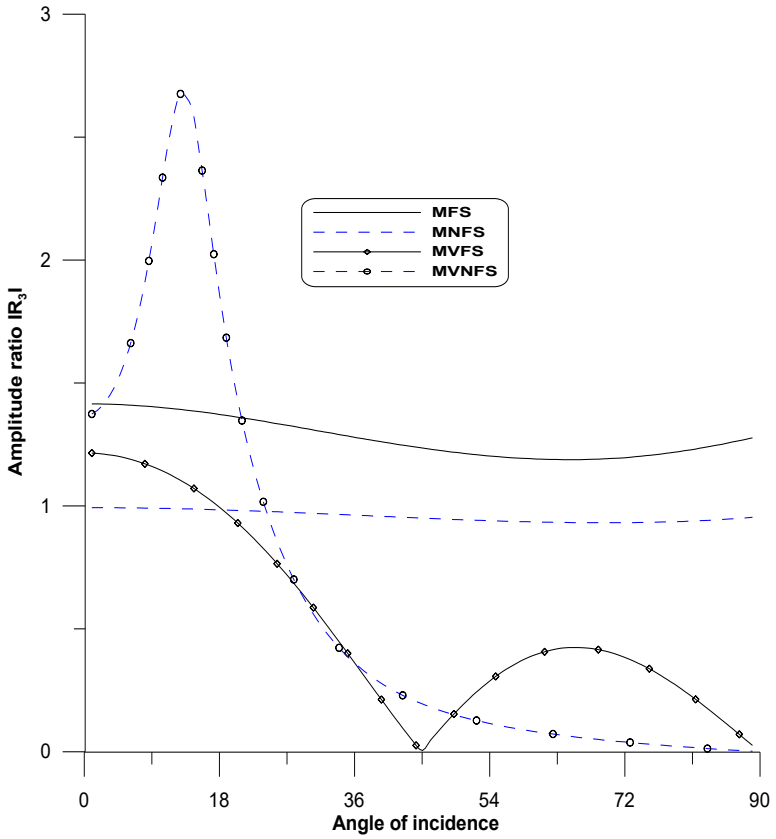

Fig. 4.16: $|R_3|$ vs. θ_0
(CD-II wave)

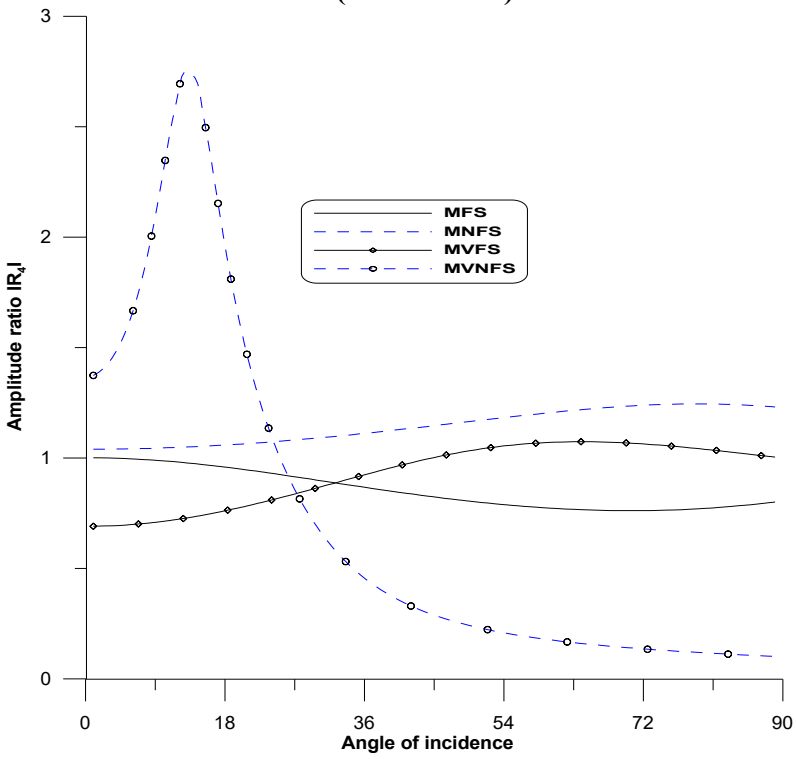

Fig. 4.17: $|R_4|$ vs. θ_0
(CD-II wave)

Chapter 5

Deformation induced by normal force and thermal source within the micropolar Moore-Gibson-Thompson theory of thermoelasticity, considering hyperbolic two-temperature and non-local effects

The work from this chapter has been published in the form of research papers entitled as "Mathematical modelling of micropolar thermoelastic problem with nonlocal and hyperbolic two-temperature based on Moore–Gibson–Thompson heat equation", Canadian Journal of Physics, 101(11), 2023, https://doi.org/10.1139/cjp-2022-0339.

Indexing: SCI, Scopus, Impact Factor: 1.2

Chapter 5

Deformation induced by normal force and thermal source within the micropolar Moore-Gibson-Thompson theory of thermoelasticity, considering hyperbolic two-temperature and non-local effects

5.1 Introduction

Sharma (2011) [134] examined the deformation caused by an inclined load in a generalized thermoelastic diffusive media. Abouelregal (2020) [2] used non-local (N-L) theory of thermoelasticity with higher-order time derivatives and two-phase lags to study thermoelastic interactions in a N-L medium subjected to a magnetic field and periodic heat source. Marin et al. (2020) [103] proposed a domain of impact theorem for the combined initial-boundary value problem in Moore-Gibson-Thompson (MGT) thermoelasticity theory for dipole bodies. Sharma and Khator (2021 [144], 2022 [145]) investigated issues related to power generation from renewable sources and also explored micro-grid planning in the renewable-inclusive prosumer market.

Abouelregal et al. (2022) [12] performed a computational study on a N-L isotropic magneto-thermoelastic semi-space influenced by a periodically varying heat source, utilizing the MGT heat equation. Kumar et al. (2022) [86] developed a novel model to estimate the response of thermomechanical and carrier density loading in an anisotropic photothermoelastic plate. They obtained the displacement components, stresses, temperature distribution, and carrier density distribution. Kumar et al. (2023) [80] calculated physical quantities such as displacements, stresses, conductive temperature, and thermodynamic temperature using the MGT theory of thermoelasticity in the presence of thermal load and normal distributed force, as well as a moving heat source, and studied the impacts of hyperbolic two-temperature (HTT) and N-L on the results.

Abouelregal et al. (2023) [10] used the normal mode analysis approach to study the effects of the higher-order derivatives and Hall current on tangential couple stress, temperature, stresses, and displacements in an electromagnetic micropolar thermoelastic (MT) medium with surface heating and a transverse magnetic field. Abouelregal et al. (2024) [7] utilized a memory-based derivative in conjunction with the MGT equation to examine the viscoelastic properties of materials. They analyzed the materials' response to external loads and deformations over time, using a non-Gaussian laser radiation heat source at the boundary.

In this chapter, a two-dimensional deformation problem in homogeneous, isotropic MT half-space has been presented under the framework of the MGT heat equation, incorporating N-L and HTT parameters. The governing equations are converted into dimensionless form, and potential functions are used to simplify further under thermomechanical conditions. The problem is addressed using the Laplace transform (L.T) with respect to (w.r.t) the time variable t and the Fourier transform (F.T) w.r.t the space variable x_1. Physical quantities such as displacement components, force stresses, tangential couple stress, conductive temperature and thermodynamic temperature, are computed in the transformed domain using specified normal force and thermal source conditions at the boundary surface. These values are then retrieved in the original domain through a numerical inversion technique. Graphical representations exhibit the influence of HTT, N-L and two-temperature (TT) parameters on these quantities. Certain cases of interest are also discussed.

The impetus for this study arises from the well-known shortcomings of classical thermoelastic theories, which fall short in capturing essential microstructural effects and the finite propagation speed of thermal disturbances. As materials and systems increasingly operate at micro and nano scales, these shortcomings become critical. The motivation behind the study is to develop a more realistic and unified theoretical framework that can accurately capture the coupled thermo-mechanical behavior of advanced materials where microrotation and N-L interactions are prominent. The novelty of this work is reflected in its integration of N-L effects and HTT within a micropolar continuum framework an approach that significantly enriches generalized thermoelasticity. By addressing both mechanical and thermal loading, this study provides a more comprehensive foundation for analyzing stress-thermal interactions in micro-engineered environments, where traditional models fall short.

5.2 Fundamental Equations

The field equations and constitutive relations for micropolar thermoelasticity under MGT heat equation, incorporating N-L and HTT effects, after excluding body couples, body forces, and heat sources, are provided in equations (3.1) - (3.6) [Chapter 3]. All symbols, including $\mathbf{u}, \boldsymbol{\phi}, T, \varphi, \beta, \gamma, K, \rho, \mu, \hat{\jmath}, K^*, K_1^*, \gamma_1, C_e, t, t_{pq}, \lambda, \alpha, m_{pq}, \tau_0, \beta^*, T_0, \xi_1, \xi_2, \delta_{pq}, \varepsilon_{pqh}, \Delta, \nabla$ are as defined in section 2.2 [Chapter 2] and in section 3.2 [Chapter 3].

5.3 Statement of the Problem

In the context of the MGT heat equation, we examine a domain of isotropic, homogeneous MT solid semi-space is examined w.r.t N-L and HTT effects. We use a rectangular Cartesian coordinate system (x_1, x_2, x_3), with the origin located at the plane boundary at $x_3 = 0$. The x_3-axis is oriented vertically downward into the medium. The semi-space is subjected to normal force and a thermal source at the stress-free boundary. If we confine our analysis to a plane strain problem parallel to x_1x_3- plane, the field variables are dependent on x_1, x_3 and t.

In two-dimensional problem, displacement components, microrotational components, thermodynamic temperature and conductive temperature are taken as given by equation (3.21) [Chapter 3].

After using equation (3.21) in equations (3.7) -(3.13), (3.16), (3.17) [Chapter 3], (2.23) [Chapter 2] and (3.20) [Chapter 3] yield the equations (3.22) -(3.29) [Chapter 3]. Therefore, for further simplification, we use equations (3.22) -(3.29) [Chapter 3].

Following dimensionless quantities are taken, in addition to dimensionless quantities given by (3.30) [Chapter 3]

$$F'_{10} = \frac{1}{\gamma_1 T_0} F_{10}, \qquad F'_{20} = \frac{c_1}{\omega_1 T_0} F_{20}. \tag{5.1}$$

Using (3.30) [Chapter 3] in equations (3.22) -(3.29) after suppressing the primes, we get the resulting equations [(3.32) -(3.39)] [Chapter 3],

and, $a_i (i = 1 \cdots 7)$ are as given by equation (2.42) [Chapter 2] and $a_i (i = 8 \cdots 15)$ are as given by equation (3.40) [Chapter 3].

5.4 Solution Procedure

Relation between displacement components and scalar potentials is same as given in equation (2.43) [Chapter 2].

Applying (2.43) on equations (3.32) -(3.35) [Chapter 3], yield

$$\Delta q - a_4 T = \left(1 - {\xi_1}^2 \Delta\right) \frac{\partial^2 q}{\partial t^2}, \tag{5.2}$$

$$a_2 \Delta\psi + a_3 \phi_2 = \left(1 - {\xi_1}^2 \Delta\right) \frac{\partial^2 \psi}{\partial t^2}, \tag{5.3}$$

$$a_5 \Delta\phi_2 - a_6 \Delta\psi - a_7 \phi_2 = \left(1 - {\xi_2}^2 \Delta\right) \frac{\partial^2 \phi_2}{\partial t^2}, \tag{5.4}$$

$$\frac{\partial}{\partial t} \Delta\varphi + a_8 \Delta\varphi = \left(1 + \tau_0 \frac{\partial}{\partial t}\right) \left(\frac{\partial^2 T}{\partial t^2} + a_9 \frac{\partial^2}{\partial t^2} \Delta q\right). \tag{5.5}$$

According to Debnath (1995) [28], the L.T of a function $g(x_1, x_3, t)$ w.r.t time variable t, where s is the L.T variable, is defined as follows, with its essential properties:

$$\bar{g}(x_1, x_3, s) = L\{g(x_1, x_3, t)\} = \int_0^\infty g(x_1, x_3, t) \exp(-st)\, dt, \tag{5.6}$$

$$\text{i) } L\left(\frac{\partial g}{\partial t}\right) = s\bar{g}(x_1, x_3, s) - g(x_1, x_3, 0), \tag{5.7}$$

$$\text{ii) } L\left(\frac{\partial^2 g}{\partial t^2}\right) = s^2\bar{g}(x_1, x_3, s) - sg(x_1, x_3, 0) - \left(\frac{\partial g}{\partial t}\right)_{t=0}. \tag{5.8}$$

Initial conditions are as follows:

$$u_1(x_1, x_3, 0) = \left(\frac{\partial u_1}{\partial t}\right)_{t=0} = 0, \qquad u_3(x_1, x_3, 0) = \left(\frac{\partial u_3}{\partial t}\right)_{t=0} = 0,$$

$$q(x_1, x_3, 0) = \left(\frac{\partial q}{\partial t}\right)_{t=0} = 0, \qquad T(x_1, x_3, 0) = \left(\frac{\partial T}{\partial t}\right)_{t=0} = 0,$$

$$\psi(x_1, x_3, 0) = \left(\frac{\partial \psi}{\partial t}\right)_{t=0} = 0, \qquad \varphi(x_1, x_3, 0) = \left(\frac{\partial \varphi}{\partial t}\right)_{t=0} = 0,$$

$$\phi_2(x_1, x_3, 0) = \left(\frac{\partial \phi_2}{\partial t}\right)_{t=0} = 0, \tag{5.9}$$

and the regularity conditions are

$$q(x_1, x_3, t) = u_3(x_1, x_3, t) = T(x_1, x_3, t) = \psi(x_1, x_3, t) = u_1(x_1, x_3, t) = 0,$$

$$\phi_2(x_1, x_3, t) = \varphi(x_1, x_3, t) = 0, \text{ for } t > 0, x_3 \to \infty. \tag{5.10}$$

Following Sneddon (1975) [156], Fourier transform (F.T) of a function $\bar{g}(x_1, x_3, s)$ w.r.t space variable x_1 is defined as

$$\hat{g}(\xi, x_3, s) = \int_{-\infty}^{\infty} \bar{g}(x_1, x_3, s) \exp(i\xi x_1)\, dx_1. \tag{5.11}$$

Appling L.T and F.T defined by equations (5.6) and (5.11) on equations (5.2) -(5.5) and (3.39) [Chapter 3], with aid of equations (5.7) -(5.9), yield

$$[(D^2 - \xi^2) - (1 - \xi_1^2(D^2 - \xi^2))s^2]\hat{q} - a_4\hat{T} = 0, \tag{5.12}$$

$$[a_2(D^2 - \xi^2) - (1 - \xi_1^2(D^2 - \xi^2))s^2]\hat{\psi} + a_3\hat{\phi}_2 = 0, \tag{5.13}$$

$$[a_5(D^2 - \xi^2) - a_7 - (1 - \xi_2^2(D^2 - \xi^2))s^2]\hat{\phi}_2 - a_6(D^2 - \xi^2)\hat{\psi} = 0, \tag{5.14}$$

$$[(D^2 - \xi^2)(s + a_8)]\hat{\varphi} - (1 + \tau_0 s)s^2\hat{T} - a_9(1 + \tau_0 s)s^2(D^2 - \xi^2)\hat{q} = 0, \tag{5.15}$$

$$\hat{T} = \hat{\varphi} - \varsigma(D^2 - \xi^2)\hat{\varphi}, \tag{5.16}$$

where

$$\varsigma = \begin{cases} \frac{\beta^*}{s^2}, & \text{for (HTT)} \\ a, & \text{for two temperature (TT)} \\ 0, & \text{for one temperature (1T)}, \end{cases}$$

and

$D = \frac{d}{dx_3}$.

Using equation (5.16) in equations (5.12) and (5.15), yield

$$[(D^2 - \xi^2) - (1 - \xi_1^2(D^2 - \xi^2))s^2]\hat{q} - a_4\big(1 - \varsigma(D^2 - \xi^2)\big)\hat{\varphi} = 0, \quad (5.17)$$

$$[(D^2 - \xi^2)(s + a_8)]\hat{\varphi} - (1 + \tau_0 s)s^2(1 - \varsigma(D^2 - \xi^2))\,\hat{\varphi}$$
$$-a_9(1 + \tau_0 s)s^2(D^2 - \xi^2)\hat{q} = 0, \quad (5.18)$$

After algebraic simplifications, equations (5.17), (5.18) (5.13) and (5.14), yield

$$(D^4 - P_{01}D^2 + P_{02})(\hat{q}, \hat{\varphi}) = 0, \quad (5.19)$$

$$(D^4 - P_{03}D^2 + P_{04})(\hat{\phi}_2, \hat{\psi}) = 0, \quad (5.20)$$

where

$$P_{01} = \frac{P_{15}P_{17} + \xi^2 P_{15}P_{16} + (1+\tau_0 s)s^2(1+\xi^2\varsigma)P_{18} + (1+\tau_0 s)s^2\varsigma P_{19}}{P_{15}P_{16} + (1+\tau_0 s)s^2\varsigma P_{18}}, \qquad P_{02} = \frac{P_{15}P_{17}\xi^2 + (1+\tau_0 s)s^2(1+\xi^2\varsigma)P_{19}}{P_{15}P_{16} + (1+\tau_0 s)s^2\varsigma P_{18}},$$

$$P_{03} = \frac{P_{13}P_{12} + P_{11}P_{14} - a_3 a_6}{P_{13}P_{14}}, \qquad P_{04} = \frac{P_{11}P_{12} - a_3 a_6 \xi^2}{P_{13}P_{14}},$$

$$P_{11} = a_5\xi^2 + a_7 + s^2(1 + \xi^2\xi_2^2), \quad P_{12} = a_2\xi^2 + s^2(1 + \xi^2\xi_1^2), \quad P_{13} = a_5 + s^2\xi_2^2,$$

$$P_{14} = a_2 + s^2\xi_1^2, \quad P_{15} = a_8 + s, \quad P_{16} = 1 + {\xi_1}^2 s^2, \quad P_{17} = \xi^2 + s^2(1 + \xi^2\xi_1^2),$$

$$P_{18} = 1 + {\xi_1}^2 s^2 + a_4 a_9, \quad P_{19} = \xi^2\big(1 + {\xi_1}^2 s^2 + a_4 a_9\big) + s^2.$$

The bounded solution of equations (5.19) and (5.20), satisfying the regularity conditions given by (5.10) are

$$\hat{q} = \sum_{i=1}^{2} (K_i e^{-\lambda_i x_3}), \quad (5.21)$$

$$\hat{\varphi} = \sum_{i=1}^{2} (l_i K_i e^{-\lambda_i x_3}), \quad (5.22)$$

$$\hat{\psi} = \sum_{j=3}^{4} (K_j e^{-\lambda_j x_3}), \quad (5.23)$$

$$\hat{\phi}_2 = \sum_{j=3}^{4} (m_j K_j e^{-\lambda_j x_3}), \quad (5.24)$$

where the roots of characteristic equations $(D^4 - P_{01}D^2 + P_{02}) = 0$, and $(D^4 - P_{03}D^2 + P_{04}) = 0$ are $\pm\lambda_i (i = 1,2)$ and $\pm\lambda_j$ $(j = 3,4)$, respectively. Arbitrary constants K_i $(i = 1,2)$ and $K_j (j = 3,4)$, as well as coupling constants l_i $(i = 1,2)$ and m_j $(j = 3,4)$, can be represented as follows:

$$l_i = \frac{(1+\xi_1^2 s^2)(\lambda_i^2 - \xi^2) - s^2}{a_4(1 + \varsigma\xi^2 - \varsigma\lambda_i^2)}, \quad m_j = \frac{s^2\big(1 + \xi^2\xi_1^2 - \xi_1^2\lambda_j^2\big) - a_2(\lambda_j^2 - \xi^2)}{a_3}, \quad (i = 1,2), (j = 3,4).$$

5.5 Boundary Restrictions

A normal force and thermal source are applied to the boundary surface of an MT half-space at $x_3 = 0$. The normal force is concentrated in spatial coordinates and distributed over time, while the thermal source is concentrated in time and distributed in spatial coordinates. Tangential force stress and tangential couple stress are set to zero. These can be stated mathematically as follows:

$$\text{(i) } t_{33} = F_1(x_1, t), \quad \text{(ii) } t_{31} = 0, \quad \text{(iii) } m_{32} = 0, \quad \text{(iv)} \frac{\partial \varphi}{\partial x_3} = F_2(x_1, t), \tag{5.25}$$

where

$$F_1(x_1, t) = F_{10} \begin{cases} \delta(x_1) \sin \frac{\pi t}{\eta}, & 0 \le t \le \eta \\ 0, & t > \eta \end{cases}, \qquad F_2(x_1, t) = F_{20} H(x_1) e^{-b x_1} \delta(t), \tag{5.26}$$

additionally, $\delta(\,)$ represents the Dirac-delta, b is a constant, H () denotes the Heaviside step function, F_{10} is magnitude of the force, and F_{20} is a constant temperature applied at the boundary surface.

Applying the dimensionless quantities given by equations (3.30) [Chapter 3] and (5.1) in equations (5.25) and (5.26), yield the non-dimensional boundary condition and after applying L.T and F.T determine,

$$\text{(i) } \hat{t}_{33} = \hat{F}_1(\xi, s), \qquad \text{(ii) } \hat{t}_{31} = 0,$$

$$\text{(iii) } \hat{m}_{32} = 0\,, \qquad \text{(iv) } \frac{\partial \hat{\varphi}}{\partial x_3} = \hat{F}_2(\xi, s), \tag{5.27}$$

where

$$\hat{F}_1(\xi, s) = F_{10} \frac{(1 + e^{-\eta s})\pi\eta}{\pi^2 + s^2\eta^2}, \qquad \hat{F}_2(\xi, s) = F_{20} \frac{1}{s(b - i\xi)}. \tag{5.28}$$

After applying L.T and F.T defined by (5.6) and (5.11) in equations (2.43) [Chapter 2], (3.36)-(3.38) [Chapter 3] and with aid of equation (5.16), yield

$$\hat{u}_1 = -\iota\xi\hat{q} - \frac{d\hat{\psi}}{dx_3}, \tag{5.29}$$

$$\hat{u}_3 = \frac{d\hat{q}}{dx_3} - \iota\xi\hat{\psi}, \tag{5.30}$$

$$\hat{t}_{33} = -\iota\xi a_{13}\hat{u}_1 + a_{14}\frac{d\hat{u}_3}{dx_3} - (1 - \varsigma(D^2 - \xi^2))\hat{\varphi}, \tag{5.31}$$

$$\hat{t}_{31} = (a_{10} + a_{11})\frac{d\hat{u}_1}{dx_3} + \iota\xi\, a_{10}\hat{u}_3 - a_{12}\hat{\phi}_2, \tag{5.32}$$

$$\hat{m}_{32} = a_{15}\frac{d\hat{\phi}_2}{dx_3}. \tag{5.33}$$

Inserting the values of $\hat{q}, \hat{\varphi}, \hat{\psi}, \hat{\phi}_2$ from (5.21) -(5.24) in the transformed boundary condition (5.27) with the aid of equations (5.29) -(5.33), yield the desired expressions as

$$\hat{u}_1 = \frac{1}{\Delta_1}[\sum_{i=1}^{2}(-\iota\xi(\Delta_{i1}\hat{F}_1(\xi,s) + \Delta_{i2}\hat{F}_2(\xi,s))e^{-\lambda_i x_3}) + \sum_{i=3}^{4}(\lambda_i(\Delta_{i1}\hat{F}_1(\xi,s) + \Delta_{i2}\hat{F}_2(\xi,s))e^{-\lambda_i x_3})], \quad (5.34)$$

$$\hat{u}_3 = \frac{1}{\Delta_1}[\sum_{i=1}^{2}(-\lambda_i(\Delta_{i1}\hat{F}_1(\xi,s) + \Delta_{i2}\hat{F}_2(\xi,s))e^{-\lambda_i x_3}) + \sum_{i=3}^{4}(-\iota\xi(\Delta_{i1}\hat{F}_1(\xi,s) + \Delta_{i2}\hat{F}_2(\xi,s))e^{-\lambda_i x_3})], \quad (5.35)$$

$$\hat{t}_{33} = \frac{1}{\Delta_1}\left[\sum_{i=1}^{4}(H_{i+4}(\Delta_{i1}\hat{F}_1(\xi,s) + \Delta_{i2}\hat{F}_2(\xi,s))e^{-\lambda_i x_3})\right], \quad (5.36)$$

$$\hat{t}_{31} = \frac{1}{\Delta_1}\left[\sum_{i=1}^{4}(H_i(\Delta_{i1}\hat{F}_1(\xi,s) + \Delta_{i2}\hat{F}_2(\xi,s))e^{-\lambda_i x_3})\right], \quad (5.37)$$

$$\hat{m}_{32} = \frac{1}{\Delta_1}\left[\sum_{i=3}^{4}(H_{i+6}(\Delta_{i1}\hat{F}_1(\xi,s) + \Delta_{i2}\hat{F}_2(\xi,s))e^{-\lambda_i x_3})\right], \quad (5.38)$$

$$\hat{\varphi} = \frac{1}{\Delta_1}\left[\sum_{i=1}^{2}(l_i(\Delta_{i1}\hat{F}_1(\xi,s) + \Delta_{i2}\hat{F}_2(\xi,s))e^{-\lambda_i x_3})\right], \quad (5.39)$$

$$\hat{T} = \frac{1}{\Delta_1}\left[\sum_{i=1}^{2}(H_{i+10}(\Delta_{i1}\hat{F}_1(\xi,s) + \Delta_{i2}\hat{F}_2(\xi,s))e^{-\lambda_i x_3})\right], \quad (5.40)$$

where

$\Delta_1 = TH_1 + TH_2$, $\Delta_{11} = \lambda_2 l_2(H_4H_9 - H_3H_{10})$,

$\Delta_{12} = H_9(H_4H_6 - H_2H_8) - H_{10}(H_3H_6 - H_2H_7)$,

$\Delta_{21} = -\lambda_1 l_1(H_4H_9 - H_3H_{10})$, $\Delta_{22} = -H_9(H_4H_5 - H_1H_8) + H_{10}(H_3H_5 - H_1H_7)$,

$\Delta_{31} = -H_{10}(\lambda_1 l_1 H_1 - \lambda_2 l_2 H_2)$, $\Delta_{32} = -H_{10}(H_1H_6 - H_2H_5)$,

$\Delta_{41} = -H_9(\lambda_1 l_1 H_2 - \lambda_2 l_2 H_1)$, $\Delta_{42} = H_9(H_1H_6 - H_2H_5)$,

$TH_1 = -\lambda_1 l_1[H_9(H_4H_6 - H_2H_8) - H_{10}(H_3H_6 - H_2H_7)]$,

$TH_2 = \lambda_2 l_2[H_9(H_4H_5 - H_1H_8) - H_{10}(H_3H_5 - H_1H_7)]$, $H_i = \iota\xi\lambda_i(2a_{10} + a_{11})$,

$H_j = -a_{10}(\xi^2 + \lambda_j^2) - a_{11}\lambda_j^2 - a_{12}m_j$, $H_{i+4} = -\xi^2 a_{13} + \lambda_i^2 a_{14} - l_i(1 + \varsigma(\xi^2 - \lambda_i^2))$,

$H_{j+4} = -\iota\xi\lambda_j(a_{13} - a_{14})$, $H_{j+6} = -a_{15}\lambda_j m_j$,

$H_{i+10} = l_i(1 + \varsigma(\xi^2 - \lambda_i^2))$, $(i = 1 - 2), (j = 3 - 4)$,

and, $\hat{F}_1(\xi, s)$ and $\hat{F}_2(\xi, s)$ are given by equation (5.28).

5.6 Validations

i) By considering $\alpha = \beta = \gamma = K = 0$ along with $\xi_2 = 0$, the equations (5.19) - (5.20) reduces as

$$(D^4 - P_{01}D^2 + P_{02})(\hat{q}, \hat{\varphi}) = 0, \tag{5.41}$$

$$(D^2 - \lambda_3^2)\hat{\psi} = 0, \tag{5.42}$$

with changed values of

$P_{01} = \frac{P_{15}P_{17}+\xi^2 P_{15}P_{16}+(1+\tau_0 s)s^2(1+\xi^2\varsigma)P_{18}+(1+\tau_0 s)s^2\varsigma P_{19}}{P_{15}P_{16}+(1+\tau_0 s)s^2\varsigma P_{18}}$, $P_{02} = \frac{P_{15}P_{17}\xi^2+(1+\tau_0 s)s^2(1+\xi^2\varsigma)P_{19}}{P_{15}P_{16}+(1+\tau_0 s)s^2\varsigma P_{18}}$,

$P_{15} = a_4 + s$, $P_{18} = 1 + {\xi_1}^2 s^2 + a_3 a_5$, $P_{19} = \xi^2(1 + {\xi_1}^2 s^2 + a_3 a_5) + s^2$,

$\lambda_3^2 = \frac{(a_2\xi^2+s^2(1+{\xi_1}^2\xi^2))}{a_2+{\xi_1}^2 s^2}$, $a_2 = \frac{\mu}{\rho c_1^2}$, $a_3 = \frac{\gamma_1 T_0}{\rho c_1^2}$, $a_4 = \frac{K_1^*}{\omega_1 K^*}$, $a_5 = \frac{\gamma_1 c_1^2}{\omega_1 K^*}$, $a_6 = \frac{\mu}{\gamma_1 T_0}$,

$a_7 = \frac{\lambda}{\gamma_1 T_0}$, $a_8 = \frac{(\lambda+2\mu)}{\gamma_1 T_0}$.

Also, equations (5.34) -(5.40) reduces as

$$\hat{u}_1 = \frac{1}{\Delta_1}[\sum_{i=1}^{2}(-\iota\xi(\Delta_{i1}\hat{F}_1(\xi, s) + \Delta_{i2}\hat{F}_2(\xi, s))e^{-\lambda_i x_3}) + (\lambda_3(\Delta_{31}\hat{F}_1(\xi, s) + \Delta_{32}\hat{F}_2(\xi, s))e^{-\lambda_3 x_3}], \tag{5.43}$$

$$\hat{u}_3 = \frac{1}{\Delta_1}[\sum_{i=1}^{2}(-\lambda_i(\Delta_{i1}\hat{F}_1(\xi, s) + \Delta_{i2}\hat{F}_2(\xi, s))e^{-\lambda_i x_3}) + (-\iota\xi(\Delta_{31}\hat{F}_1(\xi, s) + \Delta_{32}\hat{F}_2(\xi, s))e^{-\lambda_3 x_3}], \tag{5.44}$$

$$\hat{t}_{33} = \frac{1}{\Delta_1}\left[\sum_{i=1}^{3}(H_{i+3}(\Delta_{i1}\hat{F}_1(\xi, s) + \Delta_{i2}\hat{F}_2(\xi, s))e^{-\lambda_i x_3})\right], \tag{5.45}$$

$$\hat{t}_{31} = \frac{1}{\Delta_1}\left[\sum_{i=1}^{3}(H_i(\Delta_{i1}\hat{F}_1(\xi, s) + \Delta_{i2}\hat{F}_2(\xi, s))e^{-\lambda_i x_3})\right], \tag{5.46}$$

$$\hat{\varphi} = \frac{1}{\Delta_1}\left[\sum_{i=1}^{2}(l_i(\Delta_{i1}\hat{F}_1(\xi, s) + \Delta_{i2}\hat{F}_2(\xi, s))e^{-\lambda_i x_3})\right], \tag{5.47}$$

$$\hat{T} = \frac{1}{\Delta_1}\left[\sum_{i=1}^{2}(H_{i+6}(\Delta_{i1}\hat{F}_1(\xi, s) + \Delta_{i2}\hat{F}_2(\xi, s))e^{-\lambda_i x_3})\right], \tag{5.48}$$

where

$\Delta_1 = \lambda_1 l_1(H_2H_6 - H_3H_5) + \lambda_2 l_2(H_3H_4 - H_1H_6)$,

$\Delta_{11} = \lambda_2 l_2 H_3$, $\Delta_{12} = H_3H_5 - H_2H_6$, $\Delta_{21} = -\lambda_1 l_1 H_3$,

$\Delta_{22} = (H_1H_6 - H_3H_4)$, $\Delta_{31} = (\lambda_1 l_1 H_2 - \lambda_2 l_2 H_1)$, $\Delta_{32} = (H_2H_4 - H_1H_5)$,

$H_i = \iota\xi 3\lambda_i a_6$, $H_3 = -a_6(2\lambda_3^2 + \xi^2)$, $H_{i+3} = -\xi^2 a_7 + \lambda_i^2 a_8 - l_i(1 + \varsigma(\xi^2 - \lambda_i^2))$,

$H_6 = -\iota\xi\lambda_3(a_7 - a_8)$, $H_{i+6} = l_i(1 + \varsigma(\xi^2 - \lambda_i^2))$, $l_i = \frac{(1+\xi_1^2 s^2)(\lambda_i^2 - \xi^2) - s^2}{a_3(1+\varsigma(\xi^2 - \lambda_i^2))}$ $(i = 1 - 2)$.

these results are consistent with those obtained by Kumar et al. (2023) [80] (In absence of heat source).

ii) In absence of micropolar effect along with the conditions $K_1^* = \tau_0 = 0$ and $\varsigma =$

a, the equations (5.19) - (5.20), reduces as

$$(D^4 - P_{01}D^2 + P_{02})(\hat{q}, \hat{\varphi}) = 0, \tag{5.49}$$

$$(D^2 - \lambda_3^2)\hat{\psi} = 0, \tag{5.50}$$

With changed values of

$$P_{01} = \frac{P_{17}+\xi^2 P_{16}+s(1+\xi^2 a)P_{18}+saP_{19}}{P_{16}+saP_{18}}, \quad P_{02} = \frac{P_{17}\xi^2+s(1+\xi^2 a)P_{19}}{P_{16}+saP_{18}}, \quad P_{18} = 1 + {\xi_1}^2 s^2 + a_3 a_4,$$

$$P_{19} = \xi^2\left(1 + {\xi_1}^2 s^2 + a_3 a_4\right) + s^2, \quad \lambda_3^2 = \frac{(a_2\xi^2+s^2(1+{\xi_1}^2\xi^2))}{a_2+{\xi_1}^2 s^2}, a_2 = \frac{\mu}{\rho c_1^2}, \quad a_3 = \frac{\gamma_1 T_0}{\rho c_1^2},$$

$$a_4 = \frac{\gamma_1 c_1^2}{\omega_1 K^*}, \quad a_5 = \frac{\mu}{\gamma_1 T_0}, \quad a_6 = \frac{\lambda}{\gamma_1 T_0}, \quad a_7 = \frac{(\lambda+2\mu)}{\gamma_1 T_0}.$$

Also, equations (5.34) -(5.40) reduces as

$$\hat{u}_1 = \frac{1}{\Delta_1}[\sum_{i=1}^{2}(-\iota\xi(\Delta_{i1}\hat{F}_1(\xi,s) + \Delta_{i2}\hat{F}_2(\xi,s))e^{-\lambda_i x_3}) + (\lambda_3(\Delta_{31}\hat{F}_1(\xi,s) + \Delta_{32}\hat{F}_2(\xi,s))e^{-\lambda_3 x_3}], \tag{5.51}$$

$$\hat{u}_3 = \frac{1}{\Delta_1}[\sum_{i=1}^{2}(-\lambda_i(\Delta_{i1}\hat{F}_1(\xi,s) + \Delta_{i2}\hat{F}_2(\xi,s))e^{-\lambda_i x_3}) + (-\iota\xi(\Delta_{31}\hat{F}_1(\xi,s) + \Delta_{32}\hat{F}_2(\xi,s))e^{-\lambda_3 x_3}], \tag{5.52}$$

$$\hat{t}_{33} = \frac{1}{\Delta_1}\left[\sum_{i=1}^{3}(H_{i+3}(\Delta_{i1}\hat{F}_1(\xi,s) + \Delta_{i2}\hat{F}_2(\xi,s))e^{-\lambda_i x_3}\right], \tag{5.53}$$

$$\hat{t}_{31} = \frac{1}{\Delta_1}\left[\sum_{i=1}^{3}(H_i(\Delta_{i1}\hat{F}_1(\xi,s) + \Delta_{i2}\hat{F}_2(\xi,s))e^{-\lambda_i x_3}\right], \tag{5.54}$$

$$\hat{\varphi} = \frac{1}{\Delta_1}\left[\sum_{i=1}^{2}(l_i(\Delta_{i1}\hat{F}_1(\xi,s) + \Delta_{i2}\hat{F}_2(\xi,s))e^{-\lambda_i x_3}\right], \tag{5.55}$$

$$\hat{T} = \frac{1}{\Delta_1}\left[\sum_{i=1}^{2}(H_{i+6}(\Delta_{i1}\hat{F}_1(\xi,s) + \Delta_{i2}\hat{F}_2(\xi,s))e^{-\lambda_i x_3}\right], \tag{5.56}$$

where

$$\Delta_1 = \lambda_1 l_1(H_2H_6 - H_3H_5) + \lambda_2 l_2(H_3H_4 - H_1H_6),$$

$$\Delta_{11} = \lambda_2 l_2 H_3, \quad \Delta_{12} = H_3H_5 - H_2H_6, \quad \Delta_{21} = -\lambda_1 l_1 H_3,$$

$$\Delta_{22} = (H_1H_6 - H_3H_4), \quad \Delta_{31} = (\lambda_1 l_1 H_2 - \lambda_2 l_2 H_1), \quad \Delta_{32} = (H_2H_4 - H_1H_5),$$

$$H_i = 3\iota\xi\lambda_i a_6, \quad H_3 = -a_5(2\lambda_3^2 + \xi^2), \quad H_{i+3} = -\xi^2 a_6 + \lambda_i^2 a_7 - l_i(1 + a(\xi^2 - \lambda_i^2)),$$

$$H_6 = -\iota\xi\lambda_3(a_6 - a_7), \; H_{i+6} = l_i(1 + a(\xi^2 - \lambda_i^2)), \quad l_i = \frac{(1+\xi_1^2 s^2)(\lambda_i^2 - \xi^2) - s^2}{a_3(1+a(\xi^2-\lambda_i^2))} \; (i = 1 - 2).$$

these results are consistent with those reported by Lata and Singh (2020) [95] (In absence of ramp-type heat source).

5.6.1 Special Cases

i) When $F_{20} = 0$ in equations (5.34) -(5.40), we derive the corresponding results for the normal force.

ii) When $F_{10} = 0$, the expressions from equations (5.34) -(5.40) simplify for the thermal source.

5.7 Inverse Transformations

To obtain the physical domain solutions to the current problem, we must invert the converted components given in equations (5.34) -(5.40). To retrieve the function $g(x_1, x_3, t)$ in the physical domain, we begin by inverting the F.T as

$$\bar{g}(x_1, x_3, s) = \frac{1}{2\pi}\int_{-\infty}^{\infty} \hat{g}(\xi, x_3, s)\exp(-i\xi x_1)\, d\xi = \frac{1}{2\pi}\int_{-\infty}^{\infty} |\cos(\xi x_1)\, g_e - i\sin(\xi x_1)\, g_0|\, d\xi, \quad (5.57)$$

where g_e and g_0 denote the odd and even parts of $\hat{g}(\xi, x_3, s)$, respectively.

According to Honig and Hirdes (1984) [56], the inverse L.T of the function $\bar{g}(x_1, x_3, s)$ yields $g(x_1, x_3, t)$ through

$$g(x_1, x_3, t) = \frac{1}{2\pi i}\int_{C-i\infty}^{C+i\infty} \bar{g}(x_1, x_3, s)\exp(st)\, ds, \quad (5.58)$$

where C is a freely chosen real number that surpasses the real parts of all singularities of $\bar{g}(x_1, x_3, s)$.

Substituting $s = C + \iota y$ into equation (5.58), we obtain

$$g(t) = \frac{\exp(Ct)}{2\pi}\int_{-i\infty}^{+i\infty} \bar{g}(C + \iota y)\exp(\iota y t)\, dy, \quad (5.59)$$

By defining $h(t) = \exp(-Ct)g(t)$ and expanding it using a Fourier series over the interval [0, 2L], we drive the following approximation formula:

$$g(t) = F_D + g_\infty(t),$$

where

$$g_\infty(t) = \frac{C_0}{2} + \sum_{m=1}^{\infty} C_m, \qquad 0 \le t \le 2L, \quad (5.60)$$

and

$$C_m = \frac{\exp(Ct)}{L} R_e\left[\bar{g}\left(C + \frac{\iota m\pi}{L}\right)\exp\left(\frac{\iota m\pi t}{L}\right)\right], \quad (5.61)$$

By choosing a suitably large number for C, the discretization error F_D can be made arbitrarily tiny. The values of C and L are determined based on criteria established by Honig and Hirdes

(1984) [56]. In equation (5.61), the infinite series can be truncated after a finite number of N terms.

Consequently, g(t)'s approximate value

$$g_N(t) = \frac{C_0}{2} + \sum_{m=1}^{N} C_m, \qquad 0 \le t \le 2L, \tag{5.62}$$

When computing g(t) using expression (5.62), the total approximate error is obtained by combining the discretization error with the truncation error F_T.

To reduce this total error, two methods are employed. The first is the Korrektur method, which focuses on minimizing the discretization error. The second method utilizes the ε- algorithm to improve convergence speed.

The Korrektur technique uses the formula below to evaluate the function g(t):

$g(t)=F'_D - g_\infty(2L + t)\exp(-2CL) + g_\infty(t),$

where

$|F'_D| \ll |F_D|,$

Therefore, the approximate value of $g(t)$ is given by

$$g_{NK}(t)=- g_{N'_1}(2L + t)\exp(-2CL) + g_N(t), \tag{5.63}$$

where N'_1 is an integer such that $N'_1 < N$.

We will now apply the ε- algorithm to accelerate the convergence of the series in equation (5.63). Consider $N = 2q + 1$, where q is a natural number, and define $s_n = \sum_{m=1}^{n} C_m$ be the sequence of the partial sums of the series in equation (5.63).

Defining the ε-sequence as follows:

$\varepsilon_{0,n} = 0, \qquad \varepsilon_{1,n} = s_n,$

and

$\varepsilon_{a+1,n} = \varepsilon_{a-1,n+1} + \frac{1}{\varepsilon_{a,n+1} - \varepsilon_{a,n}}, a = 1,2,3 \ldots .$

$\varepsilon_{1,1}, \varepsilon_{3,1}, \ldots \varepsilon_{N,1}$ converges to $F_D + g(t) - \frac{\bar{C}_0}{2}$ quicker than the sequence of the partial sums s_n, where n is natural number. This procedure is used to invert L.T, consisting of equation (5.63) together with the ε-algorithm.

5.8 Numerical Implementation and Discussion

To examine the effects of different parameters, numerical calculations are performed for several cases: (i) HTT (ii) ξ_1 and ξ_2, taking into account normal force and thermal source in a MT

medium governed by the MGT heat equation. For the numerical results and analysis, we use a magnesium crystal-like material, utilizing the numerical data provided in section 3.8 [Chapter 3].

5.8.1 HTT Effects

We consider $\xi_1 = 0.50$ and $\xi_2 = 0.4$ for the range $0 \leq x_1 \leq 10$.

The curves with HTT ($\varsigma = 0.75$) are denoted by solid line (—).

The curves with TT ($a = 0.104$) are represented by small dashed line (---).

The curves without HTT ($\varsigma = 0$) are denoted by big dashed line ($- - -$).

Figures 5.2-5.5, show the effects of HTT and TT due to normal force on all considered cases.

Figures 5.6-5.9, show the effects of HTT and TT due to thermal source on all considered cases.

5.8.1.1 Normal Force

The figure 5.2 depicts variations of t_{33} vs. x_1. The value of t_{33} for a = 0.104 and $\varsigma = 0$, exhibits an ascending behavior in the range $0 \leq x_1 \leq 6$ and a descending trend in the rest of interval. However, for ς = 0.75, the value of t_{33} shows a declining trend throughout the range.

The trend of m_{32} vs. x_1 is depicted in figure 5.3. It is evident that for $\varsigma = 0$ and a = 0.104, m_{32} exhibits oscillatory behavior and its magnitude remains high for a = 0.104. However, the value of m_{32} drops in the range $0 \leq x_1 \leq 7$, reaching a low at x_1=7.

Figure 5.4 depicts variations of T vs. x_1. For the interval $0 \leq x_1 \leq 6$, the value of T decreases for $\varsigma = 0$ and a = 0.104 but its behavior is opposite for ς = 0.75. In the remaining range, T follows an increasing trend for all the cases.

Figure 5.5 exhibits the variations of φ vs. x_1. The trend of φ for ς = 0.75 is inverse in nature when compared to $\varsigma = 0$ and a = 0.104 for the range $0 \leq x_1 \leq 6$, and displays a similar trend in the remaining interval.

5.8.1.2 Thermal Source

Figure 5.6 shows variations of t_{33} vs. x_1. The value of t_{33} for a = 0.104 and $\varsigma = 0$ shows a descending trend over the range $0 \leq x_1 \leq 6$ and reaches its minimum value at $x_1 = 6$. In contrast, for ς = 0.75, t_{33} decreases throughout the range $0 \leq x_1 \leq 4$, and vice-versa for left over the interval.

Figure 5.7 shows a plot of m_{32} vs. x_1. It is evident that m_{32} exhibits opposite behavior for ς = 0.75 compared to the other considered cases within the interval $0 \leq x_1 \leq 7$. However, it reaches

its maximum value near the source and behaves similarly for all other cases in the remaining interval.

Figure 5.8 depicts the variations of T vs. x_1. For $\varsigma = 0.75$, the magnitude of T increase within the range $0 \leq x_1 \leq 4$ before reaching a steady state for the left over the interval. In contrast, for other considered cases, T increases inside the range of $0 \leq x_1 \leq 6$ and decreases in the remaining interval.

Figure 5.9 shows a plot of φ vs. x_1 . It is seen that the values of φ follow the same trend as noted for T, with significant difference in their magnitudes.

5.8.2 Non-Local Effect (ξ_1)

We assume, $\xi_2 = 0.4$ with HTT parameter for the range $0 \leq x_1 \leq 10$.

For $\xi_1 = 0.75$, the curves are represented by the solid line (—).

For $\xi_1 = 0.50$, the curves are denoted by the small dashed line (---).

In absence of ξ_1, the curves are represented by the big dashed line $(- - -)$.

Figures 5.10-5.13, show the impact of N-L parameter (ξ_1) due to normal force on all considered cases. Figures 5.14-5.17, show the impact of N-L parameter (ξ_1) due to thermal source on all considered cases.

5.8.2.1 Normal Force

The variations of t_{33} vs. x_1 is shown by figure 5.10. It is evident that the magnitude of t_{33} for $\xi_1 = 0.75$ and $\xi_1 = 0.50$, shows a descending trend across the entire range except some value of x_1 whereas in absence of N-L parameter (ξ_1), magnitude of t_{33} depicts increasing trend near and far away from boundary and decreasing in the rest of the interval.

Figure 5.11 shows a plot of m_{32} vs. x_1. The magnitude of m_{32} increases for highest value of N-L parameter, reaching its maximum value at the end of interval. In contrast, m_{32} shows a decreasing trend for $\xi_1 = 0.50$ in the range $0 \leq x_1 \leq 7$ and increases in the remaining interval whereas in absence of ξ_1, m_{32} depicts steady state behaviour about origin.

Figure 5.12 shows the variations of T vs. x_1. The magnitude of T shows an increasing trend throughout the entire interval for $\xi_1 = 0.75$ and $\xi_1 = 0.50$ whereas for $\xi_1 = 0.0$, T depicts oscillatory trend.

Figure 5.13 exhibits the variations of φ vs. x_1. The values of φ follow same trend as seen for T, but with significant differences across all considered cases.

5.8.2.2 Thermal Source

Figure 5.14 demonstrate the variations of t_{33} vs. x_1. The magnitude of t_{33} decreases near the source, and reaching a minimum value at $x_1 = 2$ for $\xi_1 = 0.75$. Due to presence of N-L parameter, the values of t_{33} rise as x_1 increases.

Figure 5.15 exhibits the plot of m_{32} vs. x_1. The magnitude of m_{32} depicts descending trend for all the values of ξ_1 as $x_1$increases.

The variations of T vs. x_1 are illustrated in Figure 5.16. It is evident the near the boundary, T shows escalating trend for all the considered cases. For $x_1 > 4$, T exhibits a reverse trend for $\xi_1 = 0.0$ compared to the other values of ξ_1.

The importance of N-L parameters is seen in figure 5.17, as magnitude of φ is higher for $\xi_1 = 0.75$ compared to other values of ξ_1 in the first half of interval. As x_1 increases, the trend of φ reverses i.e., the values of φ are smaller for $\xi_1 = 0.75$ compared to other considered cases.

5.8.3 Non-Local Effect (ξ_2)

We assume $\xi_1 = 0.50$ with HTT parameter for the range $0 \leq x_1 \leq 10$.

For $\xi_2 = 0.6$, the curves are represented by a solid line (──).

For $\xi_2 = 0.4$, the curves are denoted by a small dashed line (------).

In absence of ξ_2, the curves are depicted by a big dashed line (− − −).

Figures 5.18-5.21, show the impact of N-L parameter (ξ_2) due to normal force on all considered cases. Figures 5.22-5.25, show the impact of N-L parameter (ξ_2) due to thermal source on all considered cases.

5.8.3.1 Normal Force

Figure 5.18 depicts a plot of t_{33} vs. x_1. The value of t_{33} indicates an increasing trend for all values of ξ_2 in the range $0 \leq x_1 \leq 2$, with a maximum at $x_1 = 2$. As x_1 increases further, the values of t_{33} decreases, but the magnitude of t_{33} is highest for $\xi_2 = 0.6$.

Figure 5.19 shows the plot for m_{32} vs. x_1. The trend of m_{32} for $\xi_2 = 0.6$ and $\xi_2 = 0.0$ is identical for the range $0 \leq x_1 \leq 4$ but an inverse trend is observed in the remaining interval. For $\xi_2 = 0.4$, m_{32} decreases in the range of $0 \leq x_1 \leq 7$ and increases in the rest of interval.

Figure 5.20 exhibits variations of T vs. x_1. The values of T increases throughout the interval for all cases, despite the magnitude difference.

Figure 5.21 shows variations of φ vs. x_1. The values of φ follow increasing trend across the interval for all investigated scenarios, but the magnitude of φ is higher for higher values of ξ_2.

5.8.3.2 Thermal Source

Figure 5.22 exhibits the variations in t_{33} vs. x_1. The magnitude of t_{33} displays a descending behavior for the range $0 \leq x_1 \leq 4$, reaching its minimum value at $x_1 = 4$ for all cases, and then increases for the remaining interval.

Figure 5.23 reveals the variations of m_{32} with x_1. The magnitude of m_{32} declines rapidly for $\xi_2 = 0.6$ and $\xi_2 = 0.4$ across the whole range, but for $\xi_2 = 0$, there are small variations around 1.

Figure 5.24 displays the variations in T vs. x_1. The magnitude of T increases near the source for all values of ξ_2 and diminishes after $x_1 \geq 5$, with significant differences in their magnitudes.

Figure 5.25 exhibits the variations of φ vs. x_1. The magnitude of φ grows in the region $0 \leq x_1 \leq 4$ for all values of ξ_2. For $x_1 \geq 5$, it exhibits steady-state behavior.

5.9 Conclusion

This chapter presents a two-dimensional problem in an isotropic, homogeneous and MT semi-space under the MGT heat equation, together with HTT and N-L parameters. After transforming the system into a dimensionless form and applying potential functions, the revised set of governing equations is solved using L.T and F.T techniques, taking into account the application of normal force and thermal source at the boundary surface. The components of displacement, force stresses, tangential couple stress, conductive temperature and thermodynamic temperature are then recovered in the physical domain through a numerical inversion technique. The effects of HTT, TT, and N-L parameters on these quantities are examined numerically and displayed graphically.

Based on the empirical study, following observations are noted:

i) The HTT parameter amplifies the magnitude of conductive temperature, tangential couple stress, and thermodynamic temperature. However, it diminishes the magnitude of normal stress, resulting on minima compared to 1T and TT theories, when normal force applied at boundary.

ii) When normal force is applied at the boundary tangential couple stress, thermodynamic temperature and conductive temperature exhibit an ascending behavior, whereas normal stress shows a downward trend across the entire interval for higher values of the N-L parameter (ξ_1).

iii) When a thermal source is present, the HTT parameter is found to increase the magnitude of the normal force stress while reducing the magnitudes of the thermodynamic temperature and conductive temperature compared to the 1T and TT theories. In contrast, the tangential couple stress shows opposite behavior in the HTT case relative to the other theories.

iv) It is observed that as the distance increases, the normal force stress becomes significantly higher when N-L parameter ξ_1 has a larger value. In contrast, tangential couple stress shows the opposite trend under the influence of a thermal source.

v) It has been observed that as the N-L parameter ξ_2 increases, the normal stress, thermodynamic temperature, and conductive temperature increase significantly. In contrast, the tangential couple stress exhibits oscillatory behavior for all values of ξ_2 when a normal force is applied at the boundary.

vi) Thermodynamic temperature, normal stress, and conductive temperature are observed to have lower magnitudes for intermediate values of the N-L parameter ξ_2 compared to its extreme values. In contrast, the tangential couple stress exhibits a decreasing and steady-state behavior regardless of the presence or absence of N-L parameter ξ_2 when a thermal source is applied.

The theoretical framework and graphical results presented here hold substantial promise for a wide range of applications. These include thermoelastic sensors, acoustic waveguides, and advanced composite materials, where understanding the interplay between mechanical forces and thermal source at small scales is essential. Additionally, the findings offer valuable insights for geophysical modeling and energy harvesting devices, where delayed thermal responses, microrotational effects, and boundary interactions critically influence system performance. This work thus provides a robust foundation for both theoretical advancements and practical design strategies in modern materials science and micro-engineering disciplines.

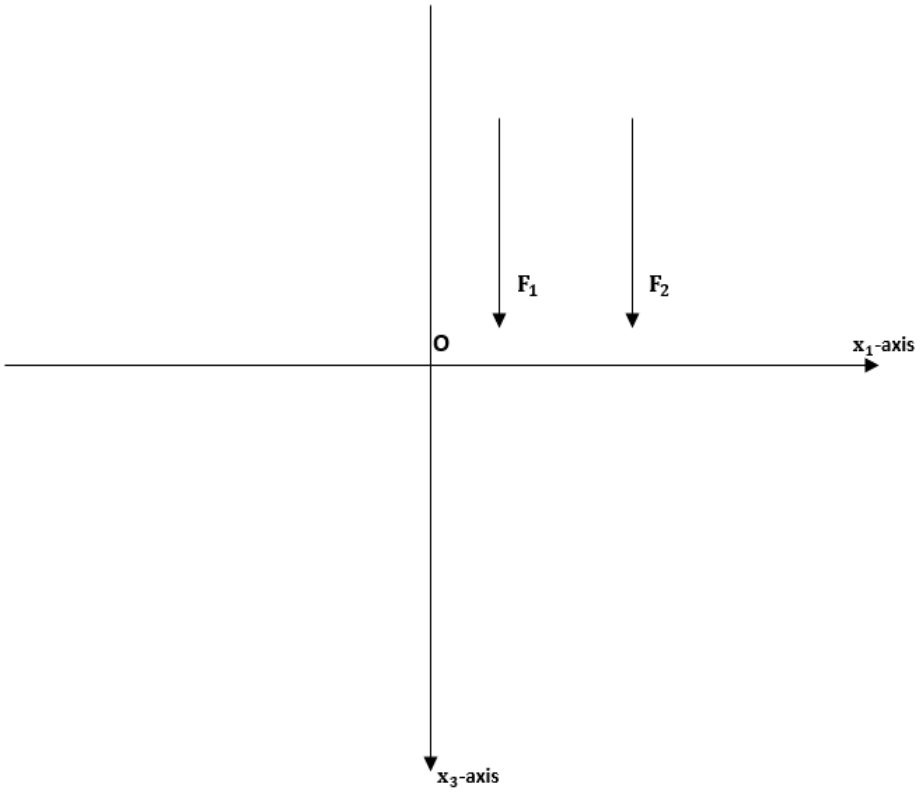

Figure 5.1: Normal Force and Thermal Source

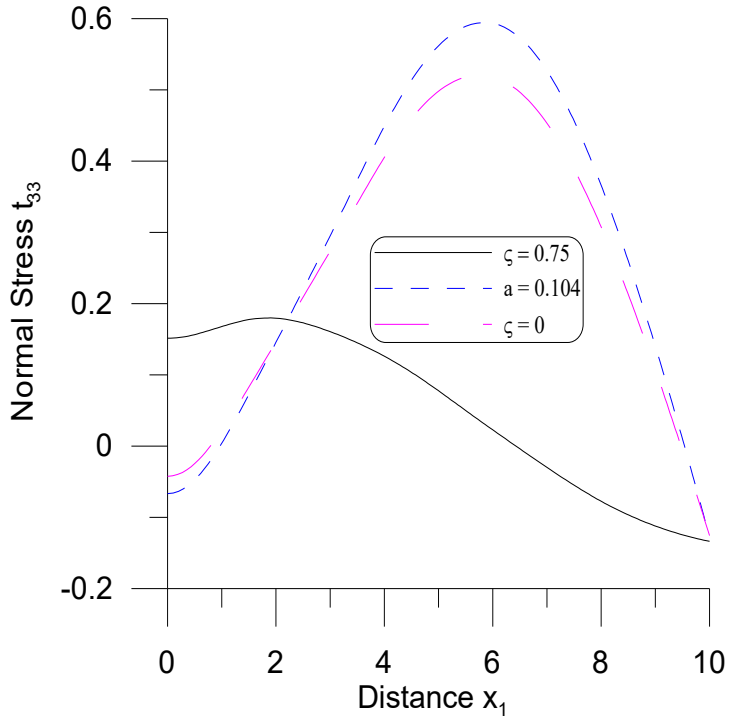

Fig.5.2 t_{33} w.r.t x_1
(Normal Force)

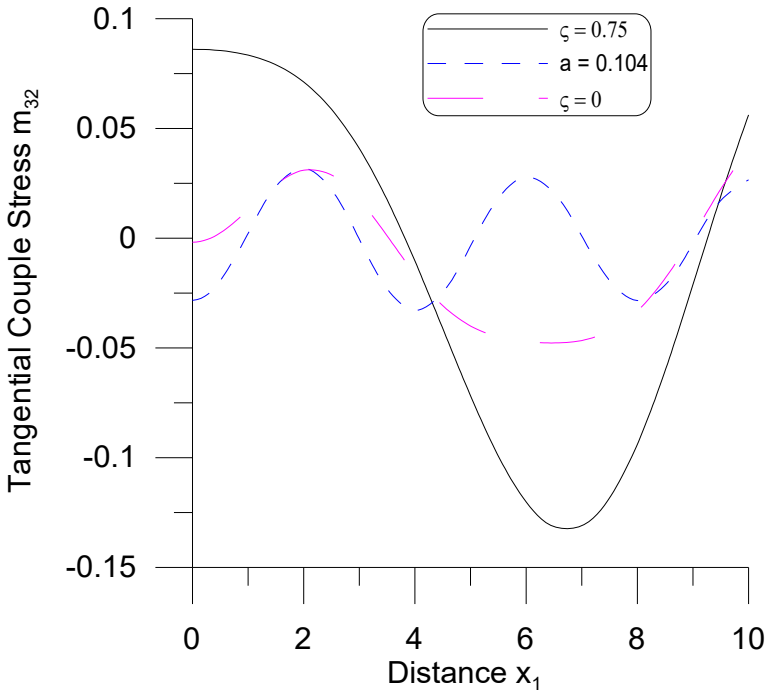

Fig.5.3 m_{32} w.r.t x_1
(Normal Force)

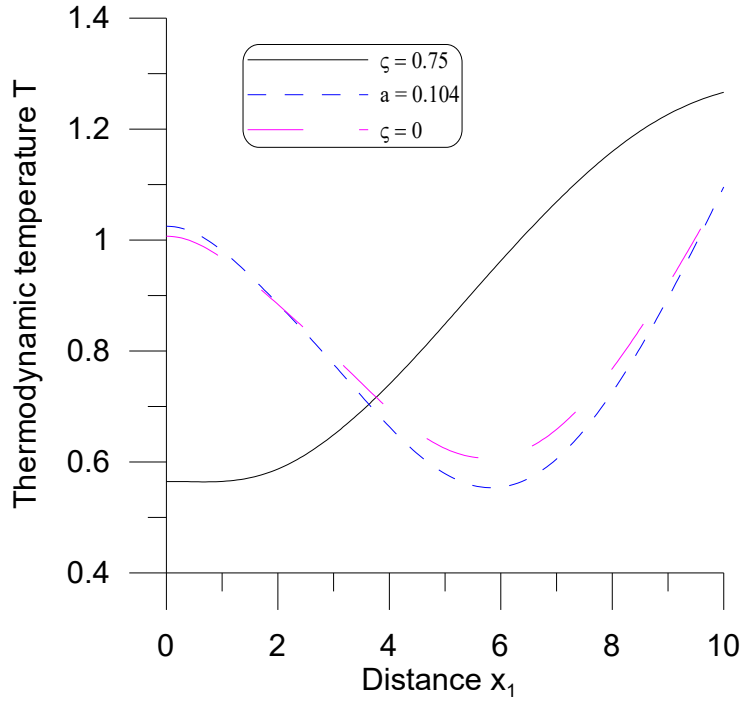

Fig.5.4 T w.r.t x_1
(Normal Force)

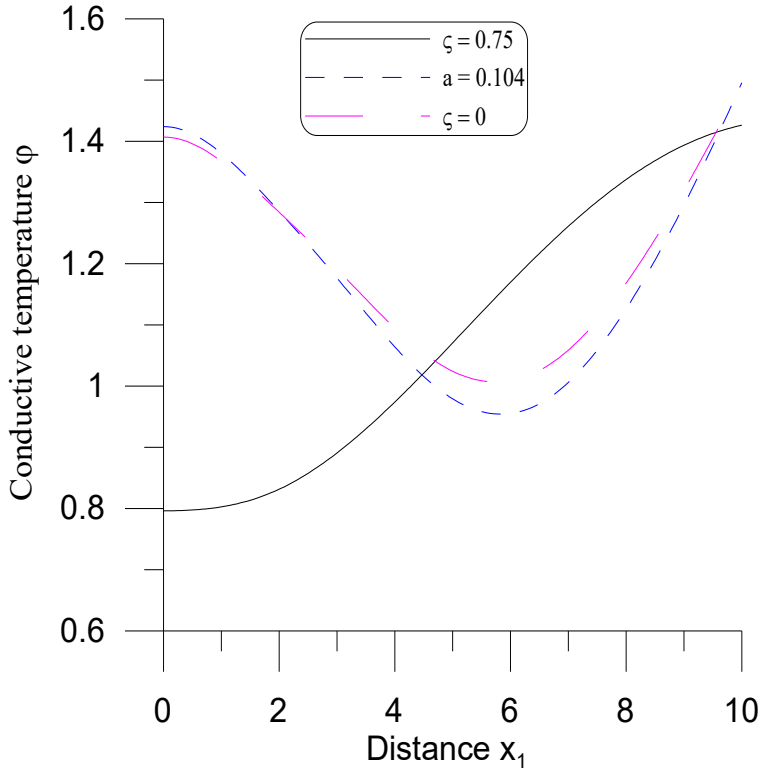

Fig.5.5 φ w.r.t x_1
(Normal Force)

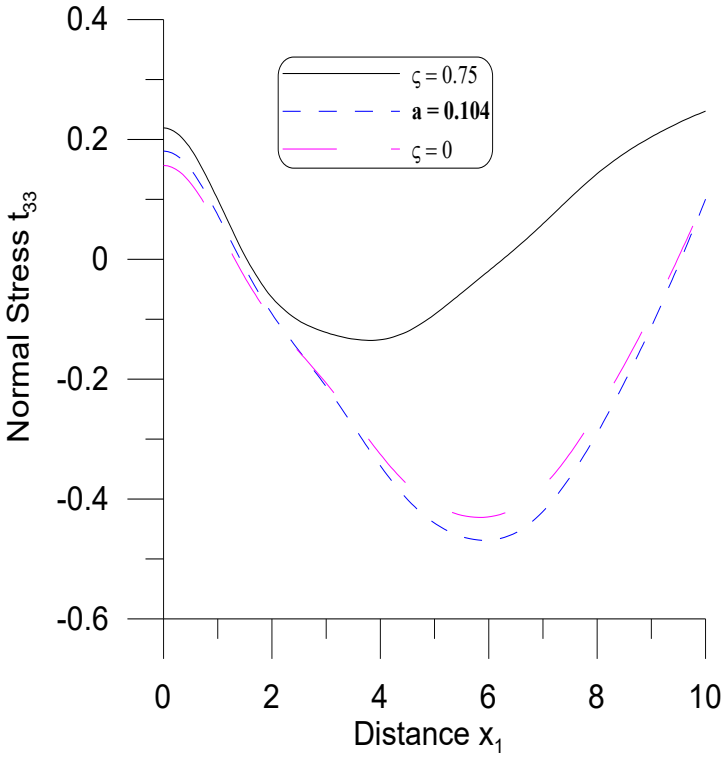

Fig.5.6 t_{33} w.r.t x_1
(Thermal Source)

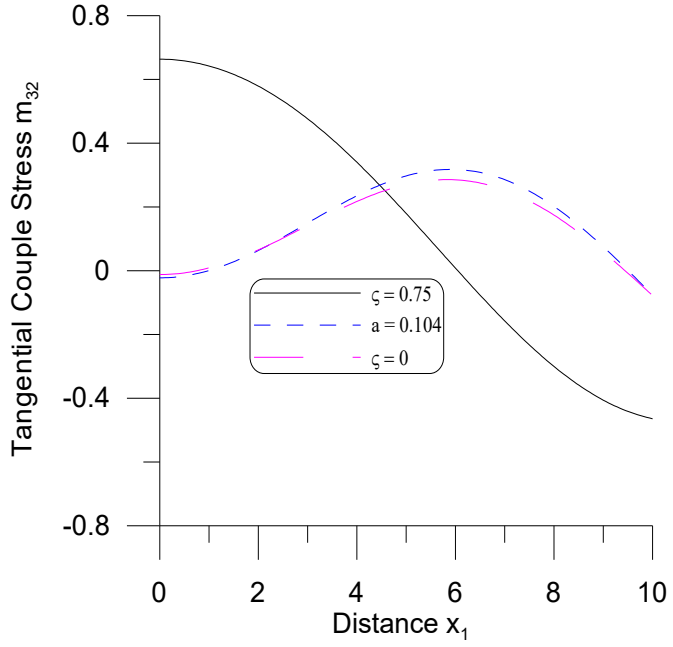

Fig.5.7 m_{32} w.r.t. x_1
(Thermal Source)

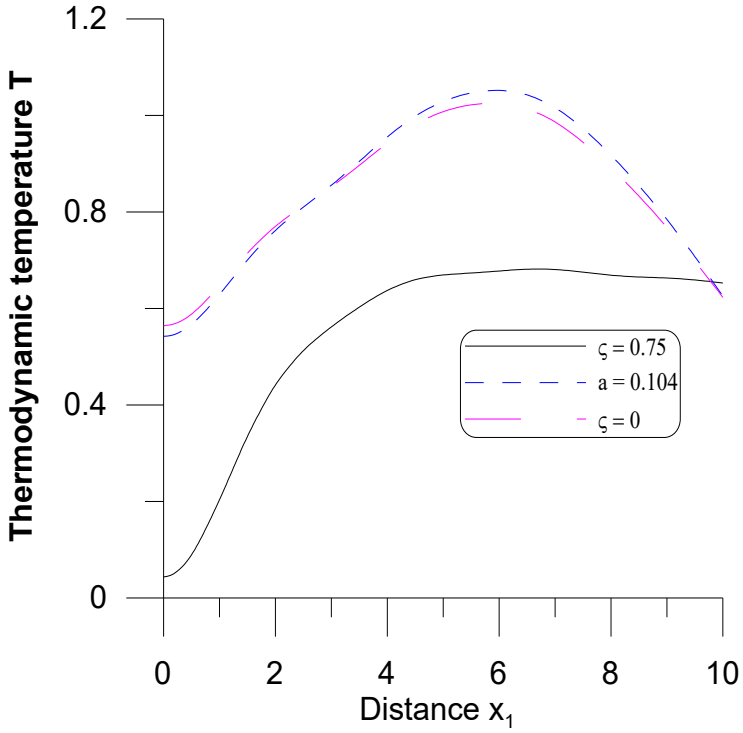

Fig.5.8 T w.r.t x_1
(Thermal Source)

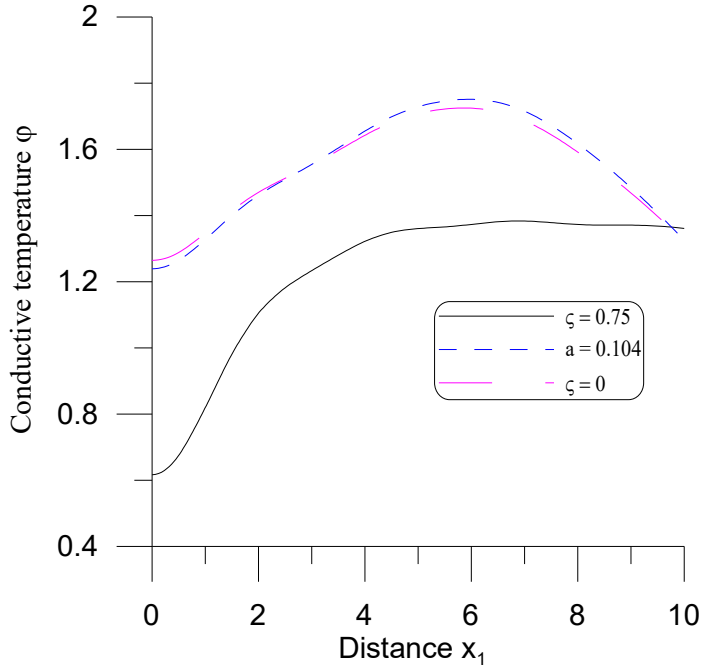

Fig.5.9 φ w.r.t x_1
(Thermal Source)

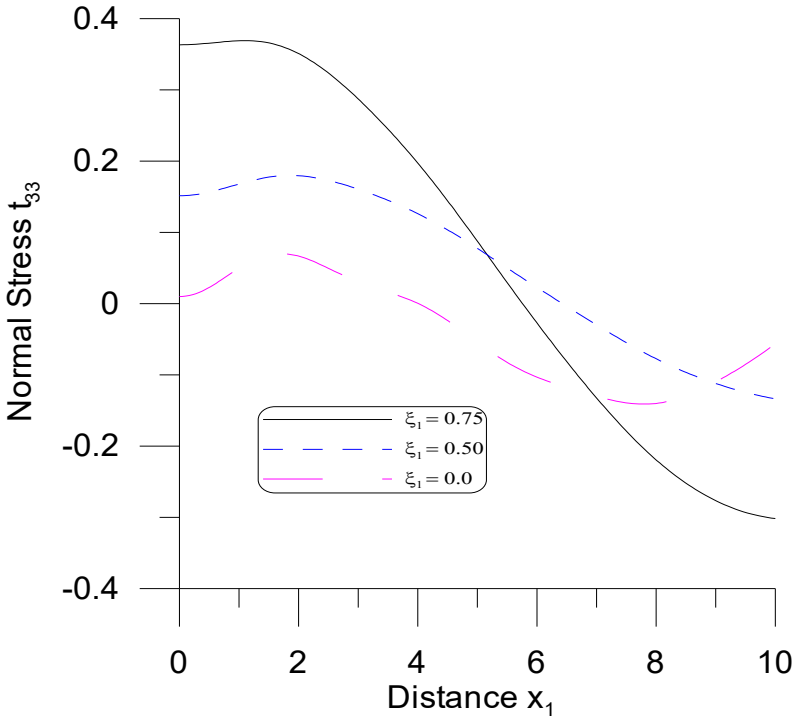

Fig.5.10 t_{33} w.r.t x_1
(Normal Force)

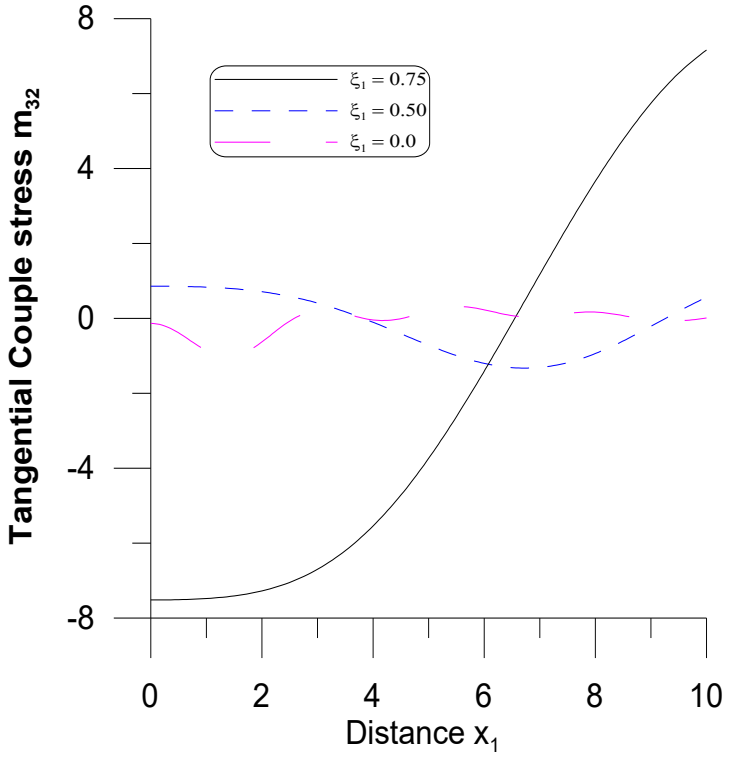

Fig.5.11 m_{32} w.r.t x_1
(Normal Force)

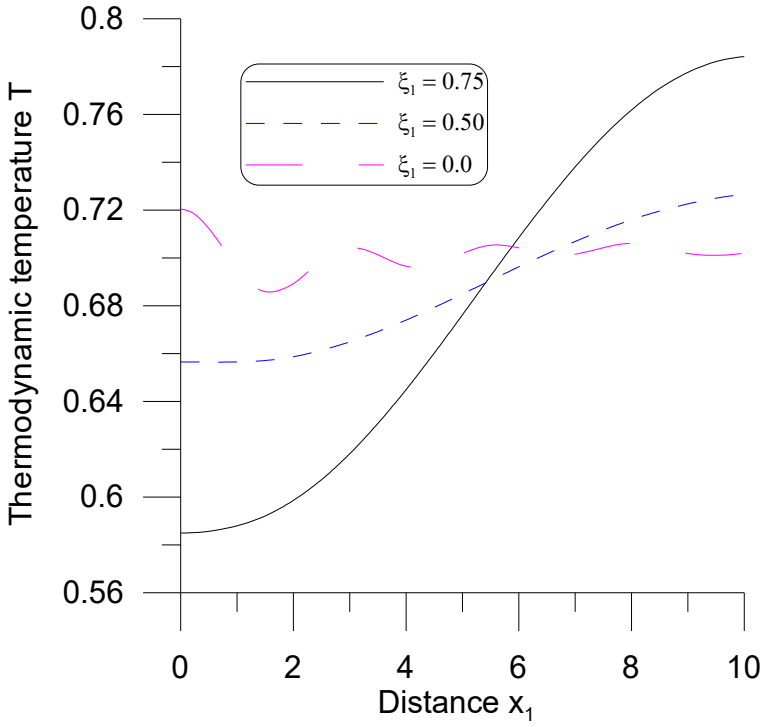

Fig.5.12 T w.r.t x_1
(Normal Force)

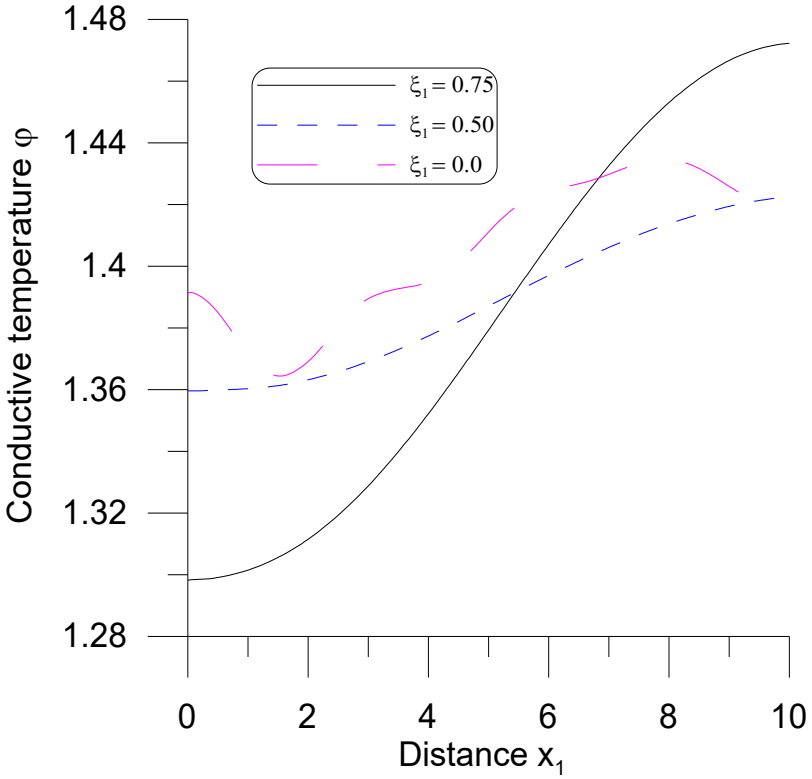

Fig.5.13 φ w.r.t x_1
(Normal Force)

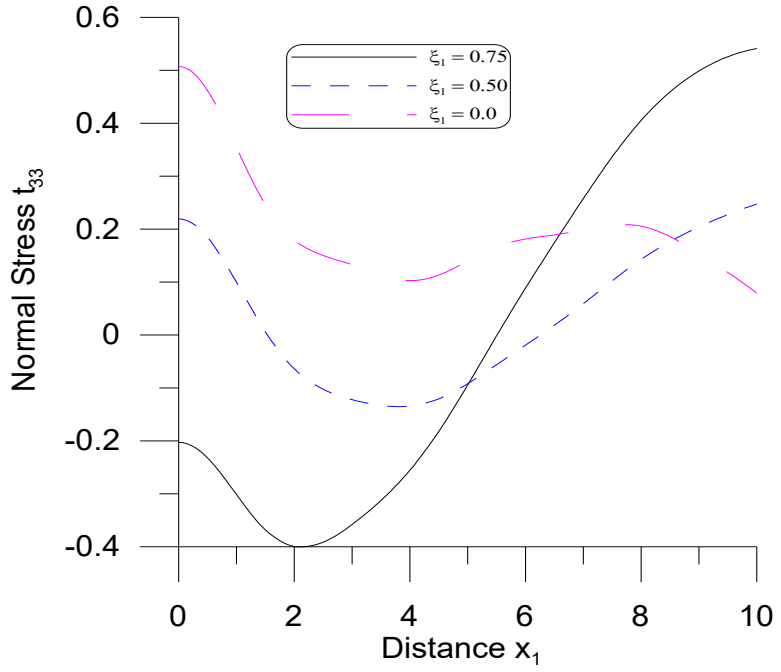

Fig.5.14 t_{33} w.r.t x_1
(Thermal Source)

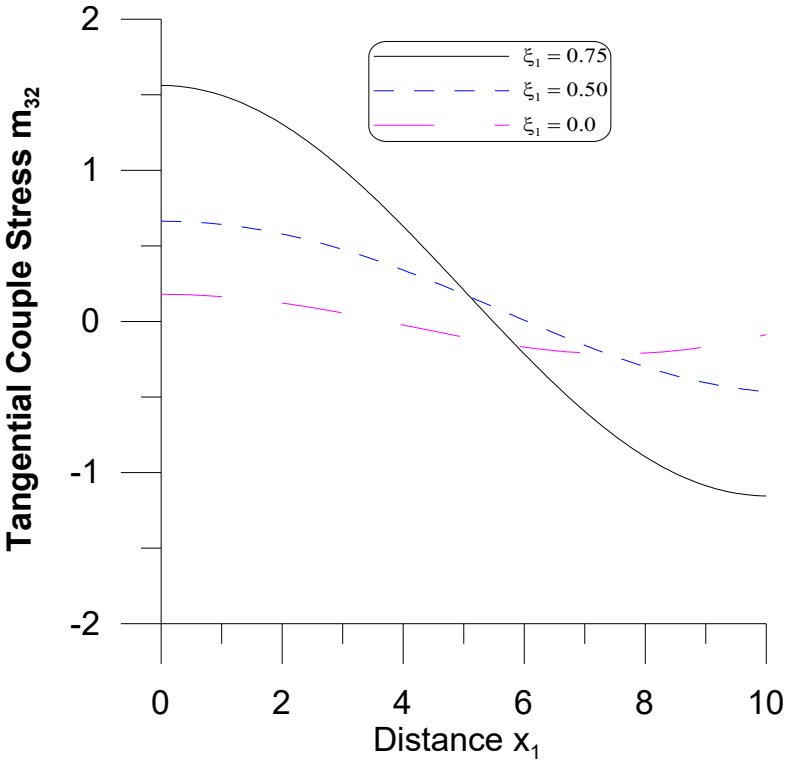

Fig.5.15 m_{32} w.r.t x_1
(Thermal Source)

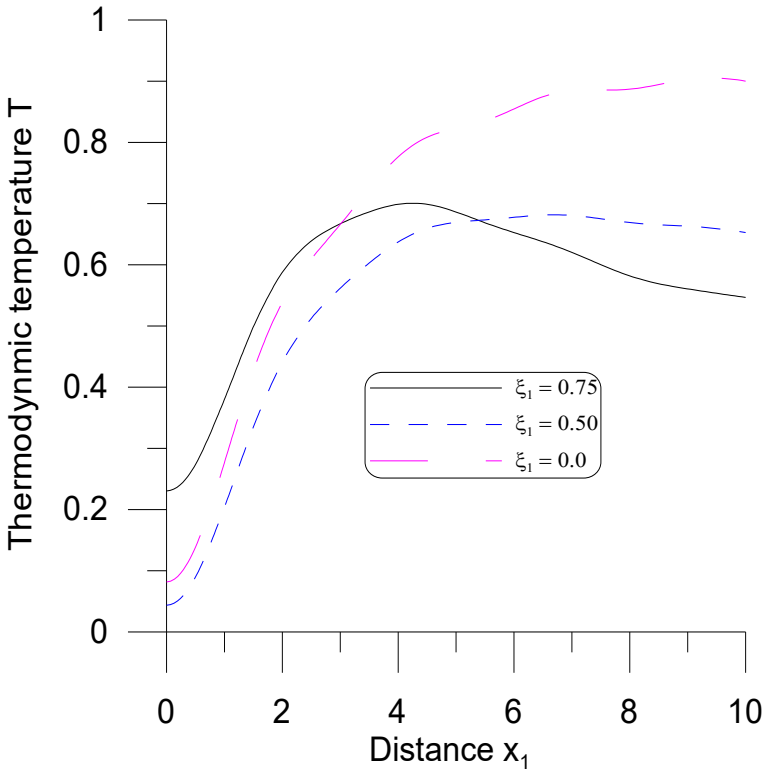

Fig.5.16 T w.r.t x_1
(Thermal Source)

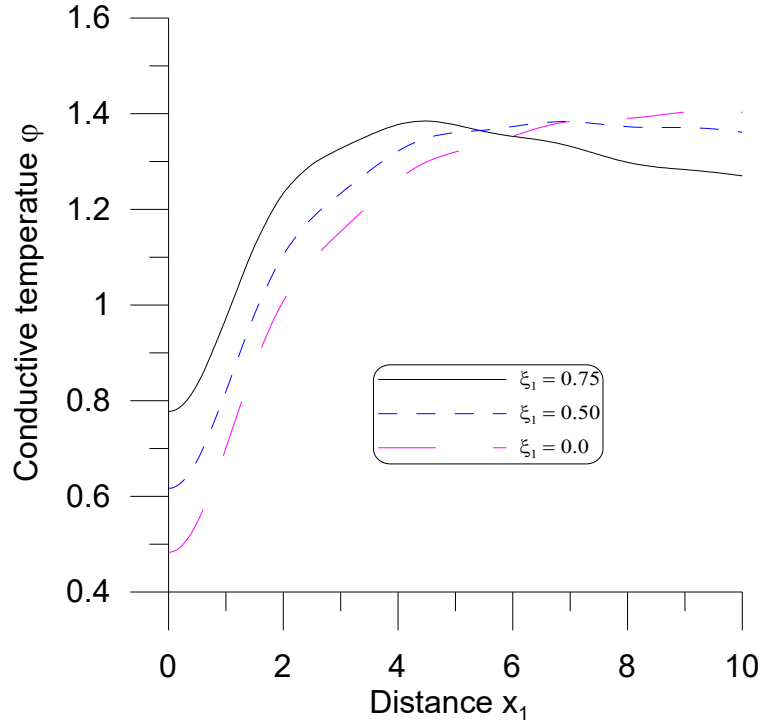

Fig.5.17 φ w.r.t x_1
(Thermal Source)

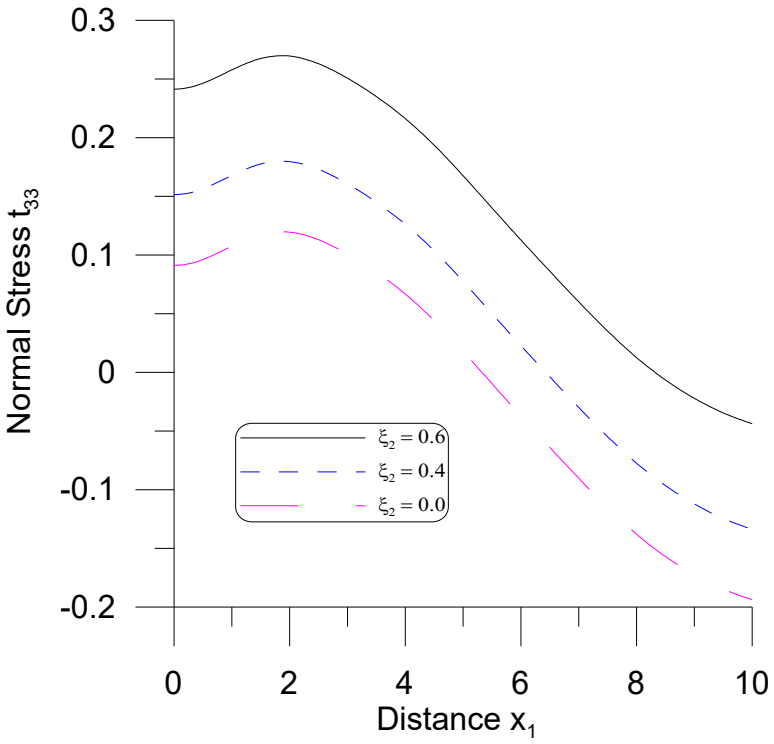

Fig. 5.18 t_{33} w.r.t x_1
(Normal Force)

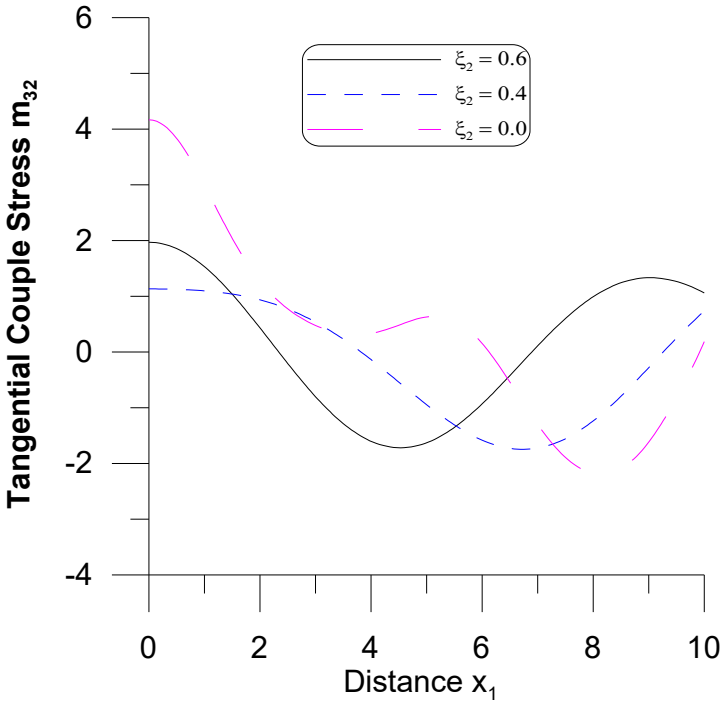

Fig. 5.19 m_{32} w.r.t x_1
(Normal Force)

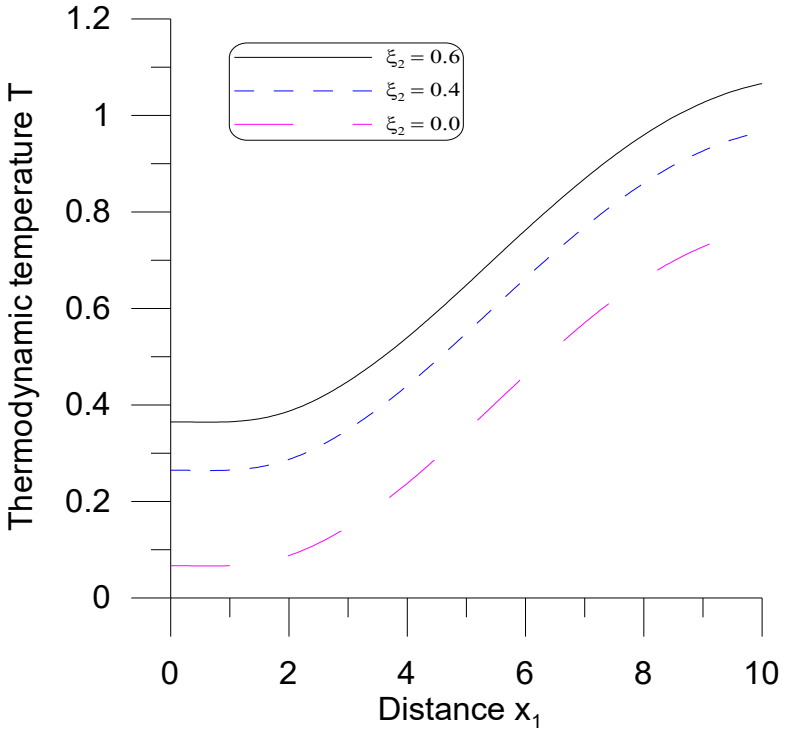

Fig. 5.20 T w.r.t x_1
(Normal Force)

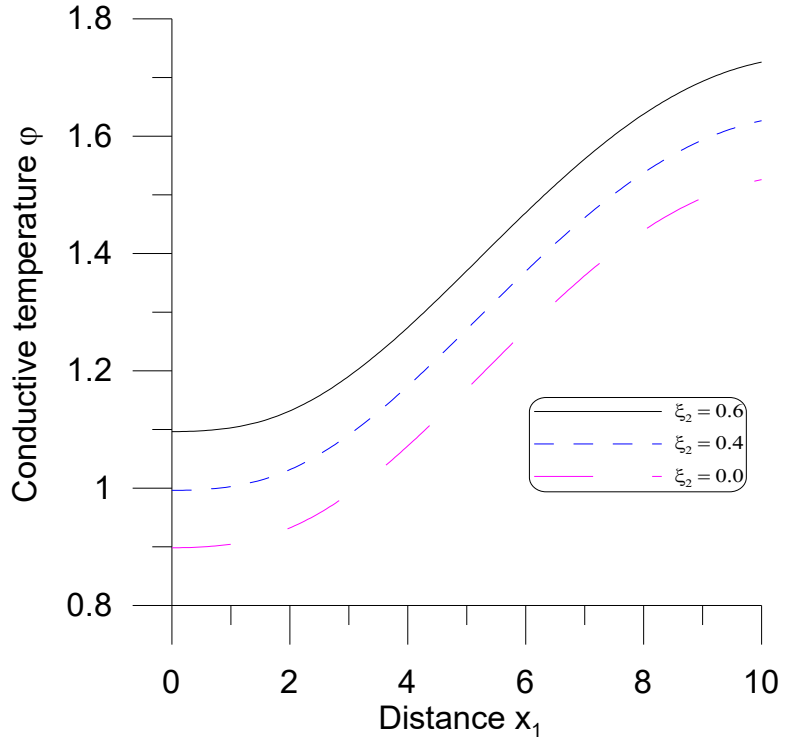

Fig. 5.21 φ w.r.t x_1
(Normal Force)

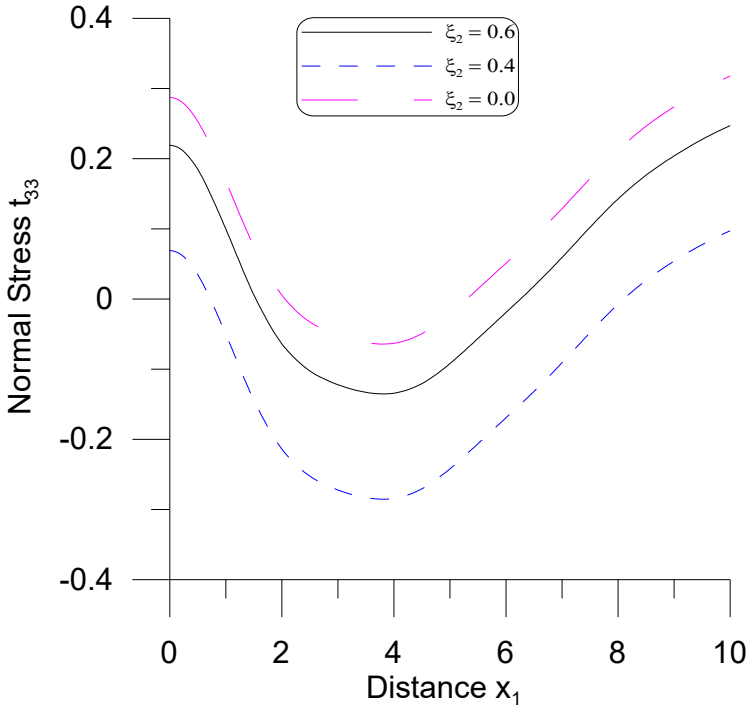

Fig. 5.22 t_{33} w.r.t x_1
(Thermal Source)

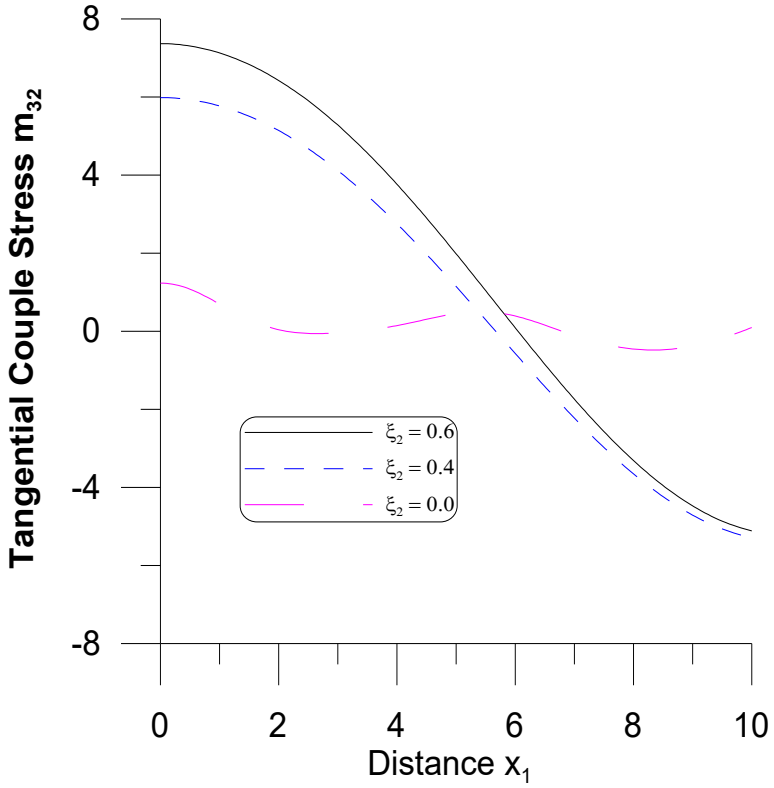

Fig. 5.23 m_{32} w.r.t x_1
(Thermal Source)

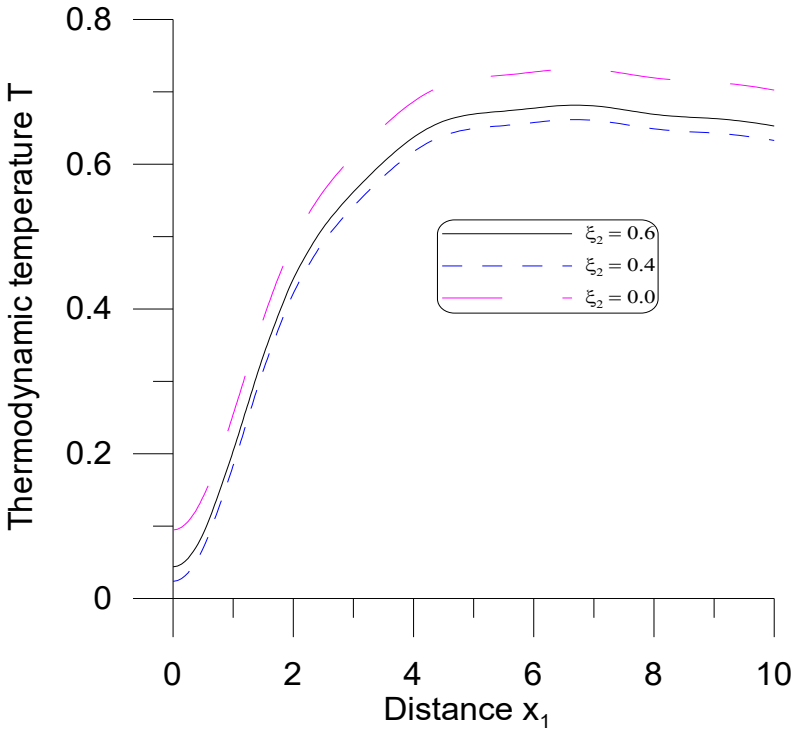

Fig. 5.24 T w.r.t x_1
(Thermal Source)

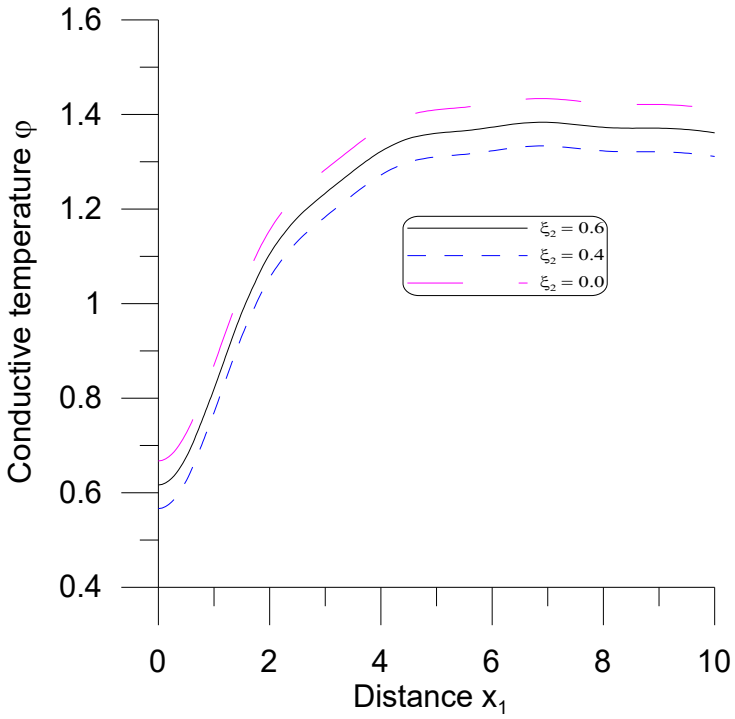

Fig. 5.25 φ w.r.t x_1
(Thermal Source)

Chapter 6

Axisymmetric deformation in a micropolar thermoelastic media, considering non-local and hyperbolic two-temperature effects under Moore-Gibson-Thompson heat equation

The work from this chapter has been published and accepted in the form of research papers entitled

a) "Analysis of axisymmetric deformation in generalized micropolar thermoelasticity within the framework of Moore-Gibson-Thompson heat equation incorporating non-local and hyperbolic two-temperature effect", The Journal of Strain Analysis for Engineering Design, 59(6), 2024, DOI:10.1177/03093247241232180.
Indexing: SCI, Scopus, Impact Factor: 1.8

b) "Frequency domain response in generalized micropolar thermoelastic media using the Moore-Gibson-Thompson heat equation and hyperbolic two temperature", International Applied Mechanics. (Accepted)
Indexing: Scopus, Q3, Impact Factor: 0.7

Chapter 6

Axisymmetric deformation in a micropolar thermoelastic media, considering non-local and hyperbolic two-temperature effects under Moore-Gibson-Thompson heat equation

6.1 Introduction

Miglani and Kaushal (2011) [106] employed the axisymmetric technique to study deformation owing to thermal source and normal force in a thermoelastic medium with two temperatures (TT) in the context of generalised thermoelasticity theories. Sharma and Sharma (2014) [146] investigated how relaxation times and heat sources affect the temperature distribution in tissues. Kumar et al. (2014) [83] computed the stresses, displacement, pore pressure, and temperature changes caused by ring and disc loads in a thermoporoelastic material, as well as the effects of porosity on the results.

Abbas and Kumar (2014) [1] explored thermally induced deformation in micropolar generalised thermoelastic materials and the effect of relaxation times on the derived quantities. Sharma et al. (2015) [143] investigated a deformation problem under an inclined load using the Green-Naghdi II (GN-II) (1992) [52] theory of thermoelasticity with TT. Kumar and Kumar (2021) [77] analysed thermoelastic vibration of micro and nano-beam resonators using Euler-Bernoulli beam theory and TT generalized theory of thermoelasticity, and compared the results with other theories of thermoelasticity. Sharma and Kumar (2021 [141], 2022 [142]) investigated some problems in photothermoelastic medium due to distributed load and inclined load respectively.

Chteoui et al. (2022) [24] used the normal mode analysis approach to investigate the effect of rotation and initial stress on various fundamental physical quantities under the Moore-Gibson-Thompson (MGT) heat equation with TT. Kumar et al. (2022) [87] used the MGT thermoelastic model to investigate the deformation caused by thermomechanical and carrier density loading in an orthotropic photothermoelastic plate. Roy and Lahiri (2024) [126] presented a problem in MT medium under higher order heat conduction and electromagnetic field due to moving heat source by using normal mode analysis and eigen value approach. Ailawalia et al. (2024) [14] studied the impact of variable thermal conductivity on components of displacement, stresses, couple stress, micro-stress, and temperature distributions in a generalized thermoelastic solid with microstretch based on Green-Naghdi theory.

In this chapter, the primary goal is to use MGT heat equation to examine the axisymmetric deformity in micropolar homogenous, isotropic MT with hyperbolic two-temperature (HTT) and non-local (N-L) parameters under different loads (ring load and disc load). The equations are reduced in two-dimensional form and then transformed by using dimensionless quantities and potential functions. A new set of governing equations is solved using the Laplace transform (L.T) and Hankel transform (H.T). The transformed forms of the components of displacement, force stresses, tangential couple stress, conductive temperature, and thermodynamic temperature are derived. A numerical inversion technique is then applied to recover these physical quantities in the original domain. The graphical representation of numerical findings for stress components, conductive temperature and tangential couple stress, highlighting the impacts of N-L, HTT and TT parameters. Specific cases of interest are also drawn.

The motivation for this work stems from the practical need to accurately analyze microstructured materials subjected to ring and disc loads, which are commonly encountered in various engineering applications. Traditional continuum theories fall short in describing key physical phenomena like microrotation and N-L interactions effects which are particularly significant in advanced systems like aerospace structures. The reason for pursuing this study is to overcome these limitations by incorporating a more advanced theoretical framework. To this end, the work integrates micropolar thermoelasticity with N-L parameters, HTT theory, and the MGT heat conduction equation. The novelty of this research lies in its unified treatment of these models under axisymmetric thermomechanical loading conditions, a combination that provides a more realistic and comprehensive approach to deformation analysis and has not been extensively addressed in the existing literature.

6.2 Fundamental Equations

Equations (3.1) -(3.6) [Chapter 3] describe the field equations and constitutive relations in an isotropic, homogeneous, MT under MGT heat equation, considering the influence of N-L and HTT factors after removing body couples, body forces, and heat sources. All symbols, including $\mathbf{u}, \boldsymbol{\phi}, T, \varphi, \beta, \gamma, K, \rho, \mu, \hat{\jmath}, K^*, K_1^*, \gamma_1, C_e, t, t_{pq}, \lambda, \alpha, m_{pq}, \tau_0, \beta^*, T_0, \xi_1, \xi_2, \delta_{pq}, \varepsilon_{pqh}$, Δ, ∇ are as defined in section 2.2 [Chapter 2] and in section 3.2 [Chapter 3].

Equations (3.1) -(3.6) in components form for cylindrical polar coordinates (r, θ, z) are expressed as:

$$(\lambda+\mu)\frac{\partial e_1}{\partial r}+(\mu+K)\left(\Delta u_r-\frac{u_r}{r^2}-\frac{2}{r^2}\frac{\partial u_\theta}{\partial \theta}\right)+\frac{K}{r}\left(\frac{\partial \phi_z}{\partial \theta}-r\frac{\partial \phi_\theta}{\partial z}\right)-\gamma_1\frac{\partial T}{\partial r}$$
$$=\rho\left(1-{\xi_1}^2\Delta\right)\frac{\partial^2 u_r}{\partial t^2}, \qquad (6.1)$$

$$(\lambda+\mu)\frac{1}{r}\frac{\partial e_1}{\partial\theta}+(\mu+K)\left(\Delta u_\theta-\frac{u_\theta}{r^2}+\frac{2}{r^2}\frac{\partial u_r}{\partial\theta}\right)+K\left(\frac{\partial\phi_r}{\partial z}-\frac{\partial\phi_z}{\partial r}\right)-\frac{\gamma_1}{r}\frac{\partial T}{\partial\theta}$$
$$=\rho\left(1-{\xi_1}^2\Delta\right)\frac{\partial^2 u_\theta}{\partial t^2}, \tag{6.2}$$

$$(\lambda+\mu)\frac{\partial e_1}{\partial z}+(\mu+K)\Delta u_z+\frac{K}{r}\left(\frac{\partial(r\phi_\theta)}{\partial r}-\frac{\partial\phi_r}{\partial z}\right)-\gamma_1\frac{\partial T}{\partial z}=\rho\left(1-{\xi_1}^2\Delta\right)\frac{\partial^2 u_z}{\partial t^2}, \tag{6.3}$$

$$(\alpha+\beta)\frac{\partial e_2}{\partial r}+\gamma\left(\Delta\phi_r-\frac{\phi_r}{r^2}-\frac{2}{r^2}\frac{\partial\phi_\theta}{\partial\theta}\right)+\frac{K}{r}\left(\frac{\partial u_z}{\partial\theta}-r\frac{\partial u_\theta}{\partial z}\right)-2K\phi_r$$
$$=\rho\hat{j}\left(1-{\xi_2}^2\Delta\right)\frac{\partial^2\phi_r}{\partial t^2}, \tag{6.4}$$

$$(\alpha+\beta)\frac{1}{r}\frac{\partial e_2}{\partial\theta}+\gamma\left(\Delta\phi_\theta-\frac{\phi_\theta}{r^2}+\frac{2}{r^2}\frac{\partial\phi_r}{\partial\theta}\right)+K\left(\frac{\partial u_r}{\partial z}-\frac{\partial u_z}{\partial r}\right)-2K\phi_\theta$$
$$=\rho\hat{j}\left(1-{\xi_2}^2\Delta\right)\frac{\partial^2\phi_\theta}{\partial t^2}, \tag{6.5}$$

$$(\alpha+\beta)\frac{\partial e_2}{\partial z}+\gamma\Delta\phi_z+\frac{K}{r}\left(\frac{\partial(ru_\theta)}{\partial r}-\frac{\partial u_r}{\partial z}\right)-2K\phi_z=\rho\hat{j}\left(1-{\xi_2}^2\Delta\right)\frac{\partial^2\phi_z}{\partial t^2}, \tag{6.6}$$

$$\left(1+\tau_0\frac{\partial}{\partial t}\right)\left[\rho C_e\frac{\partial^2 T}{\partial t^2}+\gamma_1 T_0\frac{\partial^2 e_1}{\partial t^2}\right]=K^*\frac{\partial}{\partial t}\Delta\varphi+K_1^*\Delta\varphi, \tag{6.7}$$

$$t_{zz}=\lambda e_1+(2\mu+K)\frac{\partial u_z}{\partial z}-\gamma_1 T, \tag{6.8}$$

$$t_{zr}=\mu\left(\frac{\partial u_r}{\partial z}+\frac{\partial u_z}{\partial r}\right)+K\frac{\partial u_r}{\partial z}-K\phi_\theta, \tag{6.9}$$

$$m_{z\theta}=\beta\frac{\partial\phi_z}{\partial\theta}+\gamma\frac{\partial\phi_\theta}{\partial z}, \tag{6.10}$$

$$\ddot{T}=\ddot{\varphi}-\beta^*\Delta\varphi, \tag{6.11}$$

where

$$e_1=\frac{u_r}{r}+\frac{\partial u_r}{\partial r}+\frac{1}{r}\frac{\partial u_\theta}{\partial\theta}+\frac{\partial u_z}{\partial z},\qquad e_2=\frac{\phi_r}{r}+\frac{\partial\phi_r}{\partial r}+\frac{1}{r}\frac{\partial\phi_\theta}{\partial\theta}+\frac{\partial\phi_z}{\partial z},$$
$$\Delta=\frac{\partial^2}{\partial r^2}+\frac{1}{r}\frac{\partial}{\partial r}+\frac{\partial^2}{\partial z^2}+\frac{1}{r^2}\frac{\partial^2}{\partial\theta^2}. \tag{6.12}$$

6.3 Formulation of Problem

Under the MGT heat equation, we consider an isotropic, homogeneous MT solid half-space with HTT and N-L parameters. Cylindrical polar coordinates (r, θ, z) are chosen to align with the axis of symmetry. The half-space surface is defined as the plane z=0 that points vertically into the medium. A ring or disc load is assumed to act at the origin of the cylindrical polar coordinates, as illustrated in Figure 6.1. The problem is an axisymmetric deformation problem, and we assume that all functions are dependent on spatial variables r and z, as well as temporal variable t.

As a result, we use $\mathbf{u}=(u_r(r,z,t),0,u_z(r,z,t)),\quad \boldsymbol{\phi}=(0,\phi_\theta(r,z,t),0),\ T=T(r,z,t)$ and $\varphi=\varphi(r,z,t),$ (6.13)

Because of symmetry around z-axis, the quantities are independent of θ, resulting in $\frac{\partial}{\partial\theta}=0$. With these assumptions, and using equation (6.13), equations (6.1) -(6.11) simplify as

$$(\lambda+\mu)\frac{\partial e_1}{\partial r}+(\mu+K)\left[\left(\Delta-\frac{1}{r^2}\right)u_r\right]-K\frac{\partial \phi_\theta}{\partial z}-\gamma_1\frac{\partial T}{\partial r}=\rho\left(1-{\xi_1}^2\Delta\right)\frac{\partial^2 u_r}{\partial t^2}, \tag{6.14}$$

$$(\lambda+\mu)\frac{\partial e_1}{\partial z}+(\mu+K)\Delta u_z+\frac{K}{r}\frac{\partial}{\partial r}(r\phi_\theta)-\gamma_1\frac{\partial T}{\partial z}=\rho\left(1-{\xi_1}^2\Delta\right)\frac{\partial^2 u_z}{\partial t^2}, \tag{6.15}$$

$$\gamma\left(\Delta-\frac{1}{r^2}-2K\right)\phi_\theta+K\left[\frac{\partial u_r}{\partial z}+\frac{\partial u_z}{\partial r}\right]=\rho\hat{j}\left(1-{\xi_2}^2\Delta\right)\frac{\partial^2 \phi_\theta}{\partial t^2}, \tag{6.16}$$

$$\left(1+\tau_0\frac{\partial}{\partial t}\right)\left[\rho C_e\frac{\partial^2 T}{\partial t^2}+\gamma_1 T_0\frac{\partial^2 e_1}{\partial t^2}\right]=\Delta\varphi\left(K^*\frac{\partial}{\partial t}+K_1^*\right), \tag{6.17}$$

$$t_{zz}=\lambda\left(\frac{\partial u_z}{\partial z}+\frac{\partial u_r}{\partial r}+\frac{u_r}{r}\right)+(2\mu+K)\frac{\partial u_z}{\partial z}-\gamma_1 T, \tag{6.18}$$

$$t_{zr}=\mu\left(\frac{\partial u_r}{\partial z}+\frac{\partial u_z}{\partial r}\right)+K\left(\frac{\partial u_r}{\partial z}-\phi_\theta\right), \tag{6.19}$$

$$m_{z\theta}=\gamma\frac{\partial \phi_\theta}{\partial z}, \tag{6.20}$$

$$\ddot{T}=\ddot{\varphi}-\beta^*\Delta\varphi, \tag{6.21}$$

where

$$e_1=\frac{u_r}{r}+\frac{\partial u_r}{\partial r}+\frac{\partial u_z}{\partial z},\qquad \Delta=\frac{\partial^2}{\partial r^2}+\frac{1}{r}\frac{\partial}{\partial r}+\frac{\partial^2}{\partial z^2}. \tag{6.22}$$

To further simplify, the dimensionless quantities listed below are used:

$$(r',z',u_r',u_z',\xi_1',\xi_2')=\frac{\omega_1}{c_1}(r,z,u_r,u_z,\xi_1,\xi_2),\qquad \phi_\theta'=\frac{\rho {c_1}^2}{\gamma_1 T_0}\phi_\theta,\quad (\tau_0',t')=\omega_1(\tau_0,t),$$

$$(\varphi',T')=\frac{1}{T_0}(\varphi,T),\quad (t_{zz}',t_{zr}',F_0')=\frac{1}{\gamma_1 T_0}(t_{zz},t_{zr},F_0),\quad m_{z\theta}'=\frac{\omega_1}{\gamma_1 c_1 T_0}m_{z\theta},$$

$$\beta^{*\prime}=\frac{1}{c_1^2}\beta^*, \tag{6.23}$$

where

$$c_1^2=\frac{\lambda+2\mu+K}{\rho}\ \text{and}\ \omega_1=\frac{\rho C_e c_1^2}{K^*}.$$

Using (6.23) in equations (6.14) -(6.21) after omitting the primes, yield

$$a_1\frac{\partial e_1}{\partial r}+a_2\left[\left(\Delta-\frac{1}{r^2}\right)u_r\right]-a_3\frac{\partial \phi_\theta}{\partial z}-a_4\frac{\partial T}{\partial r}=\left(1-{\xi_1}^2\Delta\right)\frac{\partial^2 u_r}{\partial t^2}, \tag{6.24}$$

$$a_1\frac{\partial e_1}{\partial z}+a_2\Delta u_z+a_3\frac{1}{r}\frac{\partial}{\partial r}(r\phi_\theta)-a_4\frac{\partial T}{\partial z}=\left(1-{\xi_1}^2\Delta\right)\frac{\partial^2 u_z}{\partial t^2}, \tag{6.25}$$

$$\left[a_5\left(\Delta-\frac{1}{r^2}\right)-a_7\right]\phi_\theta+a_6\left[\frac{\partial u_r}{\partial z}-\frac{\partial u_z}{\partial r}\right]=\left(1-{\xi_2}^2\Delta\right)\frac{\partial^2 \phi_\theta}{\partial t^2}, \tag{6.26}$$

$$\left(1+\tau_0\frac{\partial}{\partial t}\right)\left[\frac{\partial^2 T}{\partial t^2}+a_9\frac{\partial^2 e_1}{\partial t^2}\right]=\Delta\varphi\left(\frac{\partial}{\partial t}+a_8\right), \tag{6.27}$$

$$t_{zz}=a_{14}\frac{\partial u_z}{\partial z}+a_{13}\left(\frac{\partial u_r}{\partial r}+\frac{u_r}{r}\right)-T, \tag{6.28}$$

$$t_{zr}=a_{10}\left(\frac{\partial u_r}{\partial z}+\frac{\partial u_z}{\partial r}\right)+a_{11}\frac{\partial u_r}{\partial z}-a_{12}\phi_\theta, \tag{6.29}$$

$$m_{z\theta}=a_{15}\frac{\partial \phi_\theta}{\partial z}, \tag{6.30}$$

$$\ddot{T}=\ddot{\varphi}-\beta^*\Delta\varphi. \tag{6.31}$$

where $a_i (i = 1 \cdots 7)$ are as given by equation (2.42) [Chapter 2] and $a_i (i = 8 \cdots 15)$ are as given by equation (3.40) [Chapter3].

6.4 Solution Procedure

The displacement components u_r and u_z, as well as the microrotational component ϕ_θ, are written as scalar potential functions using Helmholtz decomposition:

$$u_r = \frac{\partial \psi_1}{\partial r} + \frac{\partial^2 \psi_2}{\partial r \partial z}, \qquad u_z = \frac{\partial \psi_1}{\partial z} - \left(\frac{\partial^2}{\partial r^2} + \frac{1}{r}\frac{\partial}{\partial r}\right)\psi_2, \quad \phi_\theta = -\frac{\partial \Gamma}{\partial r}. \tag{6.32}$$

With the aid of (6.32), equations (6.24) -(6.27) reduce to

$$\Delta\psi_1 - \left(1 - {\xi_1}^2 \Delta\right) \frac{\partial^2 \psi_1}{\partial t^2} - a_4 T = 0 \tag{6.33}$$

$$a_2 \Delta\psi_2 - \left(1 - {\xi_1}^2 \Delta\right) \frac{\partial^2 \psi_2}{\partial t^2} + a_3 \Gamma = 0, \tag{6.34}$$

$$a_5 \left(\Delta - \frac{1}{r^2}\right)\Gamma + a_6 \Delta\psi_2 - a_7 \Gamma = \left(1 - {\xi_2}^2 \Delta\right)\frac{\partial^2 \Gamma}{\partial t^2}, \tag{6.35}$$

$$\left(1 + \tau_0 \frac{\partial}{\partial t}\right)\left(\frac{\partial^2 T}{\partial t^2} + a_9 \left(\frac{\partial^2}{\partial t^2}\Delta\psi_1\right)\right) = \Delta\varphi\left(\frac{\partial}{\partial t} + a_8\right), \tag{6.36}$$

According to Debnath (1995) [28], the L.T of a function $g(x_1, x_3, t)$ w.r.t the time variable t, where s is the L.T variable, is defined as follows, along with its fundamental properties:

$$\bar{g}(r, z, s) = L\{g(r, z, t)\} = \int_0^\infty g(r, z, t)\, e^{-st} dt, \tag{6.37}$$

$$\text{i) } L\left(\frac{\partial g}{\partial t}\right) = s\bar{g}(r, z, s) - g(r, z, 0), \tag{6.38}$$

$$\text{ii) } L\left(\frac{\partial^2 g}{\partial t^2}\right) = s^2 \bar{g}(r, z, s) - sg(r, z, 0) - \left(\frac{\partial g}{\partial t}\right)_{t=0}. \tag{6.39}$$

Initial conditions are as follows:

$$\psi_1(r, z, 0) = \left(\frac{\partial q}{\partial t}\right)_{t=0} = 0, \qquad T(r, z, 0) = \left(\frac{\partial T}{\partial t}\right)_{t=0} = 0,$$

$$\psi_2(r, z, 0) = \left(\frac{\partial \psi}{\partial t}\right)_{t=0} = 0, \qquad \varphi(r, z, 0) = \left(\frac{\partial \varphi}{\partial t}\right)_{t=0} = 0,$$

$$u_r(r, z, 0) = \left(\frac{\partial u_r}{\partial t}\right)_{t=0} = 0, \qquad u_z(r, z, 0) = \left(\frac{\partial u_z}{\partial t}\right)_{t=0} = 0,$$

$$\Gamma(r, z, 0) = \left(\frac{\partial \Gamma}{\partial t}\right)_{t=0} = 0, \tag{6.40}$$

Following Sneddon (1975) [156], the H.T of $\bar{g}(r, z, s)$ w.r.t the variable r is defined as follows:

$$\tilde{g}(\chi, z, s) = H_n\{\bar{g}(r, z, s)\} = \int_0^\infty r\bar{g}\,(r, z, s) J_n(\chi r) dr, \tag{6.41}$$

where χ represents Hankel's parameter and $J_n()$ is the Bessel function of first kind of order n with the following essential properties:

$$H_0\left(\frac{\partial \bar{g}}{\partial r} + \frac{1}{r}\bar{g}\right) = \chi H_1(\bar{g}), \qquad H_0\left(\frac{\partial^2 \bar{g}}{\partial r^2} + \frac{1}{r}\frac{\partial \bar{g}}{\partial r}\right) = -\chi^2 H_0(\bar{g}),$$

$$H_1\left(\frac{\partial \bar{g}}{\partial r}\right) = -\chi H_0(\bar{g}), \qquad H_1\left(\frac{\partial^2 \bar{g}}{\partial r^2} + \frac{1}{r}\frac{\partial \bar{g}}{\partial r} - \frac{1}{r^2}\bar{g}\right) = -\chi^2 H_1(\bar{g}). \tag{6.42}$$

Applying L.T and H.T transforms defined in equations (6.37) and (6.41) on equations (6.33) -(6.36) and (6.31) with the aid of (6.38) -(6.40) and (6.42), yield

$$[D_0^2 b_4 - (\chi^2 + b_1)]\widetilde{\psi}_1 - a_4\widetilde{T} = 0, \tag{6.43}$$

$$[(D_0^2(a_2 + s^2\xi_1^2) - (a_2\chi^2 + b_1)]\widetilde{\psi}_2 + a_3\widetilde{\Gamma} = 0, \tag{6.44}$$

$$[-D_0^2(a_5 + s^2\xi_2^2) + (a_5\chi^2 + a_7 + b_2)]\widetilde{\Gamma} + a_6(D_0^2 - \chi^2)\widetilde{\psi}_2 = 0, \tag{6.45}$$

$$\left[b_3 s^2\widetilde{T} - (a_8 + s)(D_0^2 - \chi^2)\widetilde{\varphi}\right] + b_3 s^2(D_0^2 - \chi^2)a_9\widetilde{\psi}_1 = 0, \tag{6.46}$$

$$\widetilde{T} = \widetilde{\varphi} - \varsigma(D_0^2 - \chi^2)\widetilde{\varphi}, \tag{6.47}$$

where

$$\varsigma = \begin{cases} \frac{\beta^*}{s^2}, \text{ for (HTT)} \\ a, \text{ for (TT)} \\ 0, \text{for one temperature (1T)}, \end{cases}$$

and

$$b_1 = s^2(1 + \chi^2\xi_1^2), b_2 = s^2(1 + \chi^2\xi_2^2), b_3 = (1 + \tau_0 s), b_4 = (1 + s^2\xi_1^2), D_0 = \frac{d}{dz}.$$

Using equation (6.47) in equations (6.43) and (6.46), yield

$$[D_0^2 b_4 - (\chi^2 + b_1)]\widetilde{\psi}_1 - a_4(1 - \varsigma(D_0^2 - \chi^2))\widetilde{\varphi} = 0, \tag{6.48}$$

$$[b_3 s^2(1 - \varsigma(D_0^2 - \chi^2)) - (a_8 + s)(D_0^2 - \chi^2)]\widetilde{\varphi} + b_3 s^2(D_0^2 - \chi^2)a_9\widetilde{\psi}_1 = 0, \tag{6.49}$$

After algebraic simplifications, equations (6.48), (6.49), (6.44) and (6.45), yield

$$(D_0^4 - S_{01}D_0^2 + S_{02})\left(\widetilde{\varphi}, \widetilde{\psi}_1\right) = 0, \tag{6.50}$$

$$(D_0^4 - S_{03}D_0^2 + S_{04})\left(\widetilde{\Gamma}, \widetilde{\psi}_2\right) = 0, \tag{6.51}$$

where

$$S_{01} = \frac{[(b_3\varsigma s^2 + s + a_8)(\chi^2 + b_1)] + b_4[s^2 b_3(1 + \chi^2\varsigma) + \chi^2(s + a_8)] + a_9 b_3 s^2(1 + 2\chi^2\varsigma)}{b_4(b_3\varsigma s^2 + s + a_8) + a_9 b_3\varsigma s^2},$$

$$S_{02} = \frac{(\chi^2 + b_1)[s^2 b_3(1 + \chi^2\varsigma) + \chi^2(s + a_8)] + b_3 a_9\chi^2(1 + \chi^2\varsigma)}{b_4(b_3\varsigma s^2 + s + a_8) + a_9 b_3\varsigma s^2},$$

$$S_{03} = \frac{\left[(a_2 + s^2{\xi_1}^2)(a_5\chi^2 + a_7 + b_2)\right] + \left[\left(a_5 + s^2{\xi_2}^2\right)(a_2\chi^2 + b_1)\right] - a_3 a_6}{\left(a_5 + s^2{\xi_2}^2\right)(a_2 + s^2{\xi_1}^2)},$$

$$S_{04} = \frac{[(a_2\chi^2 + b_1)(a_5\chi^2 + a_7 + b_2)] + a_3 a_6\chi^2}{\left(a_5 + s^2{\xi_2}^2\right)(a_2 + s^2{\xi_1}^2)}.$$

The solution of equations (6.50) and (6.51), utilizing the radiation conditions $\widetilde{\psi}_1, \widetilde{\varphi}, \widetilde{\psi}_2$ and $\widetilde{\Gamma} \to 0$ as $z \to \infty$, can be expressed as

$$\widetilde{\psi}_1 = \sum_{i=1}^{2}(Q_i e^{-\lambda_i z}), \tag{6.52}$$

$$\widetilde{\varphi} = \sum_{i=1}^{2}(O_i Q_i e^{-\lambda_i z}), \tag{6.53}$$

$$\tilde{\psi}_2 = \sum_{j=3}^{4}(Q_j e^{-\lambda_j z}), \tag{6.54}$$

$$\tilde{\Gamma} = \sum_{j=3}^{4}(O_j Q_j e^{-\lambda_j z}), \tag{6.55}$$

where $\pm\lambda_i\ (i = 1,2)$ and $\pm\lambda_j\ (j = 3,4)$ are the roots of the characteristic equations $(D_0^4 - S_{01}D_0^2 + S_{02}) = 0$ and $(D_0^4 - S_{03}D_0^2 + S_{04}) = 0$, respectively. Here, $Q_i(i = 1,2)$, $Q_j(j = 3,4)$ are arbitrary constants, and $O_i(i = 1,2)$, $O_j(j = 3,4)$ are coupling constants, represented as:

$$O_i = \frac{\lambda_i^2 b_4 - (\chi^2 + b_1)}{a_4(1 + \varsigma(\chi^2 - \lambda_i^2))}, \qquad O_j = \frac{(a_2\chi^2 + b_4) - \lambda_j^2(a_2 + s^2\xi_1^2)}{a_3}, \qquad (i = 1,2), (j = 3,4).$$

6.5 Boundary Restrictions

A normal (ring/disc) load is applied at the free surface z = 0, as seen in figure 6.1. This load originates at the coordinate origin and spreads rapidly over the surface at a constant rate 'c'. Under isothermal boundary conditions, both tangential stress and tangential couple stress vanish. These criteria can be stated mathematically as

$$(i)\quad t_{zz} = F_1(r,t), (ii)\quad t_{zr} = 0, (iii)\quad m_{z\theta} = 0, (iv)\ \varphi = 0, \tag{6.56}$$

where

$$F_1(r,t) = F_0 \begin{cases} \frac{1}{2\pi r}\delta(ct - r), & \text{ring load,} \\ \frac{1}{\pi(ct)^2}H(ct - r), & \text{disc load.} \end{cases} \tag{6.57}$$

In context of above boundary conditions, the total force applied on the surface remains constant over time and is denoted as F_0 which is initially applied at r = 0. As normal ring and disc loads expand, the normal stress decays as $\frac{1}{r}$ and $\frac{1}{t^2}$, respectively. δ() is a Dirac delta function, F_0 is magnitude of force and H () is known as Heaviside step function.

Applying the dimensionless quantities given by equation (6.23) on (6.56) and (6.57), yield the non-dimensional boundary condition and applying L.T and H.T on the non-dimensional boundary condition, we get

$$(i)\ \tilde{t}_{zz} = \tilde{F}_1(\chi, s),\ (ii)\ \tilde{t}_{zr} = 0,\ (iii)\ \tilde{m}_{z\theta} = 0, (iv)\ \tilde{\varphi} = 0, \qquad \text{at } z = 0 \tag{6.58}$$

where

$$\tilde{F}_1(\chi, s) = F_0 \begin{cases} \frac{1}{2\pi\sqrt{\chi^2 + \frac{s^2}{c^2}}}, & \text{ring load} \\ \frac{1}{\pi c\chi}\left(\sqrt{\chi^2 + \frac{s^2}{c^2}} - \frac{s}{c}\right), & \text{disc load.} \end{cases} \tag{6.59}$$

Using (6.37) -(6.42) on (6.32) and (6.28) -(6.30) with the aid of (6.47), components of displacement, microrotational and stresses are obtained as

$$\tilde{u}_r = -\chi\left(\tilde{\psi}_1 + \frac{d\tilde{\psi}_2}{dz}\right), \tag{6.60}$$

$$\tilde{u}_z = \frac{d\tilde{\psi}_1}{dz} + \chi^2\tilde{\psi}_2, \tag{6.61}$$

$$\tilde{\phi}_\theta = \chi\tilde{\Gamma} \tag{6.62}$$

$$\tilde{t}_{zz} = a_{14}\frac{d\tilde{u}_z}{dz} + a_{13}\chi\tilde{u}_r - (1 - \varsigma\left(\frac{d^2}{dz^2} - \chi^2\right))\tilde{\varphi}, \tag{6.63}$$

$$\tilde{t}_{zr} = (a_{10} + a_{11})\frac{d\tilde{u}_r}{dz} - a_{10}\chi\tilde{u}_z - a_{12}\tilde{\phi}_\theta, \tag{6.64}$$

$$\tilde{m}_{z\theta} = a_{15}\frac{d\tilde{\phi}_\theta}{dz}. \tag{6.65}$$

By substituting the values of $\tilde{\psi}_1, \tilde{\varphi}, \tilde{\psi}_2$ and $\tilde{\Gamma}$ from (6.52) -(6.55) into the boundary condition (6.58), and using equations (6.60) -(6.65), we derive the following results for displacement components, stresses, tangential couple stress, conductive temperature, and thermodynamic temperature as

$$\tilde{u_r} = \frac{-\tilde{F}_1(\chi,s)\chi}{\Omega}\left[\sum_{i=1}^{2}(\Omega_{i1}\, e^{-\lambda_i z}) - \sum_{i=3}^{4}(\lambda_i\Omega_{i1}\, e^{-\lambda_i z})\right], \tag{6.66}$$

$$\tilde{u}_z = \frac{-\tilde{F}_1(\chi,s)}{\Omega}\left[\sum_{i=1}^{2}(\lambda_i\Omega_{i1}\, e^{-\lambda_i z}) - \sum_{i=3}^{4}(\chi^2\Omega_{i1}\, e^{-\lambda_i z})\right], \tag{6.67}$$

$$\tilde{t}_{zz} = \frac{\tilde{F}_1(\chi,s)}{\Omega}\left[\sum_{i=1}^{4}(U_i\Omega_{i1}\, e^{-\lambda_i z})\right], \tag{6.68}$$

$$\tilde{t}_{zr} = \frac{\tilde{F}_1(\chi,s)}{\Omega}\left[\sum_{i=1}^{4}(U_{i+4}\Omega_{i1}\, e^{-\lambda_i z})\right], \tag{6.69}$$

$$\tilde{m}_{z\theta} = \frac{\tilde{F}_1(\chi,s)}{\Omega}\left[\sum_{i=3}^{4}(U_{i+6}\Omega_{i1}\, e^{-\lambda_i z})\right], \tag{6.70}$$

$$\tilde{\varphi} = \frac{\tilde{F}_1(\chi,s)}{\Omega}\left[\sum_{i=1}^{2}(O_i\Omega_{i1}\, e^{-\lambda_i z})\right], \tag{6.71}$$

$$\tilde{T} = \frac{\tilde{F}_1(\chi,s)}{\Omega}\left[\sum_{i=1}^{2}(O_iU_{i+10}\Omega_{i1}\, e^{-\lambda_i z})\right], \tag{6.72}$$

where

$\Omega = HT_1 + HT_2, \qquad \Omega_{11} = O_2(U_7U_{10} - U_8U_9), \quad \Omega_{21} = O_1(U_8U_9 - U_7U_{10}),$

$\Omega_{31} = -U_{10}(O_2U_5 - O_1U_6), \ \Omega_{41} = -U_9(O_1U_6 - O_2U_5),$

$HT_1 = -O_1[U_9(U_4U_6 - U_2U_8) - U_{10}(U_3U_6 - U_2U_7)],$

$HT_2 = O_2[U_9(U_4U_5 - U_1U_8) + U_{10}(U_1U_7 - U_3U_5)],$

$U_i = (a_{14}\lambda_i^2 - (1 + \varsigma\chi^2)O_i + \varsigma O_i\lambda_i^2 - \chi^2 a_{13}), \qquad U_j = \chi^2\lambda_j(a_{13} - a_{14}),$

$U_{i+4} = \chi\lambda_i(a_{11} + 2a_{10}), \qquad U_{j+4} = -\chi((a_{10} + a_{11})\lambda_j^2 + \chi^2 a_{10} + a_{12}O_j),$

$U_{j+6} = a_{15}\chi\lambda_j O_j, \qquad U_{i+10} = (1 + \varsigma(\chi^2 - \lambda_i^2)), \quad (i = 1,2), (j = 3,4).$

6.6 Validations

i) In the absence of N-L parameters ($\xi_1 = \xi_2 = 0$) and micropolar parameters ($\alpha = \beta = \gamma = K = 0$), together with $\varsigma = a$, and $K_1^* = 0$, the equations (6.50) and (6.51) reduces as

$$(D_0^4 - S_{01}D_0^2 + S_{02})\left(\widetilde{\varphi}, \widetilde{\psi}_1\right) = 0, \tag{6.73}$$

$$(D_0^2 - \lambda_3^2)\widetilde{\psi}_2 = 0, \tag{6.74}$$

with changed values of

$S_{01} = \frac{(2\chi^2+s^2)+ab_1(\chi^2+s^2+a_3a_4\chi^2)+b_1(1+a\chi^2)(1+a_3a_4)}{1+ab_1(1+a_3a_4)}$, $S_{02} = \frac{\chi^2(\chi^2+s^2)+b_1(1+a\chi^2)(\chi^2+s^2+a_3a_4\chi^2)}{1+ab_1(1+a_3a_4)}$,

$\lambda_3^2 = \frac{(a_2\chi^2+s^2)}{a_2}$, $a_2 = \frac{\mu}{\rho c_1^2}$, $a_3 = \frac{\gamma_1 T_0}{\rho c_1^2}$, $a_4 = \frac{\gamma_1 c_1^2}{\omega_1 K^*}$, $a_5 = \frac{\mu}{\gamma_1 T_0}$,

$a_6 = \frac{\lambda}{\gamma_1 T_0}$, $a_7 = \frac{(\lambda+2\mu)}{\gamma_1 T_0}$, $b_1 = (1 + \tau_0 s)s$.

Also, equations (6.66) -(6.72) reduces as

$$\widetilde{u_r} = \frac{-\widetilde{F}_1(\chi,s)\chi}{\Omega}\left[\sum_{i=1}^{2}(\Omega_{i1}\, e^{-\lambda_i z}) - \lambda_3\Omega_{31}e^{-\lambda_3 z}\right], \tag{6.75}$$

$$\tilde{u}_z = \frac{-\widetilde{F}_1(\chi,s)}{\Omega}\left[\sum_{i=1}^{2}(\lambda_i\Omega_{i1}\, e^{-\lambda_i z}) - \chi^2\Omega_{31}e^{-\lambda_3 z}\right], \tag{6.76}$$

$$\tilde{t}_{zz} = \frac{\widetilde{F}_1(\chi,s)}{\Omega}\left[\sum_{i=1}^{3}(U_i\Omega_{i1}\, e^{-\lambda_i z})\right], \tag{6.77}$$

$$\tilde{t}_{zr} = \frac{\widetilde{F}_1(\chi,s)}{\Omega}\left[\sum_{i=1}^{3}(U_{i+3}\Omega_{i1}\, e^{-\lambda_i z})\right], \tag{6.78}$$

$$\widetilde{\varphi} = \frac{\widetilde{F}_1(\chi,s)}{\Omega}\left[\sum_{i=1}^{2}(O_i\Omega_{i1}\, e^{-\lambda_i z})\right], \tag{6.79}$$

$$\widetilde{T} = \frac{\widetilde{F}_1(\chi,s)}{\Omega}\left[\sum_{i=1}^{2}(O_iU_{i+6}\Omega_{i1}\, e^{-\lambda_i z})\right], \tag{6.80}$$

where

$\Omega = O_1(U_2U_6 - U_3U_5) + O_2(U_3U_4 - U_1U_6)$, $\Omega_{11} = O_2U_6$, $\Omega_{21} = O_1U_6$,

$\Omega_{31} = (O_2U_4 - O_1U_5)$, $U_i = (a_7\lambda_i^2 - (1 + a\chi^2)O_i + aO_i\lambda_i^2 - \chi^2 a_6)$,

$U_3 = \chi^2\lambda_3(a_6 - a_7)$, $U_{i+3} = 3a_5\chi\lambda_I$, $U_{i+6} = (1 + a(\chi^2 - \lambda_i^2))$,

$O_i = \frac{\lambda_i^2-(\chi^2+s^2)}{a_3(1+a(\chi^2-\lambda_i^2))}$, $(i = 1,2)$.

The above equations represent results for L-S model with TT, which are consistent to those obtained by Miglani and Kaushal (2011) [106] (In absence of normal force and thermal source at boundary).

ii) Assuming $\xi_1 = \xi_2 = \varsigma = \alpha = \beta = \gamma = K = \tau_0 = K_1^* = 0$, the equations (6.50) and (6.51) reduces as

$$(D_0^4 - S_{01}D_0^2 + S_{02})\left(\widetilde{\varphi}, \widetilde{\psi}_1\right) = 0, \tag{6.81}$$

$$(D_0^2 - \lambda_3^2)\widetilde{\psi}_2 = 0, \tag{6.82}$$

with changed values of

$S_{01} = (2\chi^2 + s^2) + s(1 + a_3a_4)$, $S_{02} = \chi^2(\chi^2 + s^2) + s(\chi^2 + s^2 + a_3a_4\chi^2)$,

$\lambda_3^2 = \frac{(a_2\chi^2+s^2)}{a_2}$, $a_2 = \frac{\mu}{\rho c_1^2}$, $a_3 = \frac{\gamma_1 T_0}{\rho c_1^2}$, $a_4 = \frac{\gamma_1 c_1^2}{\omega_1 K^*}$, $a_5 = \frac{\mu}{\gamma_1 T_0}$, $a_6 = \frac{\lambda}{\gamma_1 T_0}$, $a_7 = \frac{(\lambda+2\mu)}{\gamma_1 T_0}$.

Also, equations (6.66) -(6.72) reduces as

$$\tilde{u_r} = \frac{-\tilde{F}_1(\chi,s)\chi}{\Omega}\left[\sum_{i=1}^{2}(\Omega_{i1}\, e^{-\lambda_i z}) - \lambda_3\Omega_{31}e^{-\lambda_3 z}\right], \tag{6.83}$$

$$\tilde{u}_z = \frac{-\tilde{F}_1(\chi,s)}{\Omega}\left[\sum_{i=1}^{2}(\lambda_i\Omega_{i1}\, e^{-\lambda_i z}) - \chi^2\Omega_{31}e^{-\lambda_3 z}\right], \tag{6.84}$$

$$\tilde{t}_{zz} = \frac{\tilde{F}_1(\chi,s)}{\Omega}\left[\sum_{i=1}^{3}(U_i\Omega_{i1}\, e^{-\lambda_i z})\right], \tag{6.85}$$

$$\tilde{t}_{zr} = \frac{\tilde{F}_1(\chi,s)}{\Omega}\left[\sum_{i=1}^{3}(U_{i+3}\Omega_{i1}\, e^{-\lambda_i z})\right], \tag{6.86}$$

$$\tilde{\varphi} = \frac{\tilde{F}_1(\chi,s)}{\Omega}\left[\sum_{i=1}^{2}(O_i\Omega_{i1}\, e^{-\lambda_i z})\right], \tag{6.87}$$

where

$\Omega = O_1(U_2U_6 - U_3U_5) + O_2(U_3U_4 - U_1U_6)$, $\Omega_{11} = O_2U_6$, $\Omega_{21} = O_1U_6$,

$\Omega_{31} = (O_2U_4 - O_1U_5)$, $U_i = (a_7\lambda_i^2 - O_i - \chi^2 a_6)$, $U_3 = \chi^2\lambda_3(a_6 - a_7)$,

$U_{i+3} = 3a_5\chi\lambda_I$, $O_i = \frac{\lambda_i^2 - (\chi^2 + s^2)}{a_3}$, $(i = 1,2)$.

These results align with the classical theory of thermoelasticity, which are consistent with those reported by Kumar et al. (2014) [83] in the absence of porous media.

6.6.1 Special Cases

i) When $K_1^* \neq 0, K^* = 0$ and $\tau_0 = 0$ are considered, then expressions from (6.66) -(6.72) reduce for GN-II theory of thermoelasticity with micropolar, N-L and HTT effects.

(ii) If $K_1^* \neq 0, K^* \neq 0$ and $\tau_0 = 0$, the derived results from (6.66) -(6.72) diminish for Green-Naghdi–III (GN-III) thermoelasticity theory with N-L, micropolar and HTT effects.

(iii) To reduce the results to the MGT thermoelastic model with HTT and N-L effects, we substitute $\alpha = \beta = \gamma = K = 0$ in equations (6.66) -(6.72).

6.7 Inversion of Transformations

To address the problem in the physical realm, where the components of displacement, stresses, tangential couple stress, conductive temperature, and thermodynamic temperature are expressed as functions of $\tilde{g}(\chi, z, s)$, we need to invert the transforms. We begin by inverting the H.T utilising

$$\bar{g}(r, z, s) = \int_0^\infty \chi\, \tilde{g}(\chi, z, s)\, J_n(\chi r) d\chi, \tag{6.88}$$

Press et al. (1986) [118] detailed a method to evaluate integral (6.88) using Romberg's integration technique with adaptive step size. This approach involves iteratively refining the results using the extended trapezoidal rule and extrapolating these results as the step size approaches zero.

The expression (6.88) calculates the L.T of the function $g(r, z, t)$. Honig and Hirdes (1984) [53] propose inverting $\bar{g}(r, z, s)$ to produce $g(r, z, t)$ as

$$g(r, z, t) = \frac{1}{2\pi i}\int_{C-i\infty}^{C+i\infty} \bar{g}(r, z, s)\exp(st)\, ds, \qquad (6.89)$$

where C is a real number that exceeds the real components of all singularities $\bar{g}(r, z, s)$.

The final step involves calculating the integral in equation (6.89). The details of this method are described in section 5.7 [Chapter 5].

6.8 Discussion and Implementation of Numerical Solutions

To study the effects of various parameters, numerical simulations are performed for several cases: (i) HTT (ii) ξ_1 and ξ_2 (iii) time domain analysis, under ring and disc loads in MT media governed by MGT heat equation.

For the numerical results and discussions, a magnesium crystal-like material is considered, with numerical data as provided in section 3.8 [Chapter 3].

6.8.1 Impacts of HTT and TT

We assume N-L parameters $\xi_1 = 0.25$ and $\xi_2 = 0.35$ for the range $0 \leq r \leq 10$.

All the curves with HTT ($\varsigma = 0.75$) are represented by solid line (—).

All the curve with TT ($a = 0.0104$) are denoted by small dashed line (---).

All the curves without HTT ($\varsigma = 0$) are represented by big dashed line ($- - -$).

Figures 6.2-6.5, show the effects of HTT and TT due to ring load on all considered cases.

Figures 6.6-6.9, show the effects of HTT and TT due to disc load on all considered cases.

6.8.1.1 Ring Load

Figure 6.2 exhibits variations of t_{zz} vs. r. The value of t_{zz} shows an increasing trend in the range $0 \leq r \leq 2$ in all cases. As r increases, t_{zz} shows small variations about origin.

Figure 6.3 is a plot of t_{zr} vs. r. The magnitude of t_{zr} exhibits a descending behavior for the range $0 \leq r \leq 1$ across all considered cases. As r increases, t_{zr} shows steady state about the value '0'.

Figure 6.4 demonstrates the variations of $m_{z\theta}$ vs. r. It is evident that $m_{z\theta}$ shows opposite behavior throughout the entire range for TT and in the absence of HTT, highlighting the impact of TT parameter. While the value of $m_{z\theta}$ for $\varsigma = 0.75$ decrease with larger magnitude in $0 \leq r \leq 2$ and exhibits an oscillatory behavior in rest of the interval.

Figure 6.5 exhibits variations φ vs. r. The values of φ decreases strictly within the bounded region $0 \leq r \leq 2$ and beyond this range, small variations are noted near the origin for all the considered cases, magnitude of φ remain lower for $\varsigma = 0.75$ as compared to remaining cases.

6.8.1.2 Disc Load

Figure 6.6 illustrates the variations of t_{zz} vs. r. For $\varsigma = 0.75$, t_{zz} increases prominently for the range $0 \leq r \leq 2$, while it displays reverse behavior for a = 0.0104 and $\varsigma = 0$. As r increases, t_{zz} exhibits oscillatory behavior, with the magnitude of oscillation being greater for $\varsigma = 0.75$.

Figure 6.7 displays the variations of t_{zr} vs. r. For $\varsigma = 0.75$, the magnitude of t_{zr} decrease abruptly in the region $0 \leq r \leq 1$, whereas for TT and without HTT, it exhibits an increasing trend. As r increases, t_{zr} oscillates with decreasing magnitude for $\varsigma = 0.75$. In case of a = 0.0104 and $\varsigma = 0$, t_{zr} shows small variations about the origin.

Figure 6.8 demonstrates $m_{z\theta}$ vs. r. It is evident that the behavior of $m_{z\theta}$ for a = 0.0104 is opposite in comparison to $\varsigma = 0.75$ and $\varsigma = 0$, with significant difference in their magnitudes.

Figure 6.9 is a plot of φ vs. r. It is noticed that the magnitude of φ drops for the region $0 \leq r \leq 2$ and oscillates beyond that region for all cases. Additionally, it is noted that the magnitude of φ is higher for $\varsigma = 0.75$ when compared to other cases.

6.8.2 Non-Local Effect

In this case, we take the HTT parameter for the range $0 \leq r \leq 10$.

For $\xi_1 = 0.0, \xi_2 = 0.0$, the curves are represented by the solid line (—).

For $\xi_1 = 0.25, \xi_2 = 0.0$, the curves are denoted by the small dashed line (---).

For $\xi_1 = 0.0, \xi_2 = 0.35$, the curves are represented by the solid line (-△-).

For $\xi_1 = 0.25, \xi_2 = 0.35$, the curves are denoted by the small dashed line (-◇-).

Figures 6.10-6.13 depict the impacts of ξ_1 and ξ_2 due to the ring load on all considered cases.

Figures 6.14-6.17 depict the impacts of ξ_1 and ξ_2 due to the disc load on all considered cases.

6.8.2.1 Ring Load

Figure 6.10 illustrates the variations of t_{zz} vs. r. It is noticed that, the values of t_{zz} shows increasing trend for all considered cases near the loading surface. However, the magnitude of t_{zz} is higher for $(\xi_1 = 0.25, \xi_2 = 0.0)$ and $(\xi_1 = 0.0, \xi_2 = 0.35)$ compared to $(\xi_1 = 0.25, \xi_2 = 0.35)$ and $(\xi_1 = 0.0, \xi_2 = 0.0)$ respectively. As r increases, the values of t_{zz} exhibit oscillating behavior.

Figure 6.11 is a plot of t_{zr} vs. r. It is evident that t_{zr} follows a similar pattern across all models, with substantial differences in their magnitude. Furthermore, the values of t_{zr} are maximum for $(\xi_1 = 0.25$ and $\xi_2 = 0.0)$, and lowest in the absence of N-L parameters.

Figure 6.12 exhibits the behaviour of $m_{z\theta}$ vs. r. The magnitude of $m_{z\theta}$ varies significantly across all scenarios, despite a consistent trend.

Figure 6.13 demonstrate the variations of φ vs. r. The magnitude of φ drops in the range of $0 \leq r \leq 2$, with a greater decrement in the absence of N-L parameters. As r increases, the values of φ vary around zero with decreasing magnitude. Furthermore, the values of φ for $(\xi_1 = 0.25, \xi_2 = 0.0)$ remain higher compared to other cases.

6.8.2.2 Disc Load

Figure 6.14 exhibits variations of t_{zz} vs. r. The magnitude of t_{zz} increases in the ranges $0 \leq r \leq 2$, $4 \leq r \leq 6$, $8 \leq r \leq 10$, but decreases in the remaining range for all cases considered.

Figure 6.15 demonstrates that the magnitude of t_{zr} decreases in the ranges $0 \leq r \leq 1$, $3 \leq r \leq 5$, $7 \leq r \leq 8$, while the opposite trend is noticed in the remaining interval for all cases. Furthermore, the magnitude of t_{zr} is shown to be lowest in the absence of N-L parameters across entire range except some values of r.

Figure 6.16 displays the variations of $m_{z\theta}$ vs. r. The magnitude of $m_{z\theta}$ for $\xi_1 = 0.25, \xi_2 = 0.35$ differs significantly from other cases, indicating the impact of N-L factors.

Figure 6.17 exhibits variations of φ vs. r. It is noticed that the magnitude of φ declines throughout a limited region $0 \leq r \leq 2$, with minor changes around the origin for all considered cases. Furthermore, the values of φ remain higher for $\xi_1 = 0.25, \xi_2 = 0.0$ compared to other cases.

6.8.3 Time Domain Variation

We consider $\xi_1 = 0.25$ and $\xi_2 = 0.35$ with HTT parameter for the range $0 \leq r \leq 10$.

The solid line (—) represents the curves for $t = 0.5$ RL.

The small dashed line (---) denotes the curves for $t = 0.1$ RL.

The solid line (—△—) represents the curves for $t = 0.5$ DL.

The small dashed line (--◇--) denotes the curves for $t = 0.1$ DL.

Here, RL and DL represent ring load and disc load respectively.

Figures 6.18-6.21, show the impacts of different time domains under ring load and disc load on all considered cases.

6.8.3.1 Due to Ring load and Disc load

Figure 6.18 exhibits the variation of t_{zz} vs. r due to ring and disc loads. It is noticed that, due to the loading and different time domains, the material along the boundary surface expands in an uncontrolled direction. This suggests that stress moves initially in the negative direction, then transitions from negative to positive, and finally tends to zero to achieve a steady state

in all investigated cases. However, magnitude of t_{zz} is higher for t=0.1 RL for most of the range.

Figure 6.19 displays the trend of t_{zr} vs. r due to ring and disc loads. The values of t_{zr} for t=0.5 RL oscillate about origin for the entire range of r. For other considered cases, the values decrease monotonically within the range of $0 \leq r \leq 1.7$, and then oscillate about origin as r increase further for both time domains.

Figure 6.20 shows the variations of $m_{z\theta}$ vs. r due to ring and disc loads. The values of $m_{z\theta}$ initially increase sharply and then approaches to zero in an oscillatory manner for t=0.5 DL. In contrast, for the remaining cases, $m_{z\theta}$ shows a small initial decrement and then oscillates near the application of load.

Figure 6.21 demonstrates the trend of φ vs. r due to ring and disc loads. It is evident that magnitude of φ decreases strictly within the bounded region $0 \leq r \leq 2$. Beyond that, small variations are noticed near the origin for all cases. The magnitude of φ remains higher for t=0.5 RL compared to the remaining cases.

6.9 Conclusion

In this chapter, a two-dimensional micropolar axisymmetric problem governed by the MGT heat equation**,** incorporating HTT and N-L parameters is presented. We obtain a new set of governing equations by translating the equation system into dimensionless form and introducing potential functions. These equations are solved using L.T and H.T. The components of displacement, stresses, tangential couple stress, conductive temperature, and thermodynamic temperature are then reverted to the original domain through a numerical inversion technique. The numerical computations assess the effects of HTT, TT and N-L parameters, as well as ring and disc loads, on these physical quantities. These impacts are illustrated graphically.

From the empirical study, following observations are made:

i. Due to N-L parameters, the trend of tangential stress, normal stress, and tangential couple stress become oscillatory in presence of ring load.
ii. In the case of ring load, HTT parameter enhances the magnitude of conductive temperature, normal stress, and tangential couple stress.
iii. Due to ring load, uniform pattern is noticed for conductive temperature, tangential couple stress, and tangential stress, whereas their magnitudes show a decreasing trend in the absence of N-L parameters.
iv. Tangential stress attains a higher value for TT parameter near and far away from the boundary when a ring load is applied.

v. N-L parameters increase the magnitude of both tangential stress and conductive temperature in presence of disc load.

vi. Due to HTT parameter, normal stress, tangential stress, and tangential couple stress exhibit opposite behavior compared with other cases when a disc load is applied.

vii. In the presence of N-L parameters, the behavior of normal stress and tangential couple stress presents a mirror image of each other due to the disc loading.

viii. Due to mechanical loading, tangential couple stress, conductive temperature and tangential stress exhibit a descending behavior in both time domains near the boundary, while an opposite trend is observed for normal stress.

These findings are especially significant for practical applications involving materials with inherent microstructures subjected to ring and disc loadings. In particular, subsurface environments such as granular rock formations demand a deep understanding of these complex thermo-mechanical interactions. The insights gained from this study offer valuable contributions to fields such as geomechanics, seismic wave propagation, soil dynamics, and geo-material characterization, where the incorporation of micropolar thermoelastic behaviour markedly improves the accuracy of predictive models. By integrating microstructural effects and non-local interactions, this research provides a more realistic and robust framework for analysing material responses under real-world problems, thereby advancing both theoretical understanding and practical engineering solutions.

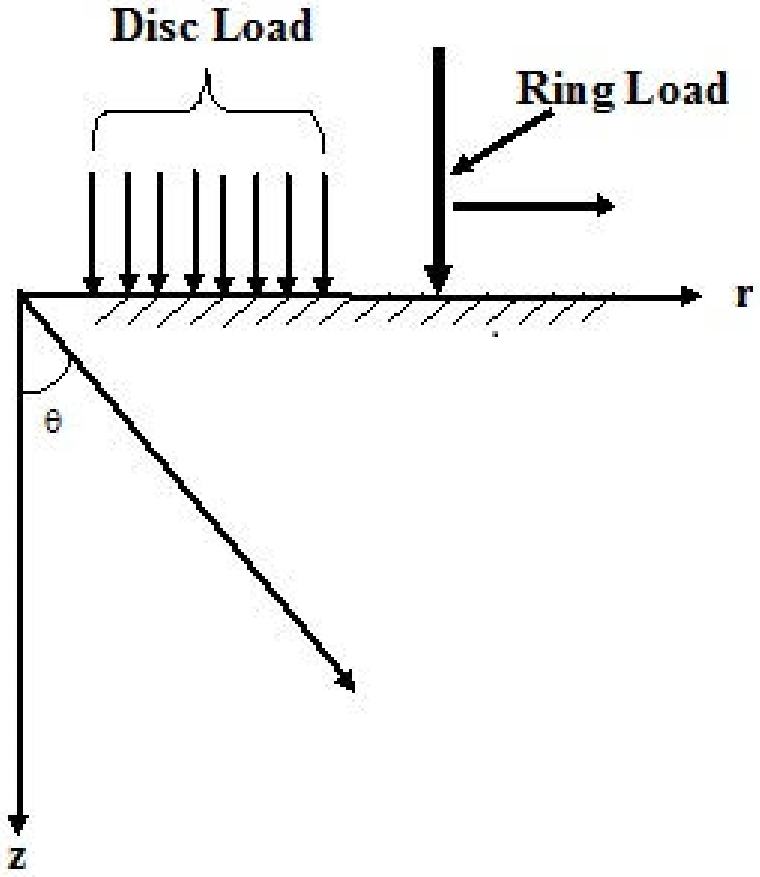

Figure 6.1: Schematic representation of the problem

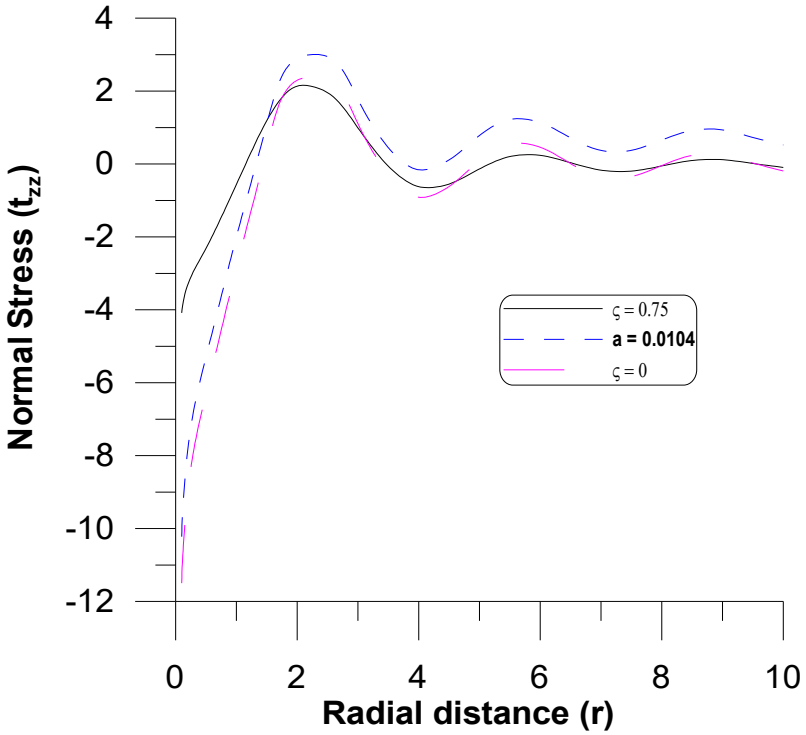

Fig. 6.2: t_{zz} vs. r
(Ring load)

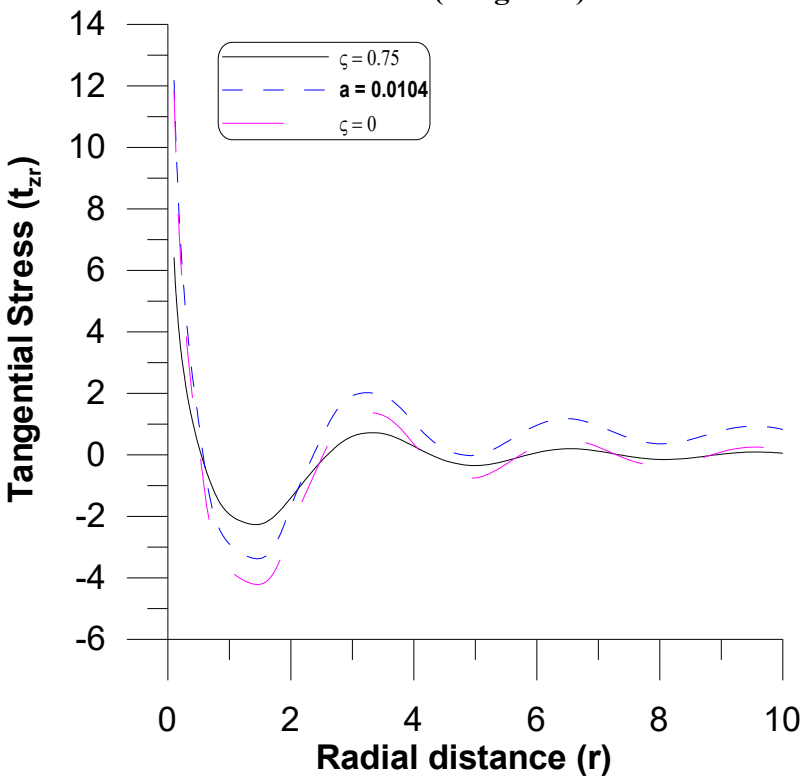

Fig.6.3: t_{zr} vs. r
(Ring load)

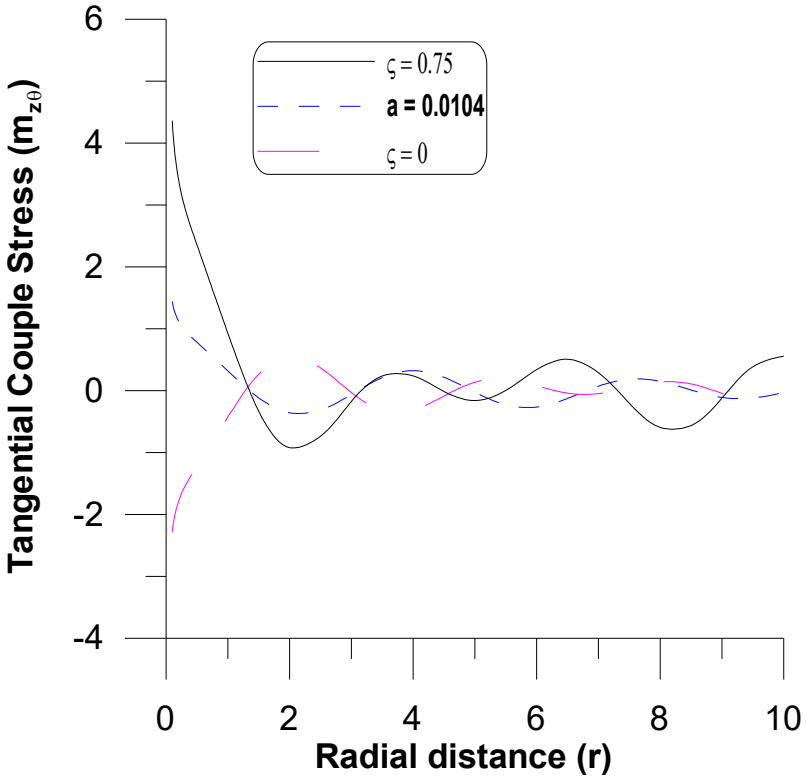

Fig.6.4: $m_{z\theta}$ vs. r
(Ring load)

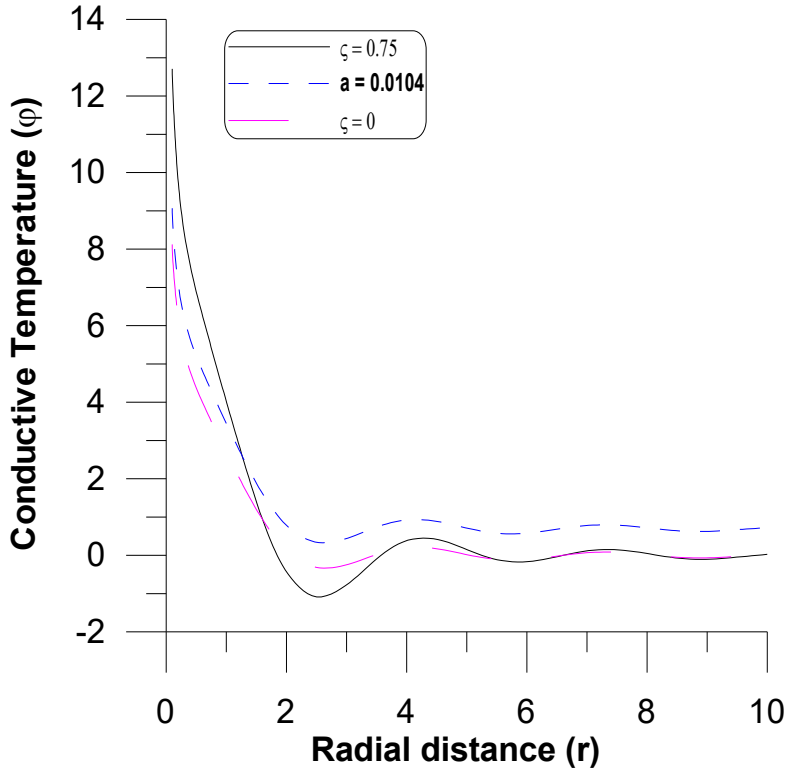

Fig.6.5: φ vs. r
(Ring load)

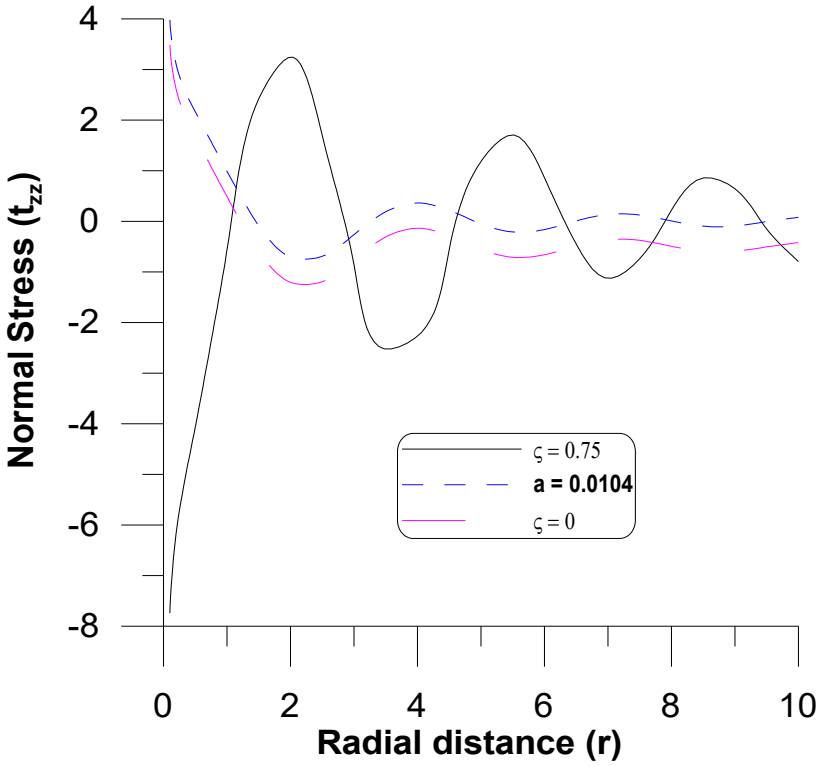

Fig. 6.6: t_{zz} vs. r
(Disc load)

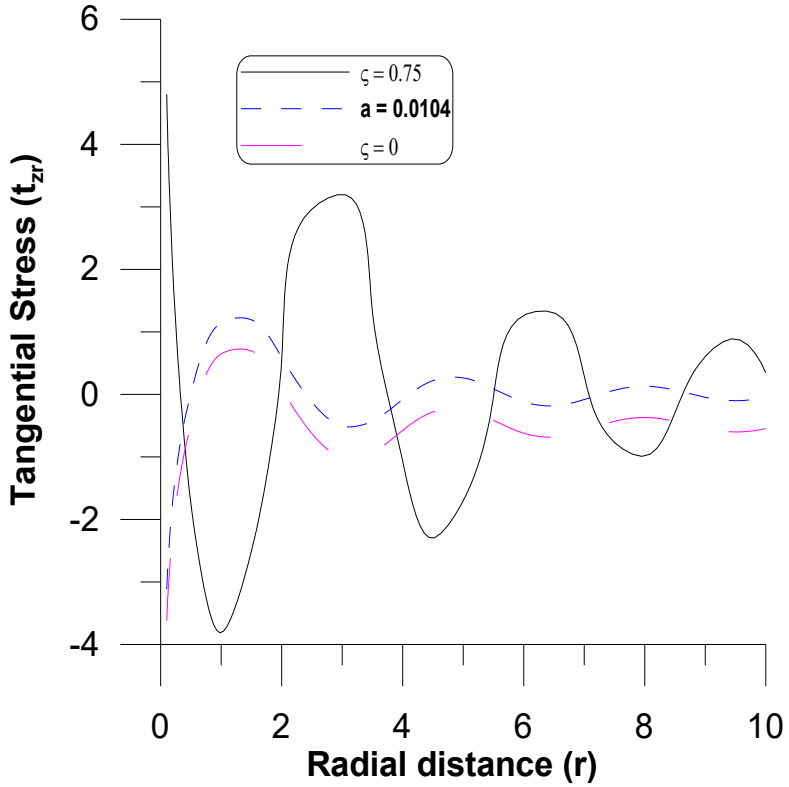

Fig.6.7: t_{zr} vs. r
(Disc load)

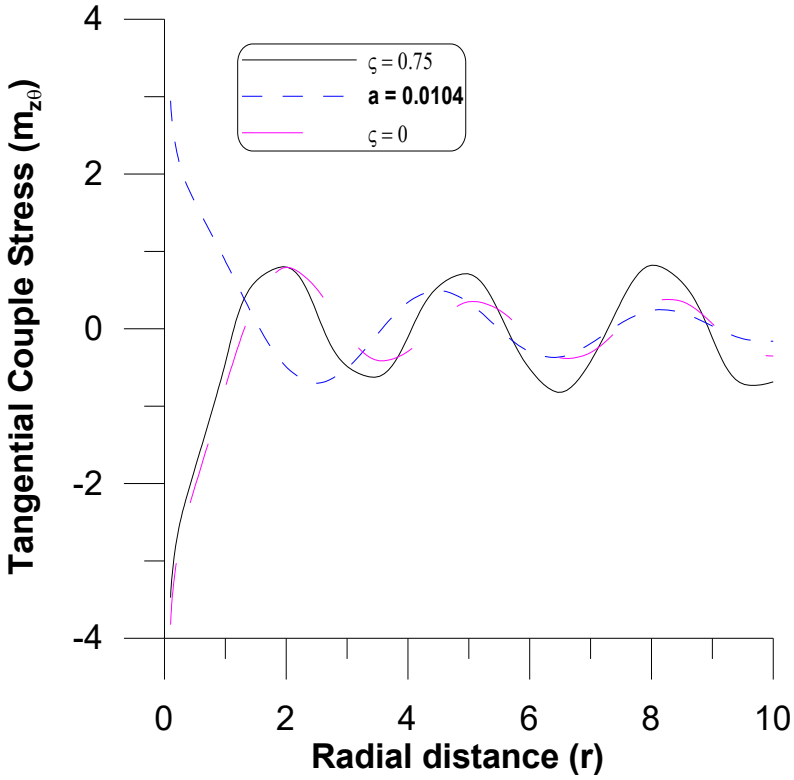

Fig.6.8: $m_{z\theta}$ vs. r
(Disc load)

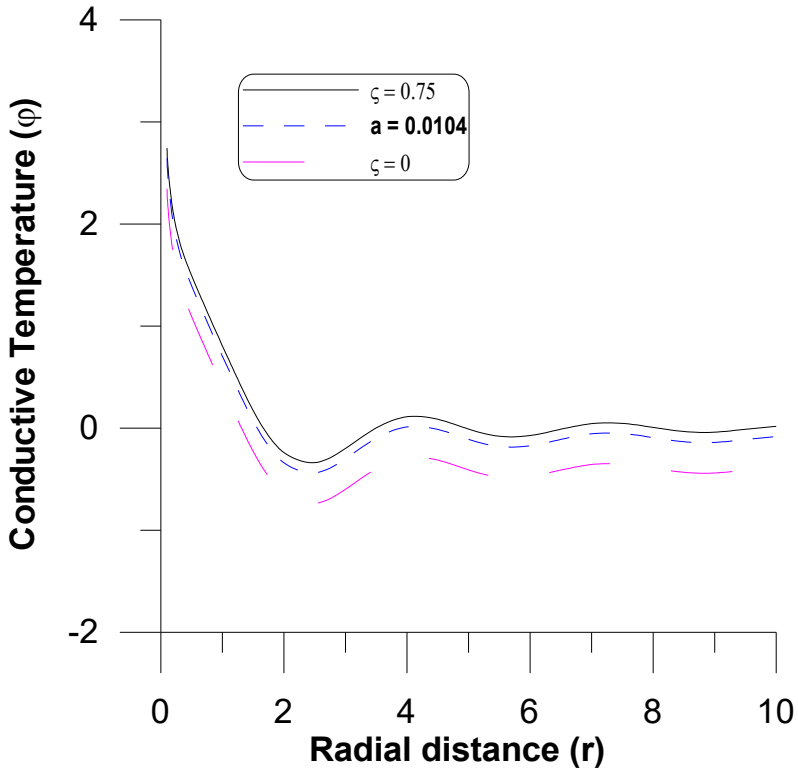

Fig.6.9: φ vs. r
(Disc load)

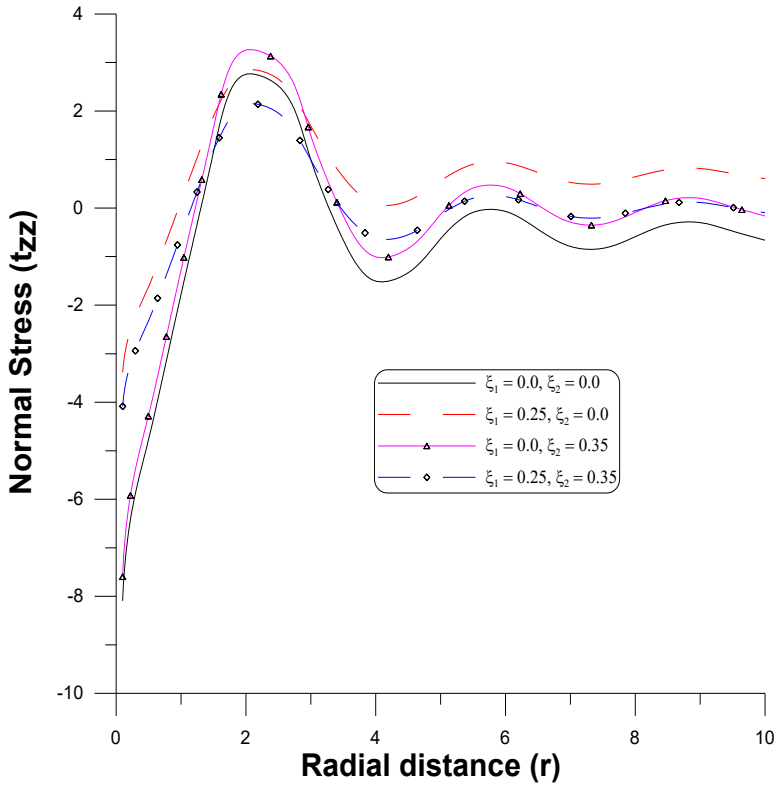

Fig. 6.10: t_{zz} vs. r
(Ring load)

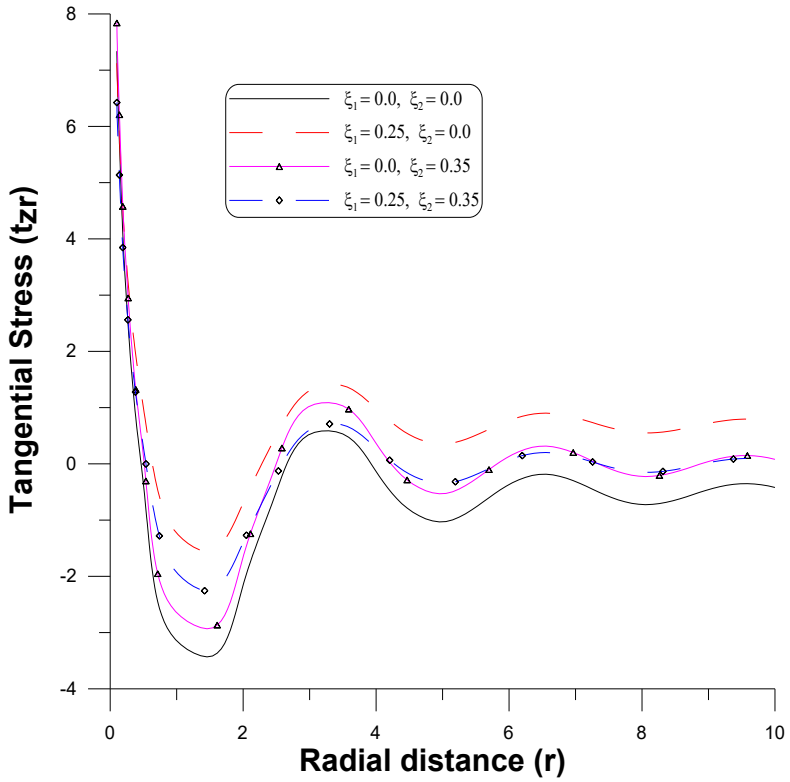

Fig.6.11: t_{zr} vs. r
(Ring load)

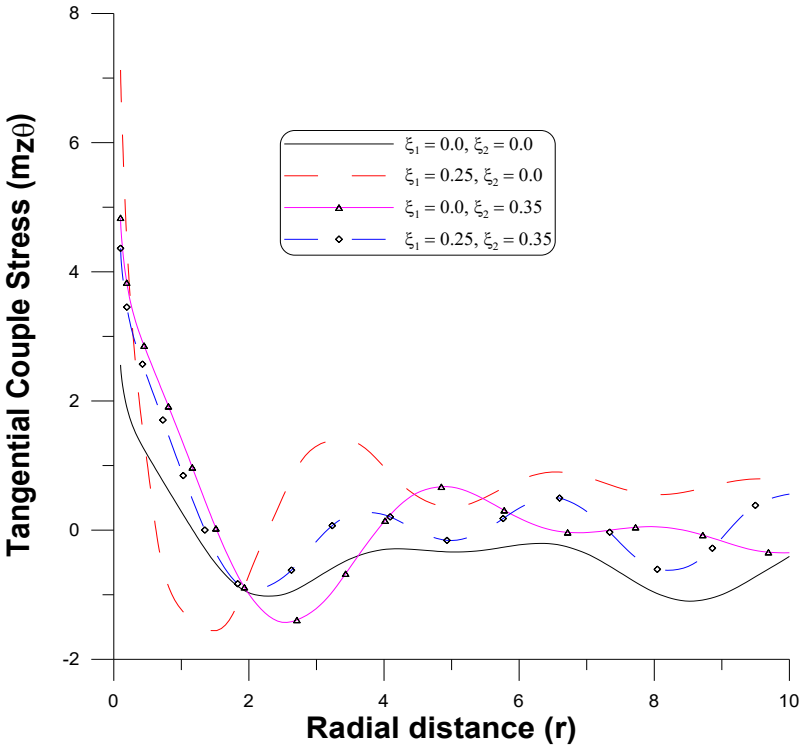

Fig.6.12: $m_{z\theta}$ vs. r
(Ring load)

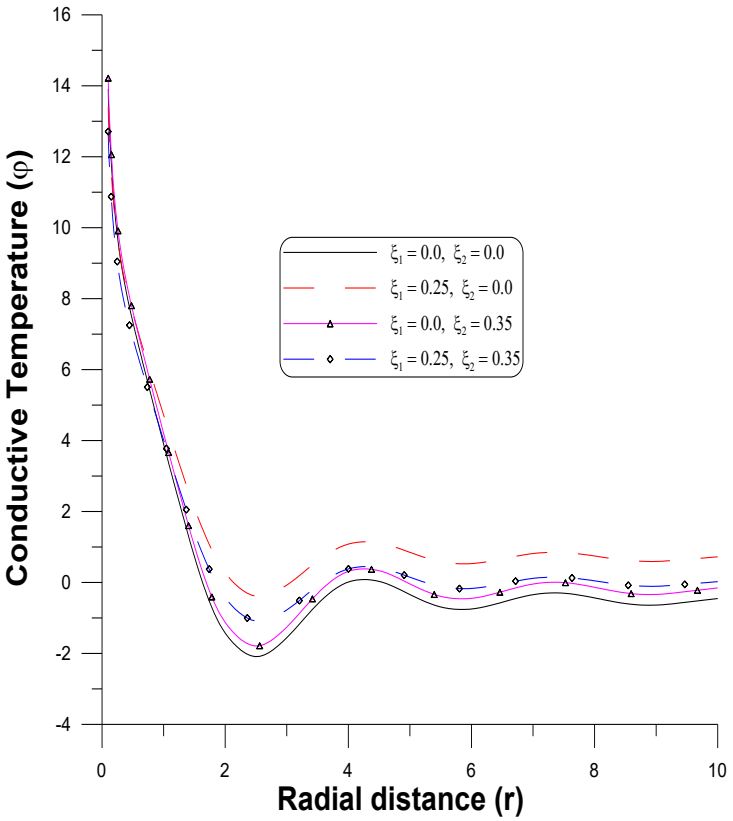

Fig. 6.13: φ vs. r
(Ring load)

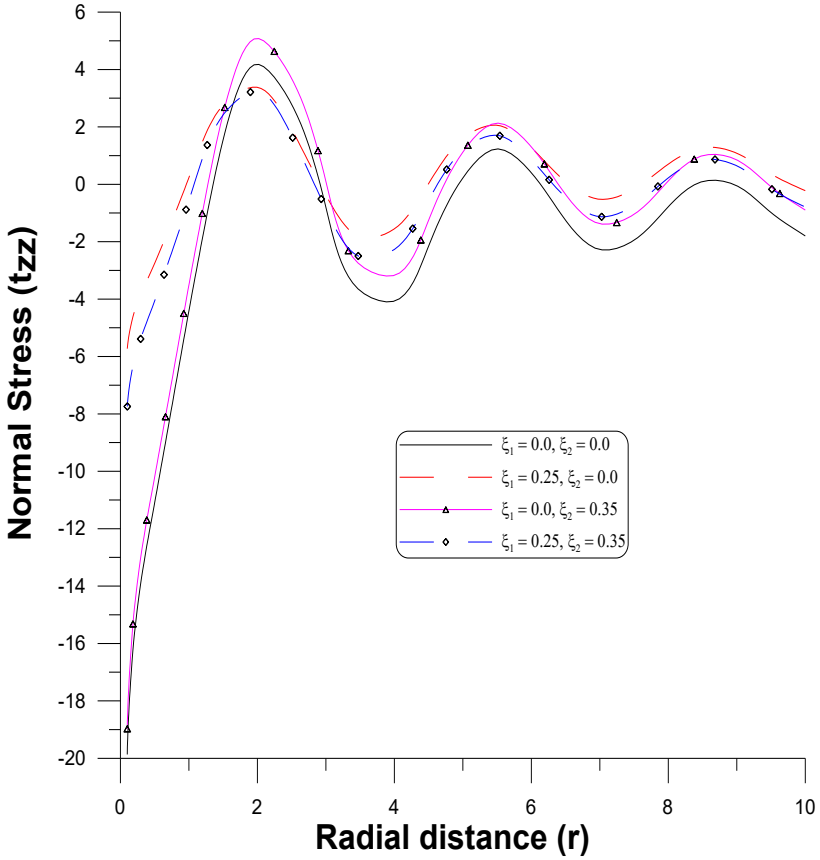

Fig. 6.14: t_{zz} vs. r
(Disc load)

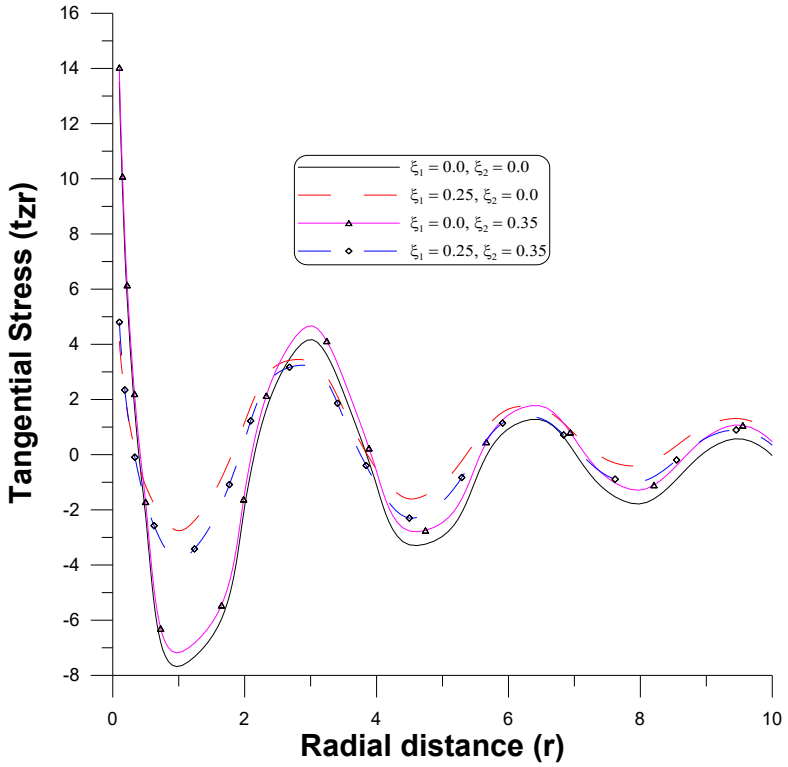

Fig. 6.15: t_{zr} vs. r
(Disc load)

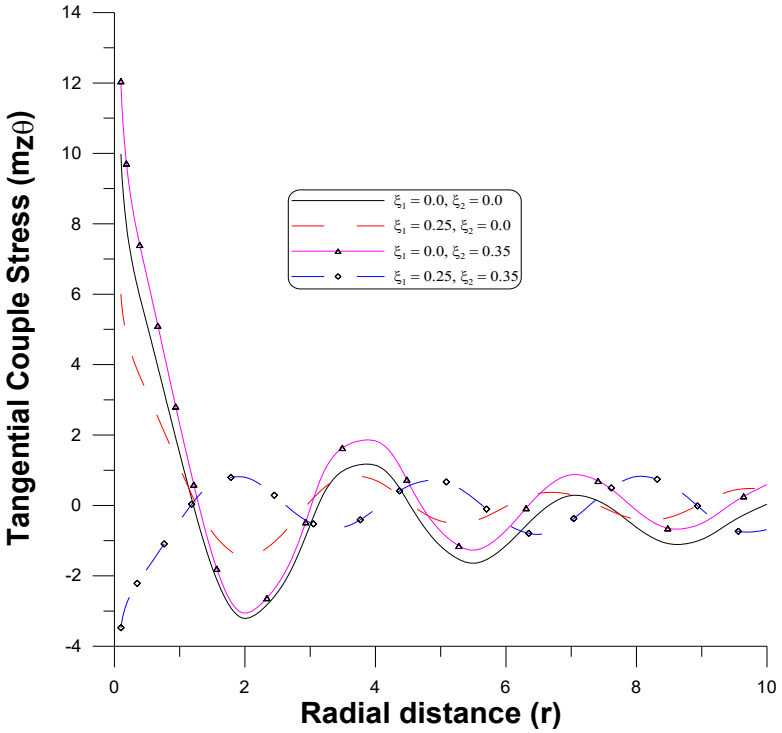

Fig.6.16: $m_{z\theta}$ vs. r
(Disc load)

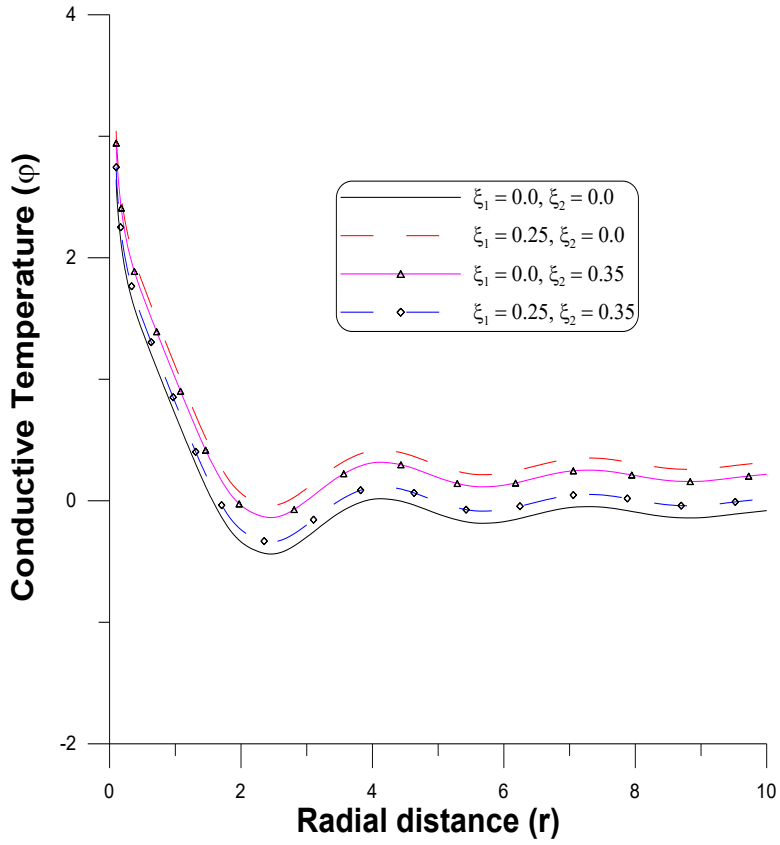

Fig.6.17: φ vs. r
(Disc load)

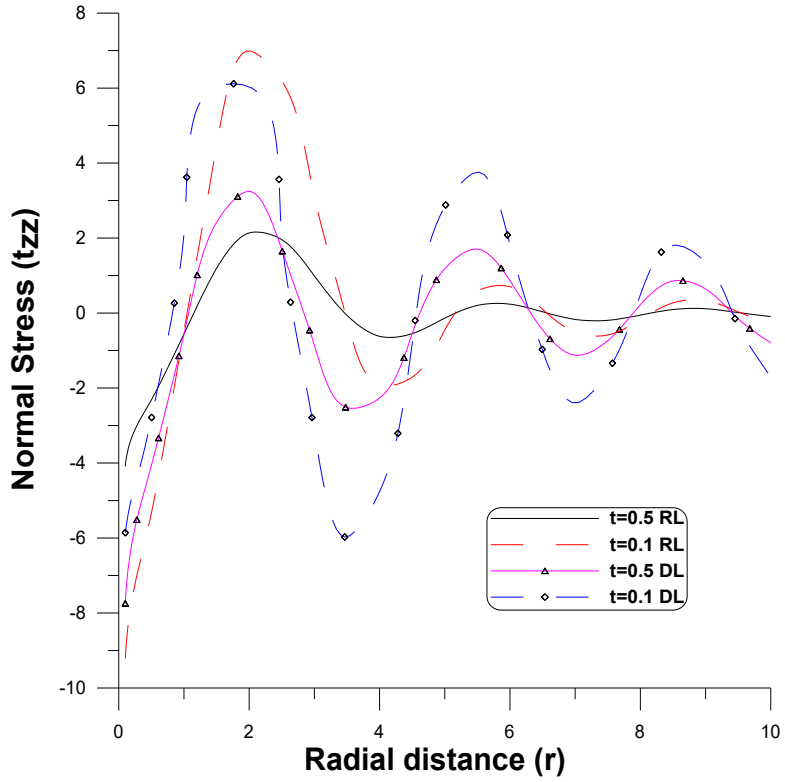

Fig. 6.18: t_{zz} vs. r
(Time Domain)

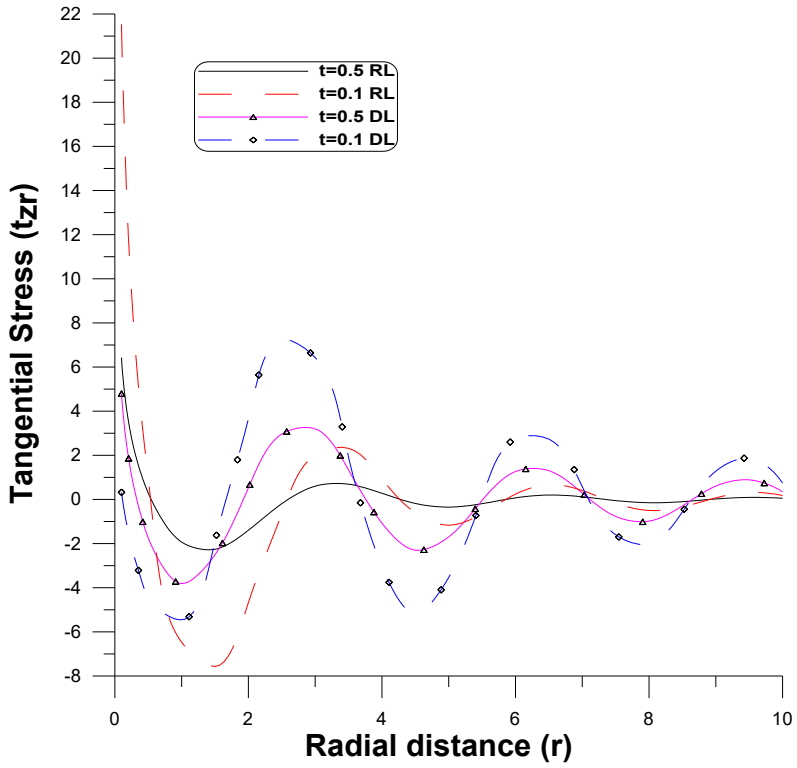

Fig. 6.19: t_{zr} vs. r
(Time Domain)

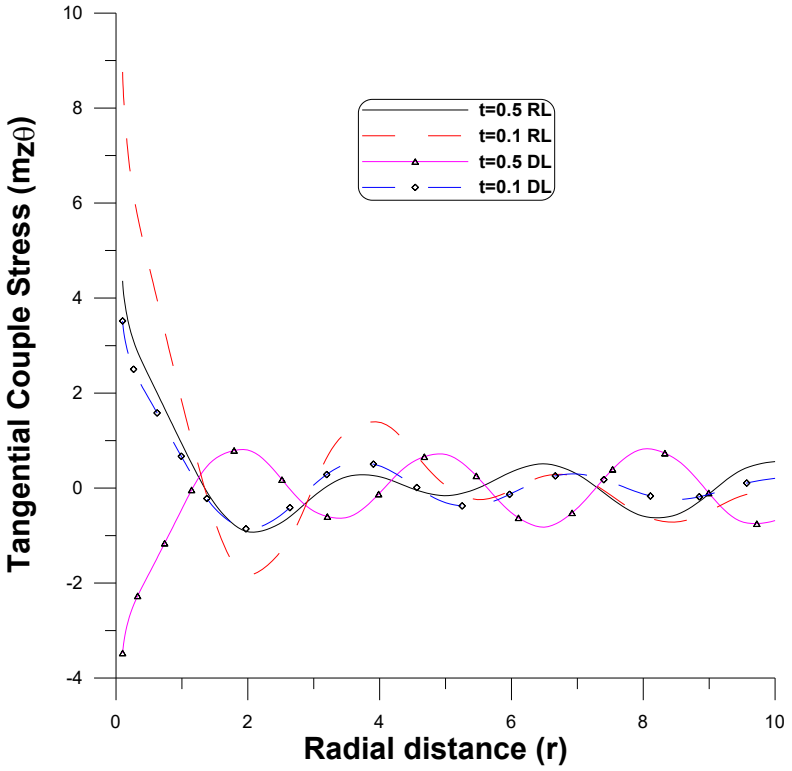

Fig.6.20: $m_{z\theta}$ vs. r
(Time Domain)

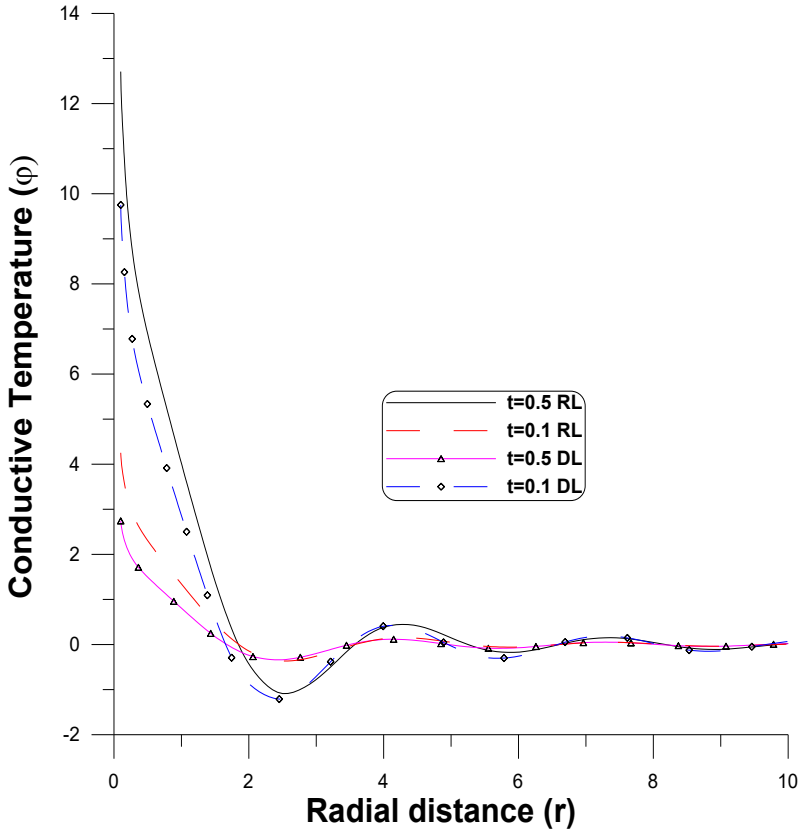

Fig. 6.21: φ vs. r
(Time Domain)

Future Scope

- Various problems related to the reflection of waves and thermomechanical deformation in micropolar elasticity and micropolar thermoelasticity have been investigated within the framework of the MG-L theory of thermoelasticity and the MGT heat equation. The effects of impedance, voids, non-local parameters, HTT, and TT are examined in the problems presented in chapters 2-6 and many more problems can be discussed. Although the models discussed in this thesis are theoretical, they hold great significance in the fields of geophysics, seismology, earthquake engineering, and other related areas, attracting researchers to contribute to this field.
- These problems can also be examined by taking into account the effects of magnetic rotation, three-phase lag, and fractional-order derivatives.
- Mathematical modeling can be illustrated using the finite element method, the homotopy perturbation method, and other numerical techniques.
- The problems discussed in this thesis can be extended by incorporating anisotropy material and higher-order time symmetries.

Bibliography

Bibliography

[1] Abbas, I. and Kumar, R.; Deformation due to thermal source in micropolar generalized thermoelastic half-space by finite element method, *Journal of Computational and Theoretical Nanoscience*, 11(1), 2014, 185-190.

[2] Abouelregal, A.E.; A novel model of nonlocal thermoelasticity with time derivatives of higher order, *Mathematical Methods in the Applied Sciences*, 43(11), 2020, 6746-6760.

[3] Abouelregal, A.E. and Rashid, A.F.; Deformation in a micropolar material under the influence of Hall current and initial stress fields in the context of a double-temperature thermoelastic theory involving phase lag and higher orders, *Acta Mechanics*, 235, 2024, 4311-4337.

[4] Abouelregal, A.E. and Zenkour, A.M.; Two-temperature thermoelastic surface waves in micropolar thermoelastic media via dual-phase-lag model, *Advances in Aircraft and Spacecraft Science*, 4(6), 2017, 711-727.

[5] Abouelregal, A.E., Marin, M. and Alsharari, F.; Thermoelastic plane waves in materials with a microstructure based on micropolar thermoelasticity with two temperature and higher order time derivatives, *Mathematics*, 10(9), 2022, https://doi.org/10.3390/math10091552.

[6] Abouelregal, A.E., Alanazi, R., Sofiyev, A.H. and Sedighi, H.M; Thermal analysis of a rotating micropolar medium using a two-temperature micropolar thermoelastic model with higher-order time derivatives, *Physical Mesomechanics*, 26, 2023, 251–266.

[7] Abouelregal, A.E., Marin, M., Askar, S.S. and Foul, A.; A modified mathematical model for thermo-viscous thermal conduction incorporating memory-based derivatives and the Moore–Gibson–Thomson equation, *Continuum Mechanics and Thermodynamics*, 36, 2024, 585–606.

[8] Abouelregal, A.E., Marin, M., Foul, A., Aksar, S.S.; Nonlocal micropolar thermoelastic half-space: a higher-order model incorporating phase lags and nonlocal effects in space and time, *Applied Physics A,* 131, 2025, https://doi.org/10.1007/s00339-025-08329-w.

[9] Abouelregal, A.E, Ahmad, H., Yavuz, M., Nofal, T. and Alsulami, M.; An orthotropic thermo-viscoelastic infinite medium with a cylindrical cavity of temperature dependent properties via MGT thermoelasticity, *Open Physics*, 20, 2022, 1127-1141.

[10] Abouelregal, A.E., Moaaz, O., Khalil, K.M., Abouhawwash, M. and E. Nasr, M.; Micropolar thermoelastic plane waves in microscopic materials caused by Hall-current effects in a two-temperature heat conduction model with higher-order time derivatives, *Archive of Applied Mechanics*, 93(5), 2023,1901-1924.

[11] Abouelregal, A.E., Moaaz, O., Khalil, K.M., Abouhawwash, M., and E. Nasr, M.; A phase delay thermoelastic model with higher derivatives and two temperatures for the hall current effect on a micropolar rotating material, *Journal of Vibration Engineering and Technologies*, 12, 2024, 1505–1523.

[12] Abouelregal, A.E., Mohammad-Sedighi, H., Shirazi, A.H., Malikan, M., and Eremeyev, V.A.; Computational analysis of an infinite magneto-thermoelastic solid periodically dispersed with varying heat flow based on non-local Moore–Gibson–Thompson approach, *Continuum Mechanics and Thermodynamics*, 34(4), 2022, 1067-1085.

[13] Ailawalia, P. and Priyanka; Effect of thermal conductivity in a semiconducting medium under modified Green-Lindsay theory, *International Journal of Computing Science and Mathematics*, 19(2), 2024,167-179.

[14] Ailawalia, P., Marin, M. and Altenbach, H.; Variable thermal conductivity in context of Green-Naghdi theory of thermo-microstretch solids, *ZAMM-Journal of Applied Mathematics and Mechanics*, 104(4), 2024, https://doi.org/10.1002/zamm.202400010.

[15] Alharbi, A.M., Abd-Elaziz, E.M. and Othman, M.I.A.; Effect of temperature-dependent and internal heat source on a micropolar thermoelastic medium with voids under 3PHL model, *ZAMM-Journal of Applied Mathematics and Mechanics*, 101(6), 2020, https://doi.org/10.1002/zamm.202000185.

[16] Bayounes, F.S., Abd-Elaziz, E.M. and Othman, M.I.; Thomson effect and two-temperature theory on a micropolar thermoelastic medium with voids under Green–Naghdi theory, *ZAMM-Journal of Applied Mathematics and Mechanics*, 102(10), 2022, doi.org/10.1002/zamm.202100473.

[17] Bazarra, N., Fernandez, J.R. and Quintanilla, R.; On the decay of the energy for radial solutions in Moore-Gibson-Thompson thermoelasticity, *Mathematics and Mechanics of solids*, 26(10), 2021, https://doi.org/10.1177/1081286521994258.

[18] Bhat, M, Manna, S. and Alkinidri, M.; Rayleigh wave fields in a multilayered micropolar media, *International Journal of Geomechanics*, 24(4), 2024, https://doi.org/10.1061/IJGNAI.GMENG-8725.

[19] Biot, M.A; Thermoelasticity and irreversible thermodynamics, *Journal of Applied Physics* 27,1956, 240–253.

[20] Boschi, E. and Iesan, D.; A generalized theory of linear micropolar thermoelasticity, *Meccanica*, 8, 1973, 154-157.

[21] Chandrasekharaiah, D.S.; Heat-flux dependent micropolar thermoelasticity, *International Journal of Engineering Science*, 24(8), 1986, 1389-1395.

[22] Chen, P.J. and Gurtin, M.E.; On a theory of heat conduction involving two-temperatures, *ZAMP-Journal of Applied Mathematics and Physics*, 19, 1968, 614-627.

[23] Chen, P.J., Gurtin, M.E. and Williams, W.O.; On the thermodynamics of non-simple elastic materials with two temperatures, *ZAMP-Journal of Applied Mathematics and Physics*, 20, 1969, 107-112.

[24] Chteoui, R., Lotfy, Kh., Seddeek, M.A., El-Dali A. and Hassanin W.S.; Moore–Gibson–Thompson Stability model in a two-temperature photonic semiconductor excited medium affected by rotation and initial stress, *Crystals*, 12(12), 2022, https://doi.org/10.3390/cryst12121720.

[25] Cosserat, E. and Cosserat, F.; *Theorie des corps deformables*, Hermann, Paris, 1909.

[26] Cowin, S.C. and Nunziato, J.W.; Linear elastic materials with voids, *Journal of Elasticity,* 13, 1983, 125-147.

[27] Das, N., De, S. and Sarkar, N.; Plane waves in Moore–Gibson–Thompson thermo-elasticity considering nonlocal elasticity effect, *Mathematics and Mechanics of Solids*, 28(9), 2023, 1978-1998.

[28] Debnath, L.; *Integral transforms and their applications*, CRC Press, 1995.

[29] Deswal, S., Kalkal, K.K., Dhankhar, P., and Poonia, R.; Reflection of plane waves in a nonlocal transversely isotropic micropolar thermoelastic medium with temperature-dependent properties, *Journal of Vibration Engineering and Technologies*, 2024, https://doi.org/10.1007/s42417-024-01378-0.

[30] Dhaliwal R.S. and Singh A.; *Dynamic coupled thermoelasticity*, Hindustan Publication Corporation, New Delhi, India, 1980.

[31] Dhankhar, P., Barak, M.S. and Poonia, R.; Nonlocal and micropolar effects in a transversely isotropic functionally graded thermoelastic solid under an inclined load, *Mechanics of Time-Dependent Materials*, 28, 2024, 1349-1373.

[32] Duhamel, J.; Second Memoire Sur Les Phenomenon Thermo-Mechanique, *Journal de l'Ecole Polytechnique*, 15, 1837, 1-15.

[33] El-Sapa, S., El-Bary, A.A. and Atef, H.M.; Modeling the viscosity and rotation on a generalized micropolar thermoelasticity with two-temperature under five theories, *Waves in Random and Complex Media*, 2023, 1–25, https://doi.org/10.1080/17455030.2023.2184646.

[34] Eringen, A.C.; Simple micro fluids, *International Journal of Engineering Science*, 2, 1964, 205-217.

[35] Eringen, A.C.; *Mechanics of micromorphic materials*, In: Görtler, H. (eds) Applied Mechanics, Springer, Berlin, Heidelberg, 1966, https://doi.org/10.1007/978-3-662-29364-5_12.

[36] Eringen, A.C.; Linear theory of micropolar elasticity, *Journal of Mathematics and Mechanics*, 15(6), 1966, 909–923.

[37] Eringen, A.C.; Theory of micropolar fluids, *Journal of Applied Mathematics and Mechanics*, 16, 1966, 1-18.

[38] Eringen, A.C.; *Theory of micropolar elasticity*, In: Liebowitz, H., Ed., Fracture, Academic Press, 2, 1968, 621-729.

[39] Eringen, A.C.; *Foundations of micropolar thermoelasticity*, International Centre for Mechanical Science, Udline Course and Lectures 23, Springer-Verlag, Berlin, 1970.

[40] Eringen, A.C.; Nonlocal polar elastic continua, *International Journal of Engineering Science*, 10, 1972, 1-16.

[41] Eringen, A.C.; Theory of nonlocal thermoelasticity, *International Journal of Engineering Science*, 12(12), 1974, 1063-1077.

[42] Eringen, A.C.; Plane waves in nonlocal micropolar elasticity, *International Journal of Engineering Science*, 22, 1984, 1113-1121.

[43] Eringen, A.C.; *Microcontinuum field theories I*, Foundations and Solids, Springer Verlag, New York, 1999.

[44] Eringen, A.C. and Edelen, D.G.B.; On nonlocal elasticity, *International Journal of Engineering Science*, 10, 1972, 233-248.

[45] Eringen, A.C. and Suhubi, E.S.; Non-linear theory of simple micro-elastic solids I, *International Journal of Engineering Science*, 2, 1964, 189-203.

[46] Fernández, J. and Quintanilla, R.; Moore-Gibson-Thompson theory for thermoelastic dielectrics, *Applied Mathematics and Mechanics*, 42(2), 2021, 309-316.

[47] Gauthier, R.D.; Experimental investigations on micropolar media, *Mechanics of Micropolar Media, CSIM Courses and Lectures*, 1, 1982, 395–463.

[48] Green, A.; Micro-materials and multipolar continuum mechanics, *International Journal of Engineering Science*, 3(5), 1965, 533-537.

[49] Green, A.E. and Lindsay, K.E.; Thermoelasticity, *Journal of Elasticity*, 2, 1972, 1–7.

[50] Green, A.E. and Naghdi, P.M.; A re-examination of the basic postulates of thermomechanics, *Proceedings of the Royal Society of London, Series A: Mathematical and Physical Sciences*, 432(1885), 1991, 171-194.

[51] Green, A.E. and Naghdi, P.M.; On undamped heat waves in an elastic solid, *Journal of Thermal stresses*, 15(2), 1992, 253-264.

[52] Green, A.E. and Naghdi, P.M.; Thermoelasticity without energy dissipation, *Journal of elasticity*, 31(3), 1993, 189-208.

[53] Green, A.E. and Rivlin, R.S.; Multipolar continuum mechanics, *Archive for rational mechanics and analysis*, 17, 1964, 113-147.

[54] Grioli, G.; Elasticita asimmetrica, *Annali di Matematica Pura ed applicata*, 50, 1960, 389-417.

[55] Gunthier, W.; Zur statik und kinematik des cosseratschen kontinuums, *Abhandlungen Braunschweigischen Wissenschaftlichen Gesellschaft*, 10, 1958, 195-213.

[56] Honig, G. and Hirdes, U.; A method for the numerical inversion of Laplace transforms, *Journal of Computational and Applied Mathematics*, 10(1), 1984, 113-132.

[57] Iesan, D.; Existence theorems in micropolar elastostatics, *International Journal of Engineering Science*, 9, 1971, 59-78.

[58] Iesan, D.; Shock waves in micropolar elastic materials with voids, *Analele Stiintifice ale Universitatu Al. l. Cuzadin lasi Seria Noua Sectiunea la matematica*, 31, 1985, 177-186.

[59] Iesan, D.; A theory of thermoelastic materials with voids, *Acta Mechanics,* 60(1-2), 1986, 67-89.

[60] Jahangir, A., Ali, H., Mahmood, A. and Zaigham Zia, Q.M.; Study on reflected waves through visco-elastic solid rotating with fixed angular frequency, *Waves in random and complex media*, 2023, https://doi.org/10.1080/17455030.2023.2171503.

[61] Jangid, K. and Mukhopadhyay, S.; A domain of influence theorem for a natural stress–heat-flux problem in the Moore–Gibson–Thompson thermoelasticity theory, *Acta Mechanica*, 232(1), 2021, 177-187.

[62] Jangra, A., Deswal, S. and Punia, B.S.; Thermoelastic interactions in a micropolar poro-elastic medium, *Journal of Thermal Stresses*, 47(8), 2024, 1028–1054.

[63] Kalkal, K., Sheoran, D. and Deswal, S.; Reflection of plane waves in a nonlocal micropolar thermoelastic medium under the effect of rotation, *Acta Mechanica*, 231, 2020, 2849-2866.

[64] Kaushal, S., Kumar, R. and Parmar, K.; Influence of diffusion and impedance parameters on wave propagation in thermoelastic medium, *International Journal of Applied Mechanics and Engineering*, 26(4), 2021, 99-112.

[65] Kaushal, S., Kumar, R., Bala, I. and Sharma, G.; Impact of non-local, two temperature and impedance parameters on propagation of waves in generalized thermoelastic medium under modified Green-Lindsay model, *Materials Physics and Mechanics*, 52(1), 2024, 1-17.

[66] Kaushal, S., Kumar, R., Bala, I. and Sharma, G., Wave propagation at free surface in thermoelastic medium under modified Green-Lindsay model with non-local and two temperature, *Structural Engineering and Mechanics*, 90(2), 2024, 209-218.

[67] Kaushal, S., Kumar, R., Kaur, K. and Sharma, G.; A mathematical model for the deformation problem in a generalized thermoelastic medium under modified Green–Lindsay model, *International Applied Mechanics*, 59, 2023, 742–753.

[68] Kaushal, S. Kumar, R., Lofty, Kh. and Bala, A.; Response of frequency domain in generalized thermoelastic medium under modified Green-Lindsay with non-local and two temperature, *ZAMM-Journal of Applied Mathematics and Mechanics*, 104(5), 2024, https://doi.org/10.1002/zamm.202301012.

[69] Khan A.A. and Tanveer S.; Transmission and reflection of SV waves at micropolar solid–liquid interface with dual-phase lag theory, *Indian Journal of Physics*, 96, 2022, 1153-1165.

[70] Kumar, D., Paswan, B., Singh, P. and Chattopadhyay, A.; Reflection and transmission of plane wave at the interface between two distinct nonlocal triclinic micropolar generalized thermoelastic half-spaces under DPL and LS theory, *Acta Mechanica*, 235(5), 2024, 3245-3270.

[71] Kumar, R. and Abbas, I.; Deformation due to thermal source in micropolar thermoelastic media with thermal and conductive temperatures, *Journal of Computational and Theoretical Nanoscience*, 10, 2013, 2241-2247.

[72] Kumar, R. and Choudhary, S.; Interaction due to mechanical sources in micropolar elastic medium with voids, *Journal of Sound and Vibration*, 266, 2003, 889-904.

[73] Kumar, R. and Deswal, S.; Wave propagation in micropolar liquid saturated porous solid, *Indian Journal of Pure and Applied Mathematics*, 31, 2000, 1317-1337.

[74] Kumar, R. and Deswal, S.; Some problems of wave propagation in a micropolar elastic medium with voids, *Journal of Vibration and Control*, 12(8), 2006, 849–879.

[75] Kumar, R. and Gupta, R.R.; Deformation due to inclined load in an orthotropic micropolar thermoelastic medium with two relaxation times, *Applied Mathematics and Information Sciences*, 4, 2010, 413-428.

[76] Kumar, R. and Kaur, M.; Effect of two temperatures and stiffness on waves propagating at the interface of two micropolar thermoelastic media, *Journal of Engineering Physics and Thermophysics*, 88, 2015, 543-555.

[77] Kumar, R. and Kumar, R.; Effect of two-temperature parameter on thermoelastic vibration in micro and nano beam resonator, *European Journal of Mechanics-A/Solids*, 89, 2021, https://doi.org/10.1016/j.euromechsol.2021.104310.

[78] Kumar, R., Kaur, M. and Rajvanshi, S.C.; Wave propagation in micropolar thermoelastic layer with two temperatures, *Journal of Vibration and Control*, 20, 2014, 458-469.

[79] Kumar R., Kaushal S. and Sharma G.; Mathematical model for the deformation in a modified Green- Lindsay thermoelastic medium with non-local and two-temperature effects, *Journal of Applied Mechanics and Technical Physics,* 63, 2022, 448–457.

[80] Kumar, R., Kaushal, S. and Sharma G.; Response of non-local and heat source in Moore-Gibson-Thompson theory of thermoelasticity with hyperbolic two temperature, *WSEAS Transactions on Heat and Mass Transfer*, 18, 2023, 310-324.

[81] Kumar, R., Kaushal, S. and Sharma, G.; Axi-symmetric problem in the thermoelastic medium under Moore-Gibson-Thompson heat equation with hyperbolic two temperature, non-local and fractional order, *Mechanics of Solids*, 59, 2024, 410–430.

[82] Kumar, R., Kumar, B. and Sharma, N.; Reflection and transmission coefficients at the boundary surface of micropolar viscothermoelastic solids with two temperatures, *Research Journal of Science and Technology*, 9(3), 2017, 323-338.

[83] Kumar, R., Kumar, S. and Gourla, M.G.; Interaction due to expanding surface loads in thermoporoelastic medium, *Material Physics and Mechanics*, 21(2), 2014, 126-134.

[84] Kumar, R., Miglani, A. and Rani, R.; Generalized two temperatures thermoelasticity of micropolar porous circular plate with three phase lag model, *Journal of Mechanics*, 34(6), 2018, 779-789.

[85] Kumar, R., Sharma, K.D. and Garg, S.K.; Effect of two temperatures on reflection coefficient in micropolar thermoelastic with and without energy dissipation media, *Advances in Acoustics and Vibration*, 2014(1), 2014, https://doi.org/10.1155/2014/846721.

[86] Kumar, R., Sharma, N. and Chopra, S.; Modelling of thermomechanical response in anisotropic photothermoelastic plate, *International Journal of Mechanical Engineering*, 6, 2022, 577-594.

[87] Kumar, R., Sharma, N. and Chopra, S.; Photothermoelastic interactions under Moore-Gibson-Thompson thermoelasticity, *Coupled System Mechanics*, 11(5), 2022, 459-483.

[88] Kumar, R., Sharma, N., Chopra, S. and Vashisth, A.K.; Representation of fundamental solution and vibration of waves in photothermoelastic under MGTE model, *Ocean Systems Engineering*, 13(2), 2023, 123-146.

[89] Kumar, R., Singh, K. and Pathania, D.S.; Propagation of Rayleigh waves in a micropolar thermoelastic half-space with impedance boundary conditions, *Material Physics and Mechanics*, 35(1), 2018, 115–125.

[90] Kumar, R., Singh, R. and Chadha, T.K.; Eigenvalue approach to micropolar thermoelasticity without energy dissipation, *Indian Journal of Mathematics*, 49(3), 2007, 355-359.

[91] Kumar, S. and Partap, G.; Analysis of waves in micropolar generalized thermoelastic plate with memory dependent derivatives, *ZAMM-Journal of Applied Mathematics and Mechanics*, 103(2), 2022, https://doi.org/10.1002/zamm.202200244.

[92] Kumar, S., Partap, G. and Kumar, R.; Impact of temperature-dependent parameters on wave motion in a micropolar thermoelastic plate involving memory-dependent derivatives, *Acta Mechanica*, 235, 2024, 429–439.

[93] Kumari, N. and Kaliraman, V.; Analysis of wave propagation at an imperfect boundary between micropolar elastic solid and micropolar porous elastic solid, *International Journal of Mathematics Trends and Technology*, 53(1), 2018, 22-37.

[94] Kundu, S., Kalkal, K.K., Sangwan, M. and Sheoran, D.; Two-dimensional deformations in an initially stressed nonlocal micropolar thermoelastic porous medium subjected to a moving thermal load, *International Journal of Numerical Methods for Heat and Fluid Flow*, 33(3), 2023, 1116-1143.

[95] Lata, P. and Singh, S.; Effects of nonlocality and two temperature in a nonlocal thermoelastic solid due to ramp type heat source, *Arab Journal of Basic and Applied Sciences*, 27(1), 2020, 358-364.

[96] Lianngenga, R.; Effect of inertial coefficients in the propagation of plane waves in micropolar porous materials, *International Journal of Computational Materials Science and Engineering*, 6(1), 2017, 1-16.

[97] Lianngenga, R.; Incident fast and slow wave at the surface of porous micropolar thermoelastic half-space, *Forces in Mechanics*, 9, 2022, https://doi.org/10.1016/j.finmec.2022.100118.

[98] Lord, H.W. and Shulman, Y.; The generalized dynamical theory of thermoelasticity, *Journal of Mechanics and Physics of Solids*, 15, 1967, 299-309.

[99] Malischewsky, P.G.; *Surface waves and discontinuities*, Elsevier, Amsterdam, 1987.

[100] Marin, M.; Generalized solutions in elasticity of micropolar bodies with voids, *Revista dele Academia Canaria de Ciencias*, 8, 1996, 101-106.

[101] Marin, M.; An approach of a heat-flux dependent theory for micropolar porous media, *Meccanica*, 51, 2016, 1127-1133.

[102] Marin, M., Chirila, A., Ochsner, A. and Vlase, S.; About finite energy solutions in thermoelasticity of micropolar bodies with voids, *Boundary Value Problems*, 89, 2019, 1-14.

[103] Marin, M., Othman, M.I.A., Seadawy, A.R. and Carstea, C.; A domain of influence in the Moore-Gibson-Thompson theory of dipolar bodies, *Journal of Taibah University for Science*, 14(1), 2020, 653-660.

[104] Megahid, S.F., Abouelregal, A.E., Askar, S.S. and Marin, M.; Study of thermoelectric responses of a conductive semi-solid surface to variable thermal shock in the context of the Moore–Gibson–Thompson thermoelasticity, *Axioms*, 12(7), 2023, https://doi.org/10.3390/axioms12070659.

[105] Miglani, A. and Kaushal, S.; Normal mode analysis of micropolar elastic medium with void under inviscid fluid, *Global Journal of Science Frontier Research*, 11(4), 2011, 39-44.

[106] Miglani, A. and Kaushal, S.; Axi-symmetric deformation in generalized thermoelasticity with two temperatures, *Arabian Journal for Science and Engineering*, 36, 2011, 1581-1595.

[107] Mindlin, R.D. and Tiersten, H.F.; Effects of couple stresses in linear elasticity, *Archives for Rational Mechanics and Analysis*, 11, 1962, 415-448.

[108] Neumann, F.; *Vorlesungen über die Theorie der Elasticität der festen Körper und des Lichtäthers*, BG Teubner, 5, 1885.

[109] Nowacki, W.; Couple-stresses in the theory of thermoelasticity, *In Irreversible Aspects of Continuum Mechanics and Transfer of Physical Characteristics in Moving Fluids: Symposia Vienna*, 1966, 1968, 259-278.

[110] Nowacki, W.; The "second" plane problem of the micropolar elasticity, *Bulletin de I' Academie Polonaise des Sciences, Serie des Sciences Techniques*, 18, 1970, 525-532.

[111] Nowacki, W.; The axial-symmetric problems in micropolar elasticity, *Bulletin de I' Academie Polonaise des Sciences, Serie des Sciences Techniques*, 19, 1971, 317-325.

[112] Nowacki, W.; The second axial symmetric problem in micropolar elasticity, *Bulletin de I' Academie Polonaise des Sciences, Serie des Sciences Techniques*, 20, 1972, 517-522.

[113] Nunziato, J.W. and Cowin, S.C.; A nonlinear theory of elastic materials with voids, *Archieve of Rational Mechanics and Analysis,* 72, 1979, 175-201.

[114] Othman, M.I.A. and Abbas, I.A.; 2-D Problem of micropolar thermoelastic rotating medium with eigenvalue approach under the three-phase-lag model, *Waves in Random and Complex Media*, 33(2), 2023, 280-295.

[115] Othman, M.I.A. and Atwa, S.Y.; Response of micropolar thermoelastic solid with voids due to various sources under Green Naghdi theory, *Acta Mechanica Solida Sinica*, 25(2), 2012, 197-209.

[116] Partap, G. and Kumar, R.; Free vibration analysis of micropolar thermoelastic cylindrical curved plate in circumferential direction*, Journal of Solid Mechanics*, 2, 2010, 267-274.

[117] Poonam, Sahrawat, R.K., and Kumar, K.; Plane wave propagation and fundamental solution in non-local couple stress micropolar thermoelastic solid medium with voids, *Waves in Random and Complex Media*, 34(2), 2024, 879–914.

[118] Press, W.H., Teukolsky, S.A., Vetterling, W.T. and Flannery, B.P.; *Numerical Recipes: The Art of Scientific Computing*, Cambridge University Press, New York, 1986.

[119] Quintanilla, R; Convergence and structural stability in thermoelasticity, *Applied Mathematics and Computation*, 135, 2003, 287-300.

[120] Quintanilla, R.; Some qualitative results for a modification of the Green-Lindsay thermoelasticity, *Meccanica*, 53, 2018, 3607–3613.

[121] Quintanilla, R; Moore-Gibson-Thompson thermoelasticity, *Mathematics and Mechanics of Solid*, 24, 2019, 4020–4031.

[122] Quintanilla, R; Moore-Gibson-Thompson thermoelasticity with two temperatures, *Applications in Engineering Science*, 1, 2020, https://doi.org/10.1016/j.apples.2020.100006.

[123] Rajkumar, G., Somaiah, K., Narasimharao, K. and Venkateswararao, B.; Propagation of elastic waves along a cylindrical rod of micropolar elastic solid with stretch under impedance boundary conditions, *Indian Journal of Science and Technology*, 17(15), 2024, 1566-1576.

[124] Rani, P., Kumar, R. and Partap, G.; Wave Analysis and Deformation in Poro-thermoelastic Medium with Microtemperature Under Nonlocal Elasticity Theory and Dual Phase Lag Model, *Iranian Journal of Science and Technology, Transactions of Mechanical Engineering* 49, 2025, 1433–1459.

[125] Rao, K.M. and Rao, B.K.; Longitudinal wave propagation in a micropolar wave guide of circular cross section, *International Journal of Engineering Science*, 21(9), 1983, 1137-1144.

[126] Roy, S. and Lahiri, A; Higher-order heat conduction model in a rotating micropolar thermoelastic medium with moving heat source and electromagnetic field, *Mechanics of Time-Dependent Materials*, 2024, https://doi.org/10.1007/s11043-024-09694-4.

[127] Sahrawat, R.K., Kumar, K., Poonam and Rani, S.; Reflection and refraction phenomenon of waves at the interface of two non-local couple stress micropolar thermoelastic solid half-spaces, *Mechanics of Solids*, 58, 2023, 216–244.

[128] Sahu, S.S., Mondal, S. and Nirwal, S.; Mathematical analysis of Rayleigh waves at the nonplanner boundary between orthotropic and micropolar media, *International Journal of Geomechanics*, 23(3), 2023, https://doi.org/10.1061/IJGNAI.GMENG-724.

[129] Said, S.M.; Effect of the gravity on a nonlocal micropolar thermoelastic media with the multi-phase-lag model, *Geomechanics and Engineering*, 36(1), 2024, 19-26.

[130] Sarkar, N. and Mondal, S.; Thermoelastic plane waves under the modified Green-Lindsay model with two-temperature formulation, *ZAMM-Journal of Applied Mathematics and Mechanics*, 100(11), 2020, https://doi.org/10.1002/zamm.201900267.

[131] Sarkar, N., Abo-Dahab, S.M. and Mondal, S.; Reflection of magneto-thermoelastic waves at a solid half-space under modified Green-Lindsay model with two temperatures, *Journal of Thermal Stresses*, 43(9), 2020, 1083–1099.

[132] Sarkar, N., De, S. and Sarkar, N.; Modified Green-Lindsay model on the reflection and propagation of thermoelastic plane waves at an isothermal stress-free surface, *Indian Journal of Physics*, 94(8), 2020, 1215–1225.

[133] Shakeriaski, F., Ghodrat, M., Diaz. J.E. and Mehnia, B.; Modified Green-Lindsay thermoelasticity wave propagation in elastic materials under thermal shocks, *Journal of Computational Design and Engineering*, 8(1), 2021, 36-54.

[134] Sharma, K.; Analysis of deformation due to inclined load in generalised thermodiffusive elastic medium, *International Journal of Engineering, Science and Technology*, 3(2), 2011, 117-129.

[135] Sharma, K.; Reflection of plane waves in thermodiffusive elastic half-space with voids, *Multidiscipline Modeling in Materials and Structures*, 8(3), 2012, 269-296.

[136] Sharma, K.; Reflection at free surface in micropolar thermoelastic solid with two temperatures*, International Journal of Applied Mechanics and Engineering*, 18(1), 2013, 217-234.

[137] Sharma, K. and Bhargava, R.R.; Propagation of thermoelastic plane waves at an imperfect boundary of thermal conducting viscous liquid/generalized thermoelastic solid, *Afrika Matematika*, 25, 2014, 81-102.

[138] Sharma, K. and Kumar, P.; Propagation of plane waves and fundamental solution in thermoviscoelastic medium with voids, *Journal of Thermal Stresses*, 36(2), 2013, 94-111.

[139] Sharma, K. and Marin, M.; Effect of distinct conductive and thermodynamic temperatures on the reflection of plane waves in micropolar elastic half-space, *UPB Scientific Bulletin, Series A: Applied Mathematics and Physics*, 75, 2013,121-132.

[140] Sharma, K., Sharma, S. and Bhargava, R.R.; Propagation of waves in micropolar thermoelastic solid with two temperatures bordered with layers or half spaces of inviscid liquid, *Materials Physics and Mechanics*, 16(1), 2013, 66-81.

[141] Sharma, N. and Kumar, R.; Photothermoelastic investigation of semiconductor material due to distributed loads, *Journal of Solid Mechanics*, 13(2), 2021, 202-212.

[142] Sharma, N. and Kumar, R.; Photothermoelastic deformation in dual phase lag model due to concentrated inclined load, *Italian Journal of Pure and Applied Mathematics*, 48, 2022, 1147-1160.

[143] Sharma, N., Kumar, R., and Lata, P.; Disturbance due to inclined load in transversely isotropic thermoelastic medium with two temperatures and without energy dissipation, *Materials Physics and Mechanics*, 22(2), 2015, 107-117.

[144] Sharma, S. and Khator, S.; Power generation planning with reserve dispatch and weather uncertainties including penetration of renewable sources, *International Journal of Smart Grid and Clean Energy*, 10(4), 2021, 292-303.

[145] Sharma, S. and Khator, S.; Micro-grid planning with aggregator's role in the renewable inclusive prosumer market, *Journal of Power and Energy Engineering*, 10(4), 2022, 47-62.

[146] Sharma, S. and Sharma, K.; Influence of heat sources and relaxation time on temperature distribution in tissues, *International Journal of Applied Mechanics and Engineering*, 19(2), 2014, 427-433.

[147] Sharma, S., Sharma, K. and Bhargava, R.R.; Plane waves and fundamental solution in an electro-microstretch elastic solids*, Afrika Matematika*, 25, 2014, 483–497.

[148] Shaw, S. and Mukhopadhyay, B.; Thermoelastic waves with thermal relaxation in isotropic micropolar plate*, Sadhana*, 36, 2011, 209-221.

[149] Sheoran, S.S., Kalkal, K.K. and Chaudhary, S.; Reflection of plane waves in a rotating micropolar double porous thermoelastic medium with temperature dependent properties, *Heat Transfer*, 53(5), 2024, 2391-2415.

[150] Singh, B. and Kaur, B.; Rayleigh surface wave at an impedance boundary of an incompressible micropolar solid half-space, *Mechanics of Advanced Materials and Structures*, 29(25), 2022, 3942-3949.

[151] Singh, B., Yadav, A.K. and Gupta, D.; Reflection of plane waves from a micropolar thermoelastic solid half-space with impedance boundary conditions, *Journal of Ocean Engineering and Science*, 4, 2019, 122–131.

[152] Singh, D., Kaur, G. and Tomar, S.K.; Waves in nonlocal elastic solid with voids, *Journal of Elasticity*, 128(1), 2017, 85–114.

[153] Singh, R. and Singh, K.; Eigenvalue approach in micropolar medium with voids, *International Journal of Applied Mechanics and Engineering*, 18, 2013, 521-536.

[154] Singh, S.S. and Lianngenga, R.; Effect of micro inertia in the propagation of waves in micropolar thermoelastic materials with voids, *Applied Mathematical Modelling*, 49, 2017, 487-497.

[155] Somaiah K. and Kumar A.R.; Rayleigh wave propagation at viscous liquid/micropolar micro-stretch elastic solid, *Communications in Mathematics and Applications*, 14(1), 2023, 89–103.

[156] Sneddon, I.N.; *Application of integral transforms in the theory of elasticity*, New York: Springer-Verlag, 33, 1975.

[157] Strunin, D.V.; On Characteristic Times in Generalized Thermoelasticity, ASME. *Journal of Applied Mech*anics, 68(5), 2001, 816–817.

[158] Suhubi, E.S. and Eringen, A.C.; Non-linear theory of simple micro-elastic solids II, *International Journal of Engineering Science*, 2, 1964, 389-404.

[159] Tauchert, T.R., Claus, W.D., Jr., and Ariman, T.; The linear theory of micropolar thermoelasticity, *International Journal of Engineering Science*, 6, 1968, 37-47.

[160] Tayel, I.M., Alebraheem, J., Asad, S., El-Bary, A. and Lotfy, Kh.; Surface absorption illumination in a 2D thermoelastic semi-infinite medium under modified Green and Lindsay model, *Alexandria Engineering Journal*, 61, 2021, 2050-2259.

[161] Thompson, P.A; *Compressible-Fluid Dynamics*, New York, McGraw-Hill, 1972.

[162] Tiersten, H.F.; Elastic surface waves guided by thin films, *Journal of Applied Physics*, 40, 1969, 770–789.

[163] Tiwari, R., Kumar, R. and Abouelregal, A.E.; Thermoelastic vibrations of nano-beam with varying axial load and ramp type heating under the purview of Moore–Gibson–Thompson generalized theory of thermoelasticity, *Applied Physics A*, 128, 2022, https://doi.org/10.1007/s00339-022-05287-5.

[164] Truesdell, C. and Toupin, R.; The Classical field theories, *Encyclopedia Physics*, 3, 1960, 226-858, https://doi.org/10.1007/978-3-642-45943-6_2.

[165] Voigt, W.; Theoretische studien uber die elastiziatverhattnisse der kristalle, *Abhandlungen, der Koniglichen Gesellschaft der Wissenschaften Gottingen*, 34, 1887, 52-79.

[166] Yadav, A.K.; Reflection of plane waves in a micropolar thermo-diffusion porous medium, *Waves in Random and Complex Media*, 34(4), 2024, 2319-2341.

[167] Youssef, H.M.; Theory of two-temperature-generalised thermoelasticity, *IMA Journal of applied mathematics*, 71(3), 2006, 383-390.

[168] Youssef, H.M., and El-Bary, A.A.; Theory of hyperbolic two-temperature generalized thermoelasticity, *Material Physics and Mechanics*, 40(2), 2018, 158-171.

[169] Yu, Y.J., Tian, X.G. and Xiong, Q.L.; Nonlocal thermoelasticity based on nonlocal heat conduction and nonlocal elasticity, *European Journal of Mechanics-A/Solids*, 60, 2016, 238-253.

[170] Yu, Y.J., Xue, Z.N. and Tian, X.G.; A modified Green-Lindsay thermoelasticity with strain rate to eliminate the discontinuity, *Meccanica*, 53, 2018, 2543–2554.

[171] Zhang, P., Wei, P. and Tang, Q.; Reflection of micropolar elastic waves at the non-free surface of a micropolar elastic half-space, *Acta Mechanica*, 226, 2015, 2925-2937.

List of Publications

1) Kumar, R., Kaushal, S. and Kochar, A.; Response of impedance parameters on waves in the micropolar thermoelastic medium under modified Green-Lindsay theory, ZAMM Journal of applied mathematics and mechanics, 102(9), 2022, DOI:10.1002/zamm.202200109 **(SCI and SCOPUS, I.F: 2.3).**
2) Kaushal, S., Kumar, R. and Kochar, A.; Wave propagation under the influence of voids and non-free surfaces in a micropolar elastic medium, Materials Physics and Mechanics, 50(2), 2022, DOI:10.18149/MPM.5022022_4 **(RSCI and SCOPUS, SJR: 0.285).**
3) Kumar, R., Kaushal, S. and Kochar, A.; Mathematical modelling of micropolar thermoelastic problem with nonlocal and hyperbolic two-temperature based on Moore–Gibson–Thompson heat equation, Canadian Journal of Physics, 101(11), 2023, https://doi.org/10.1139/cjp-2022-0339 **(SCI and SCOPUS, I.F: 1.2).**
4) Kumar, R., Kaushal, S. and Kochar, A.; Analysis of Wave Motion in Micropolar Thermoelastic Medium Based on Moore–Gibson–Thompson Heat Equation Under Non-local and Hyperbolic Two-Temperature, International Journal of Applied and Computational Mathematics, 10(50), 2024, DOI:10.1007/s40819-023-01667-4 **(SCOPUS, SJR 0.377).**
5) Kumar, R., Kaushal, S. and Kochar, A.; Analysis of axisymmetric deformation in generalized micropolar thermoelasticity within the framework of Moore-Gibson-Thompson heat equation incorporating non-local and hyperbolic two-temperature effect, The Journal of Strain Analysis for Engineering Design, 59(6), 2024, DOI:10.1177/03093247241232180 **(SCI and SCOPUS, I.F: 1.8).**
6) Kochar, A., Kumar, R. and Kaushal, S.; Frequency domain response in generalized micropolar thermoelastic media using the Moore-Gibson-Thompson heat equation and hyperbolic two temperature, International Applied Mechanics **(Accepted) (Scopus, Q3, I.F: 0.7).**

Conferences Attended/Paper Presented

1. Presented paper in International Conference on **"Emerging Trends in Engineering, Science & Management (ICETESM-2024)" organized by Global Group of Institutes Amritsar, Amritsar** held on 10th May, 2024.
2. Presented paper in International Conference on **"Recent Developments in Mathematical Sciences, Artificial Intelligence and Machine Learning (ICRMAM-2023)" organized by Sri Guru Teg Bahadur Khalsa College, Anandpur Sahib** held on 14th March to 15th March 2023.
3. Presented paper in National Conference on "**Recent Developments in Mathematics (NCRDM-2022)" sponsored by Haryana State Council of Science and Technology, and organized by Department of Mathematics Kurukshetra University, Kurukshetra** held on 26th Dec. to 27th Dec. 2022.
4. Presented paper in International Conference on "**Research and Innovation in Multidisciplinary studies (ICRIMS-2022)" organized by Sant Baba Bhag University** held on 30th May to 1st June 2022.
5. Presented paper in 4th International conference on **"Frontiers in Industrial and Applied Mathematics" organized by department of Mathematics, Sant Longowal Institute for Engineering and Technology, Longowal** held on 21-22 December, 2021.
6. Presented paper in conference on **"Application of Mathematics in Science and Technology" sponsored by Director General Higher Education, Haryana** held on 1 Feb.,2020 at Maharaja Agrasen Mahavidyalaya, Jagadhri.
7. Won **first prize** in poster presentation during the conference on **"Recent Advances in Fundamental and Applied Sciences (RAFAS 2019)"** held on November 5- 6, 2019 at Lovely Professional University, Phagwara.